Identification of the brain areas that mediate insulin action

Niannian Wang

Submitted in accordance with the requirements for the degree of
Doctor of Philosophy

University of Leeds
School of Biomedical Sciences

August 2023

Acknowledgements

Abstract

It is becoming increasingly apparent that insulin signaling regulates neural circuits in the brain, playing roles in the control of appetite, cognition and memory. Interestingly, in humans, intranasal delivery of insulin to specifically target the brain, has an effect on feeding behaviour, glucose regulation and cognition. However, the action of intranasally administered insulin in the brain has not yet been fully explained, especially in respect to food intake. Here, to determine the effect of intranasal insulin *in vivo*, the mice were placed in metabolic cages after intranasal injection of standard human insulin, the results show that intranasal insulin remarkably reduced food consumption within 2-5 hours after treatment. Then intranasal fluorescence insulin was delivered to track the distribution of insulin receptors in mouse brain to highlight the areas of the brain that intranasal insulin can reach. Results suggest that insulin receptors are located in many areas of the murine brain, including olfactory bulb, hippocampus, brainstem and a novel area nucleus of the horizontal limb of the diagonal band (HDB). Furthermore, knockdown of the insulin receptor in the HDB leads to a significant increase in food intake in male rats but not female rats. Besides, impaired insulin signaling in the HDB also results in hyperactive in female rats but not male rats. Retrograde tracing data show that the HDB receives afferents from the ventral tegmental area (VTA) and mitral cell layer of olfactory bulb, which might be involved in regulating in metabolism.

Overall, our data indicates that intranasal delivery of insulin is a good way to target areas of the brain important for controlling energy balance. Due to the metabolic effect that intranasal insulin has both in rodents and humans, further studies are warranted in order to understand which insulin sensitive brain regions and neurons are involved in this process.

Table of Contents

List of Figures

List of Tables

Abbreviations

ARC	Arcuate nucleus
AgRP	Agouti-related peptide
AP	Anterior-Posterior
APS	Ammonium persulfate
AD	Alzheimer's disease
APOE	Apolipoprotein E
ADRB3	Adrenoceptor Beta 3
ACACA	Acetyl-CoA carboxylase alpha
Ach	Acetylcholine
α–MSH	α-Melanocyte-stimulating hormone
aCSF	Artificial cerebrospinal fluid
BAT	Brown adipose tissue
BBB	Blood-brain barrier
BMI	Body mass index
BSA	Covine serum albumin
CNS	Central nervous system
CSF	Cerebrospinal fluid
Chop	DNA damage-inducible transcript 3
CLAMS	Comprehensive Lab Animal Monitoring System
ChAT	Choline acetyltransferase
CNO	Clozapine-N-oxide
CPE	Cytopathic effect
DGAT1	Diacylglycerol O-acyltransferase 1
DAG	Diacylglycerol
DV	Dorsal-Ventral
DCN	Deep cerebellar nuclei of the cerebellar cortex
DREADD	Designer Receptors Exclusively Activated by Designer Drugs
DTT	Dithiothreitol
DT	Diphtheria toxin
DMSO	Dimethyl sulfoxide
DMEM	Eagle's minimal essential medium
DEPC	Diethyl pyrocarbonate

ERK 1/2	Extracellular signal-regulated kinase 1/2
ER	Endoplasmic reticulum
ER stress	Endoplasmic reticulum stress
EEG	Electroencephalogram
ECL	Enhanced chemiluminescence
EGTA	Ethylene glycol tetraacetic acid
EDTA	Ethylenediaminetetraacetic acid
eYFP	Enhanced Yellow Fluorescent Protein
FoxO1	Forkhead box protein O 1
FOXK	Forkhead box k
FFA	Free fatty acids
fMRI	Functional magnetic resonance imaging
FITC-insulin	Fluorescein isothiocyanate-insulin
FAS_2	Fatty acid synthase_ 2
FDA	Food and Drug Administration
FBS	Fetal Bovine Serum
GSK3	Glycogen synthase kinase 3
G-6-Pase	Glucose-6-phosphatase
GLUT1	Glucose transporter 1
GLUT2	Glucose transport 2
GLUT4	Glucose transporter 4
G-6-P	Glucose 6-phosphate
GLM	Generalized linear model
GL	Glomerular layer
GFAP	Glial fibrillary acidic protein
GFP	Green fluorescent protein
HSL	Hormone-sensitive lipases
HPA	Hypothalamic-pituitary-adrenal
HRP	Horseradish peroxidase
HGP	Hepatic glucose production
HDB	Horizontal limb of the diagonal band
H&E	Haematoxylin and eosin
HYP	Hypothalamus
hM3Dq	Human Gq-coupled M3 muscarinic receptor
IL-6	Interleukin- 6

ILPs	Insulin analogues
IGF1	Insulin-like growth factor 1
IDF	International Diabetes Federation
IR	Insulin receptor
i.c.v	Intracerebroventricular
IHC	Immunohistochemistry
IRS	Insulin receptor substrates
LH	Lateral hypothalamus
LIRKO	Liver insulin receptor knockout
MAPK/MEK	Mitogen-activated protein kinase
MBH	Mediobasal hypothalamic
M/L	Medial-Lateral
ML	Mitral cell layer
MS	Medial septum
MEM-NEAA	Minimum Essentiall Medium Non-Essential amino acids
NEFA	Nonesterified fatty acid
NAc	Nucleus accumbens
Nup358	Nucleoporin 358
NFkB	Nuclear factor kappa B
NeuN	Neuronal nuclear protein
NMDG	N-methyl-D-glucamine
NAFLD	Nonalcoholic fatty liver disease
OSNs	Olfactory sensory neurons
OB	Olfactory bulb
OCT	Optimal Cutting Temperature Compound
PD	Parkinson's disease
PB	Phosphate buffer solution
PC12	Pheochromocytoma
PI3K	Phosphatidylinositol 3 kinase
PIP2	Phosphatidylinositol 4,5-biphosphate
PIP3	Phosphatidylinositol 3,4,5-triphosphate
PDK	Phosphoinositide-dependent protein kinase
PGC1α	Peroxisome proliferative activated receptor-γ coactivator 1-α
POMC	Proopiomelanocortin
PKB	Protein kinase B

PDE3B	Phosphodiesterase 3B
PKA	Protein kinases A
PEPCK	Phosphoenolpyruvate carboxykinase
PVH	Paraventricular hypothalamus
PPARγ	Peroxisome proliferators–activated receptor γ
Pol II	Polymerase II
PCL	Purkinje cell layer
PFA	Paraformaldehyde
PBS	Phosphate buffered saline
RER	Respiratory exchange ratio
PET	Positron emission tomography
RIN	RNA Integrity Number
SUR1	Sulfonylurea receptor 1
SN	Substantia nigra
STAT3	Signal transducer and activator of transcription 3
SD	Sprague Dawley
SDS	Sodium dodecyl sulfate
SEM	Standard Error of Mean
ShRNA	Short hairpin RNA
TG	Triglyceride
TH	Tyrosine hydroxylase
TNFα	Tumour Necrosis Factor α
Tu	Olfactory tubercle
TEMED	Tetramethylethylenediamine
TRPC5	Transient receptor potential canonical 5
UCP	Mitochondrial uncoupling protein
VTA	Ventral tegmental area
VEGF	Vascular endothelial growth factor
VP	Ventral pallidum
VMH	Ventromedial hypothalamus
WAT	White adipose tissue
WGA-HRP	Wheat germ agglutinin-horseradish peroxidase

1 Introduction

1 Insulin

1.1.1 The discovery of insulin

Dating back to around 1889, two German scientists, Joseph von Mering and Oskar Minkowski, pointed out that total removal of the pancreas led to the diabetes related deaths (Minkowski, 1989), which implied that the pancreas was vital in controlling carbohydrate metabolism. The key substance was named as insulin (from Latin "insula" ("island")) by Sir Edward Albert Sharpey-Schafer in 1915. On the basis of previous findings, Frederick Banting and Charles Best further discovered that dogs exhibited diabetic symptoms, such as high glucose levels in the blood and urine after removing the pancreases, while these signs were improved when pancreas extractions were given (Banting et al., 1922). However, the impurity of insulin was still an urgent issue to be addressed. The Canadian biochemist James Bertram Collip joined the team to help extract pure insulin. Finally, with the collaborative effort of many scientists, use of insulin in the clinic became possible (De Leiva-Hidalgo and De Leiva-Perez, 2020; Banting et al., 1991, 1962) and also started a new historical chapter for the treatment regimen of diabetic patients.

1.1.2 The development of insulin

The use of insulin was developed further and by the 1960s, it could be chemically synthesised in the laboratory (Katsoyannis et al., 1966). Benefiting from DNA technology, human insulin could be produced in bacteria (Crea et al., 1978) which achieved a higher yield and fewer allergic reactions (Fineberg et al., 1983). In 1988, Brange et al reported the first insulin analogue that achieved faster absorption and better mimicked the rapid augmentation of insulin in people without diabetes (Brange et al., 1988).

1.1.3 The management of diabetes mellitus

As Banting mentioned in his Nobel Prize lecture, insulin is rather a treatment than a cure for type 1 diabetes. Type 1 diabetes (Ozougwu et al., 2013) is an autoimmune disease where β cells in the pancreas are destroyed and insulin is secreted and released

to maintain normal glucose levels. A common management for type 1 diabetes is to inject short-acting insulin at meal times, combined with long-acting insulin (Owens and Griffiths, 2002) once or twice per day to control normal glucose levels. However, for the regimen of type 2 diabetes (Ozougwu et al., 2013) that is usually caused by being overweight and obesity, initial drug treatments like metformin and sulfonylurea, along with healthy diet and increasing physical activity are recommended (Gebrie et al., 2021). Insulin injection combined with licensed medications are then introduced when single medicine or dual medicine therapy are unable to control the blood glucose levels.

1.1.4 The delivery of insulin

Even though the discovery and development of insulin has brought light to the millions suffering from diabetes, it has to be delivered by injection due to the risk that enzyme digestion could destroy its function, this makes diabetes health management painful and exhausting. With the development of technologies, insulin delivery devices were invented based on monitoring patient blood glucose levels, such as the insulin pump, insulin pen (Heinemann et al., 2021) and closed-loop bihormonal delivery system (Bally et al., 2018). However, users have to test their blood sugar level several times a day or use monitors continuously, which is extremely inconvenient.

With the idea of avoiding insulin injections on the implantation of a pump, an alternative way of delivering insulin has been recently developed where insulin is administrated via inhalation (Oleck et al., 2016). In 2014, inhale insulin Afrezza was approved for the treatment of type 1 and type 2 diabetes by the Food and Drug Administration (FDA) (https://www.medscape.com/viewarticle/827539). Though some side effects were concerned, such as a cough (Bode et al., 2015), inhaled insulin Afrezza still showed great potential compared to conventional subcutaneous injection. Specifically, it was reported that type 1 diabetic patients had reduced blood glucose levels, with less hypoglycemia and less weight gain after 24 weeks of Afrezza treatment (Bode et al., 2015), suggesting that inhaled insulin could overcome the complications of applying injections of insulin for treating diabetes (Richardson and Kerr, 2003; Mccall, 2012) (Figure 1.1 shows the development of the delivery of insulin).
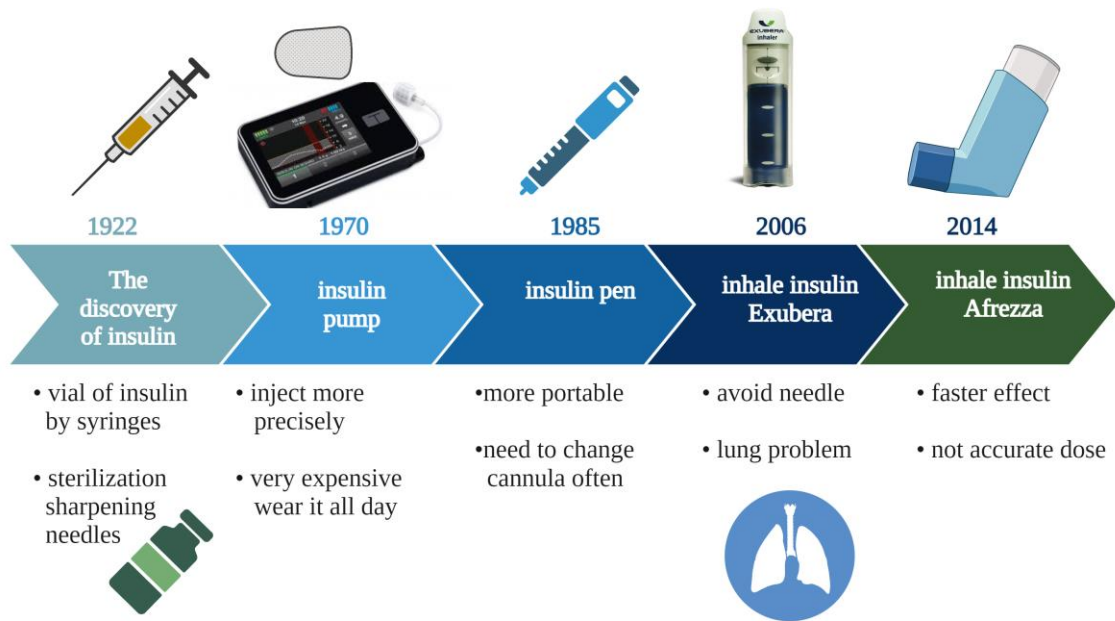
Figure 1. 1 The development of the delivery of insulin. Once insulin was discovered, insulin originally was delivered by syringes, then by insulin pumps, then insulin pens were innovated to improve the self-management of diabetes. In 2006, inhaled insulin Exubera was put onto the market. However, due to several lung problem cases that were reported, it was soon withdrawn. After that, inhaled insulin Afrezza became popular and is still used now.

1.2 The secretion of insulin

Insulin is secreted by the β cells of the pancreas. After a meal, food is digested and a person's glucose level rises. High glucose concentration is transported to the β cells of the pancreas via glucose transport 2 (GLUT2) (Kellett et al., 2008), then an abundance of ATP is produced through the process of glycolysis and the tricarboxylic acid (TCA) cycle. The increasing level of ATP binds to the ATP site in the K_{ATP} channel, leading to the K_{ATP} channel being closed and the intracellular potassium increasing. The consequence of this is a membrane depolarization that opens the voltage-gated calcium channel. Increasing Ca^{2+} influx promotes the migration of insulin vesicles into the cell membrane and the release of insulin from the vesicles. (The insulin release process is shown in Figure 1.2).

However, when blood glucose levels are low, the cells lack ATP and the K_{ATP} channels are therefore open. Potassium effluxes through the channel which generates a negative membrane potential that holds the voltage-gated calcium channels shut, which means there is no insulin secretion.
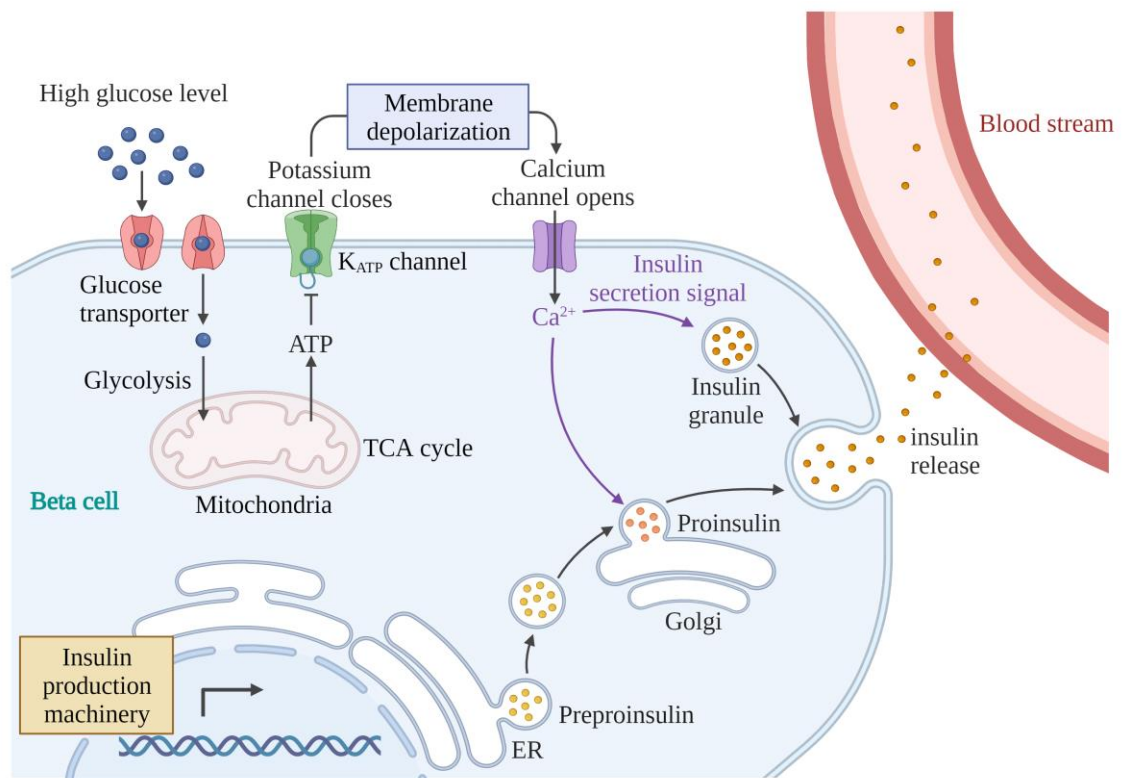
Figure 1. 2 The mechanism of insulin secretion. High levels of glucose are transported into the cells by the glucose transporter, then abundant ATP is produced through the process of glycolysis (in the cytoplasm) and TCA cycle (in the mitochondria). A high level of ATP inhibits the K_{ATP} channel, which leads to membrane depolarization and the Ca^{2+} channel opening. Ca^{2+} influx results in insulin vesicle exocytosis and insulin being released into the blood stream. ER: endoplasmic reticulum

1.3 The cellular mechanism of insulin
1.3.1 PI3K/AKT and MAPK signalling

Insulin acts via binding to the insulin receptor. The insulin receptor is a heterodimeric ligand of insulin, which comprises two α extracellular and two β intracellular subunits (Yip and Ottensmeyer, 2003). The two α subunits are extracellular while the two β intracellular traverse the membrane into the cytoplasm, which means that insulin

receptor possesses both extracellular and cytoplasmic domains. Insulin binds on the extracellular domain to trigger auto-phosphorylation of the IR, which employs and phosphorylates insulin receptor substrates (IRS) to the intracellular membrane. The phosphorylation of IRS subsequently triggers the phosphatidylinositol 3 kinase (PI3K) pathway and the mitogen-activated kinases (MAPK) pathway.

For the former, the activated PI3K phosphorylates the substrate phosphatidylinositol 4,5-biphosphate (PIP2) to form phosphatidylinositol 3,4,5-triphosphate (PIP3), which further recruits and phosphorylates other downstream proteins, such as phosphoinositide-dependent protein kinase (PDK) and Akt (also known as protein kinase B (PKB)) (Hubbard, 2013; Li et al., 1999; Ramalingam et al., 2016; Franke et al., 1997). The phosphorylation of Akt interacts with the downstream effectors, such as glycogen synthase kinase 3 (GSK3) and forkhead box protein O 1 (FoxO1). GSK3 is phosphorylated and inhibited by p-Akt which increases the glycogen synthesis (Lee and Kim, 2007). Active nuclear FOXO1 could interact with the transcriptional coactivator peroxisome proliferative activated receptor-γ coactivator 1-α (PGC1α) (Puigserver et al., 2003; Nakae et al., 2001), which further increases the expression of glucose-6-phosphatase (G-6-Pase) to induce the gluconeogenesis. In the latter case, FoxO1 is excluded from the nucleus and its transcription activity is inhibited (Kousteni, 2012), which leads to a reduction of gluconeogenic gene expression and further inhibits gluconeogenesis (Nakae et al., 1999; Matsumoto et al., 2007). In addition, the inhibited FOXO1 activity could increase the gene expression of anorexigenic neuropeptide proopiomelanocortin (POMC) and decrease the gene expression of orexigenic neuropeptide agouti-related peptide (AgRP), which induces the suppression of food intake (Iskandar et al., 2010; Kitamura et al., 2006). Together, these data suggest that the PI3K-AKT pathway is crucial for insulin in regulating glucose levels and food intake (The PI3K-AKT pathway is described in Figure 1.3).

On the other hand, insulin acts through the MAPK pathway. The phosphorylation of IRS activates Ras (a signal transduction protein), which transmits the signal by recruiting the downstream kinase Raf (Skolnik et al., 1993). The activated Raf is able to activate Mitogen-activated protein kinase (MAPK/MEK 1) and (MAPK/MEK 2) (Shaul and Seger, 2007), which further triggers the phosphorylation of the extracellular signal-regulated kinase (ERK 1/2). Increased ERK 1/2 has been found in type 2 diabetes (Carlson et al., 2003), while lacking in ERK 1 could protect mice from insulin

resistance and obesity (Bost et al., 2005). In addition, Filippi et al reported that insulin could inhibit hepatic glucose production (HGP) through activating the ERK 1/2 pathway, whereas this effect was inhibited when the ERK 1/2 was blocked, which means the MAPK pathway is also involved in controlling glucose homeostasis (Filippi et al., 2012). Altogether, these pieces of data suggest that the MAPK pathway contributes to the regulation of metabolism (The MAPK pathway is described in Figure 1.3).

1.3.2 Insulin action in the nucleus

In addition, the insulin signaling pathway is also involved indirectly in gene expression. As mentioned from last section (Section 1.3.1), Akt activates the phosphorylation of forkhead box O (FOXO), which leads to the inhibition of FOXO and is exported from the nucleus to disable its function of regulation of gene expression (Nakae et al., 2000). Phosphorylation of forkhead box k (FOXK) was imported from cytoplasm into the nucleus to down-regulate lipid metabolism and proliferation-related gene transcription (Sakaguchi et al., 2019). In addition, it has been reported that the ERK could also have been transported into the nucleus (Khokhlatchev et al., 1998; Adachi et al., 2000; Matsubayashi et al., 2001; Adachi et al., 1999), and the nuclear localization of ERK plays a crucial role in cellular proliferation and differentiation through interacting with transcriptional factors (TF) (Maik-Rachline et al., 2019; Rodriguez and Crespo, 2011), which implies that nuclear ERK may be an important target to develop anti-cancer drugs.

Insulin receptors translocating from cell surface into the nucleus to directly regulate gene expression has been studied for several decades. Goldfine et al reported that I^{125} labelled insulin was detected rapidly in the nucleus after incubation and this translocation process is also reversible (Goldfine and Smith, 1976). It was observed that insulin can also lead to the insulin receptor directly being transported into the nucleus, and interacting with TF, RNA Polymerase II (Pol II) to regulate gene transcription (Hancock et al., 2019). However, the full mechanism of how the insulin receptor translocates into the nucleus and its effects on regulating diabetes still need further study (Insulin action in the nucleus is described in Figure 1.3).
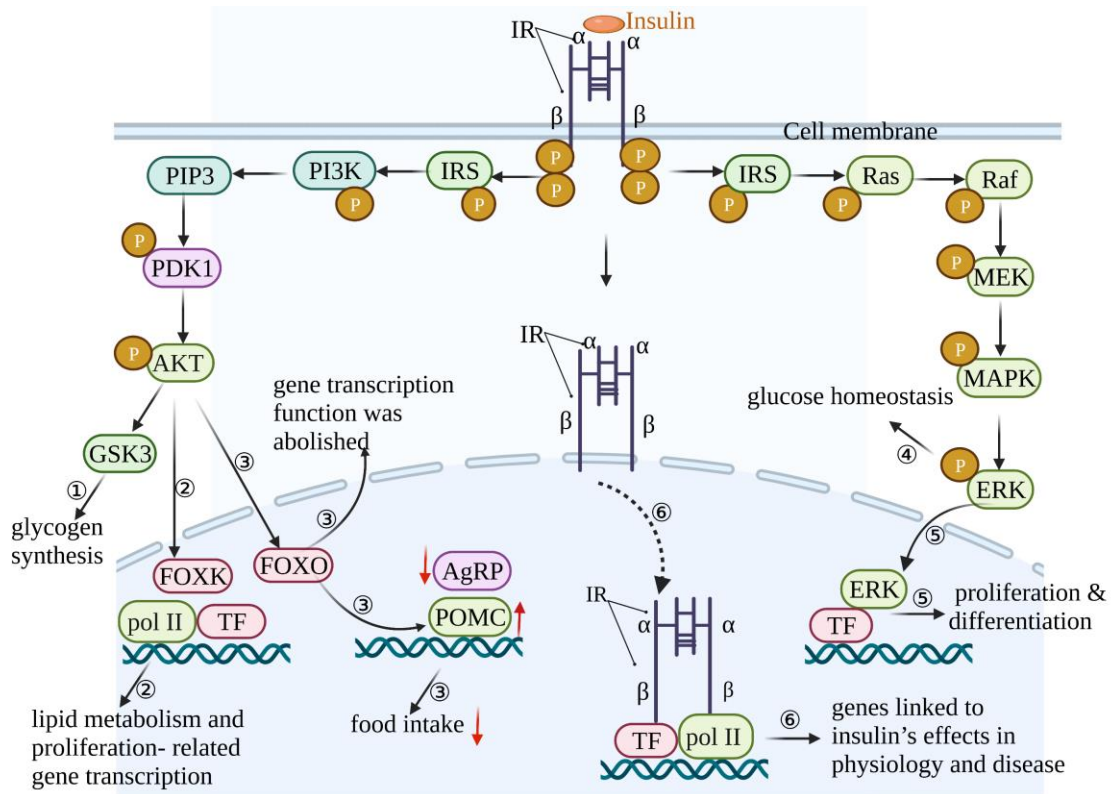
Figure 1. 3 The cellular mechanism of insulin. Insulin binds to the insulin receptor (IR), triggering the auto-phosphorylation of insulin receptor and the phosphorylation of downstream proteins, such as the phosphorylation of insulin receptor substrates (IRS), which triggers two different pathways (PI3K-Akt pathway and MAPK pathway). PI3K-Akt pathway is relevant to the regulation of glycogen synthesis by mediating glycogen synthase kinase 3 (GSK3) (shown as ①). The PI3K-Akt pathway is also involved in gene transcription in the nucleus by phosphorylation of FOXK to regulate lipid metabolism and proliferation, shown as ②, or excludes FOXO from nucleus to abolish this function to regulate food intake shown as ③). MAPK pathway is involved in the regulation of glucose homeostasis (shown as ④) and could also enter into the nucleus to regulate cellular proliferation and differentiation (shown as ⑤). The insulin receptor translocates into the nucleus, and combines with the transcriptional factors (TF) and RNA Polymerase II (Pol II) to regulate gene transcription (shown as ⑥).

1.4 Insulin action in the peripheral system

1.4.1 Insulin action in the skeletal muscles

Insulin acts on peripheral organs such as muscles and adipose tissues to increase glucose uptake (Dimitriadis et al., 2011). At the physiological level, insulin is important for glucose clearance, which involves signaling to decrease glucose production (Lu et al., 2012). In an earlier report, Cori et al discovered that compared to having no insulin injection, the difference in the sugar concentration between the arterial and venous blood of the rabbits' leg muscle became larger when insulin was subcutaneously injected, and these observations suggested that insulin was able to remove the sugar from the blood (Cori and Cori, 1925). However, it took several decades to unveil the mechanism behind it. Subsequent reports found that insulin promotes glucose uptake into the muscles via a 'carrier' or transporter instead of the phosphorylation of glucose (Park et al., 1955; Morgan et al., 1964; Elbrink and Bihler, 1975). Until around 1990, scientists from different groups reported that the 'carrier' was the glucose transporter (GLUT 4) (Charron et al., 1989; Fukumoto et al., 1989; James et al., 1988).

In most cases, glucose enters the cell for absorption and utilization is a rate-limiting process regulated by the transporter GLUT 4 (Huang and Czech, 2007). After being stimulated by insulin, GLUT 4 translocates to the plasma membrane (Sylow et al., 2021; Cushman and Wardzala, 1980; Suzuki and Kono, 1980), which has been mediated by GLUT 4-containing storage vesicles (GSV) trafficking and fusion (Leto and Saltiel, 2012; Sylow et al., 2014). Specifically knocking out GLUT 4 in the muscle results in a remarkable reduction in the glucose uptake and impaired response to insulin stimulation in mice (Zisman et al., 2000). On the contrary, the function of insulin-promoted glucose uptake was enhanced by skeletal muscle GLUT 4 overexpression, which demonstrated that GLUT 4 plays a crucial role in glucose homeostasis (Tsao et al., 1996). In addition, type 2 diabetic patients usually have normal GLUT 4 levels but impaired glucose transporters, which may be associated with GLUT 4 translocation to cell surface defects (Le et al., 2016). The incompatibility between the insulin receptor stimuli and GLUT 4 translocation could lead to insulin resistance (Xu et al., 2015b), which is characterised by a decreased sensitivity to insulin. Insulin resistance in turn lowers the efficiency of glucose uptake and utilization and leads to more insulin secretion, which consequently causes the excessive concentrations of insulin in the blood, leading to pancreatic

dysfunction and diabetes (Kasuga, 2006; Weyer et al., 2001). Besides promoting glucose uptake, insulin could also stimulate the glycogen synthesis in the skeletal muscle, and the enzyme glycogen synthase is involved in the process (Halse et al., 2001). It has been reported that physical activity could increase the rate of skeletal muscle glycogen synthesis and reduce glucose circulation in the blood (Jensen et al., 2011). Altogether, this data is evidence that GLUT 4 is closely related to regulating glucose uptake and glycogen synthesis in the muscle (how insulin acts in muscle is shown in Figure 1.4).

1.4.2 Insulin inhibits lipolysis

The process of a triglyceride (TG) breaking into a glycerol and three free fatty acids (FFA) by lipase enzymes is known as lipolysis. Insulin is an important hormone in the regulation of lipolysis (Jaworski et al., 2007). For instance, insulin could bind to the insulin receptor on the cell membrane of adipocytes and activate insulin downstream signaling pathways, such as the PI3K/Akt signaling pathway. Cyclic nucleotide phosphodiesterase 3B (PDE3B) is the main target of PI3K/Akt in the adipocytes. It has been reported that PDE3B knock-out (KO) mice displayed a decreased adipocyte size and increased TG and cyclic adenosine monophosphate (cAMP) contents in the liver, which may imply that PDE3B is involved in the cAMP signalling and lipolysis (Choi et al., 2006). It has been shown that insulin-induced phosphorylation could activate PDE3B, which leads to the inhibition of cAMP (Choi et al., 2010; Zhao et al., 2020). cAMP is required for the activation of protein kinases A (PKA) which is the enzyme that phosphorylates hormone-sensitive lipases (HSL) to promote lipolysis (Jaworski et al., 2007; Duncan et al., 2007) in the adipocyte. HSL knock-out (KO) mice caused accumulated diacylglycerol (DAG) and decreased the release of FFA in adipose tissues, which suggested that HSL is a rate-limiting enzyme responsible for DAG hydrolysis (Haemmerle et al., 2002). Consequently, the process of lipolysis is inhibited by insulin induced inactivation of HSL (how insulin acts in adipose tissue is shown in Figure 1.4).

1.4.3 Insulin action in the liver

Additionally, studies have indicated that the liver could directly respond to insulin stimulation. For example, the hepatic glucose production (HGP) rose three times when plasma insulin levels decreased by 75%, while it reduced by 50% when plasma insulin increased by 75% (Sindelar et al., 1996; Sindelar et al., 1998). A study reported by Fisher et al further supported this concept that insulin directly acts on the liver and regulates the HGP (Fisher and Kahn, 2003). By specifically knocking down the insulin receptor in the liver, mice showed an impairment in the ability of insulin to suppress the HGP (Fisher and Kahn, 2003), which suggested that hepatic insulin signaling is important for regulating normal glucose homeostasis. Sindelar et al indicated that insulin can directly inhibit the HGP by suppressing glycogenolysis (Sindelar et al., 1996) and by regulating liver gluconeogenic gene expressions such as Akt, GSK3 and FoxO1 (Cherrington, 2005; Lin and Accili, 2011) (The cellular mechanism of how insulin regulates Akt, GSK3 and FoxO1 to increase hepatic glycogen synthesis has been described in section 1.3.1). Mice with defected FoxO1 displayed a reduction of the HGP and enhanced insulin sensitivity (Matsumoto et al., 2007; Samuel et al., 2006). Mice lacking both hepatic Akt1 and Akt2 displayed impaired glucose tolerance. However, when FoxO1 was deleted in the liver, it could effectively restore these glucose-related defects (Lu et al., 2012). Interestingly, when mice had both Akt and FoxO1 deleted, they exhibited normal insulin suppression of hepatic glucose production (HGP). This suggests that the primary function of Akt is to control and limit the activity of FoxO1, which is essential for inhibiting HGP (Lu et al., 2012). These results imply that when FoxO1 is absent, Akt's role becomes significant in the suppression of HGP by insulin. In such circumstances, Akt cannot be considered dispensable for achieving the inhibitory effects on hepatic glucose production (Lu et al., 2012).

Interestingly, Buettner et al found that the acute decrease in the expression of hepatic insulin receptor did not significantly increase the HGP even though the downstream insulin signalling was changed (Buettner et al., 2005), which may imply that the action of the hepatic insulin could modulate the HGP through potential indirect mechanisms (Okamoto et al., 2005). For instance, insulin could inhibit the secretion of glucagon from the islet α cells in the pancreas to indirectly inhibit the HGP (Sun et al., 1991; Franklin et al., 2005). Glucagon is a hormone that increases the blood glucose levels by promoting glycogenolysis, gluconeogenesis and inhibiting glycogen synthesis. It has

been reported that glucagon could activate glycogen phosphorylase, which further leads to the phosphorylation of glycogen and converts glycogen into glucose 6-phosphate (G-6-P) (Krebs, 1981). G-6-P, one of the intermediates of gluconeogenesis is converted into glucose by G-6-Pase (Rajas et al., 2019). In addition, glucagon also could upregulate the expression of G-6-Pase (Band and Jones, 1980) and phosphoenolpyruvate carboxykinase (PEPCK) (Beale et al., 1984) to facilitate the process of gluconeogenesis and increase glucose production in the liver. Additionally, glucagon could reduce glycogen synthesis by inhibiting glycogen synthase (Akatsuka et al., 1985), leading to an increased glucose level in the liver. Therefore, insulin could suppress the hepatic glucose level by directly inhibiting the secretion of glucagon.

In addition to inhibiting the secretion of glucagon, the action of insulin could also decrease the release of the gluconeogenic precursor free fatty acids (FFA, also called nonesterified fatty acid (NEFA) from the adipocytes to the plasma (Sindelar et al., 1997), which consequently causes a reduction in the supply of FFA to the liver (Sindelar et al., 1997). The decreased level of FFA further leads to a reduction of ATP, and this signal will promote glycolysis which means glucose is consumed rather than produced (Sindelar et al., 1997), so that the output of the HGP is decreased (how insulin works in the liver is shown in Figure 1.4).

Notably, the indirect effect of insulin in regulation of the HGP could also act through insulin's action in the brain which sends neuronal projection to the liver (More detail will be discussed in the next section).
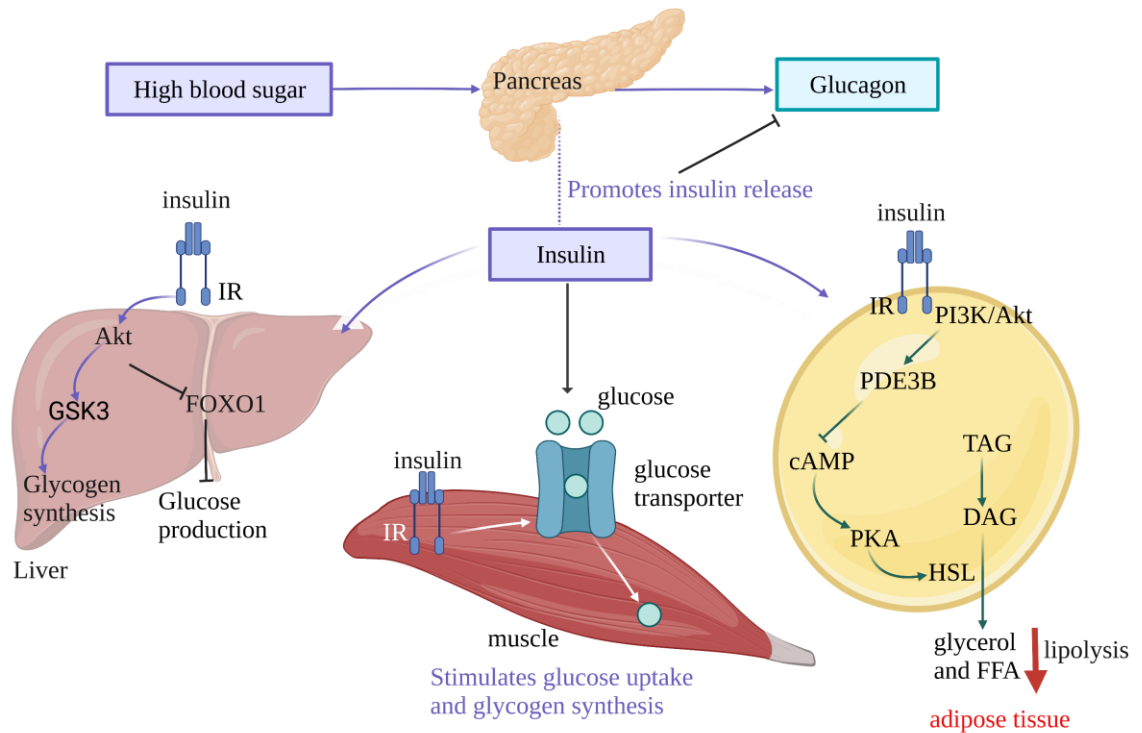
Figure 1. 4 Insulin acts in the liver, muscle and adipose tissue. High blood sugar stimulates insulin production, which leads to inhibited glucagon release. In the liver, insulin activates the Akt to promote glycogen synthesis and inhibits glucose production. Insulin could increase glucose transporter trafficking from the cytoplasm to the cell membrane to increase glucose uptake and glycogen synthesis in the muscle. In the adipose tissue, insulin activates the PI3K/Akt pathway and PDE3B. Activated PDE3B could reduce the level of cAMP, then the protein kinases A (PKA) is inhibited due to the lack of cAMP. Consequently the activity of the hormone-sensitive lipases (HSL) is inactivated, which leads to the inhibition of lipolysis.

1.5 Insulin action in the central nervous system

1.5.1 Insulin signalling in the brain

In addition to acting on the muscle, liver and adipose tissues, insulin also acts on the central nervous system (CNS) and sends information through the brain to provide a higher level of control of the hepatic glucose output (Sandoval et al., 2009), feeding behaviour (Aime et al., 2012), learning and memory (Morton et al., 2006). The accumulation of insulin in the brain could further stimulate the secretion of insulin in the pancreas (Chen et al., 1975). As a whole and dynamic biological system, it is crucial to understand how brain insulin regulates the systematic metabolism.

To better understand the role of insulin in the brain and peripheral tissues, two mouse models were created with knocked down of the IR: one model causes knocked down in all tissues including the brain (IR$^{\triangle wb}$) and the other restricts knocked down in the peripheral tissues (IR$^{\triangle per}$) (Koch et al., 2008). Down-regulation of insulin receptor expression in both models resulted in severe hyperinsulinemia, and interestingly the latter showed more pronounced hyperglycemia. Both models showed a significant up-regulation of hepatic leptin receptor expression, whereas only IR$^{\triangle per}$ mice showed increased liver STAT3 (signal transducer and activator of transcription 3) phosphorylation and Interleukin-6 (IL-6) expression. Similarly, there were reduced white adipose tissue (WAT, involves in energy storage) masses in both models, however, there was a more pronounced reduction in WAT mass and severe hypoleptinemia in IR$^{\triangle wb}$ mice. Taken together, these data suggest that the brain insulin signaling is also important to determine the whole body metabolic balance.

1.5.2 Brain insulin regulates hepatic glucose production

Insulin receptor is widely dispersed in the olfactory bulb, hypothalamus, hippocampus, cerebral cortex, brainstem and cerebellum (Havrankova et al., 1978; Unger et al., 1989). It has been reported that many areas in the brain are involved in regulating glucose production, including the hypothalamus (Pocai et al., 2005a), brainstem (Niu et al., 2011) and striatum (Heni et al., 2017). By injecting antisense oligodeoxinucleotides against the insulin receptor in the third ventricle to target the hypothalamus, Obici et al showed the involvement of insulin sensing in the control of the HGP (Obici et al., 2002a). Data

from the hyperinsulinemic clamp (Euglycemia is maintained via glucose infusion and the glucose infusion rate is an indicator of insulin-induced glucose production) suggested that physiological hyperinsulinemia (refers to a natural and healthy increase in the levels of insulin in the bloodstream in response to certain physiological conditions) reduced glucose production in rats treated with control oligodeoxynucleotides by 55%, whereas rats treated with insulin receptor antisense oligodeoxynucleotides only decreased the hepatic glucose production by 25%. This data indicates that the insulin receptor in the hypothalamus can regulate glucose production and the absence of insulin receptor in the brain will compromise the function of insulin in inhibiting the level of HGP (Obici et al., 2002a). These data evidently suggest that brain insulin also plays a significant role in regulating of HGP.

Although previous study has demonstrated that insulin signalling in the hypothalamus or the third ventricle is involved in the regulation of HGP (Obici et al., 2002a), what types of neuronal populations participated in this process are still not investigated. Data from two-photon microscopy (to image the neuronal activity in living tissues) showed that insulin administration in the recording chamber could regulate hypothalamic AgRP neuronal activity through insulin-mediated PI3K pathway (Xu et al., 2005). In parallel, Könner et al further pointed out that insulin receptor in hypothalamic AgRP neurons but not POMC neurons was required for suppression of HGP by specifically knocking out insulin receptor in the AgRP or POMC neurons *in vivo* (Konner et al., 2007). Another elegant work attempted to understand this question from another angle. Knocking-in insulin receptor in the AgPR neurons could restore the ability of insulin to suppress HGP, whereas the restoration of insulin signal in the POMC neurons enhanced HGP. This delineated that different subpopulations of hypothalamic neurons might be implicated in brain insulin signaling related HGP regulation (Lin et al., 2010).

The level of HGP is closely related to the activity of hypothalamic potassium (K_{ATP}) channels through the vagal outflow to the liver (Pocai et al., 2005a; Matsuhisa et al., 2000). K_{ATP} is made up of the Kir6.2 potassium channel and the sulfonylurea receptor 1 (SUR1), which regulates the secretions of insulin (Ashcroft, 2005). For example, loss of SUR1 in mouse pancreatic β cells causes a lack of insulin secretion, leading to an increased blood glucose level. However, when the fasting blood glucose concentration is lowered, the loss of SUR1 in the mouse pancreatic β cells causes excessive secretion of insulin, leading to hypoglycaemia (Seghers et al., 2000). In another study, however,

pancreatic SUR1 null mice did not show a fluctuating insulin level in response to glucose compared to normal mice. This is likely due to choline-stimulated insulin secretion which compensates for the loss of SUR1 (Shiota et al., 2002). Activation of the mediobasal hypothalamic (MBH) K_{ATP} channel can inhibit gluconeogenesis and reduce blood glucose concentration. Inversely, blockers of hypothalamic K_{ATP} channel impaired the regulation of HGP (Pocai et al., 2005a; Zhang et al., 2004; Coomans et al., 2011). The deliberate knockout of the Kir6.2 gene, specifically targeted to the ventromedial hypothalamus (VMH) in mice, leads to a loss of glucagon secretion from pancreatic islets, which further demonstrates that the K_{ATP} channel in the hypothalamus plays an essential role in the regulation of systemic glucose balance (Miki et al., 2001).

The following question needs to be answered is how brain insulin acts on the K_{ATP} channel to regulate HGP? It was proposed that brain insulin could activate insulin downstream signaling such as PI3K and PIP3 in the hypothalamic AgRP neurons (Konner et al., 2007; Qiu et al., 2014; Plum et al., 2006) (as previously described in section 1.3.2). This could lead to the opening of the K_{ATP} channel and K^+ ions efflux, which consequently could result in the termination of action potentials and the reduction in firing activity of AgRP (Andersson, 1992; Kuang et al., 2015). In addition, hyperpolarization of AgRP neurones could trigger a neuronal relay to the liver, the reduction of AgRP neurons and G6Pase expression in the liver could account for the suppression of HGP (Konner et al., 2007; Matsuhisa et al., 2000). Although insulin activated PI3K and PIP3 signaling in the POMC neurons, the following transduction acted in the transient receptor potential canonical 5 (TRPC5) channel across the cell membrane, inducing the influx of Na^+ and Ca^{2+}, which triggered the depolarization and excitations of POMC neurons (Song and Yuan, 2010). Consistent with this finding, optogenetic stimulation of the projection of POMC to the liver could elevate hepatic gluconeogenesis and hepatic glucose output (Kwon et al., 2020). Altogether, these studies suggest that AgRP and POMC neurons play as an opposite role to modulate HGP.

1.5.3 Brain insulin regulates food intake

Brain insulin regulating food intake might be associated with Neuropeptide Y and Agouti-Related Peptide (NPY/AgRP) neurons in the hypothalamus (Schwartz et al., 1992a; Erickson et al., 1996). In the diabetic induced hyperphagia state, the expression of NPY in the hypothalamus is increased as well as a low level of plasma insulin (Jones et al., 1992; Kalra et al., 1991; Sahu et al., 1992). While this increased NPY was inhibited by intracerebroventricular (i.c.v) injection insulin in the third ventricle (Schwartz et al., 1992b; Schwartz et al., 1991; Sipols et al., 1995), and moreover diabetic hyperphagia was significantly reduced compared to the i.c.v saline infusion (Sipols et al., 1995). A study conducted by Clark et al further showed that i.c.v injection NPY directly increased food intake in rats (Clark et al., 1984). Ablation of NPY/AgRP in adult mice results in rapid starvation (Luquet et al., 2005; Gropp et al., 2005). Benefiting from chemogenetic technology, the study has shown that specific activation of AgRP neurons could rapidly induce intense feeding (Krashes et al., 2011; Krashes et al., 2014). Altogether, these data suggested that higher expression of NPY/AgRP may contribute to overeating, and brain insulin signal could alter the expression of NPY/AgRP to influence feeding behaviours.

In addition to NPY/AgRP, hypothalamic melanocortin precursor molecule pro-opiomelanocortin (POMC) is another main target of brain insulin to regulate food intake. It has been reported that POMC neurons reduced food intake dependent on the melanocortin receptor signaling (Aponte et al., 2011). Also i.c.v infused insulin in the third ventricle could increase the expression of POMC and profoundly reduce food intake (Benoit et al., 2002). Data from patch recording also showed that insulin could excite POMC neurons in guinea pigs and mice, and significantly increase the percentage of POMC expressing c-fos (serving as a marker for neuronal activity) (Qiu et al., 2014). Consistent with the alteration of c-fos expression, insulin robustly inhibited food intake and energy expenditure (Qiu et al., 2014). Furthermore, insulin both significantly decreased meal size and meal frequency (Qiu et al., 2014). These data suggested that brain insulin might suppress food intake through this hypothalamic melanocortin system.

1.5.4 Brain insulin regulates lipogenesis

A mouse line with a neuron-specific disruption of insulin receptor (NIRKO) gene expression was constructed to study the functions of central insulin sensing in the regulation of metabolic balance (Bruning et al., 2000). The results indicated that the NIRKO female mice showed increased food intake, whereas both male and female mice had exhibited diet-sensitive obesity and increased body fat and plasma leptin levels, mild insulin resistance, elevated plasma insulin levels and hypertriglyceridemia. Chronic insulin therapy of control mice increased fat mass, adipocyte size and adipose tissue lipoprotein lipase expression, which suggested that the action of insulin in the CNS is also involved in regulating lipogenesis (Koch et al., 2008).

Work has also shown that insulin signaling particularly in the hypothalamus plays an essential role in lipolysis and lipogenesis in the WAT (Scherer et al., 2011). Specifically, insulin infused into the MBH could inhibit the expression of HSL which further reduced lipolysis in the WAT (Scherer et al., 2011), while mice with impaired neuronal insulin receptor showed increased lipolysis and dampened lipogenesis in the WAT (Scherer et al., 2011). In line with this finding, Carvalheira et al indicated that insulin stimulated p-AKT signalling in the hypothalamus was significantly lower in the obese rats than in the lean rats, which implies that insulin related p-AKT signalling may be associated with insulin resistance induced obesity (Carvalheira et al., 2003). Furthermore, Scherer et al firstly reported that knockdown of the insulin receptors in the hypothalamus led to uncontrolled lipolysis and decreased lipogenesis (Scherer et al., 2011). In 2017, the same group find out that this is POMC-dependent (Shin et al., 2017). Specifically, mice in which the insulin receptor knocked out in POMC neurons failed to inhibit lipolysis in the adipose tissue, while the ability of insulin to suppress lipolysis was unaffected in the mice that where insulin receptor was knocked down in AgRP neurons. That showed that the melanocortin pathway might be required for brain insulin regulating of adipose tissue lipolysis (Shin et al., 2017). Another study further confirmed this hypothesis in which i.c.v infusion melanocortin agonist in the third ventricle led to an increase in lipolysis (Brito et al., 2007). These data suggest that brain insulin signalling might suppress adipose lipolysis by inhibiting the firing activity of POMC neurons, which provides a new prospective on body fat weight management and anti-obesity.

In addition to suppressing lipolysis in the adipose tissue, brain insulin is also involved in

tuning the lipid metabolism in the liver. It has been reported that i.c.v infusion of insulin in the third ventricle significantly increased the release of hepatic TG from the liver (Scherer et al., 2016), and consequently the reduced hepatic TG accumulation could protect the liver from steatosis and non-alcoholic fatty liver disease (NAFLD) (Fabbrini et al., 2008). Notably, most of TG was circulated in the form of very-low-density lipoproteins (VLDL), which could be further hydrolysed to produce FFA and utilized by adipose tissue (Duwaerts and Maher, 2019). FFA, the products of lipolysis, are oxidized by β-oxidation to produce acetyl CoA and glycerol. Acetyl-CoA is the main source of the TCA cycle, which is a joint metabolic pathway of carbohydrate, fat, and protein. On the contrary, mice in which the insulin receptor was knocked out the CNS exhibited a reduction in hepatic TG export (Scherer et al., 2016). Altogether, these data suggest that brain insulin could serve as a regulator to promote triglyceride secretion and reduce lipid content in the liver.

1.5.5 Insulin action in human brain

Much work has focused on insulin sensing and insulin signaling in the rodent brain, however there is now accumulating evidence which shows that there is also insulin signaling in the human brain. For example, Sara et al detected specific binding site of insulin receptors in the post-mortem tissue (Sara et al., 1982), where the amount of insulin in the brain is directly related to the sensitivity of peripheral insulin as compared to insulin resistance patients; the insulin level in the brain is higher in normal subjects (Heni et al., 2014b). The process of insulin entering the brain from the blood may occur through a receptor-mediated transport process, which is affected by health conditions or diet habits (Woods et al., 2003). More specifically, the effect of insulin on regulation of cerebrocortical activity was attenuated in obesity induced insulin resistant subjects (Tschritter et al., 2006; Kern et al., 2006), which the brain circuit mainly relevant to the regions controlling appetite and reward (Anthony et al., 2006). Like peripheral insulin resistance, brain insulin resistance in humans not only causes metabolic disorders (Obici et al., 2002b), but causes cognitive impairment. We live in an increasingly aging (Tschritter et al., 2009) and obesogenic society, and therefore the incidence of insulin resistance in the human brain is also increasing (Heni et al., 2015). To deeply understand the mechanism of how brain insulin regulates metabolism is also helpful to tackle these challenges.

With the development of advanced technology, researchers nowadays have achieved great breakthrough on which brain regions might be involved in eating behaviour. Functional magnetic resonance imaging (fMRI) data indicated that a large bilateral network was reduced after a standardized caloric intake, among them the basal ganglia and paralimbic regions are more notable (Kroemer et al., 2013). Interestingly, an increased plasma insulin levels in response to a standardized caloric intake was associated with the decreased neuronal activity in limbic and paralimbic regions (Kroemer et al., 2013). In this study, however, the brain insulin levels data was missing, and the question of whether the brain insulin is responsible for the changed neuronal activity was left unevaluated. Fortunately, clearer evidence has been shown in recent studies about intranasal insulin applied in scientific and clinical research.

1.6 Intranasal insulin

1.6.1 The safety of intranasal insulin

In 1932, it was first reported that intranasal insulin could restore the blood sugar level to normal in diabetics in the same manner as hypodermic insulin (Collens and Goldzieher, 1932). Research studies examining the safety of intranasal insulin in the human body have not reported any significant safety issues (Schmid et al., 2018). A problem that commonly occurs with subcutaneous insulin administration is the tendency for insulin administered by this route to cause weight gain and hypoglycemia, whereas intranasal insulin has not been shown to cause these negative side effects (Dash et al., 2015). Furthermore, administration is also advantageous as it has been shown that insulin that was transported through the intranasal route only accumulated in the brain without entering the bloodstream (Salameh et al., 2015). The level of intranasal insulin in the circulatory system mainly depends on the dose of intranasal insulin used. When the dose is relatively low (40U), intranasal insulin does not enter the circulatory system, but with a higher dose (160U), a small amount of intranasal insulin can be detected in the circulatory system, but this was found to be not enough to cause changes in blood glucose level (Kullmann et al., 2018).

1.6.2 The distribution of intranasal insulin

Intranasal transport is an efficient route of delivery of drugs to the brain, this is likely due to the involvement of some extraneural pathways, such as entering the brain through gaps between the olfactory epithelium (Renner et al., 2012). When I^{125}-labelled insulin was delivered intranasally in mice, insulin spread to all brain regions 1 hour after administration (Salameh et al., 2015). The olfactory bulb exhibited the highest I^{125} concentration compared to other areas, such as the cerebellum, brainstem, and hippocampus (Brabazon et al., 2017). Following intranasal administration of Alexa Fluor 647 succinimidyl ester labelled insulin in mice, insulin was found to enter the mucosa of the olfactory epithelium, travel into the olfactory bulb nerve bundle, passing through the cribriform plate to reach the bulbs within just 30 mins (Renner et al., 2012). Nanogold-insulin has been shown to be endocytosed into the olfactory nerve layer and glomerular layer also within 30 minutes (Renner et al., 2012). Intranasal flourescently-tagged insulin (Alex546-Ins) reaches most areas of a rat brain, including the cerebellum, substantia nigra/ventral tegmental area, striatum, hippocampus, and thalamus/hypothalamus; the olfactory bulb and brainstem showed the most abundant staining within 30 minutes of delivery (Fan et al., 2019). These data indicate that intranasal delivery provides an efficient pathway for drugs to reach the CNS. However, due to the different types of labelled insulin, different injection doses and methods of detection, the accumulation of insulin receptor in the brain are also different.

Table 1. 1 Studies using intranasal insulin in rodents.

Species	Insulin	Method of detection	Dose of injection	Most intense signals	Time	Pathway	References
Rats	Alex546-insulin	IHC	10 µg in 10 µl PBS	Cerebellum, OB	15-60 mins	PI3K- Akt	(Fan et al., 2019)
Mice	Alexa Fluor 647 succinimidyl ester	Microscope	60 µg in 12 µl PBS	Olfactory nerve layer, glomerular layer of the OB.	30 mins	olfactory nerve pathway	(Renner et al., 2012)
Mice	non-labelled insulin	PET	3 U/30 µl in saline	Hippocampus	---	Activates Akt2 signaling	(Gabbouj et al., 2019)
Rats	I^{125}- insulin	gamma counter	1 uCi/5 µl in saline	Cerebellum, OB	---	---	(Brabazon et al., 2017)
Mice	I^{125}- insulin	gamma counter	1 µl of 400,000 cpm/µl	cribriform plate via the nasal route	---	Controlled by PCK inhibitors	(Salameh et al., 2015)

1.6.3 How insulin enters the central nervous system

1.6.3.1 How peripheral insulin enters the brain

Brain insulin plays a crucial role in the regulation of metabolism, mood and body weight, but where the brain insulin originates is still unclear. A report indicated that when labelled human insulin was subcutaneously injected into mice, the level of human insulin in the brain was increased with the increasing dose of human insulin, while the level of hepatic insulin in the mice was inhibited (Banks et al., 1997). This is because the increased human insulin in the peripheral tissue resulted in a decrease in the blood glucose which inhibited the secretion of insulin from the pancreas. Since the mouse cannot make human insulin, the sole source of increased mice brain insulin was from the infusion of human insulin (Banks et al., 1997), these results indicated that peripheral insulin is able to enter the brain. Another study conducted on normal male subjects first reported that the insulin concentration in cerebrospinal fluid (CSF) was increased by infusion of insulin when compared to the infusion of saline in the peripheral blood, which suggested that peripheral insulin could affect the level of brain insulin (Wallum et al., 1987).

Such results raise an important question: how does peripheral insulin pass through the blood-brain barrier (BBB), a highly tightly wrought structure that protects the brain from potential infections? Compared with other brain regions, the pons-medulla and the hypothalamus showed the highest insulin level after intravenous injection of I^{125} labelled insulin (Banks and Kastin, 1998). This is likely due to the fact that different brain areas possess different BBB permeability (Wong et al., 2013) or selective permeability of the BBB to different substances (Banks and Kastin, 1998). The CSF is extracellular fluid of the CNS, which could provide nutrients to the brain or remove products from the brain metabolism (Skipor and Thiery, 2008). It has been reported that the CSF is formed in the third and fourth ventricles by the choroid plexus. The capillaries of the choroid plexus are fenestrated and leaky (Czosnyka et al., 2004), which provides a possibility for substances such as insulin to reach the CNS. Notably, the insulin level in the brain could also be affected by diet. A high fat diet could induce higher fasting CSF insulin compared to normal rats, while the transport of insulin to the brain was inhibited in high fat diet groups by the input of peripheral insulin (Begg et al., 2013).

The study by Bank and colleagues showed that the amount of human insulin in the brain is not linear with the doses of subcutaneously infused labelled insulin (Banks et al., 1997). Specifically, with an increasingly low dose of insulin, the amount of insulin in the mouse brain shows a linear increase, however when the infused insulin amount exceeded a certain level, the level of labelled insulin in the mouse brain was unchanged. These data indicated that the insulin can be transported to the CNS, maybe in a saturable way (Banks et al., 1997). Furthermore, Baura et al investigated the kinetics of blood insulin entry into the CSF, and the data indicated that the amount of insulin in the CSF is not changed with the level of plasma insulin, which implies that the process of plasma insulin entering the brain is a saturation transport (Baura et al., 1993), and is possibly regulated by transporters in the BBB sites (Zlokovic, 2008). Born et al reported that intranasal insulin could reach the CNS through the CSF without circulating in the peripheral system (Born et al., 2002), which provides a possibility to the researcher to study the effect of intranasal insulin on the CNS and periphery system separately.

In addition, insulin receptor mediated transport has also been studied. Compared with the fourth ventricle and the third ventricle, the choroid plexus has the highest intensity of I^{125} binding sites, suggesting that the choroid plexus contains a relative higher insulin receptor density and sites, which is likely the route of insulin into the brain (Baskin et al., 1986). Receptor-mediated insulin endocytosis has been investigated (King and Johnson, 1985). Firstly, blood insulin binds to the insulin receptor in the endothelial cells of the brain, where it then undergoes endocytosis to form vesicles which are then transported into the brain (King and Johnson, 1985); the process is mediated by two proteins, clathrin and caveolin. Finally, insulin in the vesicles is then released via exocytosis. Specific insulin receptor knockdown in the endothelial cells caused a delayed systemic response to insulin (Konishi et al., 2017), which suggested that insulin receptor in the endothelial cells plays an important role in the regulation of insulin action. However, this mechanism has been challenged recently.

An experiment using *in vitro* BBB cell models showed that insulin receptor expressed in the brain endothelial cells are involved in insulin-binding to the brain endothelial cells but do not mediate insulin's transport across the BBB (Hersom et al., 2018). These findings were also confirmed by *in vivo* experiments by Rhea et al (Rhea et al., 2018). It

was reported that I[125]-labelled insulin transported from the BBB to the brain was not significantly affected in the endothelial insulin receptor knockout mice model (Rhea et al., 2018). Furthermore, insulin transport was still maintained when insulin receptor was inhibited by insulin receptor antagonist S961 (Rhea et al., 2018). These data potently suggested that insulin receptor in the endothelial cells is not essential for mediating insulin cross the BBB. However, the ability of insulin to bind to endothelial cells was significantly inhibited in both conditions (Rhea et al., 2018), which further implied that insulin receptor might be crucial for insulin binding but not insulin transport. Notably, a recent report indicated that insulin receptor in the tanycytes rather than the endothelial cells is required for peripheral insulin transported into the hypothalamic arcuate nucleus (ARC) and this process is involved in regulating glucose metabolism and feeding behaviour in a rodent model (Porniece Kumar et al., 2021). Together, these data imply that insulin receptor in the brain endothelial cells is not required in the process of insulin overcoming the BBB (Rhea et al., 2018) as previously thought (See Figure 1.5 Peripheral insulin passes the BBB and reaches the brain).
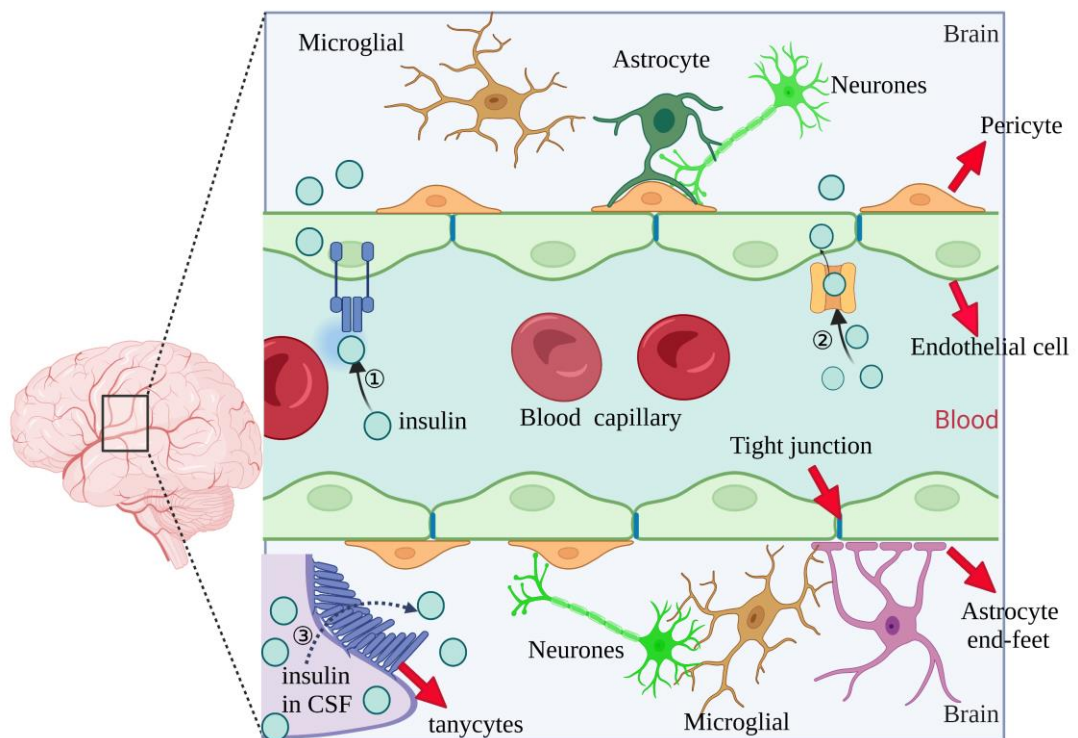
Figure 1. 5 Peripheral insulin passes the BBB and reaches the brain. The blood–brain barrier (BBB) consists of the brain endothelial cells, tight junction, pericytes, and astrocyte end-feet, which together form a continuous and tight brain

structure. ① insulin receptor in the endothelia mediates insulin endocytosis cross the BBB. ② Insulin enters the brain through transporter mediated pathway. ③ Tanycytes in the third ventricle gate that insulin in the CSF reaches the brain.

1.6.3.2 How intranasal insulin enters the brain

Intranasal delivery drugs have been developed for the treatment of CNS-related diseases (Calva and Fadel, 2020; Hanson and Frey, 2008). Studies examining how these drugs are delivered from the nasal cavity to the CNS focus on the path involving the olfactory, trigeminal nerves, vasculature, CSF and lymphatic system (Dhuria et al., 2010). For example, horseradish peroxidase (HRP, molecular weight, 40KD) was able to reach the olfactory bulb through olfactory nerve axons within 45 to 90 mins both in rodents and squirrel monkeys (Balin et al., 1986). On the one hand, the dendrites of olfactory receptor neurones localise into the olfactory epithelium which detects the odours or substances. On the other hand, the axons of olfactory receptor neurons pass through cribriform plate, CSF and localise in the mitral cell layer of olfactory bulb where neuronal projection extends to various brain areas. After administrating intranasal insulin, the results indicated that insulin could enter from the mucosa of the olfactory bulb into the olfactory epithelium, then the olfactory bulb nerve bundle, passing through the cribriform plate to reach the bulbs. Insulin was then endocytosed into the olfactory nerve layer and glomerular layer of olfactory bulb (Renner et al., 2012).

Intranasal administration could also reach the brain through the trigeminal nerve pathway. It was reported that compared to intravenous administration, intranasal I^{125}-labelled vascular endothelial growth factor (VEGF) represented higher concentration in the brain, with the trigeminal nerve showing the highest concentration followed by olfactory bulb, striatum and midbrain, which implies that intranasal administration might enter the brain through trigeminal nerve pathway (Yang et al., 2009; Thorne et al., 2004). Experiments conducted by Lochhead et al also confirmed that intranasal fluorescently labelled insulin was localised in the brain along perineural spaces of the trigeminal nerve (Lochhead et al., 2019).

Notably, an intranasal injection could also reach the brain through vascular pathways as

the nasal mucosa is surrounded by vessels. Clear evidence has shown that intranasal administration of drugs including insulin were detected in the blood vessels (Lochhead et al., 2019; Thorne et al., 2004). The three main routes of intranasal delivery to the CNS are shown in Figure 1.6.
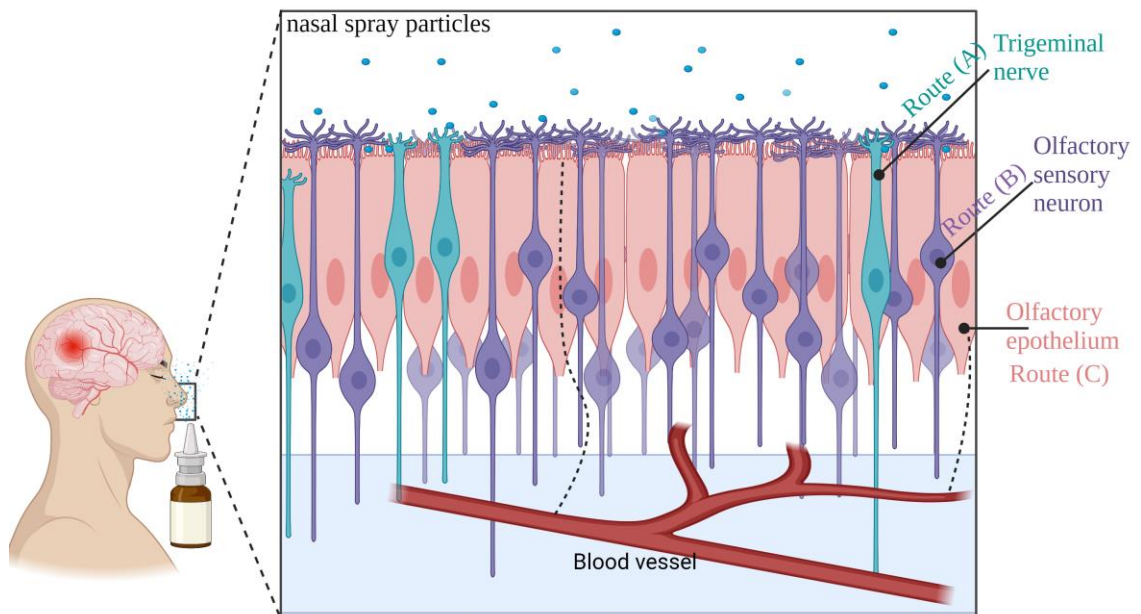
Figure 1. 6 Drug intranasal delivery routes from nasal passage to the brain. The intranasal delivery routes to the CNS are as follows: Route A: the trigeminal nerve resides in the olfactory epithelium and transports chemosensory information into the CNS. Route B: the axons of the olfactory receptor neurons reach into mitral cells in the olfactory bulb (OB). From there, projections arrive to various areas of brains. Route C: Drugs are absorbed into the blood vessels.

1.6.3.3 Is insulin produced in the brain?

The investigations about whether insulin is synthesized locally in the brain are still unverified due to the fact that the peripheral insulin can reach the brain through the BBB. Proinsulin II mRNA was detected in the mouse brain of the pancreas embryo (Deltour et al., 1993). Devaskar et al reported that insulin II genes were found in fetal and neonatal rat brains in the prepancreatic development stage (Devaskar et al., 1993), and insulin mRNA was also detected in neuroglia form cells in the cerebral cortex (Molnar et al., 2014), which might imply that insulin could locally be released in the brain. However, further studies are needed to prove that insulin can be produced locally.

1.6.4 The function of intranasal insulin

1.6.4.1 Intranasal insulin improves metabolism

Intranasal insulin has also been found to have profound effects on homeostatic energy regulation. For example, it was reported that acute intranasal insulin could increase postprandial metabolic energy expenditure (Benedict et al., 2011a), improve peripheral insulin sensitivity (Heni et al., 2014c) and markedly reduce food intake (Benedict et al., 2008) as well as the craving for sweets in healthy men (Kullmann et al., 2015b).

Plasma glucose - The effect of intranasal insulin on lowering postprandial hyperglycaemia is dose-dependent (Leary et al., 2005), where higher concentrations of intranasal insulin, results in lower plasma glucose levels in healthy subjects (Leary et al., 2005). The same research group conducted another study in seven patients with type 1 diabetes, and the results suggested that compared with subcutaneous insulin, the relative bioavailability of intranasal insulin was 16.6-19.8% over two hours and 14.0-19.8% over five hours (Leary et al., 2006). It was also shown that the effect of intranasal insulin on decreasing plasma glucose reaches the peak at 40 mins and waned after 1.5 hours post-administration (Leary et al., 2006). Intranasal insulin performed similarly to normal subcutaneous insulin in reducing postprandial hyperglycaemia, and both intranasal and subcutaneous insulin maintain their function at four hours, however intranasal insulin leads to fewer hypoglycaemic symptoms after administration compared to conventional subcutaneous insulin when given in a fasting state (Frauman

et al., 1987). These data therefore indicated that intranasal insulin is successful at controlling glucose level in humans.

Hepatic glucose - In addition, following intranasal insulin administration for four weeks eight healthy men showed lower hepatic glucose concentrations, although their venous insulin concentrations were similar compared to intranasal placebo subjects, suggesting that intranasal insulin is able to reduce HGP (Dash et al., 2015). This also indicates that intranasal insulin regulates hepatic glucose metabolism without altering the concentration of insulin in the peripheral blood, which is consistent with reports by Gancheva et al (Gancheva et al., 2015). Heni et al further reported that intranasal insulin can enhance the sensitivity of peripheral insulin (Heni et al., 2012), and this change was related to hypothalamic signalling (Heni et al., 2012; Heni et al., 2014c) and parasympathetic output (Heni et al., 2014c). Altogether, these data might indicate that intranasal insulin could be a new strategy for the treatment of excess glucose production in the diabetic patients.

Food intake and body weight - By increasing the cerebral blood flow in the insular cortex of healthy men (Schilling et al., 2014) or regulating the neuronal activity in the midbrain (Edwin Thanarajah et al., 2019), intranasal insulin may regulate eating behaviour. Research has shown that when healthy subjects were given insulin or a placebo, their brains were able to detect food pictures faster than non-food pictures (Guthoff et al., 2010). However, when intranasal insulin was administered, the cerebral activity of related objected-processing areas such as fusiform gyrus, the right hippocampus, the right temporal superior cortex and the right frontal middle cortex (images processing regions) were significantly reduced compared to intranasal placebo treatment during the process of watching videos showing food pictures (Guthoff et al., 2010). These results imply that intranasal insulin could alter the activity of the processing of food images in the human brain which may ultimately affect food intake (Guthoff et al., 2010). Furthermore, intranasal insulin can increase the human body's postprandial energy consumption, reduce the level of insulin in the postprandial circulation and FFA in the postprandial serum (Benedict et al., 2011a), which suggested that intranasal insulin might regulate caloric intake by adjusting energy homeostasis between thermogenesis and energy expenditure.

Fifteen obese men were treated with intranasal insulin for eight weeks, and the results indicate that insulin did not significantly improve body weight compared to men of normal weight, but they did improve mood and memory (Hallschmid et al., 2008), which is consistent with another report (Benedict et al., 2008). Interestingly, the role of intranasal insulin shows a gender-biased character, it can reduce the body fat of healthy men, but has no effect on women (Hallschmid et al., 2004; Benedict et al., 2008).

Palatable food - Intranasal insulin after a meal can reduce the intake of high-calorie sweets in healthy women, which could be employed as a new regime to control excessive eating (Hallschmid et al., 2012). In contrast, a recent study noted that intranasal insulin did not reduce palatable cookie intake in healthy lean women but was effective in obese women in the postprandial state (Schneider et al., 2022). This report is contrary to the results from Hallschmid et al (Hallschmid et al., 2012) in which participants were provided with a wide range and choice of palatable cookies instead of one (Schneider et al., 2022). Therefore, whether intranasal insulin is able to decrease palatable food intake in lean women may be dependent on the options of palatable food provided (Schneider et al., 2022). However, there are also studies which indicate that intranasal insulin does not change the preference of food choice and biscuit intake in healthy young men (Rodriguez-Raecke et al., 2020), but only women (Hallschmid et al., 2012; Schneider et al., 2022). These data further support the finding that insulin signaling in the CNS has a gender difference and the effect of intranasal insulin on palatable food choice and food intake in different genders have not been thoroughly defined.

Inflammation - It has been reported that inflammation in the CNS was linked to the development of type 2 diabetes, insulin resistance and Alzheimer's disease (AD) (Tsalamandris et al., 2019; De Luca and Olefsky, 2008; Kinney et al., 2018). Intranasal insulin can effectively improve the metabolic disorders of rats, the insulin sensitivity of the liver, restore normal metabolic indexes (Derkach et al., 2017), and improve markers of inflammatory factors (TNF- α and IL-6) (Spielman et al., 2015; Beirami et al., 2017). In addition, intranasal insulin could modulate mitochondrial biogenesis and fission (Iravanpour et al., 2021), while mitochondrial dysfunction is related to endoplasmic reticulum stress (ER stress), inflammation and obesity (Filippi et al., 2017; Kim et al., 2008; Sivitz and Yorek, 2010; Chen et al., 2019). This findings provide a perspective

that intranasal insulin might be a potential treatment for mitochondrial-related diseases.

1.6.4.2 Intranasal insulin improves the cognition

It has been reported that patients with diabetes or insulin resistance have a higher possibility of developing dementia, aging and other cognitive diseases (Mogi and Horiuchi, 2011; Xu et al., 2004; Moran et al., 2013; Pang et al., 2016). Both animal experiments and human studies have proved that intranasal insulin can repair damaged cognitive function (Chapman et al., 2018). Research has also shown that intranasal insulin can improve hypometabolism in rats following i.c.v injection of streptozotocin to induce Alzheimer's, and was able to effectively alleviate neuron loss as well as reduce the number of astrocytes (Chen et al., 2018; Beirami et al., 2017). Intranasal insulin restores brain insulin signalling and strengthens synaptic proteins, reducing the size of amyloid plaques in an AD mouse model (Chen et al., 2014). Acute intranasal insulin can significantly improve the cognitive performance in patients with type 2 diabetes. fMRI results showed that this is probably related to vasodilatation in the insular cortex (Novak et al., 2014), or the functional connection between hippocampal and medial frontal cortex (Brabazon et al., 2017). This may occur due to the neurotrophic factor properties that insulin exhibits, whereby it is able to influence the development and plasticity of neurons (Chiu et al., 2008).

It has been reported that intranasal insulin treatment was able to improve memory (by evaluation of recalling word lists) in addition to enhancing mood in healthy subjects (Benedict et al., 2004). Notably, higher intranasal insulin doses were related to significant improvement in memory in Alzheimer's patients, which is likely related to the regulation of apolipoprotein E (APOE, the major genetic risk factor for AD) status (Claxton et al., 2015b) and genotype (Reger et al., 2008). Recent studies also indicated that chronic application of intranasal insulin can profoundly lead to a reduction in white matter hyperintensity volume (increased risk for AD) in deep and frontal regions (Kellar et al., 2021) or improve gait (an indicator of cognitive ability) (Novak et al., 2022; Studenski et al., 2011). Interestingly, it was also reported that the memory of recent food intake could reduce food intake later in women (Higgs, 2002), further suggesting that cognition is relevant to food intake. This perspective may aid us in understanding eating disorders and pave a new strategy to treat diet-induced obesity.

An early report demonstrated that brain insulin decreased with aging (Frolich et al., 1998; Sartorius et al., 2015; Maimaiti et al., 2016), while on the other hand, there has been evidence that intranasal insulin could improve aging brain function as shown by Akintola et al (Akintola et al., 2017). In their study, intranasal insulin was applied to 19 participants, and when compared to a placebo group, intranasal insulin significantly increased perfusion through the occipital grey matter and the thalamus, which suggested that intranasal insulin could improve brain energy demand and neuronal status in older adults (Akintola et al., 2017).

Emotion is also an important factor in reference to eating-related behaviour and body weight. Acute intranasal delivery of human insulin (40 I.U.) has been shown to reduce social stress in healthy men (Bohringer et al., 2008), which may be relevant to the effect of intranasal insulin on the hypothalamic-pituitary-adrenal (HPA, as known as an axis for the neuroendocrine) axis activity (Smith and Vale, 2006; Zou et al., 2020). In addition, it has been reported that intranasal insulin could improve mood in obese women (Schneider et al., 2022), while the study from Cha et al suggested that intranasal insulin did not show significant improvements on overall mood (Cha et al., 2017). One explanation about these disagreements is the evaluation of mood does not have an absolutely objective standard.

1.6.5 Limitations of intranasal insulin

Although patients benefit greatly from intranasal insulin, it is still not a completely realistic alternative to avoid conventional subcutaneous insulin treatment. One of the reasons for this is that the bioavailability of intranasal insulin administration is lower than subcutaneous insulin due to the clearance of the mucosa, which implies that the dose of intranasal insulin must be several times higher than that of a subcutaneous injection (Frauman et al., 1987; Hilsted et al., 1995). Fortunately, methods of improving the bioavailability of intranasal insulin have been recently tested, such as adsorption enhancers or chemical modification, and these methods make intranasal insulin more likely to be used (Duan and Mao, 2010). Another issue which needs to be mentioned is that the effectiveness of intranasal insulin sometimes varies from person to person (Lalej-Bennis et al., 2001). For example, in one study, it was shown that only three out

of ten type 2 diabetes patients with intranasal insulin alone could achieve acceptable glycaemic control (Lalej-Bennis et al., 2001). One explanation is that compared to seven other subjects, these three subjects have a lower body mass index (BMI) (23.7±4.0 vs. 27.0±1.3), which may imply less marked insulin resistance. However, the reasons for this, and how we may overcome such problems, needs to be fully explored if we are to ever consider intranasal insulin treatment as a viable alternative to subcutaneous insulin injection.

1.7 Aims and objectives

Diabetes has become a severe public health issue around the world. According to the latest report from International Diabetes Federation (IDF), there are around 537 million adults suffering from diabetes, and this data will increase to 643 million in 2030. Diabetes causes many diabetic complications, such as kidney failure, heart stroke, amputation and central nervous disease (Emerging Risk Factors et al., 2010; Blindness et al., 2021; Mccrimmon et al., 2012; Manschot et al., 2007). In 2021, there were around 6.7 million deaths caused by diabetes and the expenditure on diabetes was 3.2 times higher compared to the last 15 years (https://diabetesatlas.org/). Healthy food and diet habit, regular exercise, maintaining a reasonable BMI and blood glucose level could profoundly improve patients' condition. Studying how body weight and food intake are regulated is crucial to understand and prevent diabetes and obesity in the future.

Insulin as one of the anorectic hormones, plays an important role in regulating metabolic balance in the body. Furthermore, insulin and insulin analogues provide more options for patients to achieve better diabetes management. Recent research has shown that brain insulin signaling is also involved in food intake regulation (Gerozissis, 2004), body weight (Bruning et al., 2000), glucose homeostasis (Pocai et al., 2005b) and body fat metabolism (Kullmann et al., 2020b). Notably, on the one hand, intranasal injection of insulin demonstrated high accumulations in the brain (Nedelcovych et al., 2018). On the other hand, intranasal insulin could markedly suppress food intake and decrease appetite in humans, which suggested that intranasal insulin could serve as a satiety signal in the brain to regulate eating (Hallschmid et al., 2012). Beside, data also indicated that intranasal insulin could reduce blood glucose levels without leading to hypoglycaemia (Salzman et al., 1985). These data demonstrate that intranasal insulin is

involved in the regulation of food intake and metabolism. To understand how intranasal insulin behaves is vital in unveiling the mechanism of brain insulin signal-related metabolic diseases, such as obesity and diabetes.

The study of intranasal insulin has yielded encouraging results, however there is still much more to be done. For example, the function and mechanisms of intranasal insulin in regulating food intake are still elusive. Even though studies using labelled insulin highlighted several insulin sensitive regions (Renner et al., 2012), a more detailed map of how intranasal insulin enters the brain and where it reaches is still missing. Furthermore, how these insulin sensitive brain regions regulate feeding behaviour and what types of neuronal populations are involved in this process are still not fully understood. Importantly, a study have shown that intranasal insulin has gender differences in energy homeostasis and cognitive performance (Benedict et al., 2008). However, more evidence is needed to explain this difference.

With these considerations in mind, in this project we aim to (Figure 1.7):

(1) Explore the effect of intranasal insulin on metabolic function *in vivo*.

(2) Identify the brain regions in which intranasal insulin accumulates and identify the cell types in these regions with insulin receptor.

(3) Determine which of the brain regions identified in Aim 2 contribute to the metabolic effects observed in Aim 1 by knocking down of the insulin receptor within these regions using an adenoviral delivery system.

(4) Build a map of neuronal circuits in the brain by studying how areas identified in Aim 2 are communicating with other regions or neuronal populations to influence food intake.
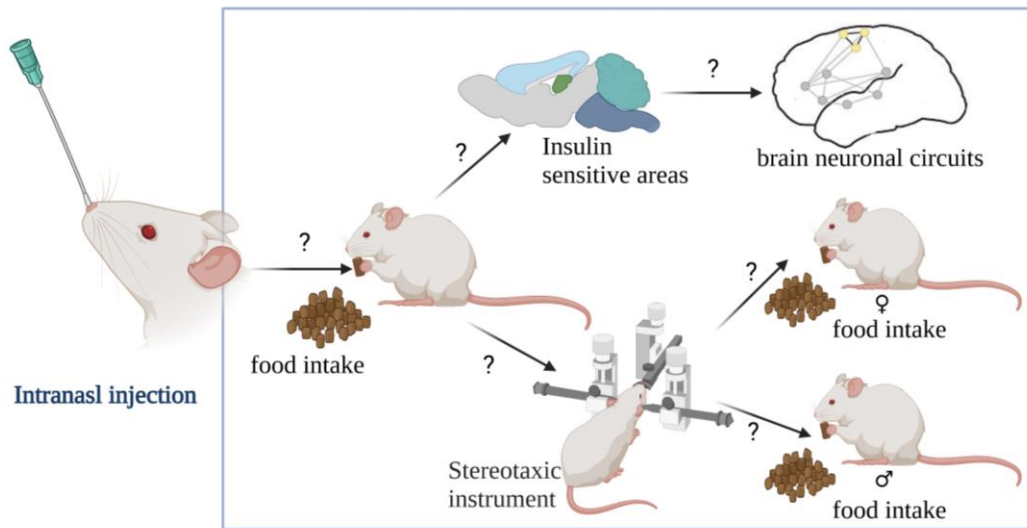
Figure 1. 7 Aims of current research project. Does intranasal insulin influence food intake in rodents? Which brain regions sense intranasal insulin and what are the potential neuronal circuits involved in feeding behaviour? Does it show gender differences in regulating food intake?

2 Methods

2.1 Materials and Chemicals

0.4 M Phosphate buffer solution (PB) (g/Liter)

Sodium phosphate dibasic (cBCCB3160): Molecular weight 141.96 (46 g)

Sodium dihydrogen phosphate (EMD Millipore # 13472-35-0): Molecular weight 156.0 (12 g)

Paraformaldehyde (PFA)

To make 8% PFA: Paraformaldehyde powder in dH_2O, stir and heat up until dissolved.

To make 4% PFA: 50% 8% PFA, 25% 0.4 M PB, 25% dH_2O

Lysis Buffer

50 mM Tris-HCl pH 7.5 (Fisher BioReagents # 183003),1 mM Ethylene glycol tetraacetic acid (EGTA) (fluorochem # FCB028343), 1 mM Ethylenediaminetetraacetic acid (EDTA) (Sigma # 101747256), 1% NP-40 (BIO BASIC CANADA INC # NDB0385), 1 mM Sodium orthovanadate (Sigma # SLBM2890V), 50 mM NaF (Sigma # 1002975197), 5 mM sodium pyrophosphate (Sigma #101720396), 0.27 M sucrose (Sigma # 102435094)

4x Sample buffer

4x Laemmli Sample buffer (BIO RAD # 1610747) with β-mercaptoethanol (Agilent Technology # 2003445-21)

SDS page gel

Resolving gels and stacking gels were made depending on the molecular weight of proteins of interest, an example of a 10%, 1.5 mm gel is given below:

The resolving gel was to separate proteins:

H_2O: 3.55 ml

Acrylamide/bis (30%, 29:1) (Bio-Rad # 1610156): 3 ml

Tris-HCl (1.5 M, pH 8.8): 2.25 ml

10% Sodium dodecyl sulfate (SDS): 90 µl

10% Ammonium persulfate (APS) (Sigma # 7727-54-0): 90 µl

Tetramethylethylenediamine (TEMED) (Bio-Rad): 22 µl

When the resolving gels were polymerized, stacking gel was made as below:

H_2O: 2.25 ml

Acrylamide/bis (30%, 37.5:1): 0.5 ml

Tris-HCl (0.5 M, pH 6.8): 188 µl

10% SDS: 30 µl

10% APS: 15 µl

TEMED: 2.5 µl

Running Buffer (1x)

25 mM Tris Base (Fisher BioReagents # 183003), 192 mM Glycine (Sigma # SLCF5576), 0.1% SDS (Sigma # 05030)

Transfer Buffer (1x)

48 mM Tris Base (Fisher BioReagents # 183003), 39 mM Glycine (Sigma # SLCF5576), 20% methanol (Honeywell # 179337)

Tris-buffered saline (TBS) (10x)

200 mM Tris base, 1.5 M NaCl, adjust the pH to 7.5 with HCl

TBST

Tris-buffered saline with 0.1% Tween® 20 (PanReac AppliChem # A3839) detergent

Blot membrane Stripping buffer

Nitrocellulose stripping buffer (Alfa Aesar # S18E575)

FITC-insulin

FITC-insulin (Sigma # I3661) dissolved in 1x Phosphate buffered saline (PBS) (OXOID # BR0014G), the stock concentration is 896.5 μM. Store in -20 °C and sonic sound for 10 mins was performed prior to use to avoid agglomeration.

FITC-dye

FITC-dye (ThermoFisher Scientific # F1906) was dissolved in 1x PSB, aliquot and store in -20 °C until use.

Standard Human Insulin

10 mg standard human insulin (Sigma # I5523) dissolved in 10 ml of 0.01 M HCl, 0.1 g bovine serum albumin (BSA) and 90 ml dH$_2$O, then filter with 0.2 μm syringe filter.

Vehicle

10 ml of 0.01 M HCl, 0.1g BSA (Sigma # SLCH3828), 90 ml ddH$_2$O

Ketamine (Zoetis Ketavet® 100 mg/ml Ketamine hydrochloride 10 ml) and Medetomidine (1 mg/kg) (Domitor 1 mg/ml Medetomidine Hydrochloride 10 ml):

0.5 ml Ketamine and 0.5 ml Medetomidine in 4 ml saline, deliver 0.1 ml per 10 g mouse weight.

Antisedan (Zoetis Ketavet® 5 mg/kg atipamezole hydrochloride 10 ml):

0.5 ml Antisedan in 4.5 ml saline, deliver 0.1 ml per 10 g mouse weight.

Meloxicam (5 mg/kg) (Boehriger Ingelheim):

0.25 ml Meloxicam in 2.75 ml saline, deliver 0.3 ml per mouse.

N-methyl-D-glucamine (NMDG) (g/Liter)

18.16 g NMDG (Alfa Aesar # 5003P01W), 0.19 g KCl (Sigma # SZBF2720V), 0.17 g NaH$_2$PO$_4$ (Sigma # BCBV1183), 2.52 g NaHCO$_3$ (Sigma # SLCG3879), 4.51 g Glucose (Fisher BioReagents # 1692814), 4.77 g HEPES (Fisher BioReagents # 189482), 0.99 g Sodium ascorbate (VWR Chemicals # 13L110002), 0.15 g Thiourea (Alfa Aesar # 10186501), 0.33 g Sodium pyruvate (Alfa Aesar # Y11B013), 5 mL MgSO$_4$ • 7H$_2$O (2 M stock) (Alfa Aesar # 10220400), 250 µl CaCl$_2$ • 2H$_2$O (2 M stock) (VWR Chemicals # 13G100033), 16 ml HCl (5 M stock) (Fisher BioReagents # 1911302)

Artificial cerebrospinal fluid (aCSF) (g/Liter)

7.3 g NaCl (Sigma # 102368807), 0.289 g KCl (Sigma # SZBF2720V), 2.1 g NaHCO$_3$ (Sigma # SLCG3879), 0.172 g NaH$_2$PO$_4$ (Sigma # BCBV1183), 0.991 g Glucose (Fisher BioReagents # 1692814), 1 ml CaCl$_2$ • 2H$_2$O (2 M stock) (VWR Chemicals # 13G100033), 1 ml MgCl$_2$ • 6H$_2$O (1 M stock) (VWR Chemicals # 14H180004)

Cryoprotectant recipe

Add 10 g Polyvinylpyrrolidone-40 (Sigma, # WXBC3748V) to 500 ml 0.1 M phosphate buffer and stir until dissolved, then slowly add 300 g Sucrose (Thermo scientific # 57-50-1) and stir until dissolved. Finally add 300 ml Ethylene glycol (Sigma, # 203-473-3). The total volume is up to 1000 ml.

10% Sucrose/TENs 50mM Tris-Hcl pH 7.4, 100 mM Nacl, 0.5 mM EDTA

1 M tris-HCl pH 7.4 (Fisher bioreagents # BP 152-1): 20 ml

2.32 g NaCl

0.058 g EDTA (Sigma # BCBR6568V)

40 g Sucrose

300 ml dH20 stir until dissolved then make up to 400 ml final volume. Autoclave, store at 4 °C in 50 ml aliquots.

2.2 Cell Culture
2.2.1 F-12K medium preparation

Pheochromocytoma (PC12) cells (AddexBio # C0032002) were cultured in F-12K medium (Gibco # 21127-022) with 15% horse serum (Gibco # 1011-07), 2.5% fetal bovine serum (Gibco # 2024-01), and 1% Penicillin Streptavidin (Sigma # P0781) under 37 °C, 5% CO_2 condition. F-12K complete medium was filtered by 0.2 μm Filteropur system (SARSTEDT # 22100425). PC12 cells are derived from a pheochromocytoma of the rat adrenal medulla and exhibit characteristics of sympathetic neurons. When treated with nerve growth factor (NGF), PC12 cells differentiate into neuron-like cells, extending neurites and forming synaptic connections. This differentiation process allows researchers to study various aspects of neuronal development and function (Greene and Tischler, 1976). Cells were detached using 0.05% trypsin-EDTA (Gibco # 25300-054) and frozen in 10% dimethyl sulfoxide (DMSO) (G Bioscience # BKC-17) in complete media.

2.2.2 PC12 treatment with fluorescent FITC-insulin

PC12 cells were seeded 1:2 onto a multi-test ultraviolet treated 8-well slide (MP Biomedicals # 20190128) in a 10 cm dish. 80% confluent cells were starved with serum-free F-12K medium overnight, and then incubated with 15 μl of 800 nM FITC-insulin for different time points. After incubating, cells were fixed directly with 4% PFA, then washed with 1x PBS for three times. Excess liquid was then aspirated, and the slide left to dry. Cover slips were added and sealed with Vectamount mounting medium (Vector Laboratories, Burlingame CA, USA). Slides were examined and imaged with an upright confocal microscope (Zeiss LSM880).

2.2.3 Design and synthesis of insulin receptor knockdown plasmid

To inhibit the insulin receptor in the brain area we are interested in, vector pAAV[FLEXon]-CMV>LL:rev(tdTomato:rInsr[miR30-hRNA#3]):rev(LL):WPRE and pAAV[FLEXon]-CMV>LL:rev(tdTomato:Scramble[miR30-shRNA#1]):rev(LL):WPRE control scramble vector were designed and purchased from Vector Builder. ShRNA (short hairpin RNA) was designed to silence target mRNA of insulin receptor, named as ShIR, and cloned into the adenoviral shuttle vector to make pacAd5CMV-ShIR-tdTomato and pacAd5CMV-ShC-tdTomato, the scramble RNA had the same nucleotide composition as the ShIR but not matching with any target mRNA of IR, which was used as control vector, named as ShC. In addition, pacAd5CMV-CRECFP vector was designed and ordered in this project to introduce Cre recombinase. The mechanism to genetically switch ShRNA on is described in Figure 2.1.
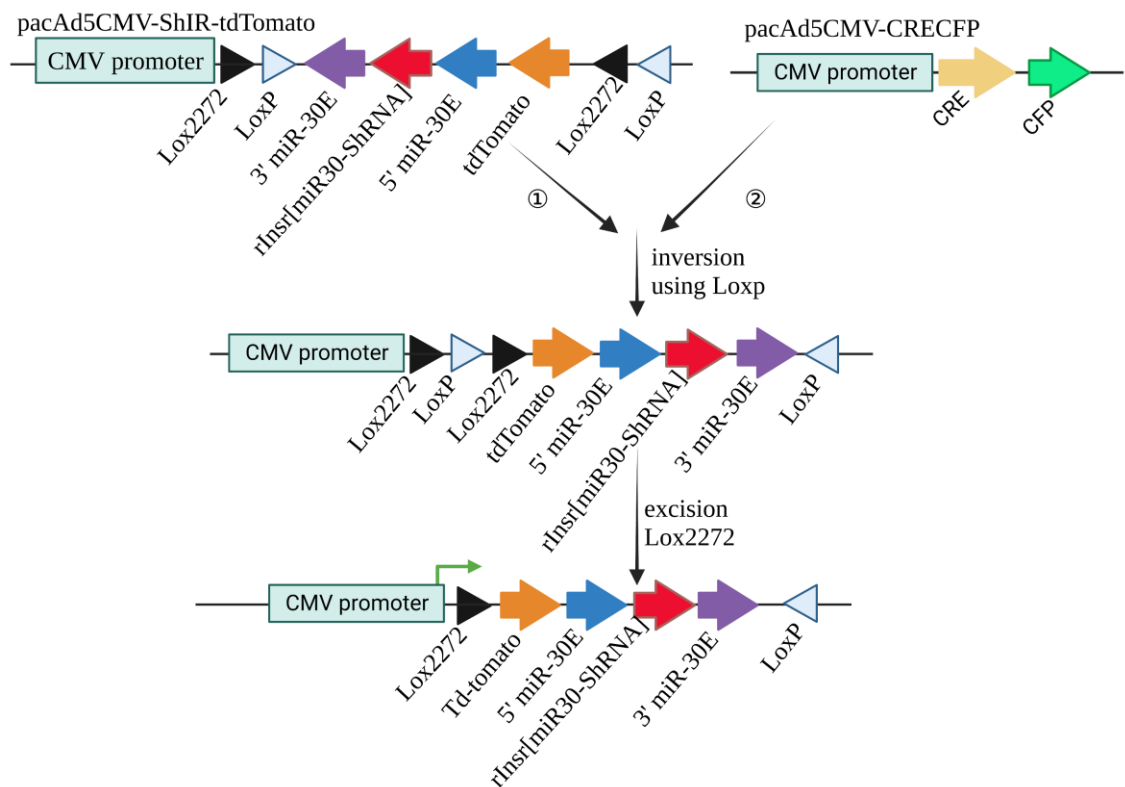
Figure 2. 1 The mechanism of genetically switch ShRNA expression on. The sequence of ShRNA (ShIR is shown here as an example) was flanked by two pairs of target sites. One is Loxp, the other is lox2272. Both loxP and lox2272 could be recognized by Cre but lox2272 sites can only recombine with other lox2272 sites, not

with loxP sites. The first recombination step will invert the ShRNA sequence using loxP site. The second recombination event then excises the loxp between the identical lox2272 sites. Since only one loxP and lox2272 site will remain on either side of the DNA fragment, any additional recombination events are impossible even in the presence of Cre recombinase.

2.2.4 Co-transfection in PC12 cells

A confluent 75 mm flask of PC12 cells was diluted 1:3 and plated in a 10 cm dish containing a multi-test 8-well slide (MP Biomedicals # 20190128). 24 hours later cells were transfected with 5 µg pacAd5CMV-CRECFP and 5 µg pacAd5CMV-ShIR-tdTomato or 5 µg pacAd5CMV-ShC-tdTomato control by using GenJet reagent (SL00489-PC12). In brief, two solutions were prepared, a solution A containing 500 µl serum-free Eagle's minimal essential medium (DMEM) (high glucose) only. And a solution B containing 500 µl serum-free DMEM (high glucose) with 5 µg pacAd5CMV-CRECFP and 5 µg pacAd5CMV-ShIR-tdTomato plasmid or 5 µg pacAd5CMV-CRECFP and 5 µg pacAd5CMV-ShC-tdTomato control plasmid. Solution A was then transferred into solution B, mixed and left at room temperature (RT) for 15 mins to form the GenJet-DNA complexes. The solution was dropwise added to the 10 cm dishes containing the multi-test 8-well slide incubated with PC12 cells. Fresh complete media was added to the cells after 24 hours transfection. 48 hours later, FITC-insulin incubation was done for 15 mins (as described in section 2.2.2). Then cells were fixed with 4% PFA.

2.2.5 Immunofluorescent staining

PC12 cells in multi-test 8-well slide were incubated for 1 hour at RT in 10% donkey serum (Sigma # D9663) to prevent non-specific binding. Each small well was applied with 15 µl solution. Cells were then subjected to incubation with 1:500 Anti-tdTomato antibody (OriGene # AB8181-200) in 0.1% PBST at 4 °C. The multi-test 8-well slide was placed in a 10 cm dish with wet tissue to keep the slide atmosphere humidified. Next day, 1:1000 Alexa Fluor 555 anti-Goat secondary antibody (Invitrogen # A-21432) was incubated at RT for 1 hour. The slides were washed with 1x PBS three times. Slides were examined and imaged with an upright confocal microscope (Zeiss LSM880).

2.2.6 Western blot

PC12 cells were seeded in 6 well plates to reach 80% confluence. Cells were fasted overnight in serum-free medium. The following day, different wells were treated with FITC-dye (200 nM or 800 nM), FITC-insulin (200 nM or 800 nM), or standard human insulin (200 nM) for different time courses. When the incubation was completed, medium was removed, and cells were washed with ice-cold 1x PBS once. Samples were lysed using lysis buffer (section 2.1) with Pierce Protease Inhibitor tablets (ThermoFisher Scientific # 88266) and dithiothreitol (DTT, 1 M) (ThermoFisher Scientific # R0861) on ice. Samples were centrifuged at 12,000 rpm for 15 mins at 4 °C, supernatants were collected, and protein concentration was determined using Pierce 660 nm Protein Assay (ThermoFisher Scientific # 22660). Proteins were separated using SDS page gel (10%, 1.5 mm thickness) (as described in section 2.1). Proteins were then transferred in Nitrocellulose membranes (GE Healthcare Life Sciences). Membranes were blocked in 5% BSA in TBST and the primary antibodies against IR, P-AKT, Total-AKT, P-ERK and Total-ERK were incubated overnight at 4 °C (see Table 2.1). Next day, TBST wash twice (10 mins each time), membranes were incubated with 1:5000 HRP conjugated secondary antibody in 5% skim milk (SERVE # 190295) in TBST for 1 hour at RT. Membranes were washed with TBST five times (5 mins each time), then enhanced chemiluminescence (ECL) (BioRad Clarity) was performed to visualise the immune-reacted bands. The bands were visualized with the iBright developer and analysed by iBright Analysis Software.

2.3 Animal Subjects

Experiments were performed in line with the UK animals (Scientific Procedures) Act 1986 and ethical standards set out by the University of Leeds Ethical Review Committee. Sprague Dawley (SD) (Charles River Laboratories) rats weighing 270-310 g were used for brain surgery. Rats acclimated for at least one week after arrival, then were randomly assigned to different groups (n=6/each group). There was at least four rats in each group in the experimental analysis. C57BL/6 male mice and Vgat-Cre-Gcamp6f mice (provide by Dr. Jamie Johnson) were maintained with ad libitum access to food and water.

2.3.1 Intranasal delivery of fluorescent FITC-insulin

8-12 weeks male C57BL/6 mice were anesthetized with ketamine (0.1 ml/10g) via intraperitoneal injection. Then 8 µl FITC-insulin (896.5 µM) was delivered to one nostril using 20 µl microloader fine tip (Eppendorf) attached to a Hamilton syringe. The tip was inserted to a depth of 10 mm, and the mice were placed in a supine position for 40 mins. A pre-warmed heat mat was used to keep mice body temperature. Finally, mice were injected with an overdose of pentobarbital (0.1 ml/30g) to perform cardiac perfusion (as describe in section 2.3.2). The brains were rapidly removed and fixed in 4% PFA overnight at 4 °C. The next day, PBS was used to wash the brains and then brains were embedded in 3% agar (Sigma # SLBS8479). Sagittal sections (50 µm thickness) were cut with a vibratome and stored in 1x PBS at 4 °C for immunohistochemistry (IHC).

2.3.2 Cardiac perfusion

Animals were fully anesthetised after intraperitoneal injection of pentobarbital. The chest cavity was opened and the heart was exposed using blunt scissors. A cannula was inserted into the left ventricle and the right atrium was cut to form a circulatory system. Then 0.1 M PB was infused intracardially followed by 4% PFA. The fixation was completed when the head of the rodent was fully stiff.

2.3.3 Acute slices

NMDG and aCSF (section 2.1) were used to stabilize the pH to 7.3-7.4. NMDG and aCSF were bubbled with 95% oxygen, 5% carbon dioxide for 15-20 mins. The male mice (4-5 weeks) were anesthetised with isoflurane (HENRY SCHEIN #988-3245), and then decapitated. The mice brain skin was opened by using a scalpel and the skull was cut carefully along the midline. The brain was trimmed to provide a flat surface to glue with and then embedded in molten 1.8% Agar (in aCSF). Sagittal sections were cut (300 µm thickness) in the holding chamber filled with chilled NMDG. The sections were transferred into NMDG for 30 mins to preserve interneurons. Then sections were transferred into aCSF to rest for 1 hour to recover from mechanical harm at RT. Slices were then divided into three groups, incubated with 800 nM FITC dye, 800 nM

FITC-insulin and 800 nM standard human insulin for 15 mins or 30 mins, respectively. Sections were washed with aCSF for three times (5 mins each time), then fixed in 4% PFA for 30 mins at 4 °C. After washing three times (5 mins each time) with PBS, sections were blocked with 10% donkey serum for 2 hours at RT. Then sections were stained either with ChAT, P-AKT (Ser473), GFP and TH primary antibodies (see Table 2.1) in 0.1% PBST for 2-3 days at 4 °C. Sections were washed using 1x PBS three times (5 mins each time), incubated with 1:50 Donkey goat Biotin for 4-6 hours at RT, then incubated with Streptavidin Alexa Fluor 647 Conjugates and Alexa Fluor 555 anti-Rabbit secondary antibody for 2-3 hours at RT. Finally, sections were washed using PBS three times (5 mins each time) and cover slips were added following using Vectamount mounting medium.

Table 2. 1 Antibodies used in this project.

Name of antibodies	Application	Concentration	Species	Catalogue Number
Insulin receptor	Western blot	1:1000	Rabbit	Cell Signalling Technology # 23413S
P-AKT	Western blot	1:1000	Rabbit	Cell Signalling Technology # 9271S
Total-AKT	Western blot	1:1000	Rabbit	Cell Signalling Technology # 9272S
ERK	Western blot	1:1000	Rabbit	Cell Signalling Technology #4370S
Total-ERK	Western blot	1:1000	Rabbit	Cell Signalling Technology #4695S
β-Actin	Western blot	1:50000	Mouse	Cell Signalling Technology # 3700
Donkey Anti-Rabbit HRP	Western blot	1:50000	Donkey	Invitrogen A16029
Choline acetyltransferase (ChAT)	IHC	1:500	Goat	AB144P
Green fluorescent protein (GFP)	IHC	1:1000	Chicken	Abcam # ab13970
Tyrosine Hydroxylase (TH)	IHC	1:1000	Rabbit	Abcam # ab6211
P-AKT	IHC	1:150	Rabbit	Cell Signalling Technology # 4060T
Neuronal nuclear (NeuN)	IHC	1:2000	Guinea Pig	Millipore # ABN90
S100B	IHC	1:2000	Mouse	Sigma # S2532
tdTomato	IHC	1:500	Goat	OriGene # AB8181

Donkey anti-rabbit IgG Alexa Fluor 555	IHC	1:1000	Donkey	Invitrogen # A13572
Donkey anti-goat IgG Alexa Fluor 555	IHC	1:1000	Donkey	Invitrogen # A21432
Donkey anti-chicken IgG Alexa Fluor 555	IHC	1:1000	Donkey	Invitrogen # A78949
Donkey anti-goat IgG Alexa Fluor 488	IHC	1:1000	Donkey	Invitrogen # A11055
Donkey Anti-Guinea Pig IgG (H+L) Biotin Conjugate	IHC	1:50	Donkey	Fitzgerald #43R-ID014bt
Donkey Anti-rabbit IgG (H+L) Biotin Conjugate	IHC	1:50	Donkey	Invitrogen A-16039
Donkey Anti-Mouse IgG (H+L) Biotin Conjugate	IHC	1:50	Donkey	Invitrogen # 16021
Streptavidin Alexa Fluor Donkey conjugate 647	IHC	1:1000	Donkey	Invitrogen # S21374

2.3.4 Cryostat preparation

After rats' brains were dissected, they were fixed for 24 hours in 4% PFA at 4 °C. The brains then were transferred into 15% sucrose (made with 1x PBS). When the brains sunk into the bottom of the solution, they were transferred to 30% sucrose (in 1x PBS) for 24 hours. Then the brains were sagittally cut into half and meninges were removed by using fine forceps. Rat brain methacrylate matrices were filled with a thin layer of Optimal Cutting Temperature Compound (OCT) (# 361603E) on dry ice. The brains were embedded with OCT and cut with 25 μm thickness using the Leica cryostat.

2.3.5 Immunohistochemistry

Brain sections were washed in 1x PBS for 10 mins on a shaker, then PBS was carefully removed and sections were incubated for 1 hour in 10% donkey serum to prevent non-specific binding. Sections were then subjected to incubation with primary antibody. ChAT, GFP, NeuN and S100B primary antibodies (see table 2.1) where incubated at 4 °C overnight. The following day sections were incubated with secondary antibody for 1 hour at RT. Washed using 1x PBS for three times, cover slips were then mounted on the stained sections using Vectamount mounting medium (Vector Laboratories, Burlingame CA, USA). Slides were examined and imaged with an upright microscope (Zeiss LSM880). Images were processed by Fiji.

2.3.6 Indirect Calorimetry and activity

A total of six male mice (8-12 weeks) were randomly assigned into two groups. Mice in the metabolic cages were not always comfortable compared to their normal housing, which could possibly affect mice mood and food intake. Firstly mice were housed singly for acclimation for two days in metabolic cages. On day 3 mice were anesthetised with isoflurane and the nasal treatment was performed as follows: The control group mice were administered with 8 μl vehicle in each nostril and the treatment group mice were administered with 8 μl standard human insulin (17.3 μM, 2 mU/μl or 0.8 UI/kg mouse body weight) in each nostril. After treatment the mice were put into the metabolic cages to track their metabolism and activity using the Comprehensive Laboratory Animal Monitoring System (CLAMS; Columbus Instruments International,

Columbus, OH, USA), such as food intake, locomotor activity, oxygen, carbon dioxide consumption and output. On day 5 the intranasal treatments were repeated where mice that received standard human insulin on day 3 were injected intranasally with vehicle, and mice that received vehicle on day 3 were injected with standard human insulin and again placed back in the metabolic cages. The CLAMS system is sensitive due to the use of respiratory gases. The measurement of O_2 and CO_2 could be randomly disturbed by changing water vapour and drierite (a drier to reduce the moisture of circulatory air in the system). The way of minimising this effect is to change water vapour and drierite when the CLAMS system is in the 'reading reference' mode. Mice were sacrificed on day 8.

2.3.7 Analysis of CLAMS data

Respiratory exchange ratio (RER) is the volume of CO_2 (VCO_2) produced per volume of O_2 (VO_2) consumed. VO_2 or VCO_2 is the volume of O_2 or CO_2 consumed per hour per kilogram mass of the animal. An air sample was recorded every 14 mins. The RER was calculated as an average for each hour. Heat production was recorded every 14 mins and averaged into 1 hour intervals. Locomotor activity was quantified as consecutive photo beam breaks along the axis (XTOT = all beam breaks in the x axis (front to back; X axis); XAMB = locomotor beam breaks (also known as Y axis); ZTOT = rearing events (mice standing on feet; Z axis) of the same CLAMS cages. Food accumulation of each hour was analysed. All the data were uploaded and analysed in CaIR (https://calrapp.org/) using R language. Taking the food consumption as an example, the relevant codes were shown in **Appendix 1**.

2.4 Brain stereotaxic surgery in rodents
2.4.1 Insulin receptor knockdown in the HDB in rats

Sprague Dawley male rats were anesthetised with isoflurane and placed in a stereotaxic apparatus (World Precision Instruments). Hair was shaved and skin disinfected with 70% alcohol. Skin was cut from the midline and tissues on the skull were removed using the blades before drilling, and two screws were places to hold the skin. After the skull had dried, the bregma and lambda in a horizontal plane (always start from bregma first, then move to the lambda) were measured. Then a cannula was moved to the

Bregma to calculate the Anterior-Posterior (A/P), Medial-Lateral (M/L) and Dorsal-Ventral (D/V) according to the coordinate of the horizontal limb of the diagonal band of Broca (HDB) (M/L: +/- 0.8 mm; A/P: + 0.6 mm; D/V: - 8.3 mm). A hole was drilled before the guide cannula was implanted into the specific brain area. Then super glue and cement were applied to close the wound. Then a dummy was put in the guide cannula. 2.5 µl of Ad5CMV-CRECFP and ADCMV-ShIR-tdTomato or Ad5CMV-ShC-tdTomato control virus (mix 1:1) were injected by using 50 µl Hamilton syringes. The cannula was held in place for 5 mins to reduce the risk of backflow of virus. After 5 mins, the injection cannula was taken out, dummy was put back and then secured with the dust cap. Each rat received subcutaneously 5 ml saline and were put on the warm cages to recover. The rats are singly housed. The daily food intake and body weight was monitored.

2.4.2 Fluoro-Gold injection in mice

Adult male mice were anesthetised (ketamine and Medetomidine (0.1 ml/10g)) via intraperitoneal injection and body temperature maintained warm by placing the animal on a hot mat during surgery. All injections were performed using a stereotaxic frame for coordinate guidelines. Lateral injections into the HDB (from bregma A/P= + 0.03 cm, D/V= - 0.58 cm, and M/L= ± 0.13 cm) was targeted. 10 nl 2% (in saline) retrograde tracer Fluoro-Gold (Biotium) was injected using a 25 µl Hamilton syringe by SPLG100 syringe pump (kdScientific), at the rate of 0.002 µl/min. When injections had finished, the cannula was left in place for 5 mins, then the line was clamped for a further 15 mins. Finally, the cannula was slowly removed. The skin was sutured to close the incision and mice were administered subcutaneously with 500 µl saline, 300 µl meloxicam (5 mg/kg) and intraperitoneally with 300 µl Antisedan (5 mg/kg). Mice were perfused for immunohistochemistry at 7 days post-injection.

2.4.3 Acute feeding study

On day 6 and day 12 after virus injection the feeding study was conducted. Body weight and food leftover were measured at 9 am, then food was removed while rats were able to access to water. At 3:30 pm rats from insulin receptor knockdown group (ShIR) were bilaterally infused with standard human insulin or a vehicle into the HDB at rate of 0.04 μl/minute for 5 mins. Rats from control virus injection group (ShC) were also bilaterally infused with standard human insulin or a vehicle into the HDB at rate of 0.04 μl/minute for 5 mins. Food was returned at 4 pm when all infusion was finished, and food intake was monitored every half an hour for 4 hours (4:30pm-8:30pm).

2.4.4 Rodent activity detector

Rats' activity was detected by using rodent activity detector (https://hackaday.io/project/160742/instructions?page=2), Adafruit Feather M0 Adalogger (https://thepihut.com/products/adafruit-feather-m0-adalogger), PIR sensor (https://www.mouser.co.uk/ProductDetail/Olimex-Ltd/MSP430-PIR?qs=%2Fha2pyFaduiyk%252B%252BqubsDJxQJhXSq%252BaD0jMP%252BoNRtYScxaJ%2FEXJ4Ntw%3D%3D), Assembled Adafruit Feather Wing OLED (128x32 OLED Add-on For Feather)(https://thepihut.com/products/adafruit-assembled-adafruit-featherwing-oled-ada3045) and Header Kit for Feather-12-pin and 16-pin Female Header Set (https://thepihut.com/products/header-kit-for-feather-12-pin-and-16-pin-female-header-set) were assembled according to the instruction).

2.4.5 Blood glucose measure

Blood glucose level was measured using a blood glucose metre (Freestyle Optium Blood Glucose 1 x 50 Test Strips), blood was tested from rats' tails while rats were awake.

2.4.6 Rat Corticosterone test

Blood samples for corticosterone analysis were token from the liver when the rats were perfused between 11am-3pm. BioVendor Mouse/Rat Corticosterone ELISA Kit (# RTC002R) was used to test rat corticosterone. All reagents and samples were brought to room temperature (21-26 °C) before use. All the steps were strictly followed by the manufacturer's instruction. 10 µl standard calibrators and samples (rats' plasma) were placed into pointed polyclonal rabbit anti-corticosterone antibody coated wells. Then 100 µl incubation buffer was added to each well followed by enzyme conjugate (50 µl /well). The plate was put on the plate shaker at RT (> 600 rpm) for 2 hours. Solution was removed after incubation; 1x wash buffer was added to the wells (300 µl/well). Then all the wash buffer was removed by beating the plate on tissue paper. The process of washing was repeated 4 times. Then 200 µl substrate solution was added and the plate was placed in the dark for 30 mins without shaking. After that, stop solution was added to terminate the reaction and the plate read under 450 nm (Hidex microplate reader). The concentration of corticosterone of each sample was calculated based on the standard curve (plotted by https://www.aatbio.com/tools/four-parameter-logistic-4pl-curve-regression-online-calculator).

2.4.7 Ad5IR-CRECFP recombinant adenovirus virus injection in the nucleus of solitary tract (NTS)

Rats were stereotactically implanted with a bilateral catheter targeting the nucleus of the solitary tract (NTS) within the dorsal vagal complex (DVC), 0.0 mm on occipital crest, 0.4 mm lateral to the midline and 7.9 mm below skull surface (Filippi et al., 2012). Ad5IR-CRECFP recombinant adenovirus virus and ADCMV-ShIR-tdTomato were mixed (1:1). Then 2 µl of viruses were injected into the each side of the NTS. Rats were perfused after one week and the viruses' expression was detected.

2.5 Brown Adipose Tissue (BAT) and the liver
2.5.1 To quantify lipid droplet from BAT and liver

The liver and BAT tissues were collected before perfusion and snap frozen in liquid nitrogen. For hematoxylin and eosin (H&E) staining, small pieces of tissue were placed

in 70% alcohol for 2 hours at 4 °C before paraffin embedding. Sections were then cut at 5 μm thickness for liver samples and 8 μm thickness for BAT and processed by the histology facility in St James hospital for H&E staining. BAT sections were imaged with the EVOS (40x) and liver sections were imaged with the slide scanner (20x). And images were analysed by Image J as following steps:

Image > Type> 16-bit; Analyze> set scale> distance in pixels (4.55)> known distance (1.0)> pixel aspect ratio (1.0)> unit of length (μm)> ok; draw an area of interest (region of interest); Image> chop; Image> adjust> Threshold> tick the box of Dark background> adjust the bar to choose the droplet of fat> click apply; Process> Binary> watershed; Analyze> analyze particles (0-314.15 μm).

Liver sections were imaged with the slide scanner (20x). And images were analysed by Image J as following steps:

Draw an area of interest (region of interest); Image> chop> Multi-point to count the number of lipid droplets.

2.5.2 RNA extraction

RNA from BAT and liver tissues were extracted by using RNeasy Lipid Tissue Mini Kit (# 74804). Tissue (around 50 mg) was homogenized in the presence of 1 ml QIAzol Lysis Reagent (optimized for lysis of fatty tissues) for around 15 seconds until no visible tissue and homogenated at RT for 5 mins to release nucleic acid from proteins. 200 μl chloroform was then added into each tube, and samples were vortex-mixed vigorously for 15 seconds. After that, samples were left at RT for 3 mins before centrifuging for 15 mins at 12,000 rpm to separate the organic phase, interphase and the aqueous phase. Then the upper aqueous phase was transferred into a new 1.5 ml tube, followed by an equal volume of fresh 70% ethanol. Then samples were mixed for several seconds to precipitate RNA from the aqueous phase. 500 μl of the samples was transferred into an RNeasy Mini spin column in a 2 ml collection tube, and centrifuged for 20 seconds at 8000x g at RT. The remainder of the samples was repeated as described above.

Then the samples were treated by using DNase digestion procedure. 350 µl buffer RW1 was applied to the column and span for 20 seconds at 8000 g at RT and the flow-through discarded. 80 µl DNase mix (10 µl DNase plus 70 µl buffer RDD) was added into the middle of the column and incubated for 15 mins at RT. After that, 350 µl buffer RW1 was added to the column and spin for 20 seconds at 8000 g at RT. Flow-through was discarded, followed by the addition of 500 µl buffer RPE to wash the column twice. Each time the flow-through was discarded. Then column was placed in a new tube and span for 1 min to further dry the column. The column was then placed in a new 1.5 ml tube and 40 µl RNAase free water was added, and centrifuged for 1 min at 8000 g.

2.5.3 Reverse transcription-PCR (RT-PCR)

Total RNA extraction was used as a template to reverse into cDNA and achieve PCR amplification to obtain many copies by using reverse transcriptase as instructed by following steps.

Table 2. 2 Reverse transcription-PCR reaction system 1:

Reagents	Volume
Oligo-dT$_{20}$ (# 18418020)	1 µl
RNA (1 µg)	11 µl
dNTP (10 mM) (# U151B)	1 µl

The total volume (13 µl) was incubated for 5 mins at 65°C to denature the RNA, then samples were incubated for 1 min at 4 °C. Then 7 µl of the following mix was added.

Table 2. 3 Reverse transcription-PCR reaction system 2:

Reagents	Volume
5x first-strand buffer (# 2105651)	4 µl
0.1 M DTT (# 2084465)	1 µl
RNasin plus (# N251B)	1 µl
Superscript III RT (# 2369473)	1 µl

The mixture was incubated for 45 mins at 55 °C and 15 mins at 70 °C. DNA was kept at -20 °C for further study.

2.5.4 Total RNA integrity assay

Total RNA integrity assay is always essential before collecting meaningful gene expressions data. There are three different types of RNA, including messenger RNA (mRNA), transfer RNA (tRNA) and ribosomal RNA (rRNA). rRNA is most of the RNA, and two sharp bands 28S and 18S (the ratio is around 2:1) are represented of intact and reliable eukaryotic RNA samples. Here Agilent RNA 6000 Nano Reagents Part 1 kit (#2120) and Agilent 2100 Bioanalyzer System were used to assess the total RNA integrity by following manufacturer's instructions.

The aliquot of ladder (# 5067-1529) was denatured at 70 °C for 2 mins before use, then immediately was put on ice or stored at -80 °C. 550 µl of Agilent RNA 6000 Nano gel matrix was added into a spin filter followed by 10 mins spin at 1500 g. Then 1 µl RNA 6000 Nano dye was added to 65 µl filtered gel in a 0.5 ml RNase-free tube. Then the gel-dye mixture was mixed and centrifuged at 13000 g for 10 mins at RT.

A new RNA Nano chip (#VM15BK20) was placed on the chip priming station. 9.0 µl of the gel-dye mix was added at the bottom of the well (means 'gel well'), and the plunger position was set at 1 ml and then the chip priming station was closed. The plunger of the syringe was pressed down until it was held by the clip. After 30 seconds, the clip was released to allow the plunger to draw back to the 1 ml position.

The chip priming station was opened and 9.0 µl of the gel-dye mix was added to each well marked G alone. 5 µl of the RNA 6000 Nano marker was added into the well (means 'marker well') and all sample wells (Do not leave empty wells). Then 1 µl of the RNA ladder was added into the well and 1 µl of each RNA was added to the sample wells. Then chips were place on IKA vortex mixer 1 mins to mix all the solutions. A cleaner chip filled with 350 µl Diethyl pyrocarbonate (DEPC) was put into the Agilent 2100 bioanalyzer for 1 min to clean the system. Agilent 2100 Bioanalyzer System was run to read the sample chip and the results were exported.
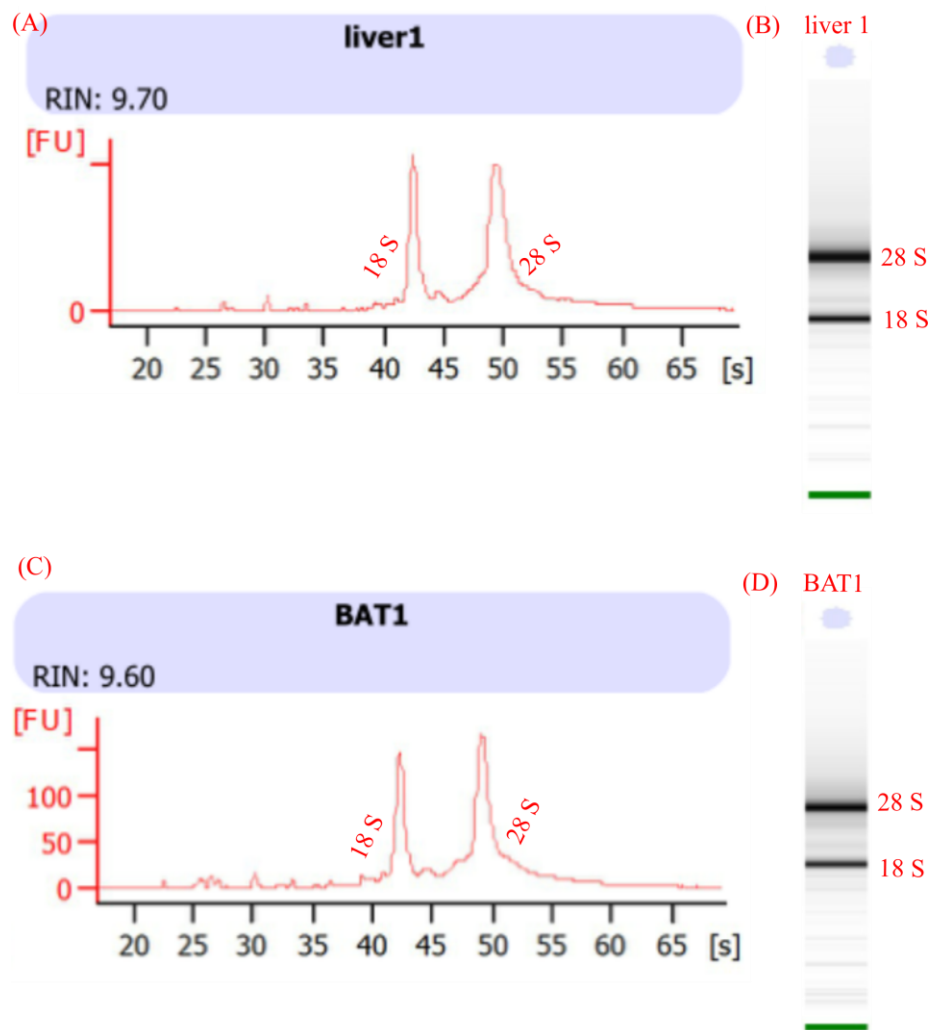
Figure 2. 2 Examples of two RNA samples by using Agilent 2100 Bioanalyzer data.
(A) RNA extracted from the liver from SD rats, and the intact RNA with a 28S:18S
rRNA ratio of approximately 2:1. (B) The 28S and 18S RNA bands from the liver
samples are indicated. (C) RNA extracted from the BAT from SD rats. (D) The 28S and
18S RNA bands from the BAT are indicated. RNA Integrity Number (RIN) indicates
the RNA integrity with a range from 0 to 10, with the maximum 10 to indicate the
highest RNA integrity.

2.5.5 Real-Time PCR/ Quantitative PCR (qPCR)

Real-Time PCR was used to evaluate gene expression by detecting a fluorescence signal as reaction occurs. In the early stage of reaction, SYBR Green fluorescence level remains too low to be detectable. Then gene amplification products keep accumulating and the number of PCR cycles at which the fluorescence signal reaches the threshold is the Ct or Cq value, which is used to measure the gene number of samples and $2^{-\Delta\Delta Ct}$ method was used to quantify the transcriptional difference between treatments.

2.5.6 Algorithm of $2^{-\Delta\Delta Ct}$ method

$2^{-\Delta\Delta Ct}$ method was used for qPCR data analysis. In our experiment, each sample was run in triplicate and there are at least 4 samples each treatment. Firstly, the average Ct value of each sample was calculated, then ΔCt of each sample is calculated by following equation:

ΔCt= average Ct (gene of interest) - average Ct (endogenous control gene)

Then $\Delta\Delta$Ct was calculated by following equation:

$\Delta\Delta$Ct= ΔCt (experimental group) - average ΔCt (control group)

Finally, the fold difference expression of gene of interest relative to the control group was calculated by the following equation:

Fold change= $2^{-\Delta\Delta Ct}$

Table 2. 4 primers used in our study.

Name of Genes	NCBI number	Primer sequence (5'–3')
Insulin Receptor (IR)	NM_017071.2	F: GGATTATTGTCTCAAAGGGCTGAA R: CGTCATACTCACTCTGATTGTGCTT
Glucose transporter 1 (GLUT 1)	NM_138827.2	F: TGGCCAAGGACACACGAATACTGA R: TGGAAGAGACAGGAATGGGCGAAT
Glucose transporter 4 (GLUT 4)	NM_012751.1	F:AGTTGGAAAGAGAGCGTCCACTGT R: GCTGCAGCACCACTGCAATAATCA
Fatty acid synthase 2 (FAS_2)	NM_139194.3	F: GCAGCTGTTGGTTTGTCCTG R: ATTCACTGCAGCCTGAGGTC
Acetyl-CoA carboxylase alpha (ACACA)	NM_022193.1	F: AGGAAGATGGTGTCCGCTCTG R: GGGGAGATGTGCTGGGTCAT
Diacylglycerol O-acyltransferase 1 (DGAT1)	NM_053437.2	F: AAGTATGGCATCCTGGTGGA R: CAGGCGCTTCTCAATCTGAA
Peroxisome Proliferator-Activated Receptor-Gamma (PPARG)	NM_013124.3	F: CCTGAAGCTCCAAGAATACC R: GATGCTTTATCCCCACAGAC
Adrenoceptor Beta 3 (ADRB3)	NM_013108.2	F: CCTTCCCAGCTAGCCCTGTT R: TGCTAGATCTCCATGGTCCTTCA
Tumour Necrosis Factor α (TNFα)	NM_012675.3	F: TCCCAGGTTCTCTTCAAGGGA R: GGTGAGGAGCACGTAGTCGG
DNA damage-inducible transcript 3(Chop)	NM_024134.2	F: GAAAGCAGAAACCGGTCCAAT R: GGATGAGATATAGGTGCCCCC

Peroxisome proliferator-activated receptor-γ coactivator (PGC1)	NM_031347.1	F: CGATGACCCTCCTCACACCA
		R: TTGGCTTGAGCATGTTGC
Nuclear factor kappa B (NFkB)	NM_001276711.1	F: AATTGCCCCGGCAT
		R: TCCCGTAACCGCGTA
Mitochondrial uncoupling protein (UCP)	NM_012682.2	R: GCCTCTACGATACGGTCCAA
		F: TGCATTCTGACCTTCACCAC
36B4	NM_022402.2	F: CGACCTGGAAGTCCAACTAC
		R: ATCTGCTGCATCTGCTTG
RPLP0	NM_022402.2	F: CCCTTCTCCTTCGGGCTGAT
		R: TGAGGCAACAGTCGGGTAGC

Table 2. 5 qPCR reaction volume:

SYBR Green (# 4309155)	6.25 μl
Forward and Reverse Primer	1.25 μl
cDNA	4 μl
RNAse free water	1 μl
Total Volume	12.5 μl

Note: the concentrations of primers were diluted to 3 μM to 5 μM in RNAse free water from the stock concentration of 100 μM. The concentration of BAT cDNA was using at 1:50 dilution and liver tissue cDNA was used at 1:100 dilution in our experiment.

Table 2. 6 qPCR reaction cycling:

Hold stage	95 °C	10 mins
PCR stage	95 °C	15 s
	60 °C	1 min
Annealing	60 °C	5 s
	95 °C	1 s

All the data was collected by QuantStudio™ Design & Analysis Software.

2.6 Recombinant Adenovirus production
2.6.1 HEK 293 AD cell culture

HEK 293 AD cells (Thermofisher) were cultured in Gibco DMEM media (high glucose, GlutaMAX Supplement) (Thermofisher # 10564011) containing 10% Fetal Bovine Serum (FBS) (Gibco # 2024-1), 1% Penicillin Streptavidin (Sigma # P0781) and 0.1 mM Minimum Essentiall Medium Non-Essential amino acids (MEM-NEAA) (Gibco # 11140-035) under 37 °C, 5% CO_2 condition.

2.6.2 Vector preparation

pAcad59.2-100 backbone vector (total 10 μg) was mixed with 2 μl Pac1 (BioLab #R0547L) and 10x CutSmart buffer (BioLab #B7204S) at 37 °C for 1 hour. pAcad5

shuttle vector (total 25 µg) containing the gene of interest (IR promoter) was mixed with Pac1 (2 µl) and 10x smart buffer at 37 ℃ for 1 hour according to the RAPAd system instruction (Vector Biolab # VPK-252). DNA was purified using the Zymo genomic DNA Clean and Concentrator (ZYMO RESEARCH #D4010) kit as manufacturer's instruction. Note: elute the DNA twice using the same elution buffer at the last step.

2.6.3 DNA Electrophoresis

0.8% Agarose gel (effective separation range is 800-10000 bp) was used for checking DNA size. 0.4 g Agarose (Fisher # BP160-500) was poured into 50 ml 1x TBE (Millipore # HC 72878577). Microwave until it was fully melted, then 2 µl SYBR safe DNA gel stain (Thermo Fisher Scientific # 2361838) was added. After mixing, the solution was poured into the gel tray to set. 6x loading buffer (Thermo Fisher Scientific # R0611) and dH_2O were added to the DNA samples. Then the samples (around 12 µl) and ladder (Thermo Fisher Scientific # 10488085) was loaded, respectively. The gel was run at 70 V for approximately 40 mins and visualised by using the blupad.

2.6.4 Cotransfection in HEK293 AD Cells

Confluent HEK293 AD cells were diluted at 1:4 and then plated in 6 cm dish the day before. On the following day, the cells were changed to 3 ml fresh completed media and transfected using PolyJet (# SL100688) with DMEM not complete media. Solutions were prepared as Table 2.7 described below:

Solutions in tube A was transferred to the tube B, after vortex, it was left at RT for 10 mins, then the mixture was dropwise added to the cells. After 3 hours, the control and transfection plate were changed to 3 ml fresh media. The expression level was monitored and checked daily. On day 3, 2 ml fresh media was added. Cells and media were harvested by using scraper when there were around 50% detached cells compare to the control. The cells and media were transferred into 50 ml falcon tubes. 3 freeze-thaw cycles alternating between the dry ice and 37 ℃ water bath was carried out to break the cells and release the viruses. Then the cell-virus mixtures were span at 3000 rpm for 5 mins to remove the cell debris. This is '**Ad5IRP-GFP virus**' stage 1 virus (S1).

Table 2. 7 Cotransfection preparation in HEK293 AD cells:

	Tube A	+	Tube B	+
	DMEM	PolyJet	DMEM	DNA
PolyJet control	100 µl	15 µl	100 µl	-
Co-transfection	100 µl	15 µl	100 µl	1 µg Pac1pacAd59.2-100 +4 µg Pac1pacAd5 vector

2.6.5 Virus amplification

Virus amplification was carried out on a 24 well plate, and HEK293 AD cells were plated at the ratio of 1:2 (500 µl/well) in the morning. The cells were settled at least 2 hours before any treatments. 500 µl PolyJet control supernatant was added into PolyJet control well, and Ad5IRP-GFP virus was added into 6 different wells (500 µl/well). 1 hour later, extra 500 µl warmed fresh media was added into all wells. The cells were checked daily under EVOS and harvested when there were more than 50% cell detached. The S1-1 to 6 media was harvested into 6 different 15 ml falcon tubes, then the supernatant was transferred into different 1.5 ml Eppendorf and stored at -80 ℃. This is stage 2 virus.

Stage 3 virus amplification was carried out in two 6 cm dishes (5 ml/each). 200 µl of S2-3 virus was dropwise added into each dish and swirled the dishes gently afterwards. The cells were incubated at 37 ℃ until most of the cells had detached. The media was harvested as stage 3 virus (S3). This will be used as the viral stock for making subsequent working stocks.

Stage 4 virus amplification was carried out in 8 confluent flasks of HEK293 AD cells. 4 flasks cells were treated with 2 ml trypsin and collected into one 50 ml falcon tube, the same treatment to the other 4 flasks. The media was discarded and the cells were resuspended using 5 ml complete media. 4 ml S3 virus was added into 200 ml complete media and then 10 ml cells were mixed into the media. 13 ml cell-virus mixture were transferred to each flask to make 16 flasks. Cells were incubated at 37 ℃ for 48 to 72 hours and harvested when all cells had detached.

Virus supernatant was slowly filtered through a 40 µm cell strainer by placing the 40

μm cell strainer on the top of the 50 ml falcon tube. Then this filtered supernatant was carefully poured into a 0.22 μm bottle top filter unit (SARSTEDT # 22100425). This is stage 4 virus (S4). This prep can be stored at -80 ℃ in 50 ml falcons or purified straight away.

2.6.6 Recombinant Adenovirus purification

30 ml of the S4 filtered virus was pipetted into a 50 ml falcon tube. 8 ml of 10% Sucrose/Tens was underlain by using a 10 ml syringe with an 18 G needle. The needle was placed into the bottom of the falcon tube and the plunger was slowly depressed to make sure the virus/media and sucrose does not mix. Virus was purified by spinning at 11,000 rpm for 4 hours at 4 ℃.

After the spin, the media and sucrose mix was carefully removed, tubes inverted onto paper and any residual media wiped off the tube. 100 μl of sterile PBS was slowly added into the bottom of each of the tubes and left for 30 mins at RT, then gently vortex. PBS from each tube was collected into a 1.5 ml Eppendorf tube and left at 4 ℃ overnight. Repeat PBS collection step for 3 time by ending up with 300 μl virus/tube. This is pure virus. Virus is stored at -80 ℃.

2.6.7 To construct PacAd5IRP-CRECFP vector

PacAd5IRP-GFP and PacAd5CMV-CRECFP were digested by restriction enzyme Sbf1 (Biolabs # R3642S) and Kpn1 (Biolabs # R3142S), respectively. The fragment of PacAd5-CRECFP band and insulin receptor promoter band were extracted (Invitrogen # K210012) and purified by ZYMO DNA Purification Kits (D4004). Insert gene (IR promoter) were inserted into the vector fragment PacAd5-CRECFP by using ligase (Table 2.8 ligation system). The total vector is 50 ng, and the vector to insert gene molar ratio is 1:3. Include a vector alone and an insert gene alone as negative control ligation. Incubate at RT for 30 mins.

Table 2. 8 ligation reaction:

T4 DNA Ligase (Biolabs # NA.54)	1 μl
2x ligase buffer (Biolabs # B0317S)	10 μl
DNA	50 ng vector
Nuclease free H_2O	up to 20 μl

2.6.8 To transform bacteria

5 μl of the ligation mix was added to 50 μl DH5α competent cells (Thermofisher) (store at -80 ℃), then the mixture was incubated on ice for 5 mins, followed by heat shock at 42 ℃ for 45 s. Then the mixture was incubated on ice for another 2 mins. Then spread onto L-Agar plates containing 100 μg/ml ampicillin in the presence of a flame, the plates were incubated at 37 ℃ overnight.

2.6.9 Mini-prep colony screening

Colonies of vector and insert genes were picked and dipped into 5 ml of L-broth containing the appropriate antibiotic. Then were put into a shaker and incubated at 37 ℃ overnight. The following day DNA was extracted using the ZYMO mini prep kit. DNA was digested to confirm that ligation is correct. PacAd5IRP-CRECFP vector was constructed successfully.

2.7 Statistical Analysis

Data were inputted on Microsoft Excel and analysed using GraphPad Prism 10 software. Each statistical test and how it is analysed were shown under each figure legends.

3 Physiological function of intranasal insulin *in vivo*

3.1 Introduction

Intranasal insulin is an inhaled insulin delivery method that not only avoids the pain and infection caused by needle injection, but also reaches the CNS (Born et al., 2002) and regulates energy balance (Benedict et al., 2011a). There is growing evidence in human studies which indicate that intranasal insulin can reduce energy consumption (Benedict et al., 2008) and palatable food intake (Hallschmid et al., 2012; Schneider et al., 2022). However, the mechanism of how intranasal insulin regulates feeding behaviour and energy expenditure through the CNS are still not fully understood. In order to explore the mechanism by which intranasal insulin affects feeding behaviour, we first must confirm the physiological function of intranasal insulin *in vivo*.

3.2 The rationale of using CLAMS system

Here we use indirect calorimetry to evaluate the metabolic function of intranasal human insulin in mice. Direct calorimetry is not feasible for this task as it requires harvesting the animal's tissues to conduct metabolic measurements of heat production in a calorimeter (Mina et al., 2018). Indirect calorimetry Comprehensive Lab Animal Monitoring System (CLAMS) is a method of collecting comprehensive metabolic data in live animals (Mina et al., 2018), which uses respiratory gases to indirectly calculate energy expenditure using equation 1

$$\text{Equation 1: } C_6H_{12}O_6 + 6H_2O + 6O_2 = 12H_2O + 6CO_2 + 2820 \text{ KJ.}$$

From the equation above, it is clear that for each 6 molecules of oxygen consumed and for 6 molecules of CO2 produced, there will be 2820 KJ of energy expended. This is the essence of how indirect calorimetry works using the CLAMS system.

The respiratory exchange ratio (RER) is a parameter which indicates which type of substrate is utilized and its equation is: $RER = VCO_2 / VO_2$. The way of measuring O_2 and CO_2 under CLAMS can be very accurate (refer to: https://www.colinst.com/products/clams-comprehensive-lab-animal-monitoring-system). The CLAMS cages used in our study were the Centre Feeder Cages, which can detect food intake with a resolution of 0.01 g, which is excellent to monitor the small amount

of food intake of mice. In addition, animal activity can also be measured by counting beam breaks within the CLAMS cage. There are 3 different measures of movement taken in the CLAMS cage: XTOT = all beam breaks in the x axis (front to back; also known as X axis); XAMB = locomotor beam breaks (also known as Y axis); ZTOT = rearing events (mice standing on feet; also known as Z axis).

3.3 Aims

(1) Does intranasal insulin affect food intake and body weight *in vivo*?
(2) Does intranasal insulin have other physiological effects on energy expenditure, activity and RER?

3.4 Results
3.4.1 Effect of intranasal insulin on metabolic balance

To explore the metabolic effect of intranasal insulin, a CLAMS system was used to measure food intake, energy expenditure, oxygen consumption, carbon dioxide production and locomotor activity after mice were intranasally administered standard human insulin. Mice were first acclimatized for 2 days in the CLAMS cages, on day 3, the cohort of 6 mice were randomly divided into control and treatment groups. The control group received vehicle in each nostril (as described in section 2.1), while the treatment group received standard human insulin in each nostril (16 μl total, 17 μM). Data regarding metabolic behaviour were collected for two days. On day 5 the experiment was repeated with the groups reversed, so that the data was paired, with each mouse receiving both vehicle and insulin (workflow is shown in Figure 3.1 A).
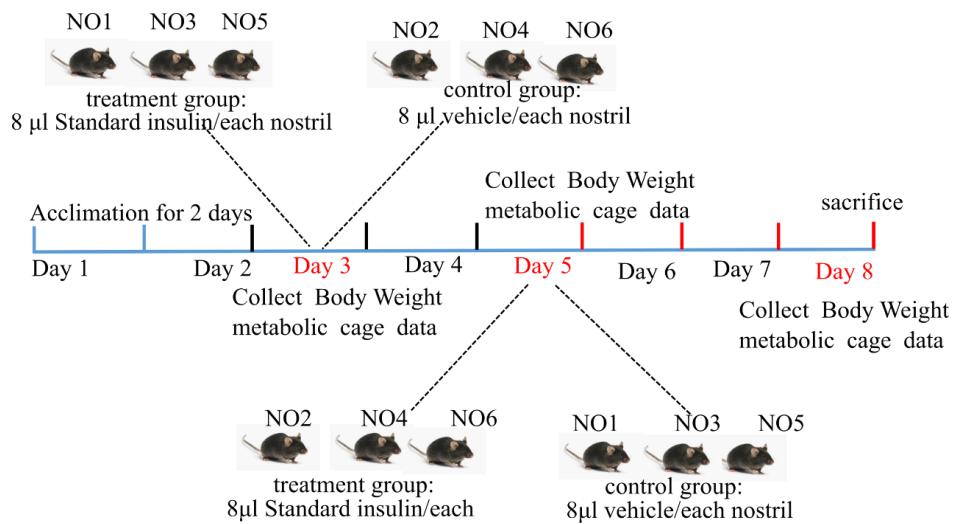
Figure 3. 1 Schematic representation of the CLAMS experimental design.

Firstly, the effect of intranasal insulin on food intake was examined. As body weight may influence food consumption, body weight was compared before intranasal injection. The results showed that the mice that were studied in each treatment group had similar body weights before treatment (Figure 3.2 A). Vehicle and intranasal insulin treated animals weighed an average of 24.051 g (SEM = 0.953, n = 10) and 24.239 g (SEM = 0.795, n = 10), respectively. Mice with intranasal injection were transferred into the metabolic cages before eating hours (4:30 pm). From Figure 3.2 B, it shows that there is a linear relationship between food consumption and the body weight of the mouse. As expected, the body weight (mass) effect P value is 0.0024, which means the food consumption was significantly correlated with body weight (Figure 3.2 B). However, the slopes of both regression lines have no significant interaction effect, which means the effect of body weight on food intake between two groups is the same (Figure 3.2 B). Both groups had increased food intake in the dark compared to the light period, consistent with their increased nocturnal activity (Figure 3.2 C). The total food consumption over two days was not significantly different between the two treatment groups (Figure 3.2 C), however, acute intranasal insulin administration significantly decreased total food intake (Kcal) in the first 2 to 5 hours in comparison to vehicle treated animals, which implies intranasal insulin has an acute effect on reducing food intake but did not lead to alterations in long term feeding patterns (Figure 3.2 D, E). Vehicle treated mice consumed a cumulative food mean of 6.436 Kcal (SEM = 0.30, n = 10) within 5 hours, while intranasal insulin treated mice ate only 5.52 Kcal (SEM = 0.32, n = 10) within the same time period (Figure 3.2 E). Results also indicated that 8 out of

10 mice exhibited an insulin-dependent decrease in food intake within 5 hours of acute intranasal insulin administration (Figure 3.1 F).
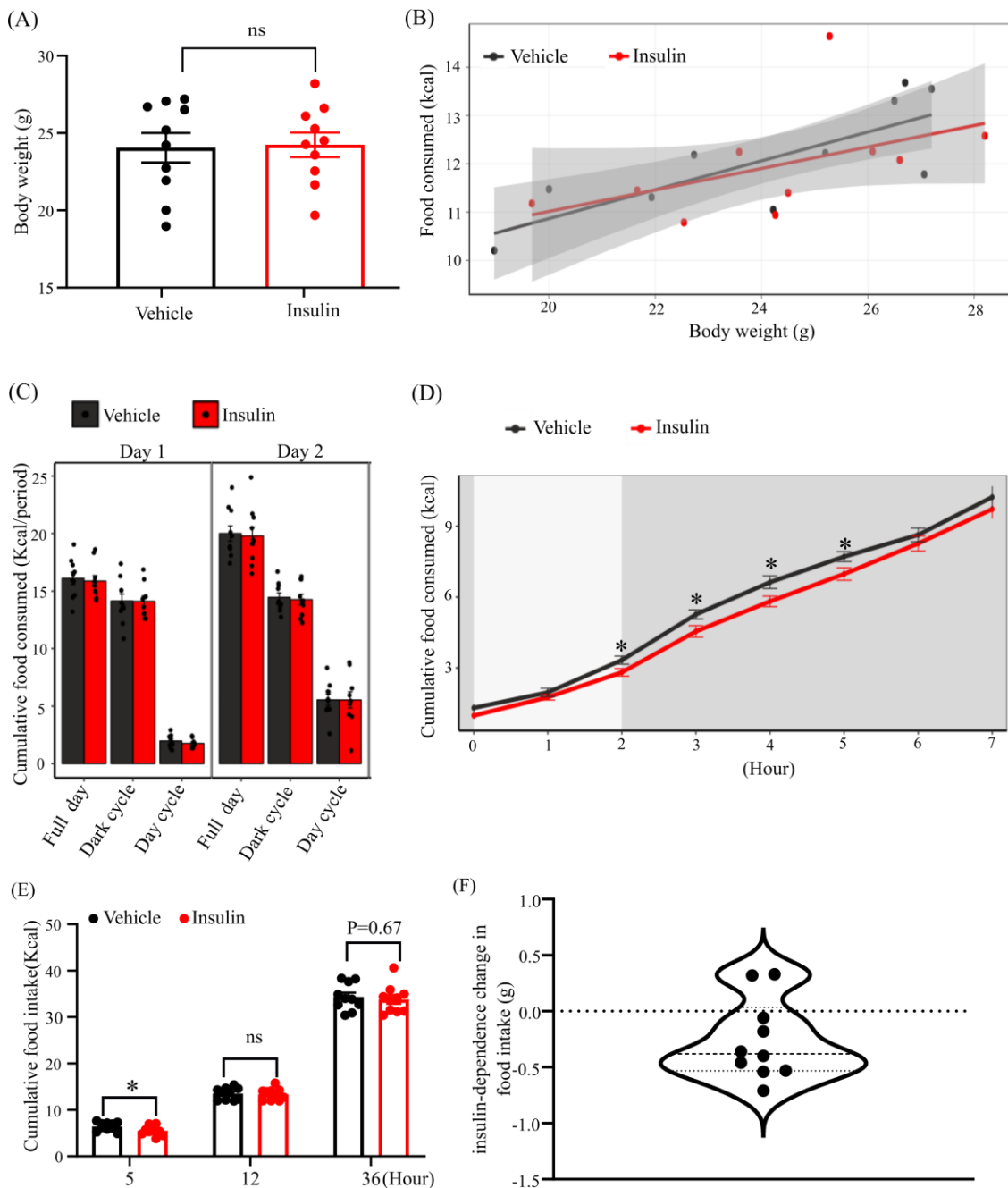
Figure 3. 2 Effect of intranasal standard human insulin on feeding behaviour in mice. (A) Body weight of mice in each group, n = 10/group. Mann-Whitney test was performed. Error bars represent Standard Error of Mean (SEM). (B) Generalized linear model (GLM) based regression plot: body weight on the effect of cumulative food consumption. ANCOVA (analysis of covariance), body weight as the covariate. Vehicle group equation: y = 0.8784x + 15.414, R² = 0.6015; Intranasal insulin group equation: y = 0.6577x + 19.988, R² = 0.2496. (C) Cumulative food consumption in light cycle and

dark cycle. (D) Cumulative food consumed (Kcal) under intranasal standard human insulin administration or same volume vehicle administration within 7 hours. Gray shadowed area represents the dark cycle, white area represents the light cycle. ANCOVA is performed, error bars represent SEM, * < 0.05. (E) Cumulative food consumption (Kcal) within 5, 12 and 36 hours after treatment, respectively. Multiple t-tests were performed, corrected for multiple comparison using the Holm-Sidak method. Error bars represent SEM. * p=0.049. (F) Insulin-dependent decrease in food intake, for each mouse cumulative insulin-treated food intake minus vehicle-treated cumulative food intake at 5th hour. Each animal was used as its own control at 5th hours. Violin chart was plotted, the upper line above zero is Third Quartile (75% of the data falls below the third quartile), the first line below zero is Median, and the second line below zero is Frist Quartile.

Our data showed that insulin decreases food intake within 5 hours after intranasal administration. Interestingly, it was also reported that intranasal insulin could increase postprandial energy expenditure in human subjects (Benedict et al., 2011a). We next tested whether energy expenditure is also changed by intranasal insulin treatment in this project. The results show that there is a linear relationship between cumulative energy expenditure and body weight. The body weight markedly affects hourly energy expenditure ($p<0.001$) (Figure 3.3 A), however the slopes of both regression lines have no interaction, which means the effect of body weight on hourly energy expenditure between the two groups is the same (Figure 3.3 A). Both treatment groups exhibited increased cumulative energy expenditure in the dark compared to the light period, consistent with their increased nocturnal activity (Figure 3.3 B). However, acute intranasal insulin did not significantly change energy expenditure neither in short term (one to seven hours) nor long term periods (39 hours) (Figure 3.3 B, C).

CLAMS was also used to measure locomotor activity of vehicle and insulin treated mice. Both groups had increased locomotor activity in the dark period compared to the light period, consistent with their increased nocturnal activity (Figure 3.3 D), however both groups exhibited similar activity levels, which suggested that acute intranasal insulin administration had no significant effect on locomotor activity (Figure 3.3 E). Additionally acute intranasal insulin treatment did not significantly affect body weight after acute intranasal insulin treatment (Figure 3.3 F). Unsurprisingly, acute intranasal

insulin did not affect body weight gain, one reason is that the body weight was measured two days post-intranasal injection and intranasal insulin only has acute effects on food intake which peaks within 2 to 5 hours following administration, which therefore dose not influence body weight. Altogether, results show that intranasal insulin reduced food consumption but did not reduce energy expenditure and locomotor activity.

Figure 3. 3 Effect of intranasal standard human insulin on energy metabolic

balance and locomotion in mice. (A) GLM based regression plot: body weight on the effect of cumulative energy expenditure. ANCOVA test, body weight as the covariate. Vehicle group equation: y = 0.8406x + 7.3327, R² = 0.3425; intranasal insulin group equation: y = 0.9434x + 5.123, R² = 0.4919. (B) Energy expenditure in light cycle and dark cycle. (C) Cumulative energy expenditure (Kcal) under intranasal standard human insulin administration or same volume vehicle administration within 7 hours. Gray shadowed area represents the dark cycle, white area represents the light cycle. Multiple t-test was performed, Error bars represent SEM. (D) Locomotor activity in light cycle and dark cycle. (E) Locomotor activity under intranasal standard human insulin administration or same volume vehicle administration within 7 hours. (F) Body weight increase after acute intranasal injection (n = 10/group), Error bars represent SEM.

Results showed acute intranasal insulin administration reduced food consumption in the acute post administration period, but did not change energy expenditure and locomotor activity. Here, the effect of intranasal insulin on oxygen consumption and carbon dioxide production were examined. The body weight as a covariate has a marked effect on hourly oxygen consumption ($p<0.001$) (Figure 3.4 A). According to the GLM slopes, both regression lines have no significant interaction effect, which means that the effect of body weight on oxygen consumption between the two groups is the same (Figure 3.4 A). Therefore, intranasal insulin injection had no significant effect on oxygen consumption and carbon dioxide production in the mice, in both the short and long time period (Figure 3.4 B, C, D, E). In addition, respiratory exchange ratio showed no difference between the intranasal injection and control group (Figure 3.4 F). These data clearly suggested that acute intranasal insulin could decrease food intake within 2-5 hours post-injection, but do not alter other metabolic parameters, such as energy expenditure, activity, body weight and RER.
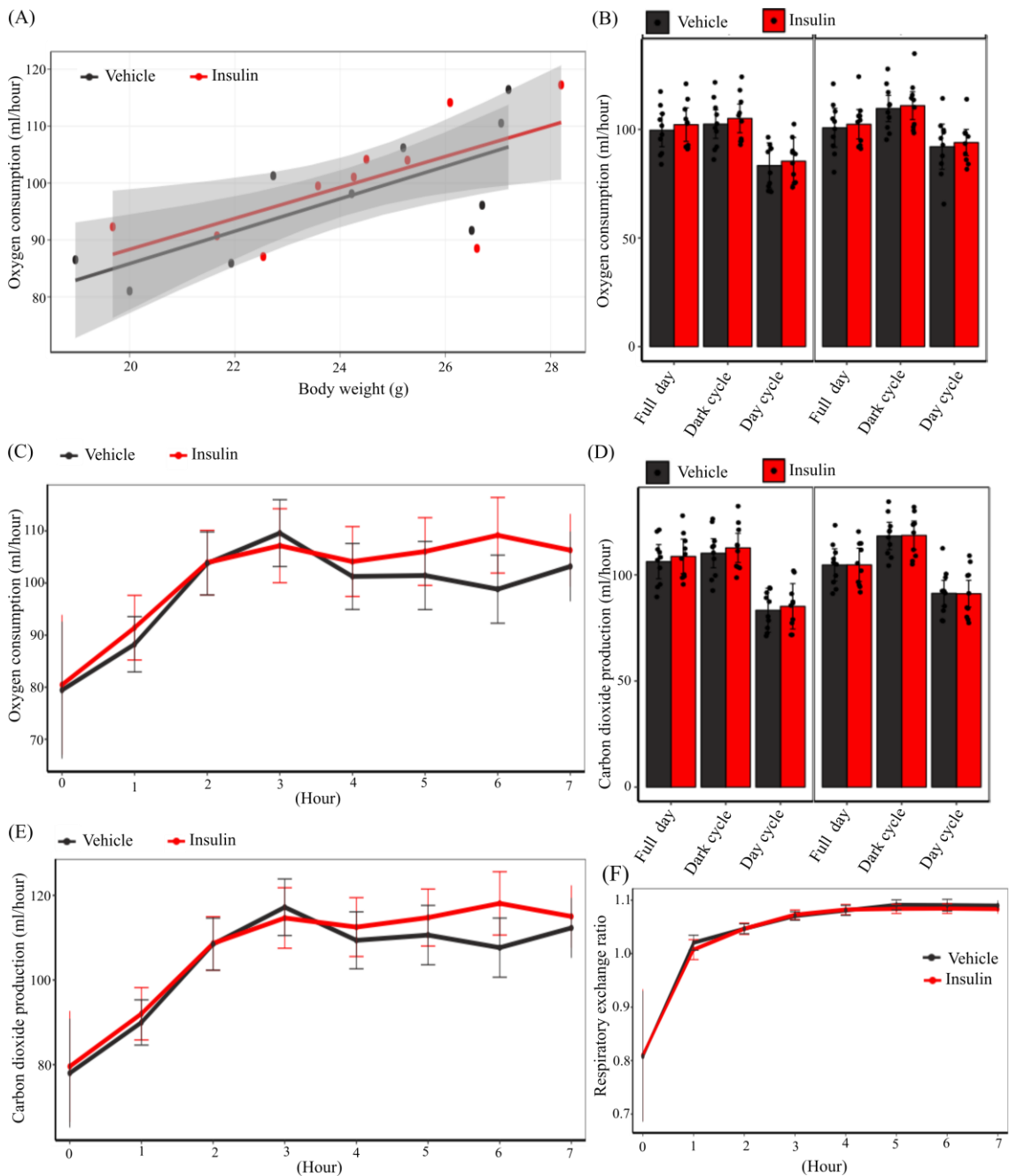
Figure 3. 4 Effect of intranasal standard human insulin on oxygen consumption and carbon dioxide production in mice. (A) GLM based regression plot: body weight on the effect of hourly oxygen consumption. ANCOVA test, body weight as the covariate. Vehicle group equation: y = 3.4223x + 10.151, R² = 0.2324; Intranasal insulin group equation: y = 4.2458x - 10.113, R² = 0.3276 (B) Oxygen consumption and carbon dioxide production (D) in the light cycle and dark cycle. Oxygen consumption (C) and carbon dioxi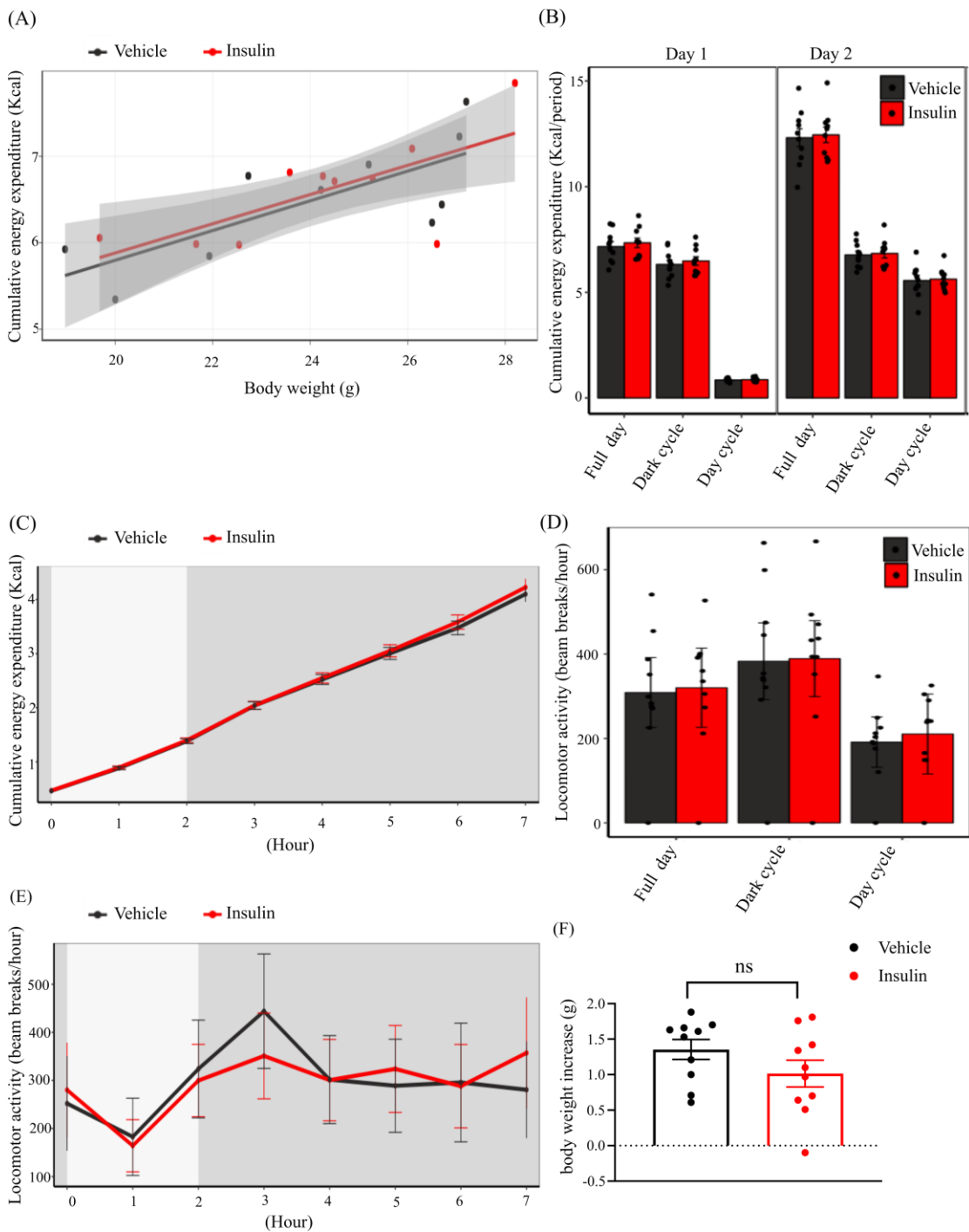de production (E) under intranasal standard human insulin administration or same volume vehicle administration within 7 hours. (F) Effect of intranasal standard human insulin administration on Respiratory exchange ratio (RER). Data was analysed under one-way ANOVA in CaIR. RER = CO_2/O_2 per min, RER around 1 means mice

use carbohydrate as their fuel.

3.5 Discussion

CLAMS is a well-established system, however, the analysis extensive raw data is one of the challenges of using this system. For example, when it comes to transgenic mice, mass-dependent parameters such as energy expenditure can be secondary to altered body weight, rather than a primary effect of the genotype alone (Speakman, 2013). Scientists propose that the effect of body weight should be taken into consideration when mass-dependent parameters are analysed. Furthermore, much debate around how to adjust such metabolic parameters has existed for many years, including whether these parameters should be directly divided by body mass or whether a using regression linear model is more physiologically relevant (Fernandez-Verdejo et al., 2019; Muller et al., 2021). The decision between directly dividing by body mass and using regression depends on the research question, the underlying assumptions of the data, and the physiological relevance of the normalization method. Both approaches can be valid and useful in different contexts. In my project, I used linear regression to explore the relationship between the cumulative food intake and body mass. When analysing measurements that are not related to mass (e.g., RER, locomotor activity), the difference between groups is assessed using a one-way ANOVA.

It has been reported that the method of directly dividing by body mass could lead to the misinterpretation of raw data, since metabolic rate is not linearly proportional to body mass and the intercept is not zero (Fernandez-Verdejo et al., 2019; Muller et al., 2021). In addition, energy expenditure is affected by different tissue compositions with different rates of metabolism (Tschop et al., 2011). When mice lose body weight, fat mass decreases more than lean mass, whereas when their body weight is increased, it does not translate to an equal or proportional increase in all tissues, and therefore energy expenditure and/or rate will be different. Under these circumstances, directly dividing by body weight will lead to artefacts when interpreting raw data. Recently, Müller et al clearly demonstrated that even though the metabolic rate in two groups were both mass-dependant, ratio-based analysis erroneously concluded significant group differences, while a regression-based liner model could distinguish between false and true group effects (Muller et al., 2021).

Since some metabolic parameters are effected by body mass or composition of body mass, such as metabolic rates and energy expenditure, ANCOVA which is based on a continuous variable analysis method is recommended for correcting such metabolic parameters (Tschop et al., 2011). The actual data in relation to body mass is highly recommended to be represent rather than plotting the data as histograms (Tschop et al., 2011). The regression-based analysis ANCOVA method usually recalculates each initial point and gives an adjusted value according to the regression slopes (more detail can refer to Module 2 from https://www.mmpc.org/shared/regression.aspx). Fortunately, an online metabolic analysis tool, CaIR, has been developed based on the regression linear model, ANOVA and ANCOVA, which makes the large amount of raw metabolic data analysis much easier to visualise, transparent and reproducible (Mina et al., 2018). In our experimental design, two groups with an acute treatment template was used for data analysis. CaIR would conduct a regression linear model between body mass and a mass-dependent measurement, such as energy expenditure. Only when there is no interaction effect reported between the two groups, which suggests that the effect of covariate body mass on energy expenditure is identical, so ANCOVA can be performed. For body mass-independent variables, such as locomotor activity and RER, data were analysed using a one-way ANOVA in CaIR.

To evaluate the role of intranasal insulin in regulating metabolic homeostasis all the mice were acclimated for 2 days in the CLAMS cage before intranasal injection based on methods described in Corrigan et al (Corrigan et al., 2020). According to the liner regression model we showed, the covariate body weight was significant, suggesting that it was an important predictor in analysing food intake, energy expenditure, oxygen consumption and carbon dioxide production. On the other hand, the effect of body weight had no preference between two groups, which means the ANCOVA could be performed.

Notably, our results showed that intranasal insulin treatment could reduce total food consumption within 2-5 hours, where this short term effect of insulin on food intake was also seen following i.c.v insulin injection in rats (Air et al., 2002) and mice (Brown et al., 2006). When we analysed the metabolic change of a single mouse treated sequentially with insulin or vehicle, our data indicated that 8 out of 10 mice decreased food intake upon insulin treatment, confirming what has been already reported in literature (Brown et al., 2006). It is possible that two mice did not receive the insulin as

the procedure did not guarantee 100% success or not all the mice response to insulin. A decrease in food intake could be due to a reduced meal size or a reduction in frequency of which food is eaten. In the future it would be beneficial to obtain data from the metabolic cages to track how many times per hour the mice would go to eat and for how long they stayed in the food area. These data will therefore illustrate the length and the frequency of the meals which will allow us to determine whether changes in food intake caused by intranasal insulin treatment are related to meal size or meal frequency. Although the influence of insulin-dependent decreased food intake was seen to disappear in the long-term, we did not observe any short term or long term effect of insulin on energy expenditure. This might be because daily energy expenditure could be affected by several other factors, such as basal metabolism rate, resting energy expenditure, daily activity and food intake (Speakman, 2013).

Although acute intranasal insulin administration is not sufficient to result in significant changes in body weight, there has been a trend toward a slight reduction in body weight increase compared to the control group. Vasselli et al reported that i.c.v injection of insulin caused a remarkable reduction in body weight after 24 hours (Vasselli et al., 2017), which is different to our data. This discrepancy may be due to the differing delivery mechanisms which are likely to target different brain areas and therefore triggering different insulin signalling circuits in the brain. It is likely that i.c.v delivered insulin can directly reach the arcuate nucleus and median eminence of hypothalamus both of which are highly involved in regulating insulin sensitivity and metabolic balance (Konishi et al., 2017; Yoo et al., 2019). While intranasal insulin may not exert its effect through the same pathway, evidence for this is provided in the following chapters.

In addition to monitoring food intake and body weight changes, examining changes in activity could also be a meaningful indicator in evaluating mice mood conditions or food searching behaviours (Wilson et al., 1976). For example, Hennige et al reported that i.c.v injection insulin increased locomotor activity in lean but not in obese mice after 24 hours (Hennige et al., 2009). In our study, however, we did not observe significant difference in locomotor activity after intranasal insulin administration compared to control treated animals. This may be due to the fact that animals were only given a single dose or the different methods of administration in our study. Locomotor activity, however, was found to be increased in the dark period compared to light period

in both mice groups, which is consistent with their increased nocturnal activity, indicating that animals in both groups exhibited normal locomotor behaviour during the experiment.

Respiratory exchange ratio (RER = VCO_2/O_2) is a parameter of fuel utilization. When RER value is near 1, this indicates that carbohydrates are the main fuel being utilised, and an RER value between 0.7 and 1 means both carbohydrates and fats were used as fuel. In our case, acute intranasal insulin injection did not change oxygen consumption and carbon dioxide production when compared with the control group. In addition there were no differences in the RER between the two groups, however, the RER in the light period was found to be much lower compared to that of the dark period, when the value of RER is always above 1, this is because increased food intake consisted of high-carbohydrate chow and carbohydrates were used as fuel in the dark period.

3.6 Conclusion

In conclusion, results presented here show that acute intranasal insulin treatment could decrease cumulative food intake in the short-term, however, single dose intranasal insulin did not have a longer term effect on food intake, energy expenditure, locomotor activity, oxygen consumption, carbon dioxide production or RER. However, there are some limitations in our experiment. Total mass was only used as a covariate in our analysis, however it is well known that different tissues composition can have an effect on metabolic rate and therefore it is important to consider the body fat and lean mass in metabolic data analysis in the future. It is possible that intranasal insulin may mediate its affects by spilling over into the circulatory system. However, to avoid this possibility, the dose of intranasal insulin used in our present study was low enough that its effect would be negligible if this were to happen (Ott et al., 2015). We have only evaluated the acute effect of intranasal insulin on metabolic homeostasis, it would be interesting to examine the effects of chromic intranasal insulin in the future and whether this can reduce caloric intake.

4 Intranasal FITC-insulin reaches to the brain

4.1 Introduction

Accumulating evidence indicates that the brain is an insulin sensitive organ, which controls eating reward, body weight, HGP and lipid metabolism (Filippi et al., 2012; Pocai et al., 2005b; Scherer et al., 2011; Guthoff et al., 2010). Insulin receptor has been discovered in a wide variety of brain regions, including the olfactory bulb, cerebellum, cortex, hypothalamus, hippocampus and brainstem (Havrankova et al., 1978; Hill et al., 1986). Dysfunction of insulin signalling in the brain has been associated with many disease, including AD, dementia, Parkinson's disease (PD) and diabetes (Ghasemi et al., 2013; Arnold et al., 2018), while activation of insulin signalling could alleviate this process (Hallschmid, 2021; Benedict et al., 2011b; Cholerton et al., 2013). For example, rats with decreased insulin receptor signalling in the hippocampus exhibited impaired spatial learning, anxiety-like and depressive-like (Grillo et al., 2011). Strikingly, learning and memory have been improved after intranasal insulin treatment (Lv et al., 2020). A plausible mechanism is that insulin could regulate the level of amyloid β peptide and phosphorylation of Tau to improve memory and other cognitive performance (Mullins et al., 2017; Hong and Lee, 1997; Rensink et al., 2004). These findings might suggest that improving insulin signalling sensitivity in the brain could be a potential therapy for the cognitive related disease.

Data produced in mice indicated that intranasal delivery of insulin could achieve similar concentrations in the brain as subcutaneous injection of insulin, but without increasing levels of insulin in the blood and therefore avoiding hypoglycaemia (Nedelcovych et al., 2018), which suggests that intranasal insulin could be a safer option to deliver insulin directly to the brain (Nedelcovych et al., 2018). There are a large number of studies that describe intranasal insulin significantly improving memory and mood in human subjects with AD (Benedict et al., 2007; Salameh et al., 2015; Schneider et al., 2022; Benedict et al., 2004; Benedict et al., 2011b; Reger et al., 2006; Stockhorst et al., 2004).

It has been reported that cerebral hypometabolism and dampened cerebral glucose uptake might be linked with cognitive diseases (Tang et al., 2016; Mosconi et al., 2009; Willette et al., 2015; Brabazon et al., 2017). Intranasal insulin significantly increase the levels of glucose, cellular energy substrates ATP and phosphocreatine in the brain after 9 days administration (Nedelcovych et al., 2018), which might partly explain the mechanism of how intranasal insulin alleviates memory and other cognitive diseases.

Brabazon et al further pointed that two week daily administration of intranasal insulin resulted in restored cerebral glucose uptake in the hippocampus that was accompanied by improved memory performance (Brabazon et al., 2017). This observation implies that intranasal insulin could improve cognitive function through changing cerebral metabolism.

Furthermore, intranasal insulin showed an effect on suppressing food intake (Jauch-Chara et al., 2012) and reducing body fat (Hallschmid et al., 2004). However, the mechanism about how intranasal insulin regulates caloric intake is still unclear. Some studies suggested that the neuronal activity of the fusiform gyrus (Guthoff et al., 2011; Guthoff et al., 2010), where responses to food stimuli, was decreased after giving intranasal insulin, which might be a potential mechanism for meal termination after intranasal insulin administration. Other neuroimaging results also indicated that insulin significantly regulates the activity of prefrontal area responses to high caloric food cue postprandial (Heni et al., 2014a; Kroemer et al., 2013). Another study further suggested that intranasal insulin reduces calorie intake by increasing brain energy ATP levels (Jauch-Chara et al., 2012). One explanation is that due to ATP severing as the currency of energy in cells, increased ATP levels will send out a signal of satiation and consequently leads to terminate eating (Lam, 2010; Cha and Lane, 2009; Lam et al., 2008). All these data imply that insulin could influence the activity of brain regions associated to the regulation of calorie consumptions. However, which brain regions are the targets of intranasal insulin acts has not been thoroughly defined.

In this chapter, we aimed to develop a viable method to detect intranasal insulin and determine which brain areas are reached by insulin upon intranasal injection.

4.2 Aims

(1) Determine whether fluorescein isothiocyanate (FITC)-insulin has the same biological function *in vivo* and *ex vivo* as standard human insulin and could it be a viable tool to follow intranasal insulin fate?
(2) Identify brain regions where intranasal insulin accumulates in the brain?

4.3 Results
4.3.1 FITC-insulin activates insulin signalling cascades in PC12 cells

To verify whether FITC-insulin is biologically active and can activate downstream insulin signalling, overnight fasted PC12 cells were incubated with FITC-dye, FITC-insulin and standard human insulin and time course was performed (Figure 4.1). We first confirmed that PC12 cells express the insulin receptors and show that expression levels are unaltered by FITC-insulin at the different time points (Figure 4.1 A). FITC serves as a fluorescent tag, enabling visualization and tracking of FITC-insulin within PC12 cells. By confirming that FITC-insulin does not interfere with insulin receptor function, we can accurately analyse insulin's cellular uptake, internalization, and subcellular localization. This information is critical for understanding insulin's interactions within the neuronal circuits and its intracellular trafficking. Our results indicated that FITC-insulin does not degrade the insulin receptor in PC12 cells and this is acting in the same way as insulin (Shi et al., 2002). Insulin binds to the extracellular domain of IR, leading to the auto phosphorylation of IR, phosphorylation of insulin receptor substrates and other downstream proteins, such as AKT and ERK (section 1.3.1). The AKT signalling and MAPK/ERK pathways were assessed by western blot. Phosphorylation of AKT (Ser 473) was increased after 5 mins of human insulin incubation and remained high for 45 mins (Figure 4.1 B). Similarly, phosphorylation of AKT (Ser 473) was significantly increased after 10 mins of incubation with low and high concentration of FITC-insulin (Figure 4.1 C, D), while ERK 1/2 phosphorylation was not changed by neither standard human insulin nor FITC-insulin (Figure 4.1 E, F). Together, these results suggest that FITC-insulin has similar biological activity to human insulin and activates the AKT pathway in *vitro*.
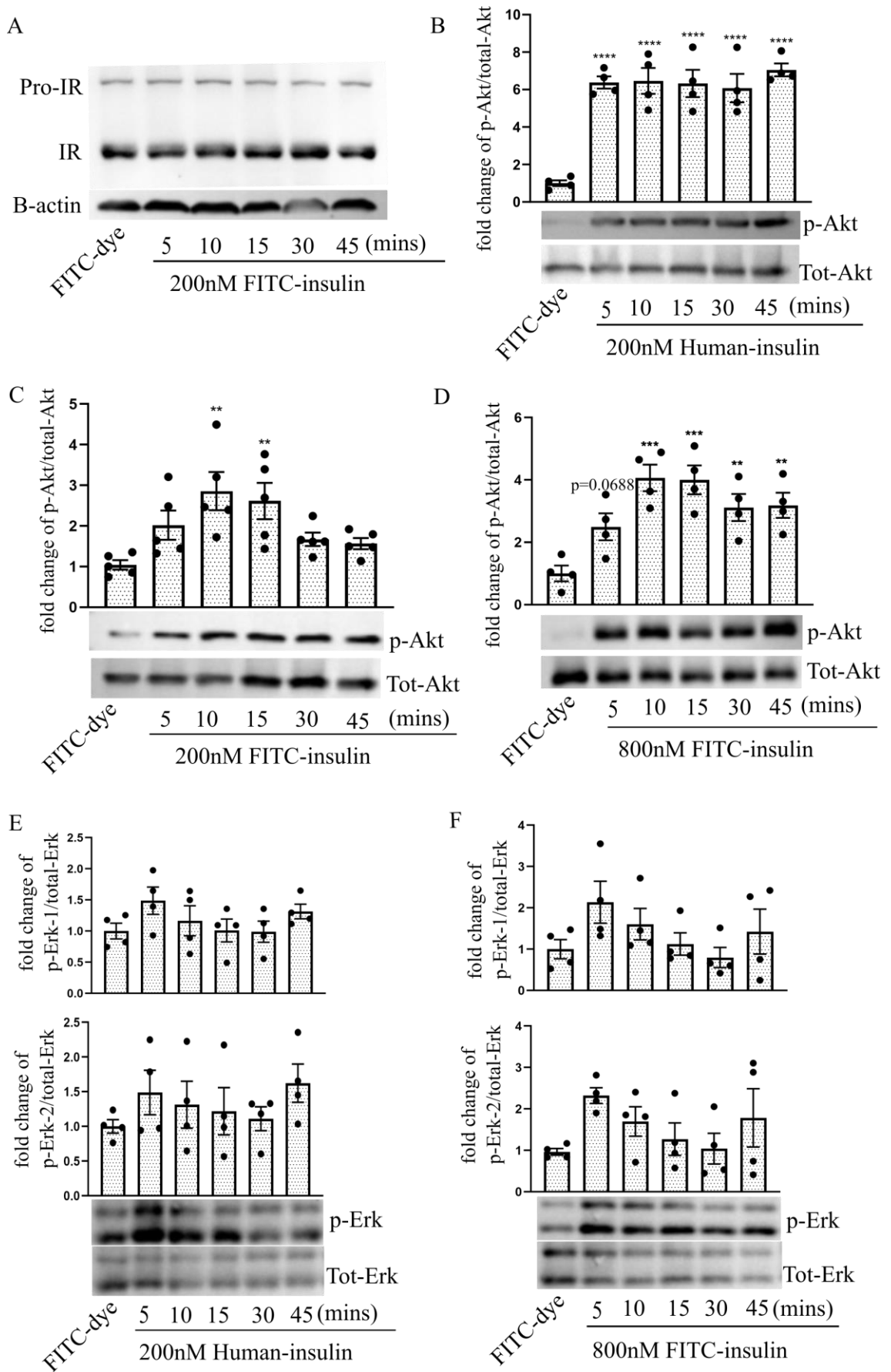
Figure 4. 1 FITC-insulin activates AKT in PC12 cells. (A) Insulin receptor (IR) levels

in PC12 cells after different incubation times with 200 nM FITC-insulin. (B) Phosphorylation levels of Akt on Ser473 after human insulin (200 nM) treatment at different time points. (C-D) Phosphorylation levels of Akt on Ser473 after low FITC-insulin (200 nM) concentration and high FITC-insulin (800 nM) concentration treatment at different time points. (E) Phosphorylation levels of ERK 1/2 (Thr202/Tyr204 and Thr185/Tyr187) after human insulin (200 nM) treatment at different time points. (F) Phosphorylation levels of ERK 1/2 (Thr202/Tyr204 and Thr185/Tyr187) after FITC-insulin (800 nM) treatment at different time points. Data are shown as mean ± SEM, n=4 samples. Data were normalized by the total proteins and the fold changes relative to FITC-dye were shown. Ordinary one-way ANOVA, Dunnett's multiple comparisons test. **$p<0.01$, ***$p<0.001$, ****$p<0.0001$.

4.3.2 FITC-insulin enters the nucleus in PC12 cells

We next examined how FITC-insulin enters PC12 cells. Cells were incubated with FITC-insulin for different times, then cells were fixed with PFA and FITC-insulin binding was detected using a confocal microscope (as previously described in section 2.2.2). No florescence was detected in cells incubated with FITC-dye (Figure 4.2 B), on the other end, FITC-insulin was able to bind the cell membrane within 5 mins treatment (Figure 4.2 B). More cells bind to FITC-insulin with incubation time (Figure 4.2 C, D), and FITC-insulin fluorescent signal in PC12 cells reached the highest intensity at 20 mins and decreased after 30 mins (Figure 4.2 E-G).

Notably with treatment between 5 to 10 mins, around 50% of cells presented membrane localization, while 20-30% had cytosolic localization and around 25% of cells presented nuclear staining (Figure 4.3 A-B). Starting from 15 mins incubation insulin was mainly localised between the cytosol and the nucleus, with the majority of the cells (~95 %) presenting nuclear localization (Figure 4.3 A-B). Overall, these data indicate that FITC-insulin can be internalized after binding to the receptors on the plasma membrane and also be transported into the nucleus.
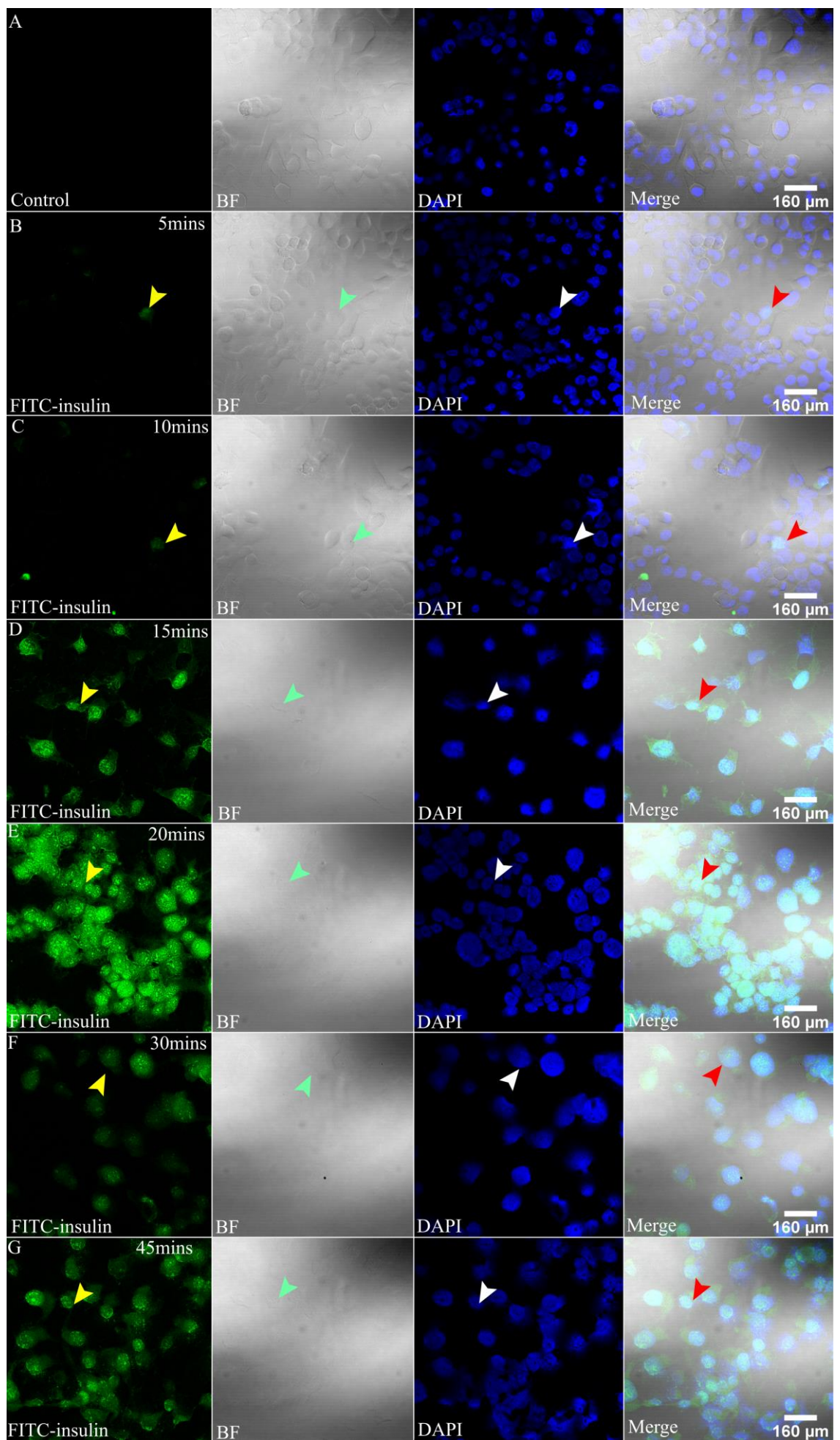
Figure 4. 2 The dynamics of FITC-insulin in PC12 cells. PC12 cells were incubated with FITC-insulin (800 nM) for different durations, control cells were incubated with FITC-dye only (A-G). Yellow arrows indicate FITC-insulin positive cells, green arrows indicate cells under bright field, white arrows indicate Dapi and red arrows indicate FITC-insulin colocalized with the nucleus.
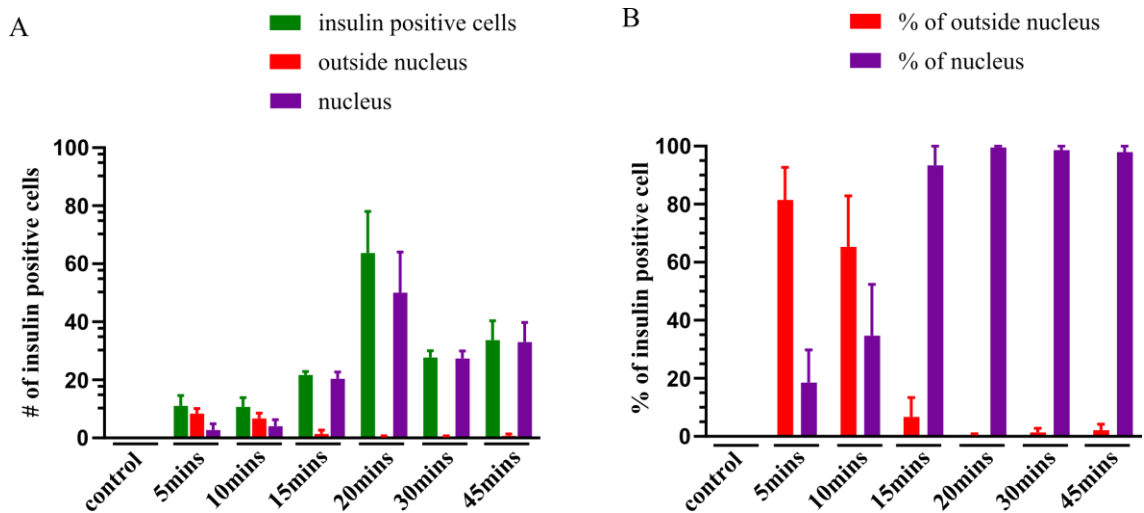
Figure 4. 3 The quantification of FITC-insulin entering in PC12 cells. (A) shows the number of FITC-insulin positive cells at different time points. (B) shows the ratio of FITC-insulin location in outside nucleus and nucleus.. Data are expressed as the mean ± SEM (Standard Error of Mean) (For each treatment, total three areas were imaged and analysed from duplicate biological experiments).

4.3.3 The internalization of FITC-Insulin is mediated by insulin receptors

As the previous section described, insulin binds to the cell membrane and is rapidly internalized and translocated to the nucleus. Here, to validate whether insulin receptors are required for insulin nuclear internalization, we knocked down insulin receptors in PC12 cells by co-transfecting pacAd5CMV-CRECFP and pacAd5CMV-ShIR-tdTomato plasmid. pacAd5CMV-ShC-tdTomato plasmid was as control (as described in section 2.2.4). Forty-eight hours post-transfection, PC12 cells were incubated with FITC-insulin for 15 mins, the time point at which insulin has its maximal effect (Figures 4.1 and 4.3). Our results indicated that there were around 80%-85% FITC-insulin positive cells after 15 mins incubation in the control group (Figure 4.4 A, D), while its binding was

significantly inhibited in the insulin receptor knockdown group (only around 14% FITC-insulin positive cells) (Figure 4.4 C, D). In contrast, FITC-insulin was not affected in pacAd5CMV-ShC-tdTomato control group (Figure 4.4 B, D). Our results also suggested that the transfection efficiency had no significant difference between pacAd5CMV-ShIR-tdTomato plasmid and pacAd5CMV-ShC-tdTomato control group (Figure 4.4 E). Notably, 76% tdTomato positive cells colocalized with FITC-insulin positive cells in nucleus in the control group, however, there were only 7.4% in insulin receptor knockdown group (Figure 4.4 F) that colocalised with FITC-insulin. These results indicated that insulin receptor is essential for FITC-insulin's internalization in PC12 cells.
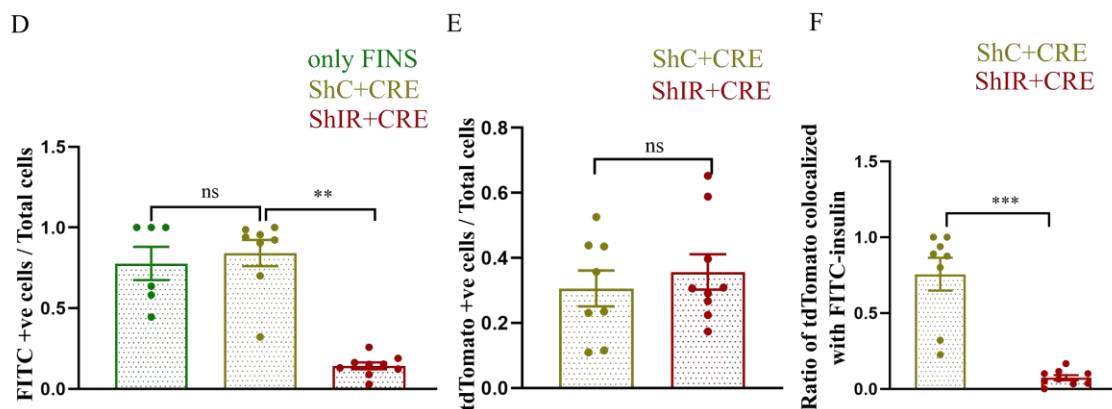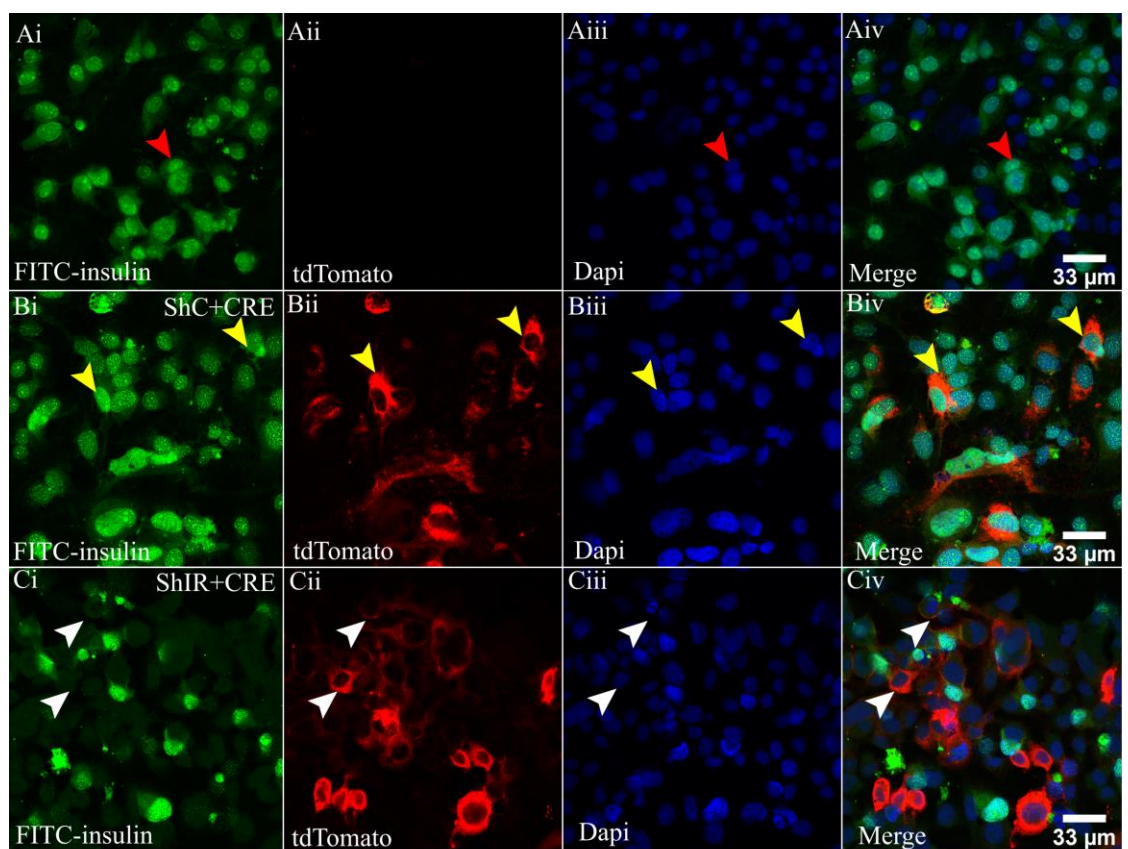
Figure 4. 4 Insulin receptor is essential for FITC-insulin internalization in PC12 cells. (A) Cells only were incubated with 800 nM FITC-insulin for 15 mins. (B) Cells were transfected with pacAd5CMV-CRECFP and pacAd5CMV-ShC-tdTomato plasmid, and then incubated with 800 nM FITC-insulin for 15 mins. (C) Cells were transfected with pacAd5CMV-CRECFP and pacAd5CMV-ShIR-tdTomato, and then incubated with 800 nM FITC-insulin for 15 mins. (D) shows the ratio of FITC-insulin to the total cell numbers in three groups, respectively. 'ShC+ CRE' presents cells co-transfected with pacAd5CMV-CRECFP and pacAd5CMV-ShC-tdTomato plasmid; 'ShIR + CRE' presents cells co-transfected with pacAd5CMV-CRECFP and pacAd5CMV-ShIR-tdTomato. Ordinary one-way ANOVA was performed. **$p<0.01$. (E) The ratio of cells expression of tdTomato to the total cell numbers in 'ShC+ CRE' and 'ShIR + CRE' group. (F) The ratio of tdTomato positive cells colocalized with FITC-insulin positive cells in 'ShC+ CRE' group and 'ShIR + CRE' group. Data are expressed as the mean ± SEM. Nonparametric t-test was performed. ***$p<0.001$. (n=6-9). Red arrows indicate FITC-insulin colocalized with the nucleus in the group only incubated with FITC-insulin (only FINS). Yellow arrows indicate FITC-insulin colocalized with tdTomato in 'ShC+ CRE' group. White arrows indicate cells express tdTomato but without FITC-insulin binding in the nucleus in the 'ShIR + CRE' group.

4.3.4 Insulin receptors were detected in the hippocampus, brainstem, olfactory bulb and cerebellum and the HDB in acute mouse brain slices

To further identify the areas of the brain where the insulin receptor is present, FITC-insulin was used to incubate with acute mouse brain slices (as previously described in section 2.3.3). In order to discard dead cells, a Dye 594 Alexa was used that would be absorbed and retained only by dead cells (Kitamura et al., 2008). The results show that only live cells absorb FITC-insulin, while not all live cells were labelled with FITC-insulin (Figure 4.5). It is probably because there are different types of neuron populations, and some of them lack insulin receptors. It probably also because that some insulin bind to insulin receptors on the surface of cell and then carry the insulin into nucleus so that cell show no insulin signal. According to the data in Figure 4.4, cells positive for FITC-insulin would have the insulin receptors. Here, intense insulin labelling was observed in brain regions such as the hippocampus and brainstem (Figure 4.5). FITC-insulin signal was abundantly detected in the CA1 (Figure 4.5 Ai),

CA3 (Figure 4.5 Aii) and dentate gyrus (DG) (Figure 4.5 Aiii) of the hippocampus. Besides, nucleus tractus solitaries (NTS) of brainstem (Figure 4.5 Bi) also showed the most intense fluoresce signals. It is worth noting that FITC-insulin signal was also detected in the glomerular and mitral cell layers of the olfactory bulb (Figure 4.6 A), the Purkinje cell layer of cerebellum (Figure 4.6 B) and the horizontal diagonal band of Broca (HDB). Our data demonstrate that using FITC-insulin seems to be a viable tool to identify insulin-sensitive regions in the brain. Nonetheless, to reinforce this argument, we suggest conducting future studies utilising immunofluorescence methods that specifically target the insulin receptors. This would facilitate the elucidation of the exact co-localization patterns of FITC-insulin with insulin receptors in specific brain regions, thus contributing to a more comprehensive understanding of its utility and specificity in delineating insulin sensitivity within the central nervous system.
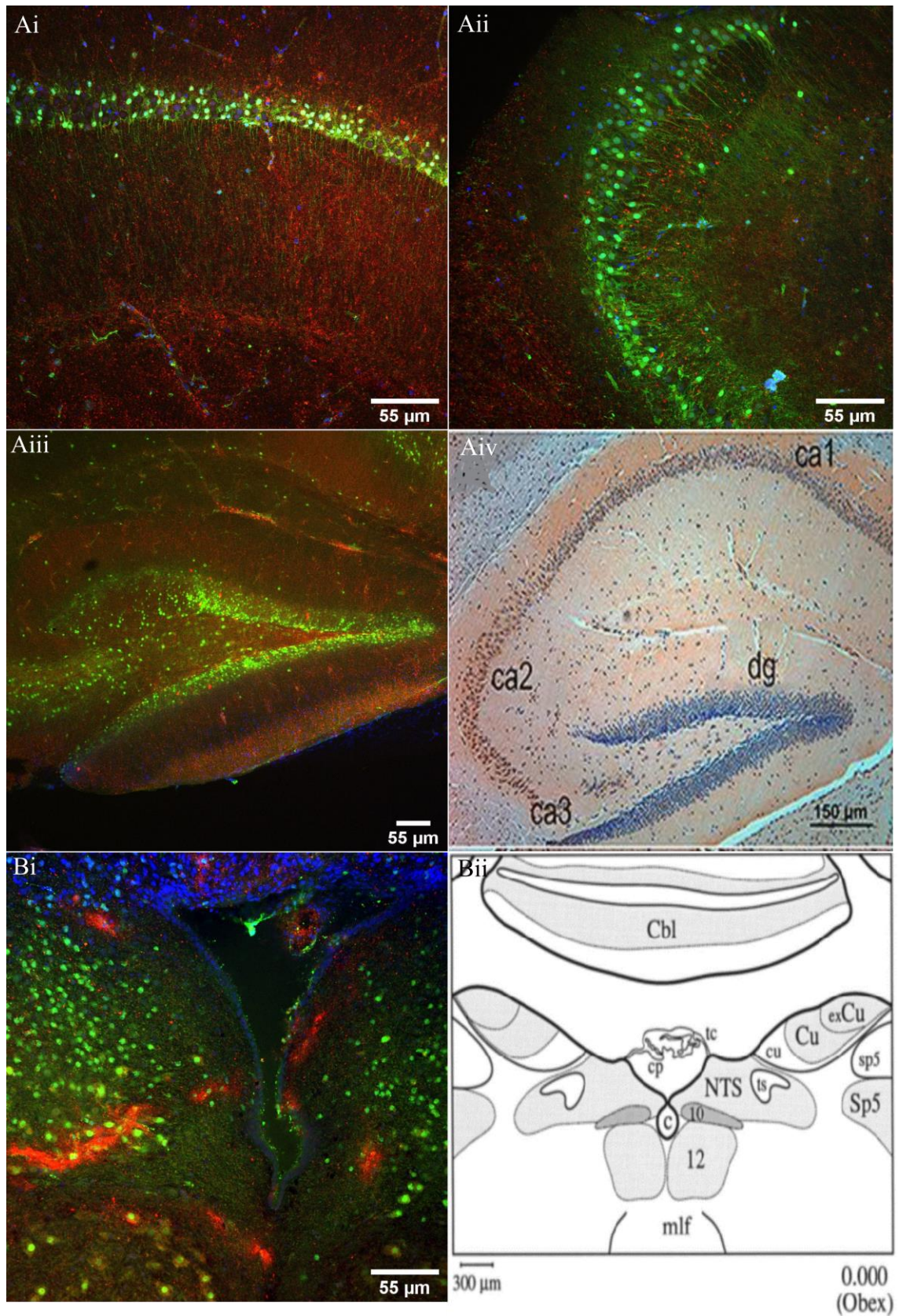
Figure 4. 5FITC-insulin in the hippocampus and brainstem of mouse brain acute slice. (Ai) to (Aiii) to show C1, C3 and dentate gyrus of hippocampus, respectively. (Aiv) to show the anatomical structure of hippocampus (Jia et al., 2017). (Bi) to shown

FITC-insulin in the brainstem. (Bii) cited from *An Atlas of the Rat Subpostremal Nucleus ractus Solitarius.* Dye 594 Alexa (red) indicate dead cells, Dapi (blue) and FITC-insulin (green). Two mice were observed in this study.
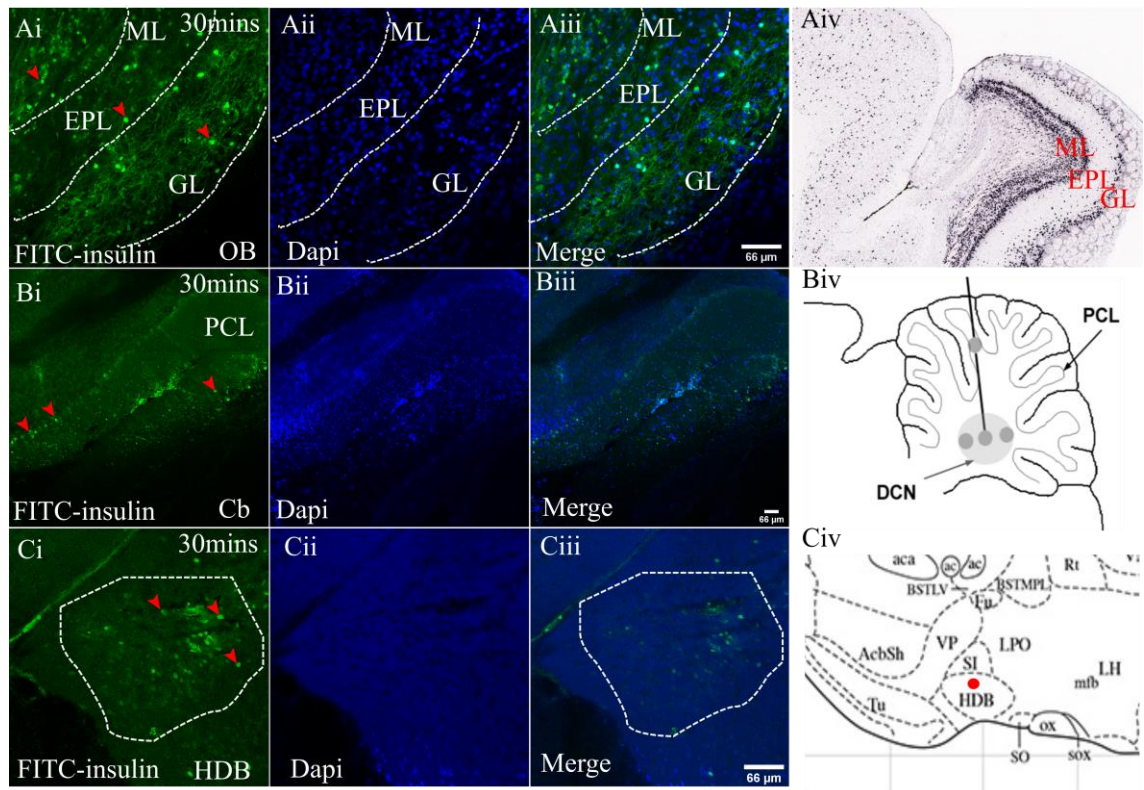
Figure 4. 6 FITC-insulin was taken by the olfactory bulb and cerebellum of C57BL/6 mice brain after 30 mins. (A) FITC-insulin in different layers of olfactory bulb (OB) of C57BL/6 mice brain. GL: glomerular layer; ML: mitral cell layer. (Aiv) to show the structure of the OB. (B) FITC-insulin in the cerebellum lobes. DCN: Deep cerebellar nuclei of the cerebellar cortex. PCL: Purkinje cell layer. Cb: cerebellum. (C) FITC-insulin in the horizontal diagonal band of Broca (HDB). Blue (Dapi), Green (FITC-insulin), Red arrows to show FITC-insulin. Three mice were observed in this study.

4.3.5 FITC-insulin activates p-Akt in acute slices of the mouse hippocampus

FITC-insulin signal was detected in various brain regions, including the hippocampus, brainstem, olfactory bulb, cerebellum and the HDB. Next, to determine whether FITC-insulin could activate insulin signalling in brain tissue, it was incubated with acute brain slices of the hippocampus for 15 mins and 30 mins, respectively, then the insulin downstream signalling, p-Akt, was detected. As expected, there is no detectable FITC signal in the FITC-dye and human insulin group either at 15 mins or 30 mins incubation (Figure 4.7 A and 4.8 A). Interestingly, there are some basal p-Akt expression even under FITC-dye treatment. This observation can be attributed to the absence of an overnight fasting period for the mice used in our study. Consequently, there was a certain degree of basal insulin secretion following their food intake, which likely accounts for the observed basal p-Akt expression. This finding highlights the significance of considering the physiological state of the animals under investigation, as the endogenous insulin secretion in response to feeding can potentially influence the activation of Akt signalling pathways in the brain. P-Akt positive cell numbers have no difference between FITC-insulin, standard human insulin and FITC-dye groups under 15 mins incubation (Figure 4.7 E) unlike in PC12 cells (Figure 4.1 C,D). While p-Akt was activated by both FITC-insulin and human insulin compared to FITC-dye at 30 mins (Figure 4.8 E). Notably, p-Akt seems to be activated by FITC-insulin in an indirect manner, since there are few colocalization between FITC-insulin and p-Akt (Figure 4.7, 4.8).
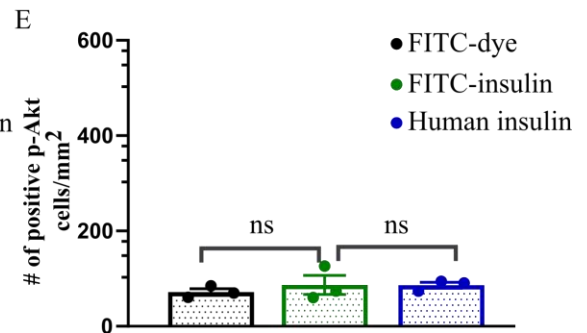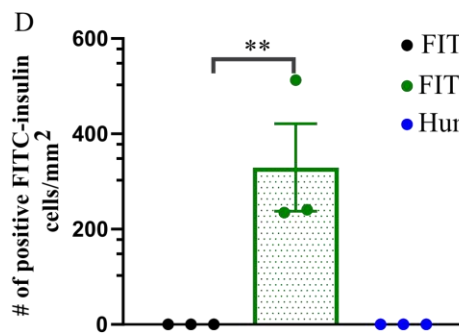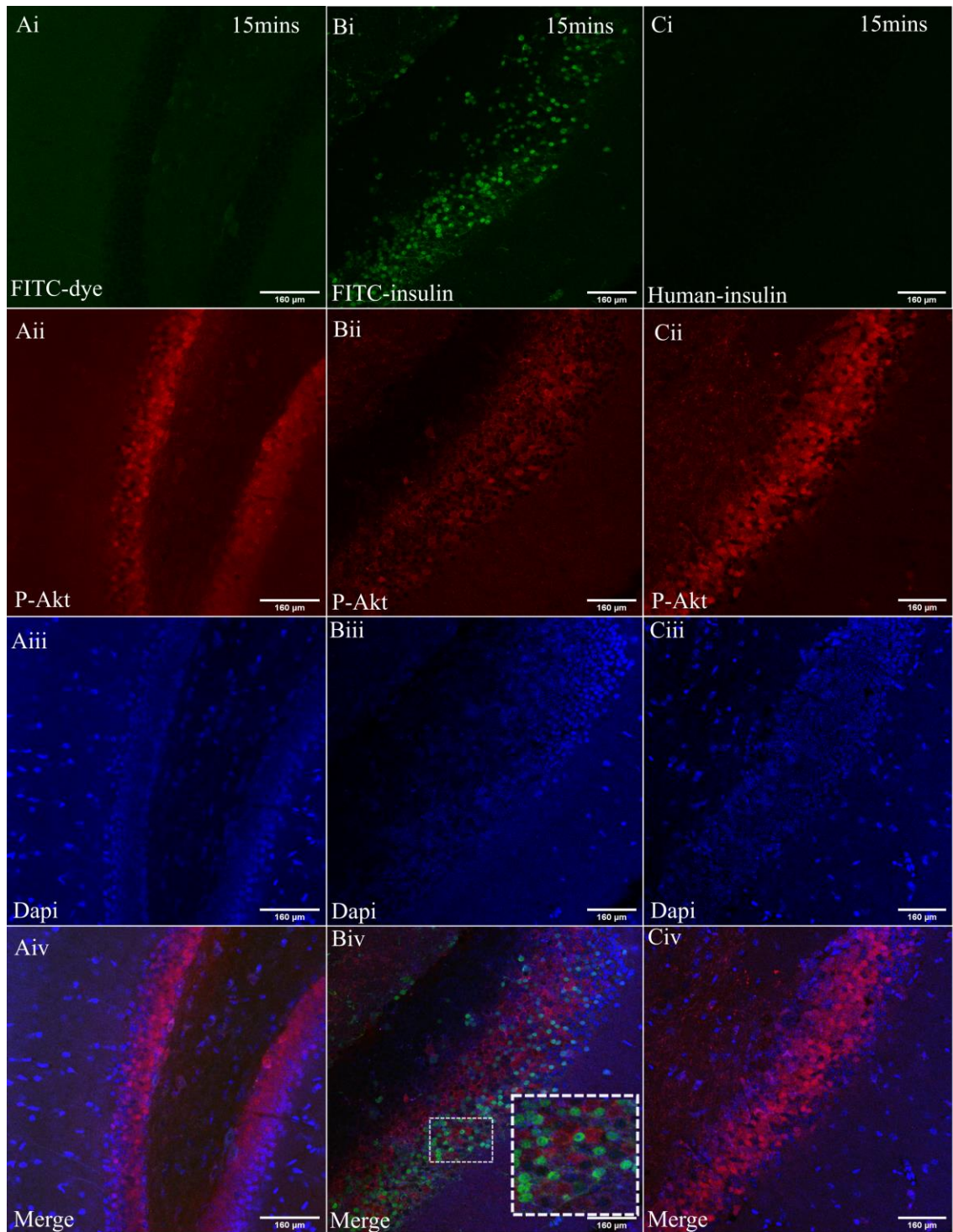
Figure 4. 7 Insulin was taken by hippocampus of C57BL/6 mice brain after 15 mins incubation. Acute slices incubated with equal concentration of FITC-dye (A), FITC-insulin (green) (B), and human insulin (200 nM) (C) for 15 mins, then co-stained with p-AKT (red) and Dapi (blue). White square is to show FITC-insulin enters into the cytoplasm instead of nuclei. (D) Cell number of positive FITC-insulin in each group. (E) Cell number of positive p-Akt in each group. N=3 from three different mice brain. Ordinary one-way ANOVA, Dunnett's multiple comparisons test was performed, $**p<0.001$.

Ai — FITC-dye — 30mins
Bi — FITC-insulin — 30mins
Ci — Human-insulin — 30mins
Aii — P-Akt
Bii — P-Akt
Cii — P-Akt
Aiii — Dapi
Biii — Dapi
Ciii — Dapi
Aiv — Merge
Biv — Merge
Civ — Merge

D
# of positive FITC-insulin cells/mm²

● FITC dye
● FITC insulin
● Human insulin

E
# of positive p-Akt cells/mm²

● FITC dye
● FITC insulin
● Human insulin
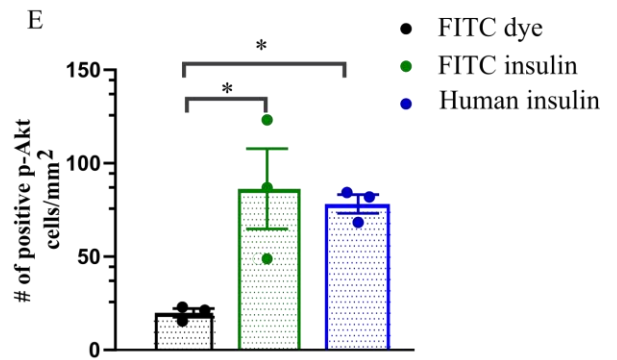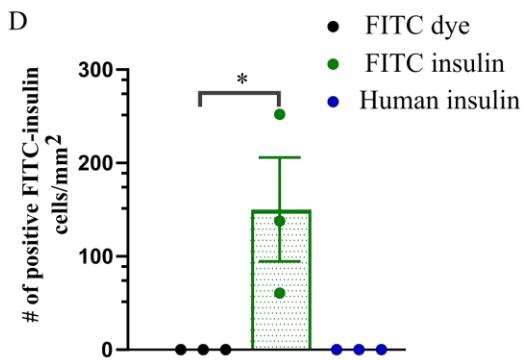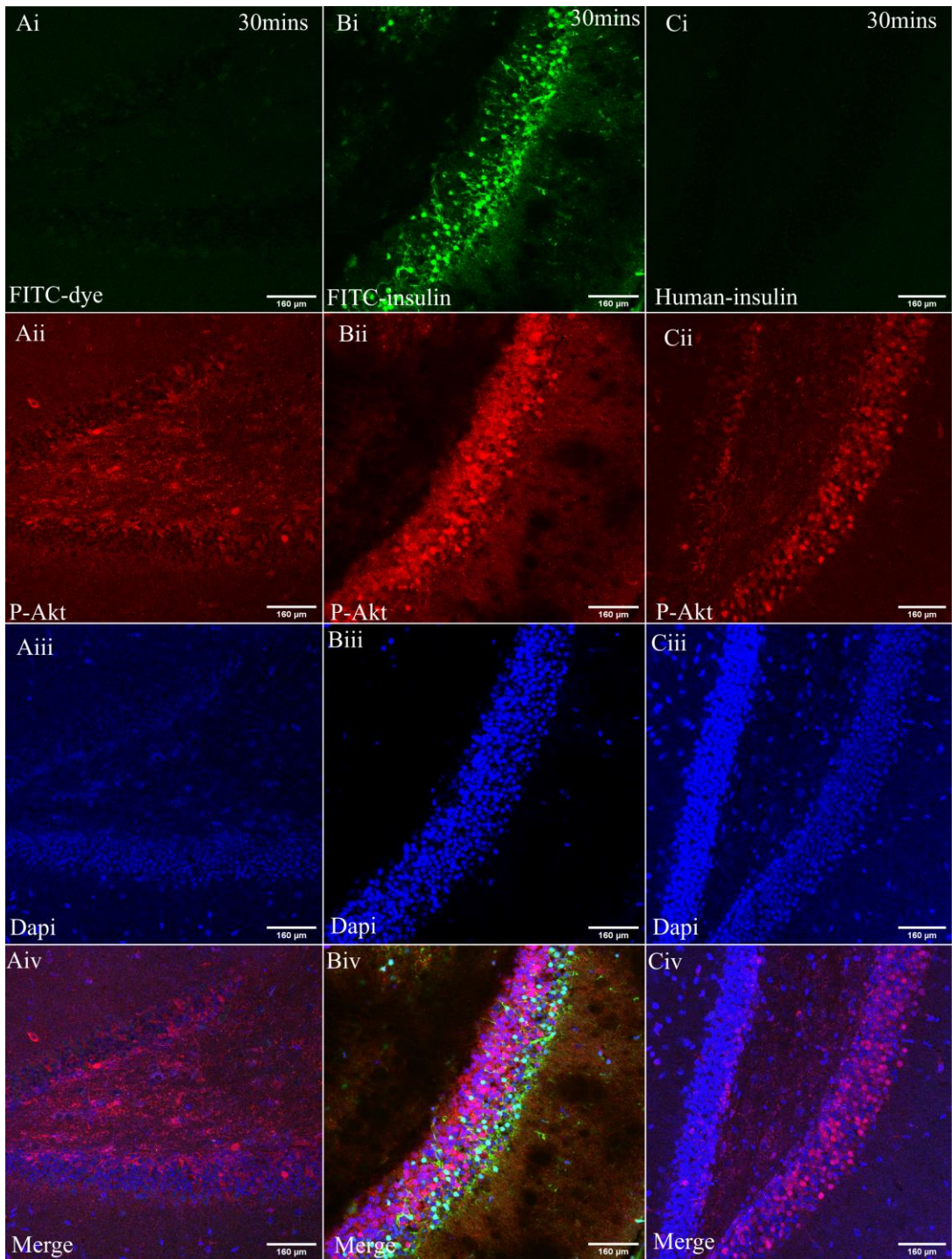
Figure 4. 8 P-Akt was activated by insulin after 30 mins incubation in hippocampus of C57BL/6 mice brain. Acute slices incubated with equal concentration of FITC-dye (A), FITC-insulin (green) (B) and human insulin (200 nM) (C) for 30 mins, then co-stained with p-Akt (red) and Dapi (blue). (D) Cell number of positive FITC-insulin in each group. (E) Cell number of positive p-Akt in each group. N = 3 from three different mice brain. Ordinary one-way ANOVA, Dunnett's multiple comparisons test was performed, $*p<0.05$.

4.3.6 Intranasal FITC-insulin tracing revealed specific binding of insulin to neurons in various brain regions

Having demonstrated the FITC-insulin is a viable way to characterise insulin receptor positive cells in different brain regions and also were able to activate insulin downstream signalling, we decided to deliver it intranasally in order to track where it spreads in the mouse brain. FITC-insulin was injected into a single nostril of mice. In our experimental approach, FITC-insulin was administered through a single nostril in mice. After 30 mins, most of the FITC-insulin remained localized within the olfactory bulb, with no discernible labelling observed in other regions of the brain. While at 60 minutes after application, showed only faint labelling in comparison. Considering these findings, we decided to select a 40 mins interval for our intranasal application studies. This choice was made to strike a balance between the localization of FITC-insulin within the olfactory bulb and its distribution to other brain areas, thus optimizing the experimental conditions for our investigation. After 40 mins, mice were cardiac perfused and fixed. After 40 mins, mice were cardiac perfused and fixed. Serial sagittal sections were prepared for either directly examining green fluorescence bindings by fluorescent microscopy or combined with IHC for further identification. The results showed that FITC-insulin was widely distributed in the brain. We found that the olfactory bulb (Figure 4.9 B) and HDB (Figure 4.9 C) presented the most intense fluorescent signals, while other regions such as hippocampus and brainstem showed faint but detectable signals (Figure 4.9 D, E).

ChAT is widely used as a marker in the HDB (Rao et al., 1987; Rye et al., 1984). ChAT was expressed in the cytoplasm and overlapped with FITC-insulin signal (Figure 4.9). Our results indicate that FITC-insulin colocalized with ChAT in the HDB, brainstem

and hippocampus (Figure 4.9 C, D, E). Interestingly, from the quantification results, the HDB area is the second high intensity of insulin-positive region and there are around 38.9% insulin-positive cells are colocalized with cholinergic neurones, which imply intranasal insulin could target both cholinergic neurons and non-cholinergic neurons in the brain. On the other hand, even though there are a few insulin positive signalling in the hippocampus (around 1.25 insulin positive cells per mm^2) and brainstem (around 14.4 insulin positive cells per mm^2) were detected compared with the olfactory bulb (around 1107 insulin positive cells per mm^2) and the HDB areas (around 307 insulin positive cells per mm^2), the insulin positive cells in the brainstem highly colocalized with cholinergic neurones (around 87%) (Figure 4.9 F, G).

To identify if FITC-insulin binds to other cell populations, NeuN and GFAP antibody were applied in our study. NeuN was used to identify mature neurones, which is mainly located in nuclei but also in cytoplasm (Mullen et al., 1992; Van Nassauw et al., 2005). Our results show that FITC-insulin colocalized with NeuN in the olfactory bulb (OB), and NeuN predominantly expressed in the glomerular layer (Figure 4.10 A). In addition, we also observed that FITC-insulin colocalized with astrocytes and other glial cells, which was characterised by GFAP antibody (Figure 4.10 B). Altogether, our data suggested that both neurons and astrocytes express insulin receptors in the olfactory bulb (Figure 4.10). It would be interesting to determine whether also in other brain areas insulin FITC-insulin can colocalize with neurons and astrocytes. Furthered experiments will be needed.
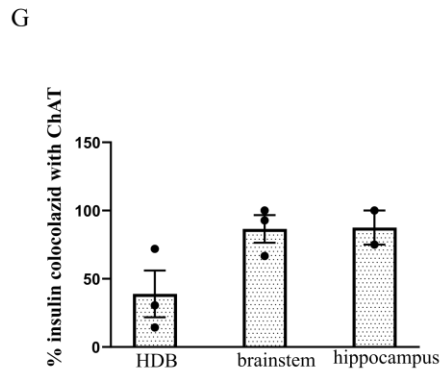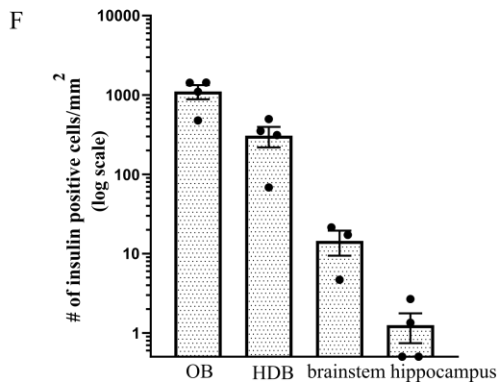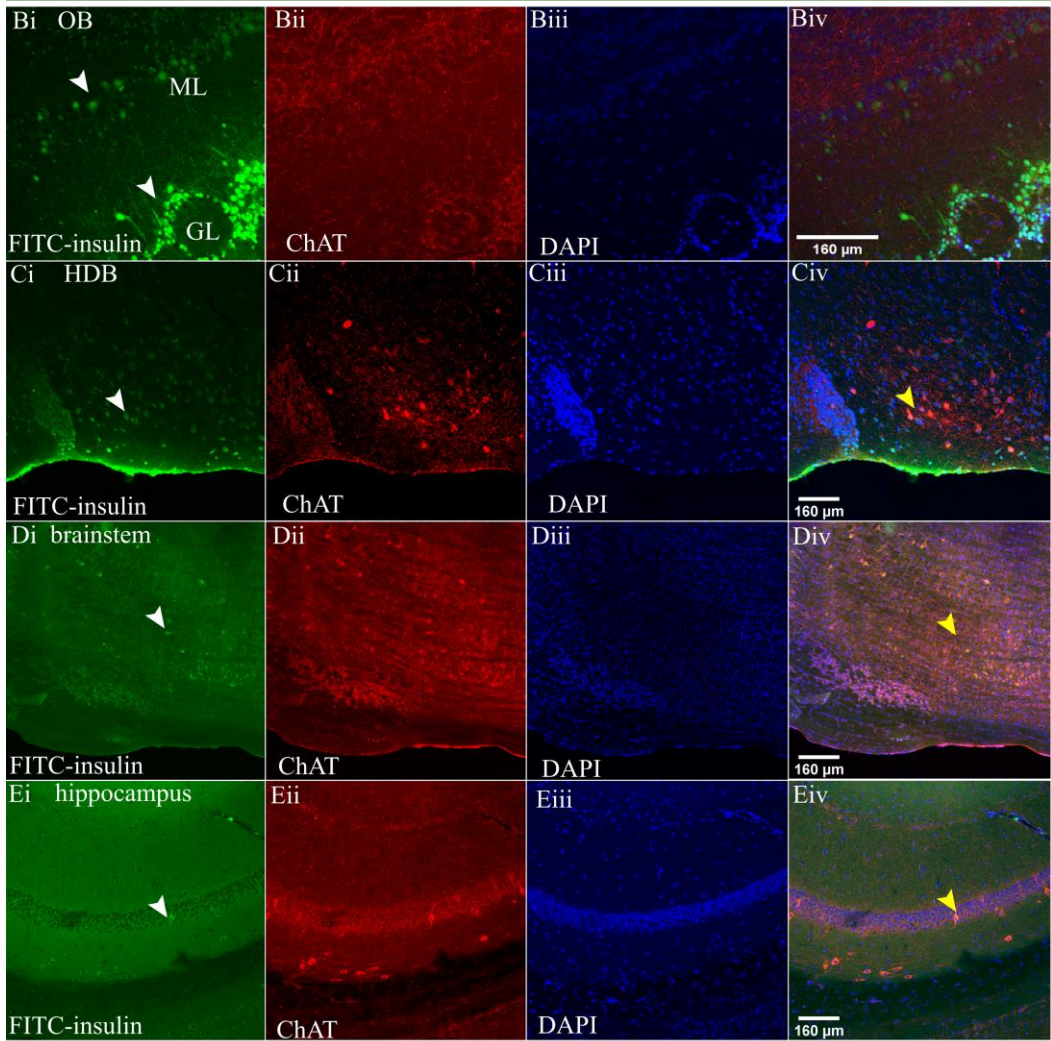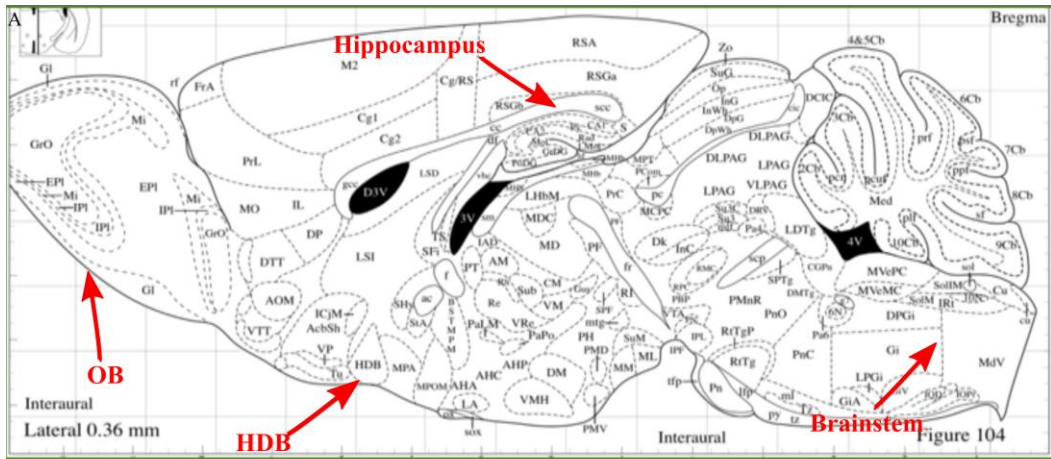
Figure 4. 9 The distribution of intranasal FITC-insulin in C57BL/6 mice brain. (A) Referenced from the Mouse Brain in Stereotaxic Coordinates to different brain areas. (B) FITC-insulin in different layers of olfactory bulb (OB) of C57BL/6 mice brain. GL: glomerular layer; ML: mitral cell layer. (C-E) FITC-insulin in the HDB, brainstem and hippocampus of C57BL/6 mice brain, respectively. ChAT immunohistochemistry (red), FITC-insulin (green), DAPI (blue). White arrows indicate FITC-insulin. Yellow arrows indicate FITC-insulin colocalized with cholinergic neurons. Data are expressed as the mean ± SEM (n=4).
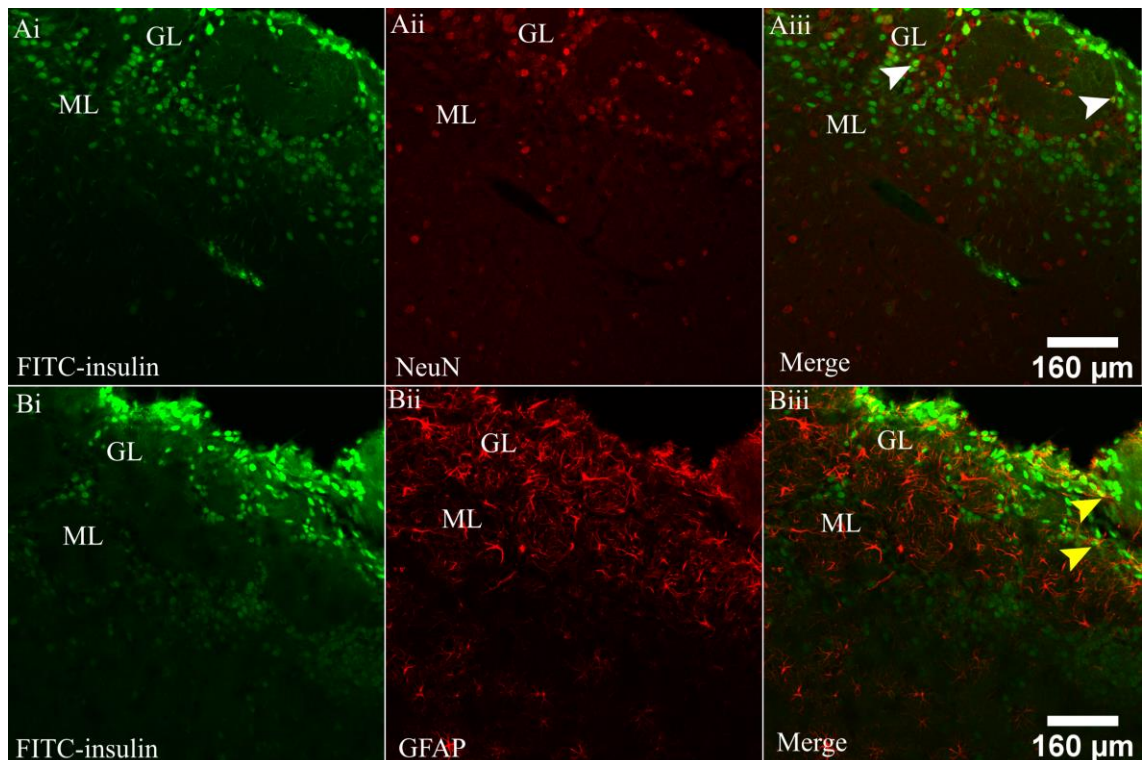
Figure 4. 10 Intranasal FITC-insulin binds with both neurons and astrocytes in the olfactory bulb of C57BL/6 mice brain. (A) White arrows show FITC-insulin (Green) colocalized with NeuN (Red) in the OB. (B) Yellow arrows show FITC-insulin (Green) colocalized with GFAP (Red) in the OB. GL: glomerular layer; ML: mitral cell layer.

4.3.7 Dopaminergic, GABAgeric and cholinergic neurons were detected in the HDB using acute mouse brain slices

The HDB is a non-canonical central region in regulating feeding behaviour (Herman et al., 2016). Next, in order to determine the neuronal cell types in the HDB, brain slices were co-stained with several antibodies. The results show that the HDB contains dopaminergic or noradrenaline neurons, which are marked by tyrosine hydroxylase (TH) (Figure 4.11 Ai-Avi). In addition, FITC-insulin was taken up by TH positive neurons, cholinergic neurons and neurons co-expressing both TH and ChAT (Figure 4.11 Ai-Avi).

On the other hand, there are around 35% insulin positive cells are GABAergic neurons, about 25% insulin positive cell are both GABAergic neurons and Cholinergic (Figure 4.11 Bi-Bv, C). While there are more than 74% FITC-insulin positive cells were colocolized with cells that are neither noradrenaline neurons nor cholinergic neurons and GABAergic (Figure 4.11 C), which implies that the majority of neuronal populations could express insulin receptors in the HDB that are still not known.
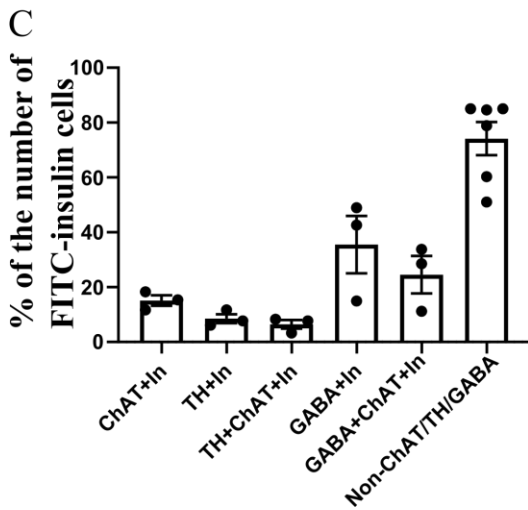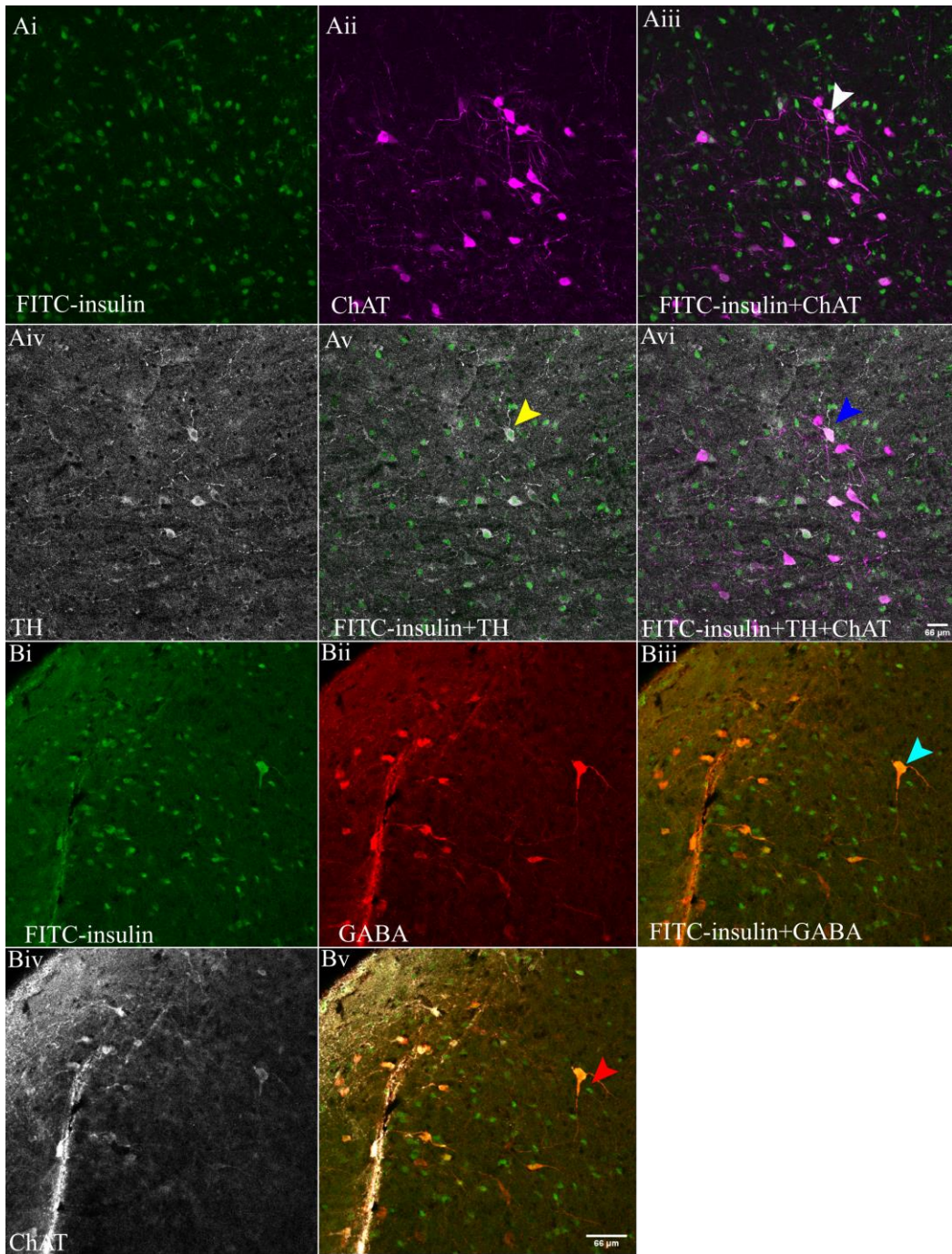
Figure 4. 11 FITC-insulin was taken by dopaminergic, GABAgeric and cholinergic neurons in the HDB. (A) C57BL/6 mice acute slices incubated with FITC-insulin (green) for 30 mins, then co-stained with ChAT-antibody (magenta) and TH-antibody (gray). White arrow indicates FITC-insulin colocalized with cholinergic neurons. Yellow arrow indicates FITC-insulin colocalized with dopaminergic neurons. Blue arrows indicate FITC-insulin was taken up by neurons co-expressing TH and ChAT. (B) Vgat-cre-Gcamp6f mice acute slices incubated with FITC-insulin (green) (200 nM) for 30 mins, then co-stained with ChAT-antibody (gray) and GFP-antibody (red), which indicates GABAgeric neurons. Cyan arrow indicates FITC-insulin colocalized with GABAgeric neurons. Red arrows indicate FITC-insulin was taken up by neurons co-expressing GABAgeric and ChAT. (C) The quantification of different cell types. Data are expressed as the mean ± SEM (Standard Error of Mean) (n=3 mice).

4.4 Discussion

We have demonstrated that FITC-insulin is a viable tool to study the distribution of insulin sensing cells in the brain (Figure 4.1, Figure 4.9 and Figure 4.11). 200 nM human insulin could rapidly activate p-Akt at 5 mins while the same concentration of FITC-insulin activated p-Akt from 10 mins to 15 mins and its effect decreased after 30 minutes. In our comparative analysis between human insulin and FITC-insulin, we observed that a higher concentration of FITC-insulin was required to elicit p-Akt activation after a 30-minute duration. This discrepancy can be attributed to the fact that one mole of FITC-insulin is composed of a mixture of mono-, di-, and tri-conjugated FITC molecules. This implies that an equal mole of FITC-insulin may not possess the same insulin composition as standard human insulin. In light of these findings, we propose that special attention should be given to the molecular weight of FITC when conducting experiments involving FITC-insulin applications. The presence of multiple FITC molecules per mole in FITC-insulin may influence its physiological behaviour and subsequently affect the activation of downstream signalling pathways, such as p-Akt activation. Therefore, accounting for the molecular weight of FITC is crucial in designing and interpreting experiments involving FITC-insulin to ensure accurate and meaningful results.

Notably, FITC-insulin just as human insulin significantly activated p-Akt pathway

instead of p-Erk in PC12 cells, which might because that insulin p-Akt pathway involved in hypothalamus-mediated glucose utilization (Obici et al., 2002b), while p-Erk pathway is essential in dorsal vagal complex-mediated glucose homeostasis (Figure 4.1) (Filippi et al., 2012).

Our *in vitro* work suggested that localisation of FITC-insulin is dynamic being translated from the cell surface to the nucleus. In the beginning, FITC-insulin localised mostly on the cell membrane and cytoplasm within 5 to 10 mins incubation and reached the nucleus after 15 mins. Interestingly, it was recently reported that insulin receptors, upon insulin binding, can translocate to the nucleus and directly control RNA polymerase II-mediated gene expression (Batista et al., 2019). The active insulin receptor was internalized by clathrin or caveolin mediated endocytosis, and nucleoporin 358 (Nup358) protein was involved in insulin receptor's nuclear localization (Qiu et al., 2022). Our data also suggested that FITC-insulin's binding to the cells was significantly inhibited when insulin receptor expression were attenuated, which suggested that FITC-insulin's internalization was mediated by insulin receptors, however, whether insulin receptors mediates FITC-insulin's nuclear localization still need to further study.

Translocation of insulin into the nucleus to regulate gene expression is an alternative way to canonical phosphorylation signalling cascade of insulin. It was reported that proinsulin C-peptide could enter into the nucleus and localize in nucleoli, and in this way control proliferation (Lindahl et al., 2010). And our results showed that FITC-insulin entered into the nucleus and colocolized with nuclear marker DAPI. In addition, FITC-insulin also localised to the nucleoli in PC12 cell, which are identified as a dark pocket in the nucleus after DAPI staining (Pontvianne et al., 2016). Nucleoli are involved in the synthesis of ribosomes, which is vital components in translation (Lafontaine and Tollervey, 2001). The role of insulin in the nucleoli involving in gene regulation is still unanswered. To verify that FITC-insulin colocolized with nucleoli, nucleolar marker SYTORNASelect could be applied in future experiments.

In addition, our acute slice experiment results showed that there was abundant expression of insulin receptors in the CA1, CA3 and dentate gyrus of the hippocampus and brainstem. The different layers of olfactory bulb, cerebellum and the HDB also exhibited insulin positive neurons. Our data on FITC-insulin labelling of neural populations in the hippocampus is in line with experimental evidences produced both in

mice and humans where brain insulin was shown to improve cognitive function (Chapman et al., 2018; Claxton et al., 2015a), where insulin is regarded as a neurotrophic factor that affects the development and plasticity of neurons (Chiu et al., 2008). Compare to FITC-dye, p-Akt positive cells were increased after 30 mins application of FITC insulin and human insulin in the brain regions of hippocampus, which suggested that FITC-insulin could also activate insulin signalling cascades *in vivo*-like environment and might be helpful to understand the mechanism of how insulin improves cognitive disease in the future.

Our results indicated that intranasal FITC-insulin (< 8 KDa protein) could bypass the blood brain barrier and reach various brain regions 40 mins after administration. The rapid nature of FITC-insulin-delivery into the CNS from the nasal passages (Born et al., 2002) is most consistent with FITC-insulin transport by an extracellular route along components of the peripheral olfactory and trigeminal systems (Dhuria et al., 2010). In addition, our study also indicated that the positive cell number of intranasal FITC-insulin varied in different brain regions. There was a high insulin uptake in the olfactory bulb and the HDB, followed by hippocampus and the brainstem.

Intranasal delivery results showed that there was a high FITC-insulin uptake in the mitral cell layer of olfactory bulb, which is an area of the brain involved in feeding regulation (Soria-Gomez et al., 2014; Riera et al., 2017). Similar to the canonical metabolic sensor, the hypothalamus, there is also a high density of hormone receptors in the olfactory bulb, such as insulin receptors (Marks et al., 1990), leptin receptors (Caillol et al., 2003) and ghrelin receptors (Tong et al., 2011). Mitral cells are the principal neurons of the olfactory bulb, they convey odour information to other brain regions. For example, Murata et al reported a novel area in olfactory cortex that could receive synaptic inputs from mitral cells and send inhibitory output to the lateral hypothalamus, which may modulate odour-guided lateral hypothalamus-related behaviours (Murata et al., 2019). Two cell types in the arcuate nucleus of the hypothalamus, AgRP and POMC (Konner et al., 2007) may be involved in this process. The former is activated by fasting and promotes foraging, while the latter is activated by satiety and inhibits food intake. This provided us a hypothesis that intranasal insulin might induce changes in mitral cells projecting from the olfactory bulb, transmitting olfactory information to hypothalamus to regulate appetitive behaviour. Increasing the amount of insulin in the olfactory bulb reduces the detection of odours in the rat,

thereby reducing the food search during a fed state (Aime et al., 2012). It is noteworthy that the insulin-dependent glucose transporter GLUT 4 co-localised with insulin receptor in mitral cells and glomeruli of the olfactory bulb, which implies intranasal insulin in the olfactory bulb, could also regulate glucose uptake (Al Koborssy et al., 2014). Marks et al reported that chronic intranasal insulin administration could induce phosphorylation of voltage-gated potassium channel Kv1.3 and increase olfactory discrimination in mice, but have no effect on body weight (Marks et al., 2009). Riera et al reported that ablation of olfactory sensory neurons (OSNs) can prevent diet-induced obesity, increase thermogenesis in brown adipose tissue and reduces insulin resistance, suggesting the involvement of the olfactory system in maintaining energy homeostasis (Riera et al., 2017). In addition to neurons, astrocytes could also uptake FITC-insulin in the olfactory bulb according to our study. Astrocytes conduct multiple roles in the brain, which includes inputting and/or outputting neurotransmitters and provide an interface between neurons and blood vessels (Verkhratsky and Nedergaard, 2018). Impaired insulin receptor in astrocytes compromise the response to glucose changes and reduce the expression of GLUT 1 (Garcia-Caceres et al., 2016; Simpson et al., 1999). Astrocytes mediated insulin signalling is also involved in mood and depression (Cai et al., 2018). The aforementioned evidences point out that insulin could play an important role in regulating olfactory bulb activity and controlling metabolic functions. Further studies are needed to fully understand this process.

The HDB is a major component of the cholinergic basal forebrain. It was reported that abundant mRNA expression of insulin receptors was highly restricted to the cholinergic neurons in the HDB of the rats (Tsujimoto et al., 1995). The ablation of the HDB could increase daily food intake in mice, causing hyperphagia (Herman et al., 2016). Selective knock-out of cholinergic neurotransmission from the HDB increased body mass, while activating HDB cholinergic neurons suppressed food intake *in vivo*, demonstrating that cholinergic signalling plays an important role in regulating food intake (Herman et al., 2016; Cassidy et al., 2019). Our results suggested that intranasal insulin could enter the HDB and co-localised with the cholinergic-specific marker, ChAT, which implies that the HDB may be one of the key brain areas that responds to intranasal insulin and participates in the regulation of food intake.

The HDB consists of various cell populations, including GABAergic and somatostatin neurons (Zhu et al., 2017). However, in our study we reported more cell populations,

such as dopaminergic neurons, cholinergic as well as GABAergic neurons in the HDB. Interestingly, TH-positive cells in the HDB, some of which overlapped with cholinergic neurons. Insulin could promote the release of dopamine in the nucleus accumbens (NAc) to influence food choices, and the process of dopamine release in NAc was mediated by cholinergic interneurons that express insulin receptor in striatum (Stouffer et al., 2015). Another study also showed that insulin activates Akt signalling in dopaminergic neurons of the substantia nigra (SN) (Fan et al., 2019). Understanding the relationship between TH, cholinergic neurones and other neurones might contribute to how insulin plays a role in regulating metabolism *in vivo*.

Electrical stimulation of the HDB could enhance spontaneous activity in mitral cell of olfactory bulb, which confirms that the HDB is connected with the olfactory bulb and could modulate the odour information from the olfactory bulb (Zhan et al., 2013). With prolonged odour exposure time, glomerular layer of olfactory bulb responded less to odours stimulations, a phenomenon that is called habituation. However, when basal forebrain cholinergic neurones were activated, glomerulus of olfactory bulb receiving cholinergic inputs reversed the decrease in response time to restart odour exploration (Ogg et al., 2018). Optogenetic activation of basal forebrain cholinergic neurons modulate neuronal excitability and sensory responses in the main olfactory bulb (Ma and Luo, 2012) and further change animal behaving states like habituation. Altogether, these observations imply that cholinergic activity in the HDB increases olfactory discrimination capability and further modulate foraging and eating behaviour.

There was also some fluorescence insulin in hippocampus and brainstem after intranasal administration, which corresponded to what Dhuria et al (2009) reported that intranasal insulin could enter deep brain structure like brainstem through trigeminal nerve (Dhuria et al., 2010; Lochhead et al., 2019). In our study, we also observed that there were sparse amounts of cholinergic neurons expressed in hippocampus, which is consistent with other reports (Frotscher et al., 2000; Knox and Keller, 2016; Tago et al., 1987). Obviously, FITC-insulin was uptaken more in the hippocampus and brainstem of acute mouse brain slices than that of intranasal delivering method, which could be in consequence of clearance of nasal mucosa *in vivo*. The cerebellum was previously reported to consume a large portion of glucose compared to other brain regions (Mergenthaler et al., 2013), and insulin signalling plays a curial role in this process (Peeyush et al., 2010). It was also reported that insulin receptors are abundantly

expressed in the cerebellum of human brain (Kullmann et al., 2020a; Peeyush et al., 2010), and flourescent insulin was also observed in cerebellum after delivering intranasal Alex546-Insulin in rats (Fan et al., 2019). Besides, insulin receptors in rat brains were detected by *in situ* hybridization, and the expression of insulin receptor mRNA in cerebellum was more significant compare to other brain areas (Marks et al., 1990). In our experiments, we could not detect any insulin-positive cells in the cerebellum by intranasal administration of FITC-insulin, however, some detectable FITC-insulin signal was found in the cerebellum in acute brain slice, which probably account for different experiment methods.

4.5 Conclusion

We intranasally administered FITC-insulin into the mouse to track which brain regions are sensitive to insulin. The olfactory bulb and the HDB show the most abundant insulin receptors than other caudal brain areas such as the hippocampus and brainstem. The HDB may be as the one of the potential structure where responses to intranasal insulin in regulation of feeding behaviour.

Additionally, various types of cell populations possess insulin receptors, such as neurones, astrocytes, cholinergic, GABAergic and dopamine/norepinephrine cells. Notably, insulin positive cells could co-express cholinergic, GABAergic and dopaminergic/norepinephrinergic neurones, and there exist majority of cell types we did not study that are also insulin positive.

5 Insulin signalling in the HDB regulates feeding behaviour and activity

5.1 Introduction

The basal forebrain is an area located in the medial and ventral part of telencephalon, which consists of several heterogeneous structures, including the ventral pallidum (VP), medial septum (MS), diagonal band nuclei (the HDB and VDB), substantia innominata/extended amygdala, and peripallidal regions (Bloem et al., 2014). In addition to being involved in attention (Pinto et al., 2013), learning (Harrison et al., 2016) and sleep (Xu et al., 2015a; Anaclet et al., 2015), the basal forebrain area is also implicated in regulating feeding behaviour (Cassidy et al., 2019; Herman et al., 2016). Excitatory VGlut2-expressing neurons in the basal forebrain could be activated by re-feeding or food odour stimuli (Patel et al., 2019). The inhibition of VGlut2 neurons significantly increased cumulative food intake, while activation of VGlut2 neurons caused reduced daily food intake, hypophagia, severe body weight loss, starvation and death, which might account for the basal forebrain-lateral hypothalamus (LH) circuits related to food avoidance behaviour (Patel et al., 2019).

Microinjections of GABAA receptor antagonists in the VP area resulted in increased ingestive hedonic saccharin intake in rats, while the activation of GABAA receptor in the VP area led to a suppression (Shimura et al., 2006), which suggested that GABAA receptors in the VP might be related to control feeding behaviour (Shimura et al., 2006; Taha et al., 2009). Using an optogenetic technique further confirmed that the activation of GABAergic neurons in the VP could promote food intake both in regular chow and high fat diet (Zhu et al., 2017).

In addition, several studies have investigated that VGAT neurons and glutamatergic neurons in the medial septum exert anorexic effects through governing different neuronal circuits. Sweeney et al (Sweeney and Yang, 2016) demonstrated that the activation of GABA neurons in the medial septum markedly reduced food intake in mice by inhibiting GABAergic neurons in the lateral hypothalamus, considered to be hyperphagia-inducing neurons (Navarro et al., 2016; Wu et al., 2015). In addition, activation of glutamatergic neurons in the medial septum suppressed food intake both in light and dark cycles by stimulating excitatory projections to the paraventricular hypothalamus (PVH) instead of lateral hypothalamus (Sweeney et al., 2017).

An elegant study by Herman *et al* has indicated that cholinergic neurons in the HDB are

associated with regulation of feeding behaviour (Herman et al., 2016). Specifically ablated cholinergic neurons using diphtheria toxin (DT) resulted in hyperphagia and obesity in mice (Herman et al., 2016). It was suggested that cholinergic neurons might regulate feeding behaviour and body weight by modulating the activity of POMC but not AgRP neurons in the hypothalamus (Herman et al., 2016). Retrograde tracing studies further suggested that POMC neurons received afferents from the HDB (Wang et al., 2015) and the Pomc RNA expression levels were remarkably reduced when the cholinergic neurons were abolished using diphtheria toxin in the HDB (Herman et al., 2016). Furthermore, to better understand how cholinergic neurons exert an effect on the POMC neurons, transgenetic Pomc-eYFP$^{+/-}$ mice were constructed, with POMC neurons in the mice labelled with enhanced Yellow Fluorescent Protein (eYFP) and the activity of POMC neurons could be recorded by electrophysiological methods. The results indicated that the neuronal firing activity of POMC neurons in Pomc-eYFP mice were significantly decreased when cholinergic neurons were abolished using DT in the HDB (Herman et al., 2016). Notably, the firing activity of POMC neurons were increased after administration of acetylcholine in the recording bath under the blue light stimulation, while it was diminished by a nicotinic acetylcholine receptor blockade (Wang et al., 2015). These data imply that cholinergic neurons in the HDB may mediate satiety signalling to modulate food intake.

The HDB is also the main source that sends cholinergic efferents to various brain areas (Rye et al., 1984). It has been reported that the olfactory bulb received afferents from the HDB, among them 10-20% are ChAT-positive (Rye et al., 1984). In the hippocampus, there are around 35-45% cholinergic efferents that come from the HDB (Rye et al., 1984). In an earlier report, Záborszky et al showed that only about 17% of the neurons in the medial septum are cholinergic, which were mainly concentrated in the HDB (Zaborszky et al., 1986). Various neurotransmitters were discovered in the HDB (Villar et al., 2021), and cholinergic and no-cholinergic neurons were reported to co-express in the HDB (Herman et al., 2016). While cholinergic neurons appeared to be strong modulators of food intake, how other cells types in the HDB influence feeding and if other brain circuits or neuronal signalling involved in modulating this process is still elusive.

Fortunately, the development of fMRI contribute to the understanding how different brain regions respond to food intake. fMRI results reported by Heni *et al* indicated that

hypothalamic neuronal activity was reduced in lean men after glucose and food stimuli (Heni et al., 2014a), while the inhibitory response was not observed in insulin resistant, obese (Matsuda et al., 1999) and diabetic subjects (Vidarsdottir et al., 2007), which suggested that glucose could induce signal responses in an specific brain area. Further research on intranasal insulin demonstrated that an increased insulin level in the brain was responsible for the changed neuronal activity in the hypothalamic area, that is associated with food reward (Kullmann et al., 2013; Kullmann et al., 2015b). In addition to the hypothalamus, other eating-related brain areas such as brainstem and striatum also were involved in an insulin-induced neuronal activity response (Kullmann et al., 2015a).

Insulin signalling in the CNS is involved in regulating food intake (Carlson et al., 2003), body weight (Carlson et al., 2003), energy balance (Filippi et al., 2012), fat deposition (Carlson et al., 2003) and blood glucose levels (Obici et al., 2002b; Pocai et al., 2005b; Varela and Horvath, 2012). Rodent studies further suggested that many neuronal populations including NPY neurons, POMC neurons, astrocytes, GABAergic and glutamatergic neurons are the targets of insulin action to regulate metabolic homeostasis (Loh et al., 2017; Varela and Horvath, 2012; Gonzalez-Garcia et al., 2021; Evans et al., 2014). Given that insulin receptor were also expressed in the HDB (Schulingkamp et al., 2000) and our results from the previous chapter also demonstrated that insulin positive cells highly accumulated in the HDB by intranasal insulin administration (as described in section 4.3.6). However, the relationship between insulin signalling in the HDB and metabolism has not yet explored. Here our hypothesis is that insulin signalling in the HDB may be involved in mediating metabolism, food intake and energy balance.

5.2 Aims

(1) To determine if insulin receptors in the HDB has a physiological role in influencing food intake and body weight in rats.
(2) To explore whether there is a sex difference in how insulin signalling in the HDB regulates metabolism.
(3) To determine if knockdown of insulin receptors in the HDB influences peripheral metabolism of the liver and BAT.
(4) To investigate if knockdown insulin receptors in the HDB results in behaviour

change.

(5) To identify the potential neuronal circuits interacting with the HDB to regulate metabolism.

5.3 Results
5.3.1 Insulin signalling in the HDB is involved in regulating feeding behaviour

It has been shown that the basal forebrain is involved in regulating food intake in mice, and which cholinergic neurons are closely associated with this process (Herman et al., 2016). There are also abundant insulin positive cells in the HDB area (as presented in Figure 4.9 B). Here, to determine if insulin signalling within the HDB modulates food intake, Ad5CMV-CRECFP and Ad5CMV-ShIR-tdTomato viruses (as described in section 2.3.3) were stereotaxically co-injected into the HDB. After two weeks expression, tdTomato which is associated with ShRNA of insulin receptor expression were colocalized with ChAT in the HDB (Figure 5.1 A-C), which suggested that the viruses was specifically delivered in the HDB.
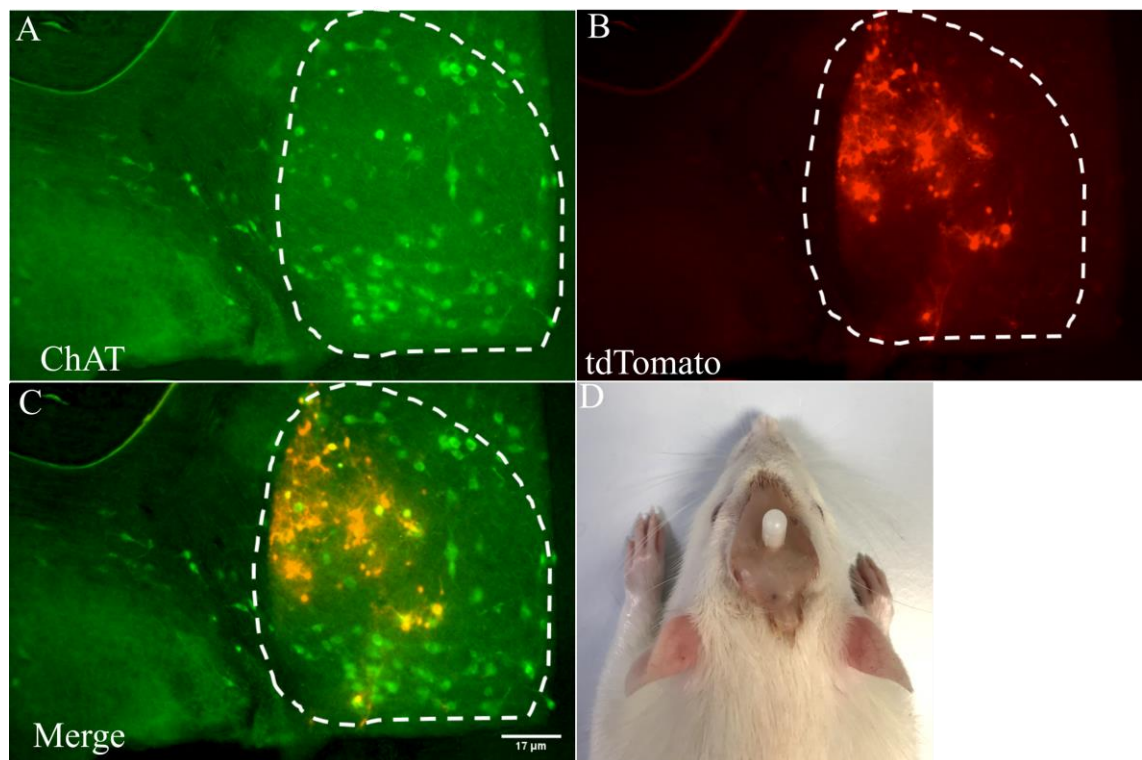
Figure 5. 1 Targeted delivery of ShRNA for the insulin receptor via adenovirus injection in the HDB. (A) ChAT immunohistochemistry as the marker in the HDB

(shown as white dotted circle). (B) tdTomato expressed in the HDB by co-injecting Ad5CMV-CRECFP and Ad5CMV-ShIR-tdTomato viruses. (C) tdTomato merged with ChAT in the HDB. (D) Representative rat after brain surgery.

Within two weeks after the viral injection of the 'ShIR+CRE' viruses, male rats exhibited a significant increase in cumulative food intake (average cumulative food intake is 354 g, n=4 animals, SEM=14.0 g) compare to the control group injected with scramble ShRNA and CRE virus ('ShC+CRE') (average cumulative food intake is 310.2 g, n=4 animals, SEM=6.3 g) (Figure 5.2 A). In contrast, insulin receptor knockdown in the female rats did not cause hyperphagia (Figure 5.2 Ai). Interestingly, insulin receptor knockdown did not change body weight in either male rats or female rats (Figure 5.2 B, Bi). Additionally, there was no remarkable effect on fat weight, blood glucose level in male or female rats after insulin receptor knockdown in the HDB (Figure 5.2 C-D, Ci-Di). Together, these data indicated that insulin receptor knockdown in the HDB results in significant increased food intake in male rats but not in female rats, without affecting body weight, fat and blood glucose levels in both male and female rats.
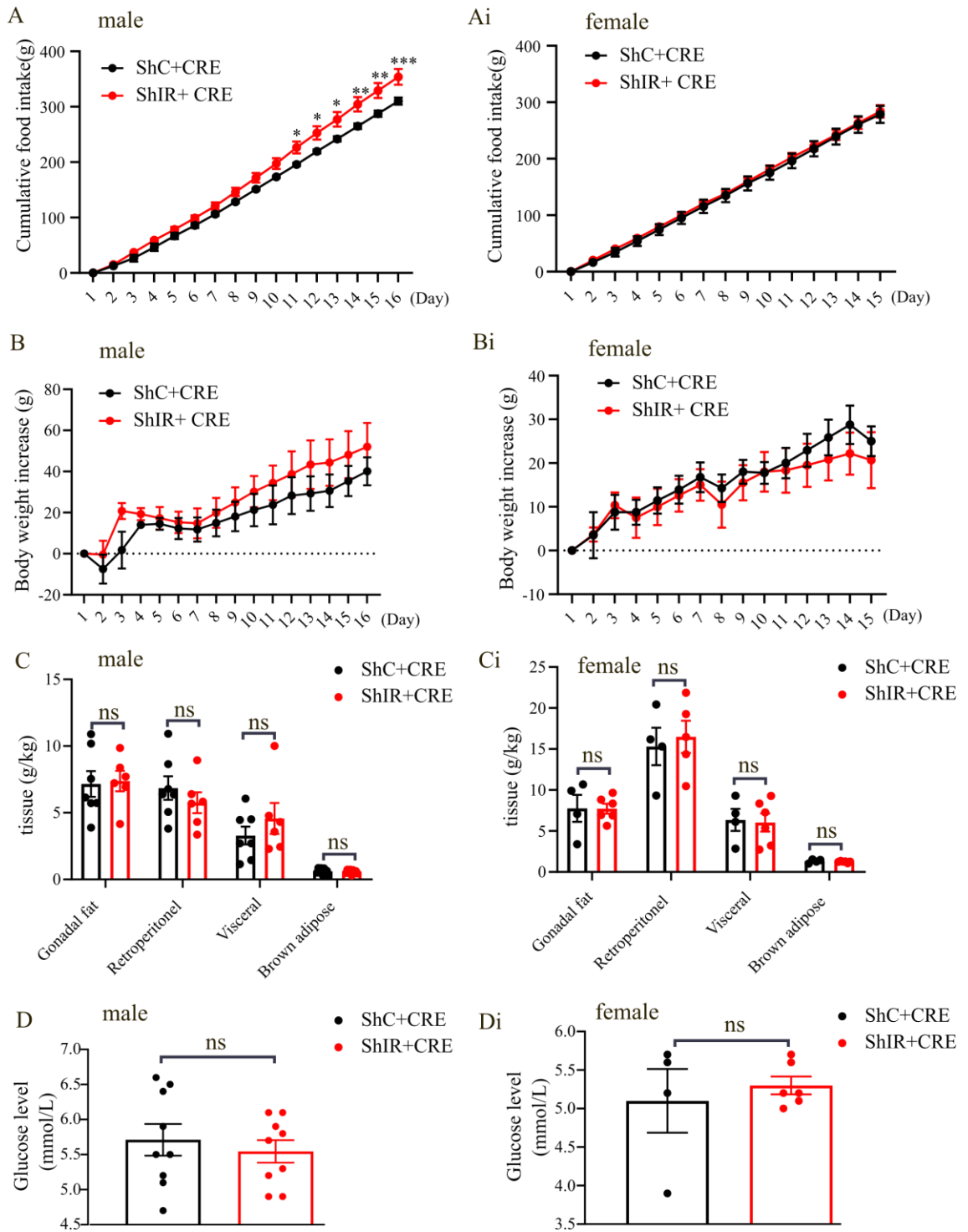
Figure 5. 2 Effect of specifically knockdown insulin receptor in the HDB on metabolism. Effect of knockdown of the insulin receptor in the HDB on cumulative food intake in male (A) and female (Ai), body weight in male (B) and female (Bi), normalized tissue weight in male (C) and female (Ci), blood glucose level in male (D) and female (Di) rats. Data are expressed as the mean ± SEM (n = 4-9 rats/group). Two-way Repeated ANOVA was performed for analysis cumulative food intake and body weight increase. Sidak's multiple comparisons test was performed * p<0.05 **

p<0.005 *** p<0.0001. Multiple t-test (correct for multiple comparisons using the Holm-Sidak method) was performed for analysis fat tissue and nonparametric test (Mann-Whitney method) was performed for analysis glucose level.

IR knockdown in the HDB could significantly increase cumulative food intake in male rats, thus suggesting that insulin signalling is involved in regulating feeding behaviour. To determine whether insulin in the HDB can modulate food intake in male rats, we conducted an acute feeding study performed on day 6 and day 12 post-knockdown of the insulin receptor in the HDB (as previously described in section 2.4.3). A previous research (Filippi et al., 2014) indicated that compared to the saline infused rats, rats that received an infusion of insulin in the DVC ate less. Insulin was effective within a range of concentrations from 0.02 μU/μl to 2 mU/μl, while 2 mU/μl was commonly used in feeding study (Clegg et al., 2003; Filippi et al., 2014). Thereby, 2 mU/μl is chosen in the current feeding study experiment to mimic the ability of insulin in the regulation of food intake. Rats were fasted for 6 hours and then infused bilaterally into the HDB with a total 0.2 μl of standard human insulin (2 mU/μl) or a vehicle over 5 minutes. Food was returned before dark cycle time period and food intake was measured every 30 mins for 4 hours. We compared the effect of insulin injection in the HDB in the male control rats (injected with the 'ShC+CRE' viruses) and male rats where insulin receptor was knocked down in the HDB. We expect that compared to vehicle injection, insulin infusion in the HDB would reduce food intake in the male control rats, while the ability of insulin in suppression food intake would be blocked in insulin receptor knockdown group rats. However, our results suggested that insulin injection in the HDB did not affect feeding behaviour in either control groups or knockdown group (Figure 5.3). The unexpected results observed in the study could potentially be attributed to two factors: the low dosage of insulin administered and the anxiety levels of the rats. Firstly, the dosage of insulin used in current study might not have been sufficient to elicit the desired effects or produce significant changes in the measured variables. In the future, investigating the effects of various doses of insulin can help establish a dose-response relationship and determine the optimal dosage for the desired effects. Secondly, the anxiety levels of the rats could have confounded the results and masked the true effects of insulin. Assessing anxiety levels using established behavioural tests such as open field test could help to understand anxiety-related factors.
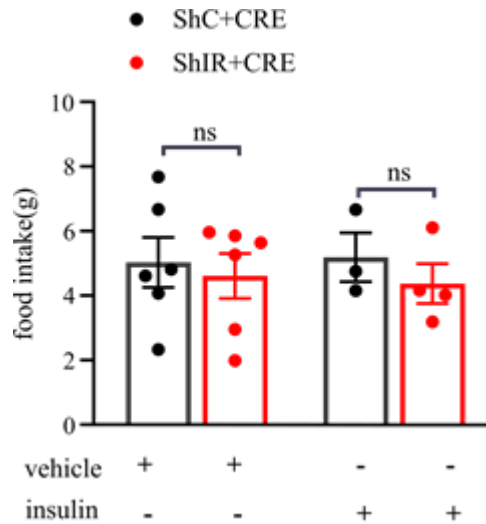
Figure 5. 3 Acute feeding study in insulin receptor knockdown HDB rats. Cumulative food intake within 4 hours after insulin injection in the HDB in the male rats. Two-way ANOVA was performed, post-hoc Tukey's multiple comparisons was used.

5.3.2 Knockdown of the insulin receptor in the HDB did not change the morphology and expression of key genes in the brown fat tissue (BAT)

As discussed in the introduction (section 1.5.2 and 1.5.4), brain insulin could affect peripheral metabolism, including lipolysis, lipogenesis (Koch et al., 2008; Scherer et al., 2011; Shin et al., 2017; Iwen et al., 2014), hepatic glucose production (Obici et al., 2002b; Pocai et al., 2005a; Dodd et al., 2018; Kimura et al., 2016) and energy expenditure (Lin et al., 2010). Thus whether knockdown of the insulin receptor in the HDB leads to the changes in peripheral tissues such as the BAT and liver are investigated here.

Our results indicated that knockdown of the insulin receptor in the HDB caused an increase in food intake in male rats compared to the control group, which might alter the pathway of energy expenditure and output. When food consumption exceeds the energy needs of an animal, this is one of contributors to being obese (Ruhm, 2012). On the other hand, it was reported that the BAT played an important role in the development of obesity (Nedergaard et al., 2007), which might be related to adipocyte proliferation and differentiation, and macrophage infiltration (Kuo et al., 2007). Obese rats exhibited

hyperplasia and enlargement of adipocytes compared to the normal lean rats (Harishankar et al., 2011; Weisberg et al., 2003). Here H&E staining was performed to examine the morphology of the BAT on 16 day post-knock down insulin receptor in the HDB. Results indicated that there is no significant difference in the lipid droplet number of the BAT between insulin receptor knockdown group (5619, mean +/- SEM =332, n = 4 animals) and the control group (4861, mean +/- SEM =236, n = 4 animals) in male rats (Figure 5.4 A-D). There is no significant difference in the lipid droplet number of the BAT between insulin receptor knockdown group (3073, mean +/- SEM =315, n = 4 animals) and the control group (2749, mean +/- SEM =318, n = 4 animals) in female rats (Figure 5.5 A-D). Additionally, compared to the control group (average size is 3.7, mean +/- SEM =0.19, n = 4 animals), knockdown of insulin receptor in the HDB (average size is 3, mean +/- SEM =0.27, n = 4 animals) did not demonstrate changes in the average size of the lipid droplet (Figure 5.4 A-D). And the average size of the lipid droplet between control group (average size is 3.1, mean +/- SEM =0.55, n = 4 animals) and knockdown group (average size is 3.5, mean +/- SEM =0.7, n = 3 animals) is also similar in female rats (Figure 5.5 A-D). Altogether, our data shows that impaired insulin signaling in the HDB did not lead to hyperplasia and infiltration in the BAT neither in male rats or female rats.

In addition to regulating fat accumulation, BAT is also related to thermogenesis and energy balance (Fenzl and Kiefer, 2014). Next several genes associated with energy expenditure and lipid metabolism were further investigated. qPCR was performed to test the expression of these key genes in the BAT, such as GLUT1, GLUT4, PPARγ, UCP1, ADRB 3 and PGC-1. Specifically, GLUT4 is responsible for the glucose transport into adipose cells (as described in section 2.5.6). PPARγ is a key gene in the process of adipogenesis, lipid metabolism and insulin signaling. UCP1, ADRB 3 and PGC-1 play an important role in thermogenesis and energy expenditure. There was no significant change in the level of expression of these genes between insulin receptor knockdown group and control group neither in male rats nor female rats (Figure 5.4, 5,5 E) either, which implies that knockdown insulin receptor in the HDB did not affect morphology and metabolism in the BAT.
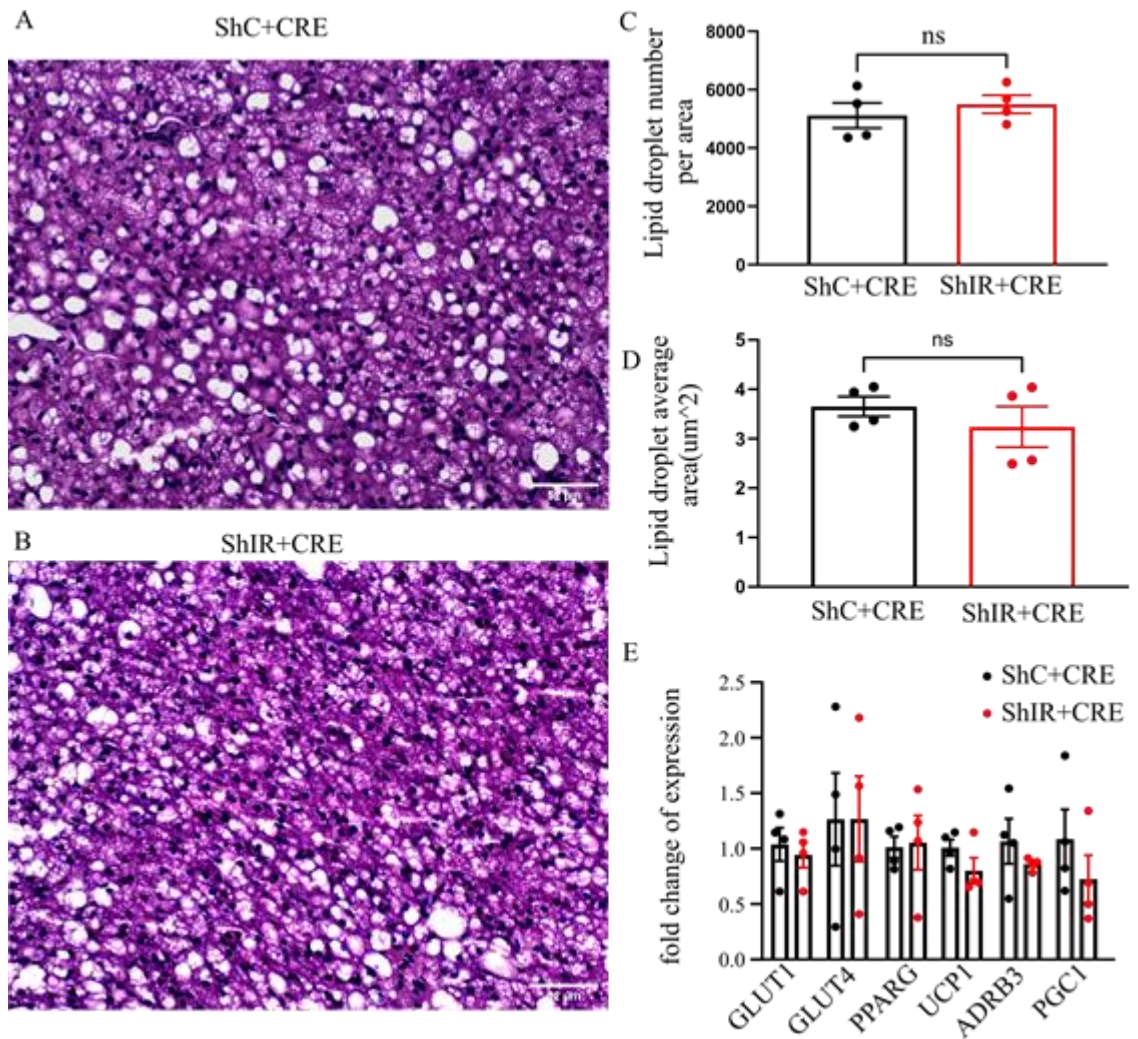
Figure 5. 4 Effect of knockdown insulin receptor in the HDB on BAT in male rats. Representative haematoxylin and eosin (H&E) staining of brown fat in control rats (A) and insulin receptor knockdown rats (B). (C) Quantification of lipid droplet number per area. (D) Lipid droplet average size per area. 2-3 images were processed from each rat (n = 4 rats/group). Nonparametric test (Mann Whitney method) was performed. (E) Fold change of key genes expression, data are expressed as the mean ± SEM (n = 4 rats/group). Multiple t-test (correct for multiple comparisons using the Holm-Sidak method) was performed.
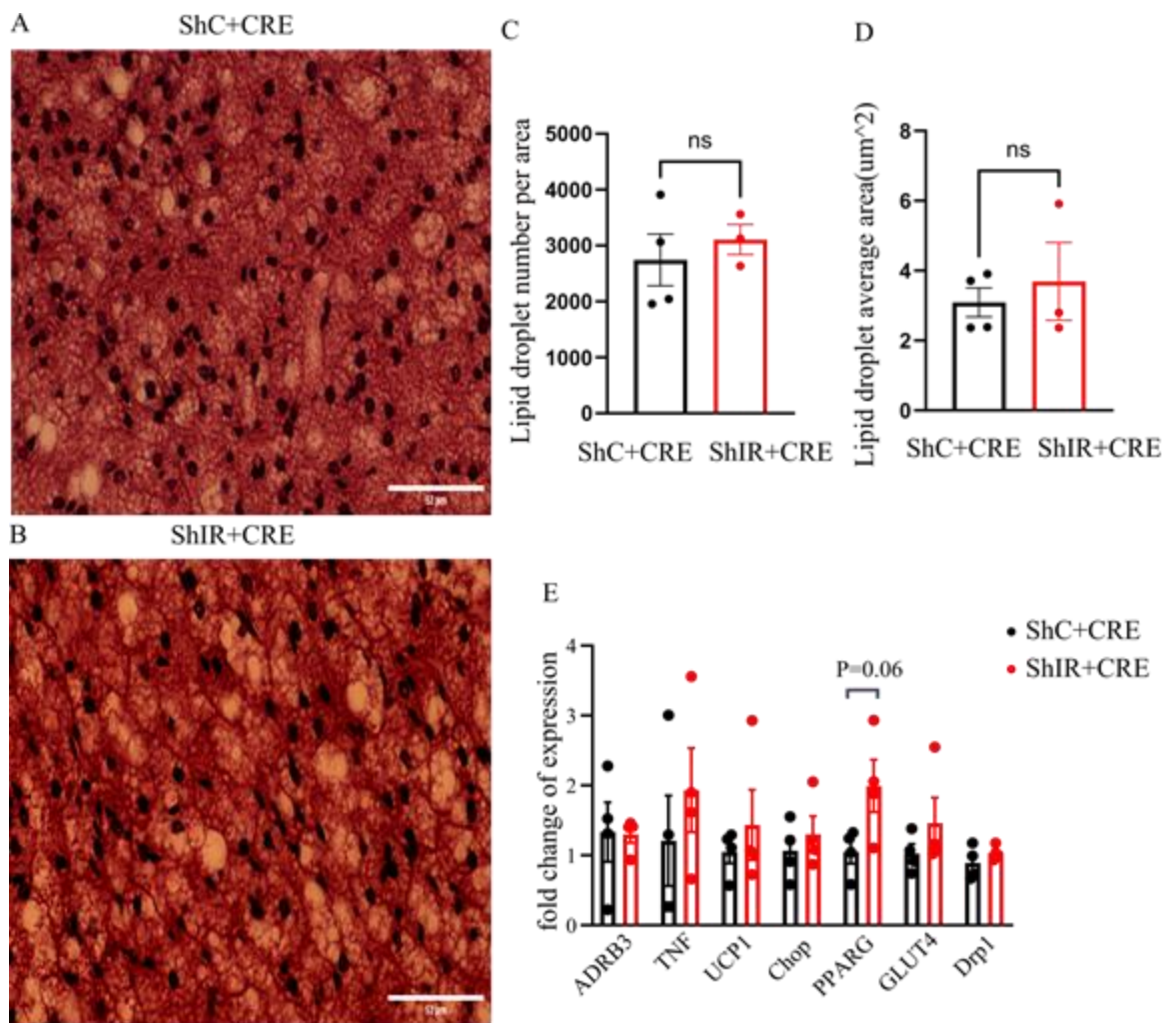
Figure 5. 5 Effect of knockdown insulin receptor in the HDB on BAT in female rats. Representative haematoxylin and eosin (H&E) staining of brown fat in control rats (A) and insulin receptor knockdown rats (B). (C) Quantification of lipid droplet number per area. (D) Lipid droplet average size per area. 4 images were processed from each rat (n = 4-6 rats/group). Nonparametric test (Mann Whitney method) was performed. (E) Fold change of key genes expression, data are expressed as the mean ± SEM, 4 images were processed from each rat (n = 3-4 rats/group). Multiple t-test (correct for multiple comparisons using the Holm-Sidak method) was performed. This part results were quantified by a master student Dauad Asghar.

5.3.3 Knockdown of the insulin receptor in the HDB did not change the morphology and expression of key genes in the liver

The liver is an important organ for the storage of free fatty acid and plays a crucial role in lipid homeostasis (Alves-Bezerra and Cohen, 2017). Excess lipid accumulation in the liver would further lead to hepatic steatosis and non-alcoholic fatty liver disease (NAFLD) (Liu et al., 2010). In addition, it has been reported that insulin signaling in the brain is involved in the regulation of hepatic metabolism, such as glucose hemostasis and very low density lipoprotein (VLDL) secretion (Obici et al., 2002b; Pocai et al., 2005a). Here, in order to determine whether impaired insulin receptor in the HDB will affect the liver function, firstly the morphology of the liver was examined. The quantification results indicated that knockdown of the insulin receptor in the HDB did not significantly affect the fat droplets infiltration in the male liver, and the number of the lipid droplets in both groups are similarly close to zero (Figure 5.6 A-D), which implies that insulin signaling in the HDB did not markedly affect the fat droplets in the male rats' liver. There is no significant difference in the average number of the lipid droplets between knockdown female group (76, SEM=15, n=12 sections) and control female group (34, SEM=13, n=6 sections) (Figure 5.7 A-C) either.

Additionally, qPCR was performed to further test the expression of several key genes in the liver, such as IR, GLUT1, Chop, TNF-α, PPAR-γ, FAS, NFKβ, ACACAC (as described in section 2.5.6). Chop gene is endoplasmic reticulum (ER) stress-regulated transcription factor (Marciniak et al., 2004), which is closely involved in inflammation and fatty liver disease (Updegraff and O'donnell, 2013). Cytokines such as TNF-α could also promote inflammation, and overexpression of TNF-α in the liver is one of the key markers in the pathogenesis of fatty liver (Tilg and Diehl, 2000). PPAR-γ gene plays an important role in regulation of insulin sensitivity and glucose metabolism. The suppression of PPAR-γ could impair insulin-induced glucose uptake (Picard and Auwerx, 2002; Liao et al., 2007), while the activation of PPARγ has been shown to enhance whole-body insulin sensitivity and promotes lipid accumulation in the liver (Gavrilova et al., 2003). ACACAC encodes for an enzyme that coverts acetyl-CoA to malonyl-CoA, an intermediate substrate for fatty acid synthesis (Abu-Elheiga et al., 2000). However, the data from qPCR here suggested that there were no significant changes in the expression of these key genes in the liver between insulin receptor

knockdown group and control group nether in male rats nor in female rats (Figure 5.6, 5.7 E), which implies that knockdown insulin receptor in the HDB did not affect these liver functions.
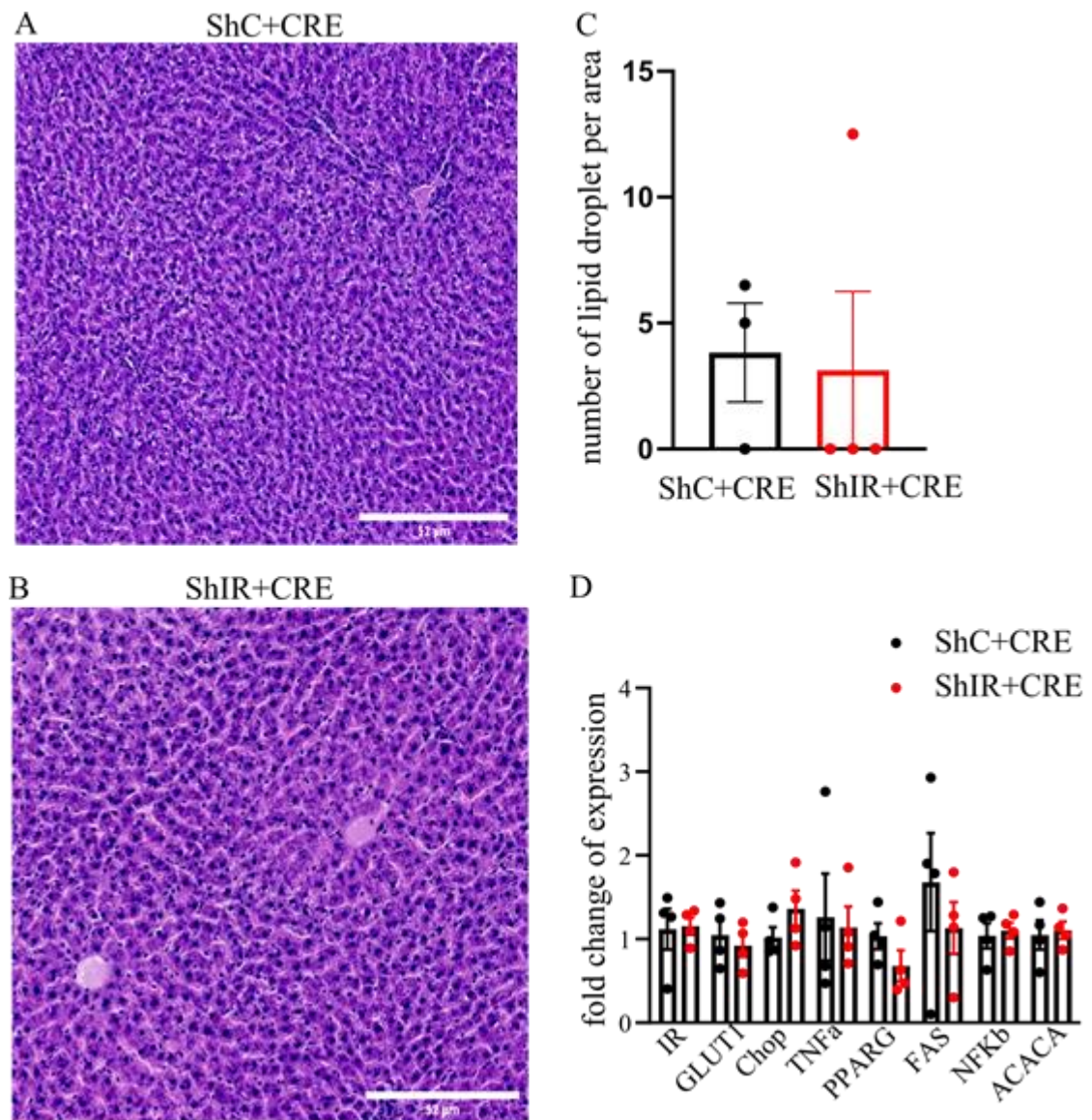
Figure 5. 6 Effect of knockdown of the insulin receptor in the HDB on liver tissue in male rats. Representative haematoxylin and eosin (H&E) staining of liver tissue in control rats (A) and insulin receptor knockdown rats (B). (C) Quantification of lipid droplet number per area. Two images were processed from each rat (n = 3-4 rats/group). Nonparametric test (Mann Whitney method) was performed. (D) Fold change of key genes expression, data are expressed as the mean ± SEM (n = 4 rats/group). Multiple t-test (correct for multiple comparisons using the Holm-Sidak method) was performed.
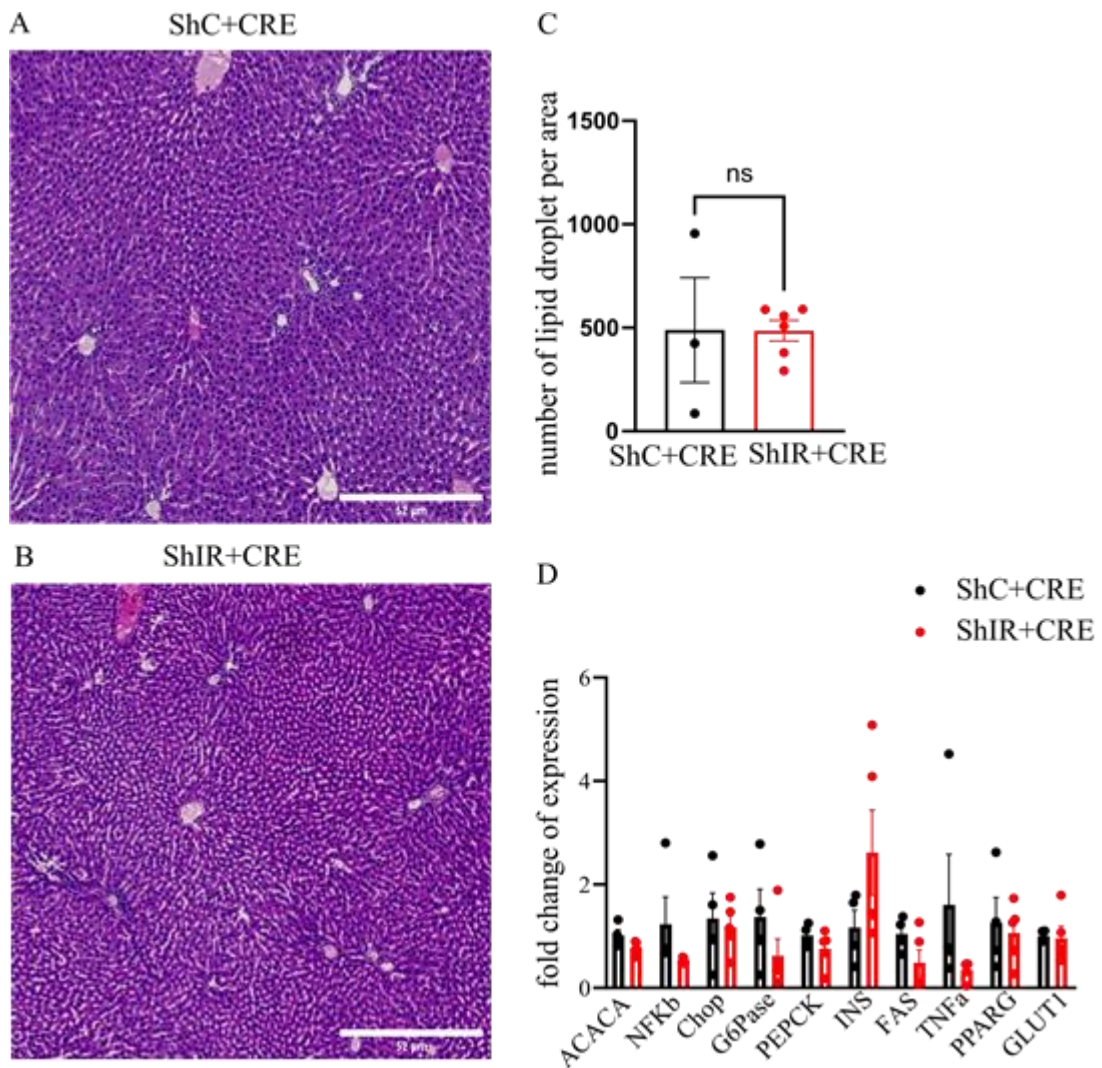
Figure 5. 7 Effect of knockdown of the insulin receptor in the HDB on liver tissue in female rats. Representative haematoxylin and eosin (H&E) staining of liver tissue in control rats (A) and insulin receptor knockdown rats (B). (C) Quantification of lipid droplet number per area. Two images were processed from each rat (n = 3-6 rats/group). Nonparametric test (Mann Whitney method) was performed. (D) Fold change of key genes expression, data are expressed as the mean ± SEM (n = 4-6 rats/group). Multiple t-test (correct for multiple comparisons using the Holm-Sidak method) was performed.

5.3.4 Knockdown of the insulin receptor in the HDB results in hyperactivity in male and female rats

The HDB region is also involved in responses to stress, fear and learning. In this study, a rodent activity detector was used to monitor the movements of the rats (Matikainen-Ankney et al., 2019). Knockdown of the insulin receptor in the HDB significantly increased total activity in male rats (n=3 rats each group) without significant change in hourly movement (Figure 5.8 A and Ai). Notably, there was no difference in activity between the control rats and the rats before surgery, while knockdown of the insulin receptor in the HDB (n=6 rats) resulted in hyperactivity in female rats compared to the control group (n=4 rats) and basal activity level (n=4 rats) (Figure 5.8 B). Interestingly, this hyperactivity was more significant in the dark cycle instead of the light cycle (Figure 5.8 Bi). Our findings indicated that knockdown of the insulin receptor in the HDB results in hyperactivity in female rats but not male rats, with a stronger effect in female.
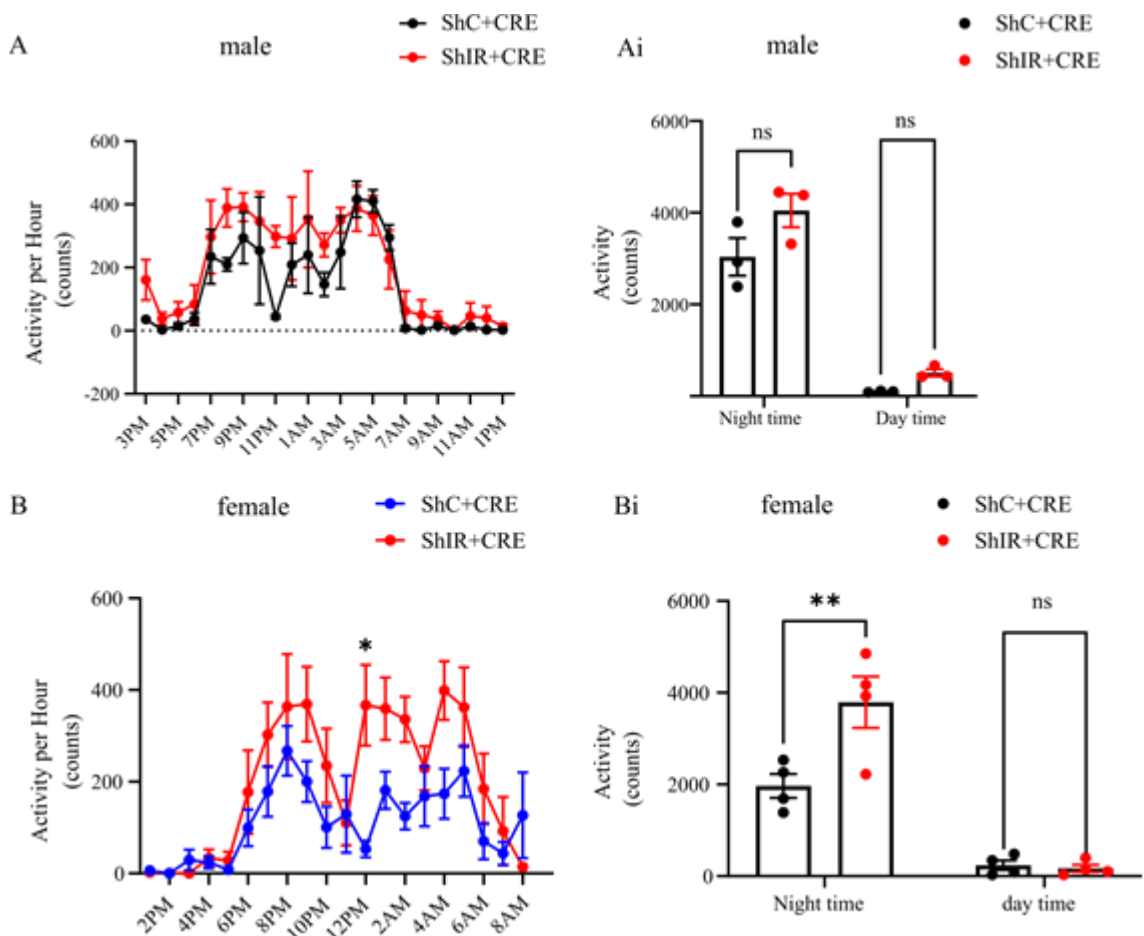
Figure 5. 8 Effect of specifically knockdown of the insulin receptor in the HDB on

activity. Activity between injected control virus and insulin receptor knockdown virus in male rats (A) and female rats (B) at different time points. Nocturnal and day time accumulated activity in male (Ai) and female rats (Bi). Data are expressed as the mean ± SEM (n=3-6 rats/group). In male rats study, 3 rats in each group were monitored, each rat was monitored once. In female rats study, random 4 rats before surgery were monitored as basal activity, each rat was monitored once. After surgery, 4 female rats in control group ('ShC+CRE') were monitored, each rat was monitored 3 times. 6 female rats in knockdown group ('ShIR+CRE') were monitored, each rat was monitored twice. Two-way ANOVA (Bonferroni's multiple comparisons test) was performed. * $p<0.05$, **** $p<0.0001$.

5.3.5 Knockdown of the insulin receptor in the HDB did not change corticosterone level in male and female rats

It has been reported that the HDB area is also involved in regulating stress, which may affect food intake and activity (Hardaway et al., 2015; Cassidy et al., 2019). To determine whether the hyperactivity we observed in male and female rats is associated with the level of stress, we next measured the corticosterone levels from the rats' plasma. The data indicated no significant difference in corticosterone levels between the insulin receptor knockdown and control groups in both male and female rats (Figure 5.9). Thus the hyperactivity led by knocking down insulin receptor in the HDB may not account for the mediation of corticosterone hormones. We did not observe the difference between male and female. This may due to the small sample size, which the study might lack the statistical power to detect true effects even if they exist. Additionally, missing data, such as the failed corticosterone analysis in one male, can further impact the statistical analysis and interpretation of results. Furthermore, studying stress levels in rats can be challenging due to various factors that can influence the results such as handling, sex of the handler, time of day, and speed of analysis. In future experiment, we can increase the sample size to improve statistical power and account for potential data loss. The mechanisms of hyperactivity need further investigation.
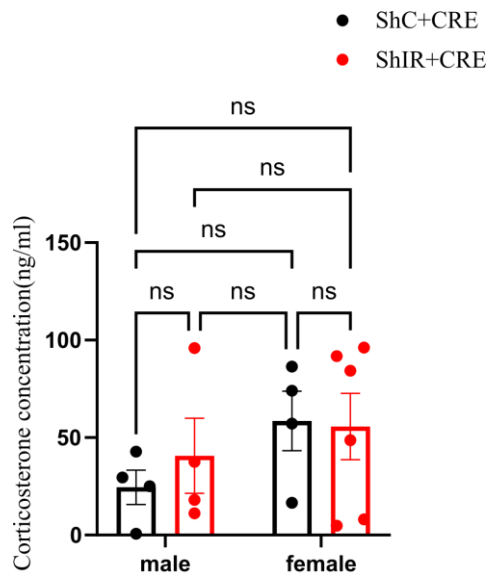
Figure 5. 9 ELISA test corticosterone level from the plasma of male and female rats. Two-way ANOVA was performed, post-hoc Turkey's multiple comparisons was used.

5.3.6 HDB received input from the ventral tegmental area (VTA) and olfactory bulb

It was reported that basal forebrain regulates various physiological functions through a complex network (Zaborszky et al., 2015; Zheng et al., 2018; Li et al., 2018; Zheng et al., 2022). In our study, we reported that the insulin signalling in the HDB is involved in regulating food intake and locomotion. Next to determine which brain areas functionally connect with the HDB, we use retrograde tracer Fluoro-Gold (Sanchez-Perez et al., 2015; Saleeba et al., 2019) to inject into the HDB (as described in section 2.4.2). The majority of Fluoro-Gold was located in the injection site, while dense projections were detected in the ventral tegmental area (VTA) and the mitral cell layer of olfactory bulb (Figure 5.10), which is consistent with the report by Zheng et al (Zheng et al., 2018). Altogether, our results implied that the HDB could receive input from the VTA and the olfactory bulb.

Next, dopaminergic neuron markers (TH) and GABAergic neuron markers (GAD) were used to identify which type of neuronal populations sent the afferents to the HDB. The IHC results indicated that mitral cell layer of olfactory bulb put into afferents into HDB, but this is not through GABAergic neurons as there is no colocalization between Fluoro-Gold and GAD (Figure 5.10 D). This is expected, only mitral/tufted cells send

projections out of the olfactory bulb and these are known to be glutamatergic (Imai, 2014). While abundant Fluoro-Gold in the VTA area was colocalized with TH, implying that the VTA sent input to the HDB through dopaminergic neurons (Figure 5.10 C).
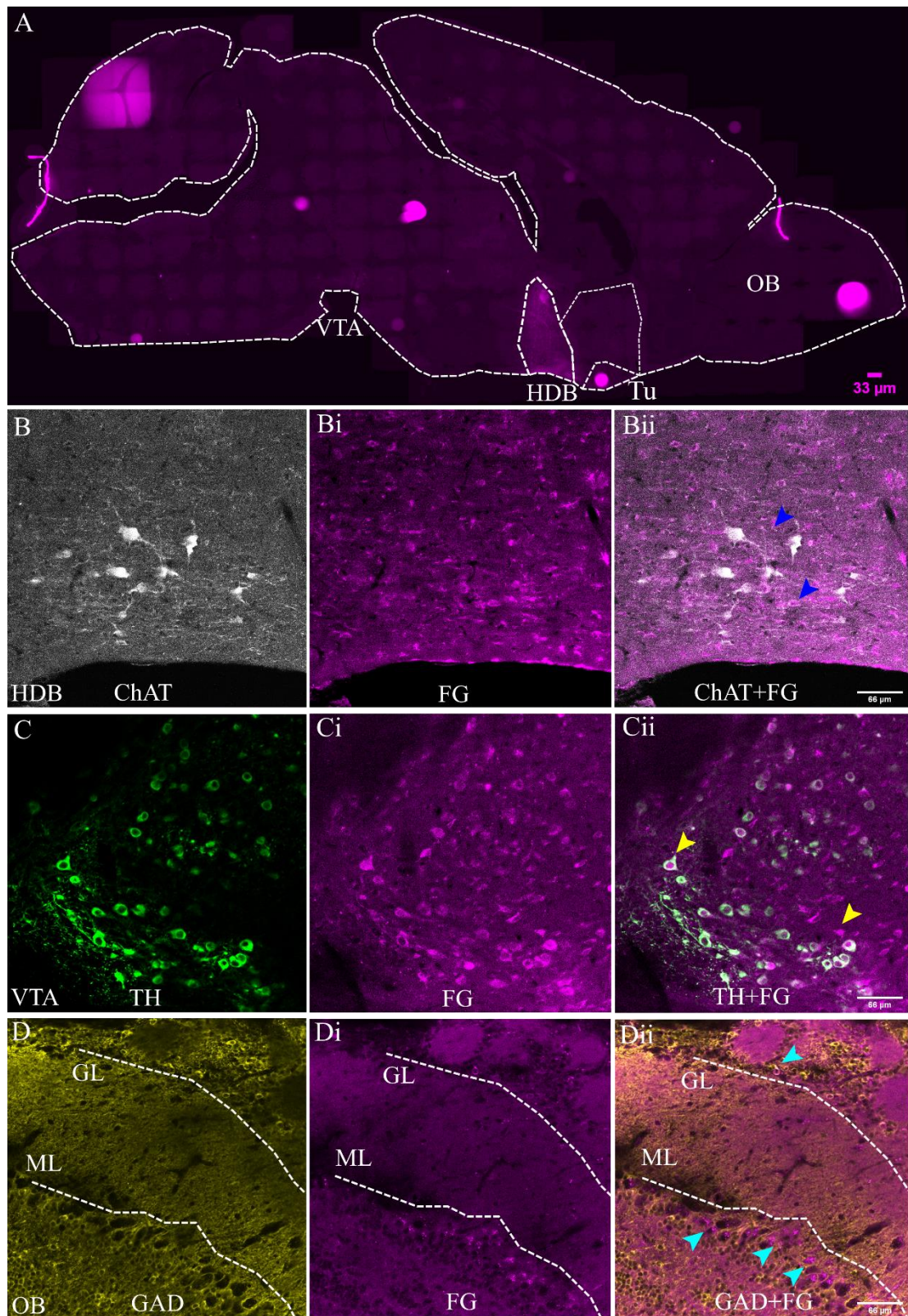
Figure 5. 10 The HDB received input from the VTA and OB. (A) whole brain view to show retrograde tracer Fluoro-Gold targeting the HDB. (B) Zoom in of injection site of the HDB (20x), n= 3 mice. ChAT-antibody immunohistochemistry (Gray), Fluoro-Gold (Magenta). (C) Fluoro-Gold was observed in the VTA, stained with TH-antibody immunohistochemistry (Green). (D) Fluoro-Gold was observed in mitral cell layer (ML) of the olfactory bulb, stained with GAD-antibody immunohistochemistry (Yellow). Tu: olfactory tubercle; HYP: hypothalamus.

5.4 Discussion

Intranasal delivery of insulin is a non-invasive administration method. It has been shown that intranasal insulin could suppress appetite and reduce energy consumption, which might be useful for diabetes or obese patients. However, more needs to be known about its effects and actions. fMRI and neuroimaging evidence indicated that the effect of intranasal insulin on feeding behaviour was mainly due to its effects in the hypothalamus (Kullmann et al., 2013), hippocampus (Guthoff et al., 2010) or cortical brain regions (Kullmann et al., 2015a). However, our study has revealed a novel brain area involved in regulating food intake.

The HDB is a major component of the cholinergic basal forebrain. Selective knock-out of cholinergic neurotransmission from the HDB was found to increase daily food intake and body mass in mice, causing hyperphagia, while activating HDB cholinergic neurons suppressed food intake *in vivo*, demonstrating that cholinergic signalling from the HDB plays an important role in regulating food intake (Herman et al., 2016). This data, together with my data showing the effect of insulin receptor knockdown in the HDB (Figure 5.2), suggests that insulin activates the cholinergic HDB neurons regulating food intake and that this is the likely mode of action for intranasal insulin in reducing food intake.

In our results, we observed that knockdown of the insulin receptor in the HDB results in a significant increase in food intake in male rats, which indicated that the insulin receptor plays an important role in the control of feeding behavior by the HDB. Interestingly, we did not observe any changes in food intake following insulin receptor knockdown in the HDB of female rats. There is clear evidence that insulin signaling in

the CNS exhibits sex differences. Clegg et al reported that insulin infusion in the third ventricle leads to a vigorous reduction in food intake in male rats but not female rats (Clegg et al., 2003), while female rats were more leptin-sensitive in reducing food intake compared to the male rats (Clegg et al., 2003). These observed sex differences might be due to the hormone estrogen which has also been shown to decrease insulin sensitivity (Clegg et al., 2006), which may explain that there is no significant effect on food intake after knocking down insulin receptor in the HDB in female rats. In the future, we can conduct the ovariectomy and hormone replacement experiment to test that oestrogen was implicate in the sex differences. Furthermore, sex differences in insulin signaling have been observed in human studies. For example, intranasal insulin reduced food intake in healthy men but had no effect in women (Benedict et al., 2008). However, the mechanisms which underlie these sex differences of anorexigenic signaling of insulin still require further investigation.

Visceral fat is fat that surrounds the internal organs, including the liver, kidneys and intestines, and it is regarded as a more reliable parameter for evaluating metabolic pathology (Stolk et al., 2003). Adipose composition also highly impacts the levels of several parameters, such as plasma glucose, leptin, insulin and triglycerides (Riccardi et al., 2004). In addition, insulin signaling in the MBH inactivates hormone-sensitive lipase, and promotes lipogenesis in white adipose tissue, which suggests that brain insulin could suppress lipolysis (Scherer et al., 2011). White, brown and beige adipose tissue are the three main types of adipose tissue. White adipose tissue mainly consists of unilocular lipid droplets and is involved in energy storage, while brown adipose tissue is responsible for energy release. Beige adipose tissue is considered to be the combination of white adipose tissue and brown adipose tissue (Ikeda et al., 2018). There are two ways for white adipose tissue to induce obesity: one is through increasing the number of adipose cells, which is also called hyperplasia; and the other way is through enlarging the adipocyte size, which is known as hypertrophy (Berry et al., 2014). In our experiment, insulin receptor knockdown in the HDB did not significantly change body weight both in male and female rats, which is consistent with the body fat mass data. These results are consistent with data from Herman et al which also suggested that specifically abolishing cholinergic neurons in the HDB did not change lean mass and body fat mass within 3 week post-ablation (Herman et al., 2016). Significant differences in lean mass and body fat mass were only observed around 12 week post-ablation (Herman et al., 2016), which suggests that alteration of fat mass in our insulin receptor

knockdown animals might occur in a more long term study.

It has been shown that insulin-mediated suppression of hepatic glucose production occurs by reducing the level of raw material available for liver glucose synthesis, such as acetyl CoA and pyruvate carboxylase (Perry et al., 2015). Insulin has been shown to inhibit lipolysis in the white adipose tissue, leading to less free fatty acid entering to the liver, reduced concentrations of acetyl CoA and pyruvate carboxylase in the liver, and further suppression of hepatic glucose production (Perry et al., 2015). However, in our study, insulin receptor knockdown in the HDB did not result in significant changes of blood glucose level, which is in line with previous report by Herman et al (Herman et al., 2016) which suggested that specifically abolishing cholinergic neurons in the HDB did not change blood glucose level neither short terms post-ablation (3 weeks) nor long term post-ablation (12 weeks). Therefore, insulin receptor knockdown in the HDB does not seem to directly influence the peripheral blood glucose level.

The brown adipose tissue morphological results indicated that there are no significant differences in the number of adipose cells and lipid droplet size in the brown adipose tissue. The expression of several key genes related to lipometabolism including GLUT1, GLUT4, PPARγ, UCP1, ADRB 3 and PGC-1 were examined in the brown adipose tissue of male rats, however we did not observe any expression differences between control and insulin receptor knockdown groups. Together, our study implies that insulin receptor in the HDB may not be involved in the control of peripheral lipometabolism through changes in these genes.

The liver is another crucial organ responsible for lipid metabolism. Under healthy condition, only small amount of triglycerides was stored in the lipid droplets in the liver, while excess triglycerides accumulation is the character of non-alcoholic fatty liver disease (Alves-Bezerra and Cohen, 2017; Liu et al., 2010). In our experiment, the effect of impaired insulin receptor in the HDB on the liver lipid metabolism was examined. We did not observe significant changes in the number of lipid droplet after knocking down insulin receptor in the HDB. In addition, insulin is also involved in liver metabolism by regulating gene expression. For example, insulin promotes glycogen synthesis by AKT mediating inhibiting of the GSK3 pathway (Wang et al., 2022). In our study, the expression of several key genes related to glucose transport, inflammation and lipometabolism including GLUT1, Chop, TNFα, PPARγ, FAS, NFK β and ACACA

were examined in the liver of male rats, however we did not observe any expression differences between control and insulin receptor knockdown groups, which imply that insulin signalling in the HDB did not change the liver lipometabolism through these genes. Biddinger et al reported that insulin signalling in the liver is not required for lipogensis under normal physiological stimuli of fasting and feeding (Haas et al., 2012). It was reported that even though liver insulin receptor knockout (LIRKO) mice presented severe insulin resistance, these mice did not develop accumulated TG and fatty liver disease (Haas et al., 2012). However, high fructose diet induces lipogenic gene expression in LIRKO mice, which means there exists a compensatory insulin-independent signalling pathway to involve in regulating insulin-induced lipogenic gene expression in the liver (Haas et al., 2012). This may be one of the reasons that disruption of insulin signalling the HDB did not alter the lipid metabolism in the liver.

In our experiment, hyperactivity was observed in female rats but not male rats compared to the control, which might be correlated to disrupted insulin receptor signaling in the HDB following insulin receptor knockdown. Our finding is consistent with a previous report by Wishart et al (Wishart et al., 1973). Data from electroencephalogram (EEG) recordings showed that higher stimulation of the MS (also known as one area of the basal forebrain) could evoke hippocampal or cortical electrical activity, which led to behavior alterations, such as vigorous eating, shaking and hyperactivity in male rats (Wishart et al., 1973).

There are several possibilities to explain why knockdown of the insulin receptor in the HDB could lead to hyperactivity. Firstly, it has been reported that the ventral hippocampus receives cholinergic input from the HDB, and disturbed efferent input from the HDB to the hippocampus leads to fear behaviour (Staib et al., 2018). Another report also confirmed this observation; when acetylcholine (Ach) signalling in the hippocampus was abolished, mice exhibited anxiety and depression-like behaviour (Mineur et al., 2013). In our study, the HDB area was targeted by insulin receptor knockdown viruses which might interfere with this efferent signal to the hippocampus and therefore lead to stress and anxiety. Secondly, cholinergic neurones are involved in attention (Turchi and Sarter, 1997), sleep, memory (Bartus et al., 1982) and depression (Warner-Schmidt et al., 2012). More specifically, higher Ach levels are associated with depression-like behaviour (Mineur et al., 2013), decreased numbers of cholinergic

neurons has been detected in aging-related memory loss and AD (Bartus et al., 1982) and damaged cholinergic neurons have been correlated to impaired attention (Mcgaughy et al., 2002). Cholinergic neurons originate from the basal forebrain, also mainly in the HDB (Maurer and Williams, 2017). In our study, knockdown of the insulin receptor in the HDB might affect the cholinergic neurons in the HDB, which further influence the attention status that associated with active movement. Finally, studies in rodents and humans both suggested that impaired astrocytic insulin signalling results in anxiety and mood disturbances, which were associated with a decrease in downstream dopamine signalling and release (Cai et al., 2018; Mansur et al., 2018). Another study referred that hyperactivity probably related with dopamine transporter (DAT) (Ralph-Williams et al., 2003) that transports dopamine into the cell and reduces dopamine levels in the synaptic cleft and reduces locomotion. It was reported that mice lacking DAT displayed hyperactivity (Ralph-Williams et al., 2003), which demonstrated that DAT-related dopamine level is associated with locomotor movements. In our study, we observed that the HDB received input from dopaminergic neurons from the VTA. There is a possibility that alteration in dopamine signalling from VTA might account for the hyperactivity after knockdown of the insulin receptor in the HDB (Figure 5. 11 Summary of the effect of insulin receptor knockdown in the HDB).
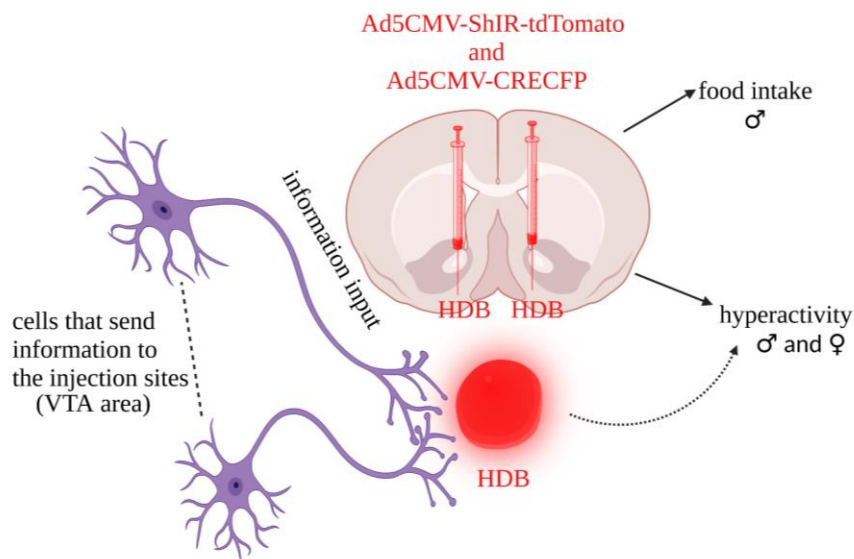
Figure 5. 11 Summary of the effect of insulin receptor knockdown in the HDB. Impaired insulin receptor in the HDB increased food intake in male rats and led to hyperacativity in female rats but not male rats which may be related to information input from the VTA.

5.5 Conclusion

Our results suggested that insulin receptor knockdown in the HDB leads to increased food intake in male rats but this was not seen in female rats after 2 weeks. However, insulin receptor knockdown in the HDB did not significantly change the body weight both in male and female rats. On the other side, knockdown of the insulin receptor in the HDB does not seem to directly affect metabolism in peripheral tissues since we did not find significant changes in blood glucose level, white adipose tissue weight, morphology and lipid droplet composition of the liver and brown adipose tissue, and expression of several key genes involved in lipometabolism and inflammation. Unexpectedly, it was found that insulin receptor knockdown in the HDB results in hyperactivity in male and female rats. Work has shown that brain insulin signalling plays a crucial role in regulating the maintenance of synapses, which helps to process sensory information and preserve brain circuit (Chiu et al., 2008). Impaired insulin signaling in the HDB might obstruct the function of other neuronal transmitters and lead to hyperactivity (Figure 5. 8 Summary of the effect of insulin receptor knockdown in the HDB). Further studies should focus on the mechanism of how insulin signaling in the HDB alters in locomotor activity and the mechanisms behind the sex difference in food intake.

6. Targeting the insulin receptor expressing cells in the HDB

6.1 Introduction and rationality

Knockdown of the insulin receptor in the HDB leads to increased food intake and hyperactivity, thus suggesting that insulin signalling in the HDB plays an important role in regulating energy balance. However, it is still not clear how insulin sensing in the HDB can modulate feeding and activity. Insulin could either activate or inhibit certain neurones in the HDB to trigger the neuronal signals that lead to the changes in feeding and activity. A potential experimental approach that could answer this question is to directly activate or inhibit insulin receptor-expressing neurones in the HDB. We attempted to develop a chemogenetic approach that uses designer receptors exclusively activated by designer drugs (DREADDs) (Roth, 2016). DREADDs system is a promising approach to control and modulate cellular activity by activation of the Gq- (stimulatory receptors) or Gi (inhibitory receptors) protein-coupled signalling pathways, which make it possible to understand the functions and mechanisms of neurons in regulating feeding behaviour and hyperactivity.

In current experimental hypothesis, human Gq-coupled M3 muscarinic receptor (hM3Dq) combined with drug clozapine-N-oxide (CNO) will be used to activate insulin receptor activity in the HDB area. The CNO can be used as a remote inducer to activate G protein-coupled receptors and modulate neuronal activity *in vivo* (Alexander et al., 2009), which provide possibility to monitor feeding behaviour and locomotor activity in freely moving rats. Now hM3Dq combined CNO system has been widely applied in studying of food intake (Krashes et al., 2011), energy expenditure (Kong et al., 2012), locomotion (Kozorovitskiy et al., 2012) as well as memory (Garner et al., 2012). We expect that the activation of the neurones that express the insulin receptor in the HDB would reduce the food intake and locomotion in the rats.

Using rats as experimental model limits our ability to target specific neurones. To work around this problem, a specific promoter (IR promoter) was used to target the insulin receptor positive cells in current project, which makes it possible to activate insulin receptor activity in the HDB area by using hM3Dq combined CNO system. The next problem is how to exclusively enhance the activity in the insulin receptor positive cells. Fortunately, Cre-dependent system combined with FLEX-hM3Dq would restrict the modulation of activity only in the specific neuronal populations. Two viruses will be

applied, one carries the flexed DREADDs channel and the other expresses the cre-recombinase under the insulin receptor promoter. FLEX switch system has two pairs of loxp sites and the sequence of hM3Dq was flanked by these target sites. One is Loxp, the other is lox2272. Both loxP and lox2272 are recognized by Cre recombinase but lox2272 sites can only recombine with other lox2272 sites, not with loxP sites. The first recombination step will invert the hM3Dq sequence using loxP site. The second recombination event then excises the loxp between the identical lox2272 sites. Since only one loxP and lox2272 site will remain on either side of the DNA fragment, any additional recombination events are impossible in the presence of Cre recombinase. Cre recombinase would be driven by insulin receptor promoter labelled with CFP, which means only insulin receptor positive cells will express the Cre recombinase and insulin receptor positive cells will be activated in the presence of FLEX-hM3Dq system. The synapsin promoter is known for its specificity in driving gene expression primarily in neurons and, more specifically, in presynaptic terminals. So under the human synapsin promoter, insulin receptor can exclusively be activated in the neurones (Figure 6.1 to show the mechanism of chemogenetically enhance the activity of insulin receptor neurones).
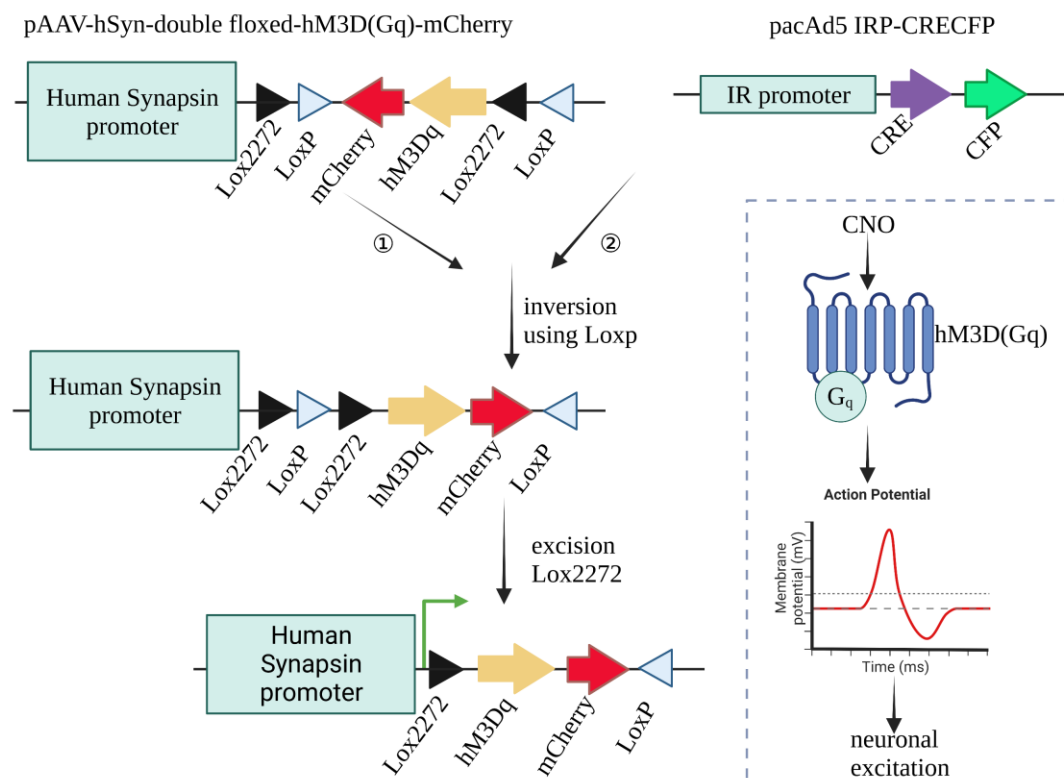
Figure 6. 1 The mechanism of genetically enhance the activity of insulin receptor neurones. The sequence of hM3Dq was flanked by loxp and lox2272. Both loxP and lox2272 could be recognized by Cre but lox2272 sites can only recombine with other lox2272 sites, not with loxP sites. The first recombination step will invert the hM3Dq sequence using loxP site. The second recombination event then excises the loxp between the identical lox2272 sites. hM3Dq is an engineered human M3 muscarinic (hM3) receptor that could be activated by CNO. Consequently, hM3Dq coupled to the Gq signalling cascade leading to Ca^{2+} influx and the neuronal excitations. Since Cre recombinase exclusively is driven by insulin receptor promoter labelled with CFP, so only insulin receptor positive cells will be activated in the presence of CNO.

To construct insulin receptor promoter mediated Cre recombinase, in current project, insulin receptor positive cells expressing GFP driven by the insulin receptor promoter (IRP) was firstly made (Ad5IRP-GFP). Then Ad5 IRP-GFP vector was digested and ligated with PacAd5CMV-CRECFP vector to construct insulin receptor promoter mediated Cre recombinase vector (PacAd5 IRP-CRECFP), which means that Cre recombinase only expressed in insulin receptor positive cells (Figure 6.2 to show the workflow of constructing PacAd5IRP-CRECFP). Then PacAd5IRP-CRECFP virus will be co-injected with pAAV-hSyn-double floxed-hM3D(Gq)-mCherry virus in the HDB to exclusively activate insulin receptor (as descried in Figure 6.1).

Ad5IRP-GFP virus and PacAd5IRP-CRECFP virus have been successfully made in this chapter, however, due to limited time, PacAd5IRP-CRECFP virus will be co-injected with pAAV-hSyn-double floxed-hM3D (Gq)-mCherry virus in the future to explore the effect of insulin signalling in the HDB on regulating metabolic balance.
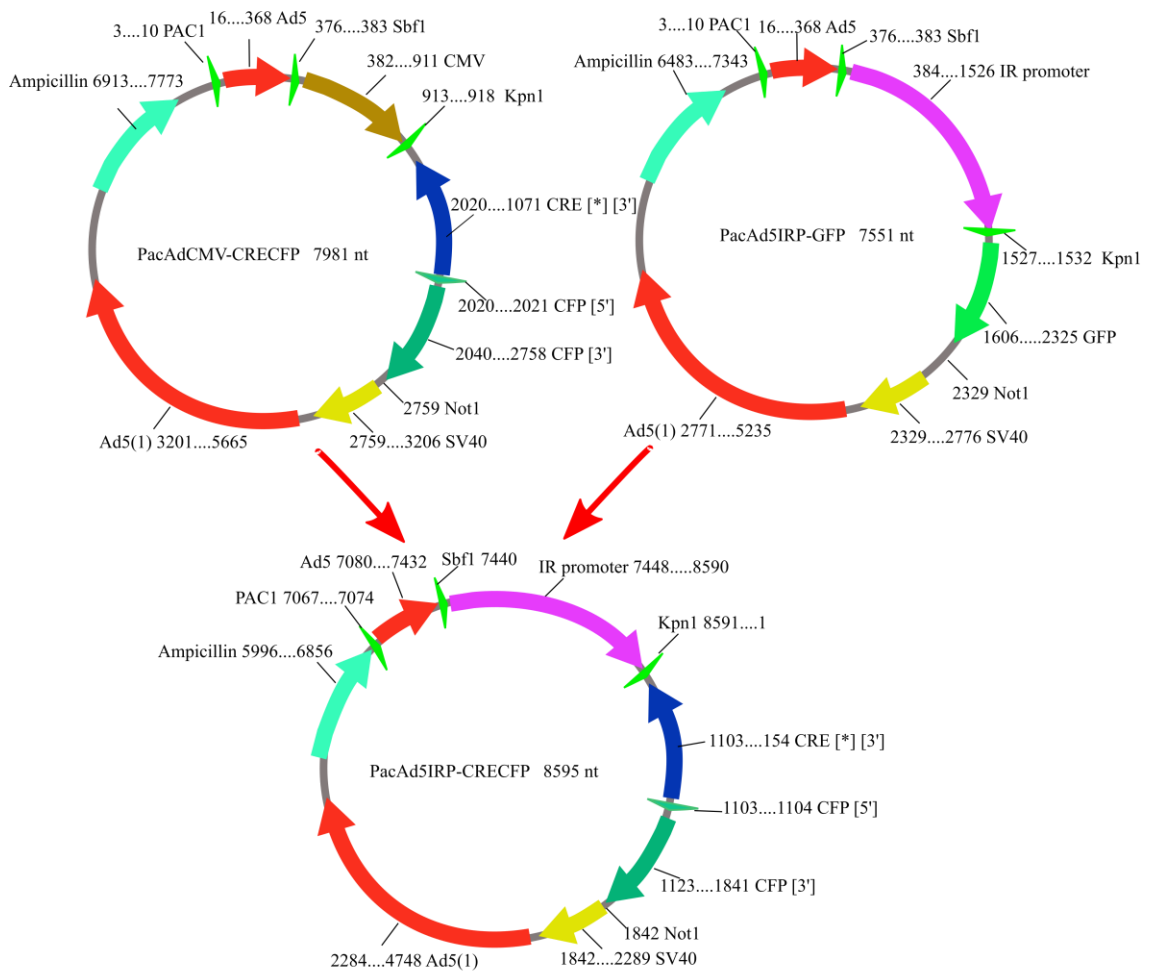
Figure 6. 2 Schematic of constructing PacAd5IRP-CRECFP. The principle is that CMV promoter from PacAd5CMV-CRECFP vector is replaced by insulin receptor promoter from PacAd5IRP-GFP. Vector PacAd5CMV-CRECFP and PacAd5IRP-GFP are digested by restriction enzyme Sbf1 and Kpn1. Then the band insulin receptor promoter is ligated to the PacAd5-CRECFP to construct PacAd5IRP-CRECFP vector.

6.2 Aims

(1) Produce a recombinant adenovirus expressing GFP from the insulin receptor promoter (Ad5IRP-GFP).

(2) Develop an insulin receptor promoter mediated Cre-CFP expression vector (PacAd5IRP-CRECFP) and produce a recombinant adenovirus Ad5IRP-CRECFP.

6.3 Results

6.3.1 Produce a recombinant adenovirus expressing GFP from the insulin receptor promoter (Ad5IRP-GFP)

IR promoter used in this project was published in GenBank (AJ006071.1), which was rats specific promoter and could achieve decent protein expression in rats. And the Ad5 vector expressing GFP under the insulin receptor promoter was previously cloned in the Filippi lab. In order to determine the specificity of the insulin receptor promoter to target only insulin receptor expressing cells, we first produced an adenovirus that express GFP under the insulin receptor promoter (Ad5IRP-GFP). The vector PacAd5IRP-GFP and the virus backbone vector pacAd59.2-100 were digested with Pac1 restriction enzyme and then co-transfected into the HEK293 AD cells (as previously described in section 2.6.2). The cell control only transfected with polyjet transfection reagent. An EVOS microscope was used to daily check the GFP expression. On day 3, there was abundant GFP expression compared with the polyjet alone (Figure 6.3 Ai, Bi). Several virus plaques (When a virus infects the host cells in the culture, it replicates and spreads, leading to the death of the infected cells. The viruses then infect neighbouring cells, causing a cascade of cell death that results in the formation of visible plaques) were also detected under bright field (Figure 6.3 Bii). On day 10, compared to the polyjet control group, most cells were detached because of the virus infection, and the virus were released into the medium (Figure 6.3 Ci, Cii, Di, Dii). The virus was collected (as describe in Methods 2.3.3) as stage 1 virus. This experiment showed that the Ad5IRP-GFP virus started to replicate in the HEK293 AD cells.
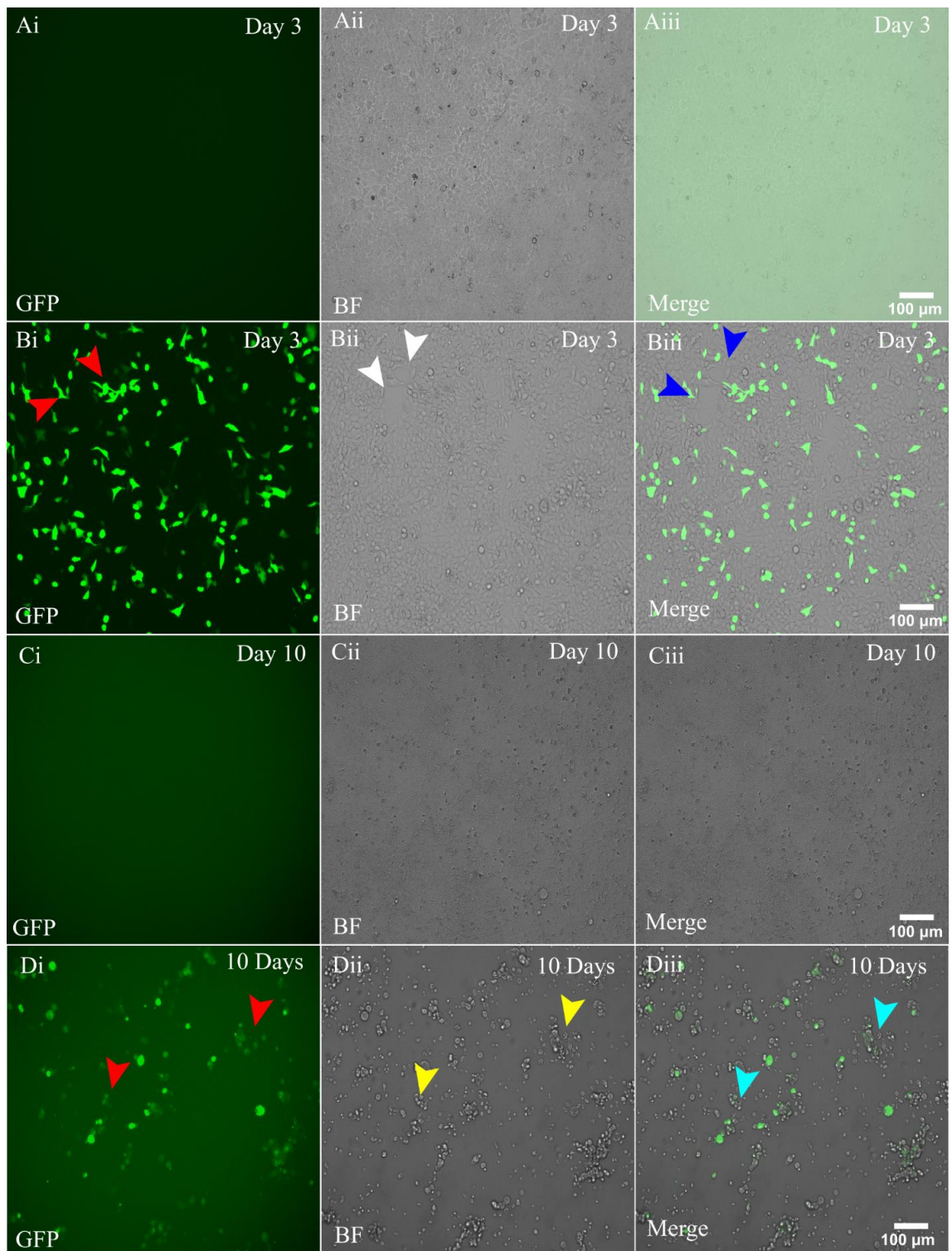
Figure 6. 3 PacAd5IRP-GFP expressed in HEK293 AD cells. (Ai-Aiii): Polyjet reagent treated HEK293 AD control cells. (Bi-Biii) PacAd5IRP-GFP and pacAD 59.2-100 plasmids were co-transfected into HEK293 AD cells. Expression on day 3 post-transfection. Red arrows to show GFP (Bi), (Bii) bright field (BF) to show cells states, (Aiii) image merged with GFP and bright field. White arrows to show infection plaques. (Ci-Ciii): On day 10 post-transfection, only polyjet regent was transfected into

the HEK293 AD cells. (Di-Diii): On day 10 post-transfection, PacAd5IRP-GFP and pacAd59.2-100 plasmid were co-transfected into HEK293 AD cells. Red arrows to show GFP (Di), Yellow arrows to show the detached cells (Dii). Image merged with GFP and bright field (Diii) (Cyan). Pictures were taken under 10x EVOS.

Next, to screen the optimal virus 'sub clones' (refer to individual cells or organisms that are derived from a common parent cell or organism and share similar genetic characteristics), stage 1 virus supernatant was used to infect the HEK293 AD cells in six different wells of 24 well plate. Interestingly, in our experiment, the virus expressed abundantly on day 2, which was quick than we expected. S1-1 to 6 all expressed viruses equally well. They are all considered as the 'best' virus sub clone (the well with the most virus plaques and chosen for further amplification). On day 3 post-infection, GFP expression and significant cytopathic effect (CPE) was observed. The cells were detaching in round clusters (Figure 6.4 B, C, D). There is no virus plaques in the control group, while virus in another three wells seems to equally express and with the similar virus plaques (shown as S1-1, S1-2 and S1-3) (Figure 6.4 Bi, Ci, Di), which implies that any of the 'sub clones' can be used for virus amplification. More than 50% of the cells were detached. Supernatants were collected, as virus stage 2.
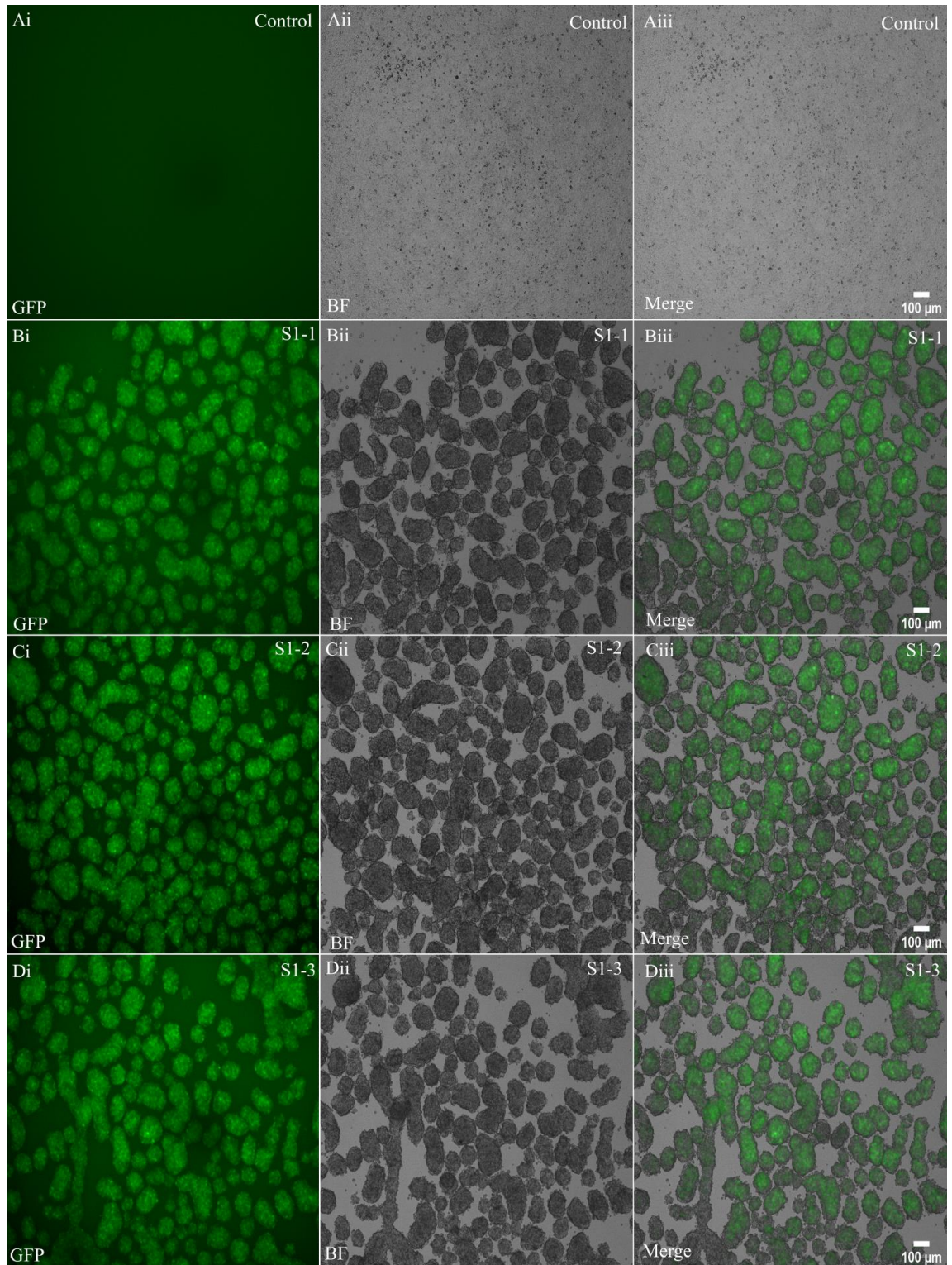
Figure 6. 4 Virus screen from stage 1. (Ai-Aiii) polyjet control group. (Bi-Biii), (Ci-Ciii) and (Di-Diii): stage 1 virus infected HEK 293 cells into six different wells, due to the expression from all six wells are similar, here only present three wells, labelled as S1-1, S1-2, S1-3 respectively. BF to show bright field (BF), virus expressed GFP. The infected cells are detaching in clusters. Pictures were took under 4x EVOS.

Then S2-1 virus was chosen to infect HEK293 AD cells in a 10 cm dish. On day 1 post-infection, Ad5IRP-GFP virus expressed abundantly, however there was little plaques formation (Figure 6.5 Ai-Aiii). While on day 3 and 4 post-infection, much more virus plaques were formed (Figure 6.5 B, C). More than 80% cells were detached and virus were collected as stage 3.
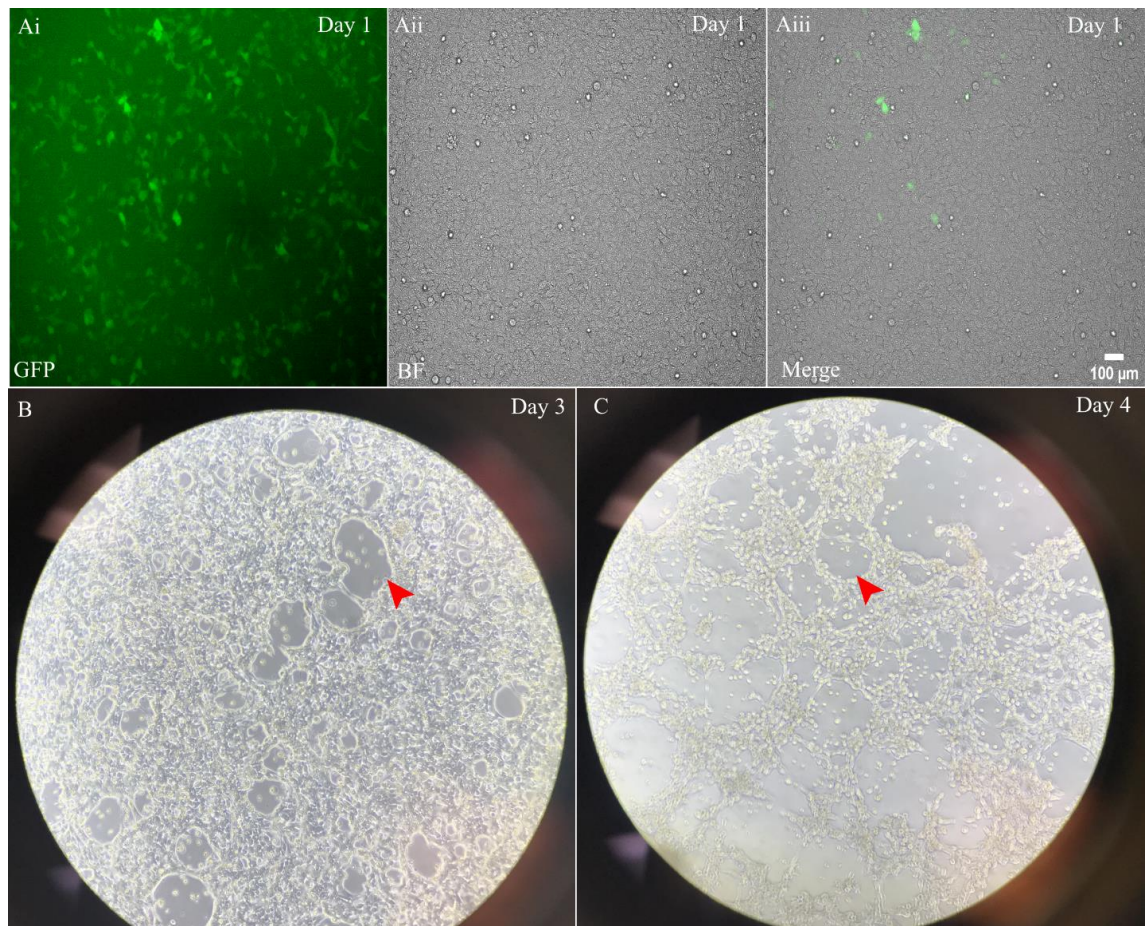
Figure 6. 5 Virus amplification stage 3. HEK293 AD cells were infected with Stage 2 virus in a 10 cm dish. (Ai) Virus expressing GFP on day 1 post-infection, (Aii) Bright field (BF), (Aiii) image merged with GFP and BF. (B) and (C) to show virus plaques forming on day 3 and day 4 post-infection, respectively. Red arrows indicate plaques.

Then stage 3 virus was used to infect in HEK293 AD cells to scale up the virus preparation in 16 flasks, and the virus was collected when 80% of the cells were detached. Virus was purified as described in section Method 2.6.6 and the virus titration was 1.7×10^{11}.

6.3.2 To make PacAd5IRP-CRECFP vector

As RNAscope results showed, GFP was highly colocalized with the insulin receptor probe, which suggests that the Ad5IRP-GFP virus exclusively targets insulin receptor positive neurons. Next PacAd5IRP-CRECFP vector was made. To construct PacAd5IRP-CRECFP vector, PacAd5IRP-GFP and PacAd5CMV-CRECFP vector were digested by restriction enzyme Sbf1 and Kpn1, respectively to remove the promoter sequences. DNA electrophoresis agarose gel showed each of vector was cut into two fragments with correct DNA size (Figure 6.6 A). Then the vector band of PacAd5-CRECFP and insulin receptor promoter were cut and extracted from the gel (Figure 6.6 A). Vector fragment (PacAd5-CRECFP) and the insert gene (IR promoter) were ligated and transformed into LB-agar plate. To confirm that the PacAd5-IRP-CRECFP vector was correctly made, three colonies were chosen and plasmid DNA extracted. DNA digestion with restriction enzymes (Sbf1 and Not1) indicated that CMV promoter from PacAd5CMV-CRECFP vector was successfully replaced by insulin receptor promoter sequence from PacAd5IRP-GFP vector and the PacAd5IRP-CRECFP vector was correctly constructed (Figure 6.6 B).

Since PacAd5IR-CRECFP vector was constructed, Ad5IR-CRECFP recombinant adenovirus virus was made by Dr. Joanne Griffiths (as described in Methods section 2.6). To verify whether this pure virus specifically expresses in the insulin receptor positive neurons, here, Wistar rats were sterotaxically injected bilaterally into the NTS area with the Ad5IRP-CREGFP virus and ADCMV-ShIR-tdTomato (as described in section 2.4.7). One week later, rats were perfused and brain sections were cut at 14 μm in cryostat. As it was shown in Figure 6.7, tdTomato highly expressed in the NTS, which suggested that Ad5IRP-CREGFP virus could drive ADCMV-ShIR-tdTomato expression.
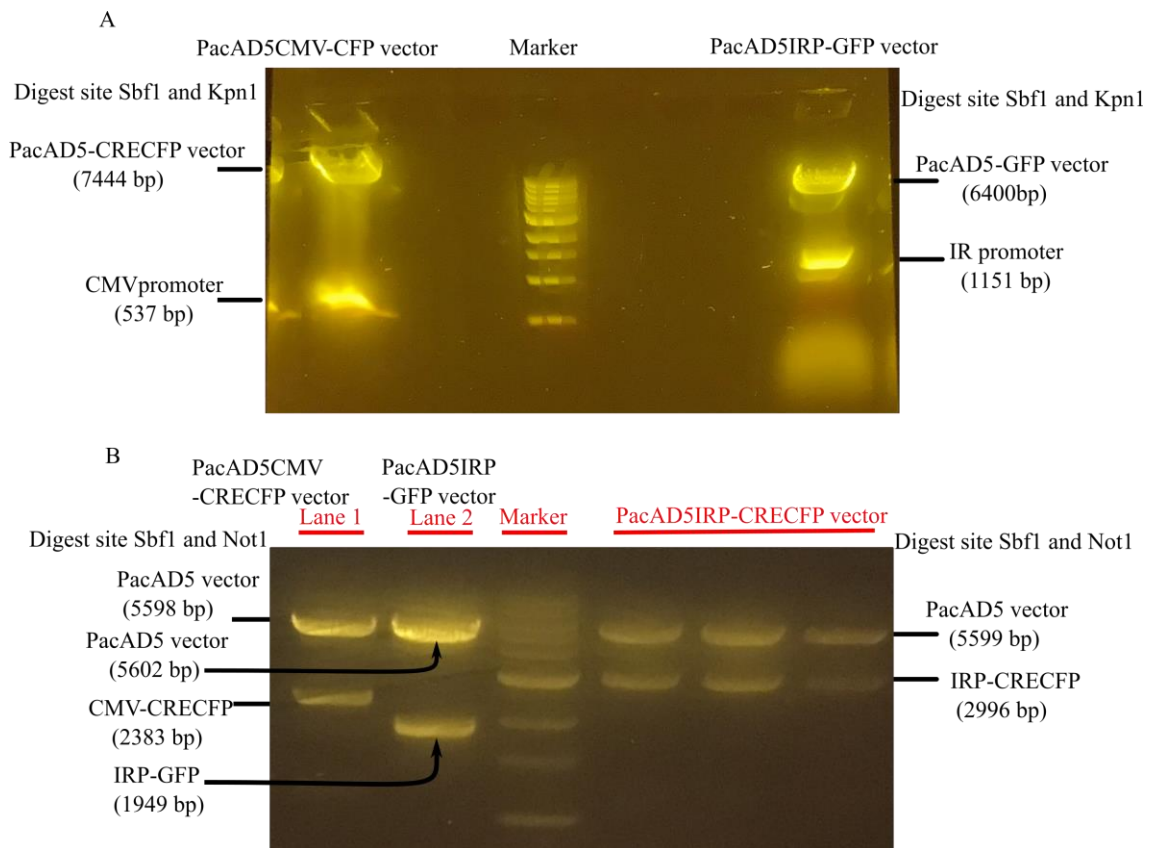
Figure 6. 6 Construction of PacAd5IRP-CRECFP vector. PacAd5IRP-GFP and PacAd5CMV-CRECFP vector were digested by restriction enzyme Sbf1 and Kpn1, respectively. Electrophoresis agarose gel was used to check band size. Two bands separated from PacAd5CMV-CRECFP vector (7981 bp): PacAd5-CRECFP (7444 bp) and CMV promoter (537 bp). Two bands were separated from PacAd5IRP-GFP vector (7551 bp): PacAd5-GFP (6400 bp) and insulin receptor promoter (1151 bp). (B) PacAd5IRP-GFP, PacAd5CMV-CRECFP and PacAd5IRP-CRECFP vector were digested by restriction enzyme Sbf1 and Not1, respectively. Electrophoresis agarose gel was used to check band size. Two bands separated from PacAd5CMV-CRECFP vector (7981 bp): PacAd5 vector (5598 bp) and CMV-CRECFP (2383 bp). Two bands were separated from PacAd5IRP-GFP vector (7551 bp): PacAd5 vector (5602 bp) and IRP-GFP (1949 bp). Two bands were separated from PacAd5IRP-CRECFP vector (8595 bp): PacAd5 vector (5599 bp) and IRP-CRECFP (2996 bp).
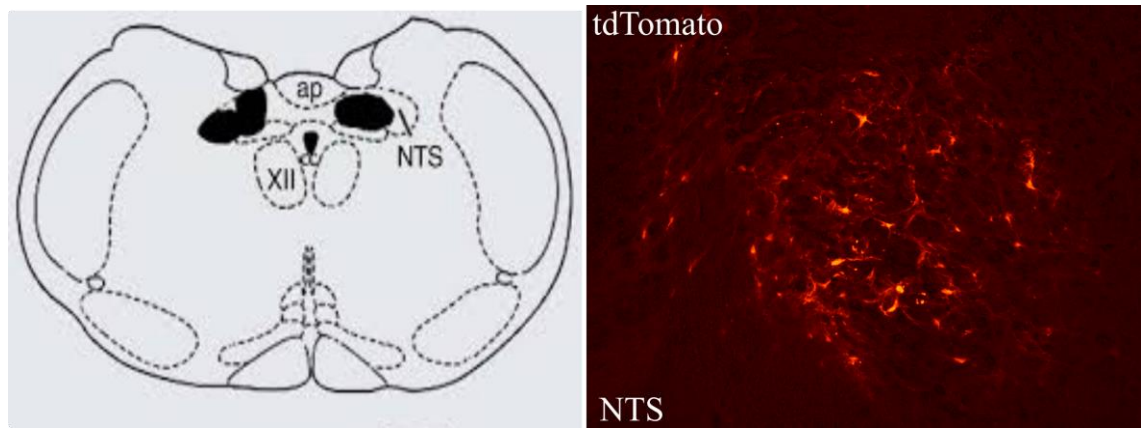
Figure 6. 7 Ad5IRP-CREGFP virus co-injected with ADCMV-ShIR-tdTomato in the NTS. tdTomato (Red) was expressed after one week.

Then Ad5IR-CRECFP recombinant adenovirus combined with pAAV_EF1a FLEX-HA-hM3D (Gq)-mCherry virus will be used to enhance insulin receptor neurons activity in the HDB by i.p injection of CNO to monitor feeding behaviour and locomotor activity in the future experiment.

7 General discussion

7.1 Final discussion and clinical application

The data collected from metabolic cages suggests that acute intranasal insulin could reduce accumulative food intake within 2-5 hours without changing body weight, respiratory exchange ratio or locomotor activity in male mice. This finding implies that intranasal insulin acts as an anorexigenic acute signal to suppress eating in the fasted state, which is in line with the report by Clegg et al (Clegg et al., 2003). Data from human subjects also indicated that acute intranasal insulin could decrease food intake in fasted healthy men compared to the intranasal placebo (Benedict et al., 2008). Compared to systemic drug treatments, intranasal delivery might achieve significant effects with less amount of administration and directly targeting the brain without affecting the peripheral organs (Fehm et al., 2000; Grassin-Delyle et al., 2012). Our results suggest that intranasal insulin might be an effective therapy for the treatment of eating disorders, excessive food consumption, obesity and diabetes.

To track the route of intranasal insulin administration, fluorescent labelled insulin (FITC-insulin) was used as a viable tool in our experimental setting. To our knowledge, our results are the first to report that the HDB area is an insulin positive region through the intranasal delivery method. Note that some elements such as method of administration, deposition, head angles, assistant agents become critical factors in the study of intranasal insulin delivery routes (Dhuria et al., 2010; Rhea et al., 2017), which may explain the difference between our findings and others. For example, van den Berg et al reported that a supine position with the head angle at 70° or 90° was found to be most suitable for efficient delivery to the CSF using this method of intranasal administration (Van Den Berg et al., 2002). The precise nasal transport route to the HDB remains unclear. Three pathways from the olfactory epithelium to the olfactory bulb have been proposed, a transcellular pathway, a paracellular pathway as well as olfactory nerve pathway. Previous studies suggested that intranasal insulin reaches various brain regions within 30 to 60 mins (Born et al., 2002; Fan et al., 2019). However, the transneuronal pathway takes hours for the drugs to reach to the olfactory bulb (Thorne et al., 1995), which is mostly transported by receptor-mediated endocytosis. It was reported that protein albumin (Molecular weight is 66.6 KD) reached the glomeruli of the olfactory bulb after 24 hours, and ultrastructural images confirmed that albumin was detected in the vesicles of bulbous apical endings of the dendrites, which extend to the epithelium (Kristensson and Olsson, 1971), which suggested that transneuronal pathway

cannot be able to explain that the fast transport (45 mins) for FITC-insulin reach to the brain in our study. Here we proposed that intranasal insulin might reach the olfactory bulb through a paracellular pathway, which transports substances through the space of the tight junction between olfactory epithelium cells (Garcia et al., 1998). In addition, intranasal insulin could also reach the brain through the olfactory nerve pathway. Electron microscope results suggested that intranasal gold particles were found in the olfactory receptor neurons within 15 mins and then travelled to the olfactory bulb in 30 to 60 mins (De Lorenzo, 1970), which implies that intranasal substances could reach the olfactory bulb through the olfactory neurons-mediated pathway, which projects to different brain regions (Itaya, 1987). For example, it has been reported that intranasal delivery wheat germ agglutinin-horseradish peroxidase (WGA-HRP) was found in the deep brain structures, such as midbrain and pons within 45 to 60 mins (Shipley, 1985). Altogether, the fast transport of intranasal insulin from nose to the brain is likely through the paracellular pathway and olfactory nerve pathway rather than transcellular pathway (Figure 7.1 to show how intranasal insulin could reach the HDB).
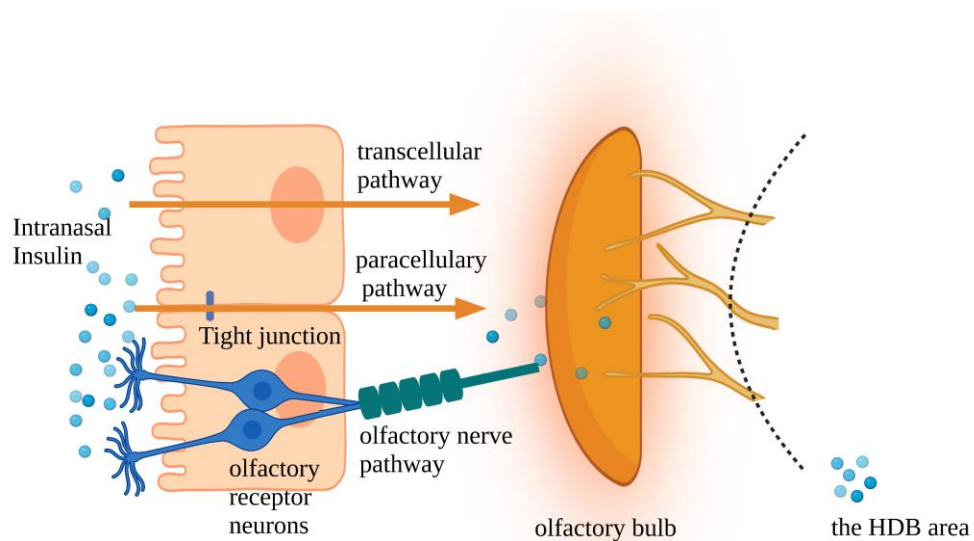
Figure 7. 1 The hypothesis of how intranasal insulin reach the HDB. Transneuronal pathway is receptor-mediated endocytosis, which usually take hours to transport insulin to the OB. Intranasal insulin is transported by paracellulary pathway which transports intranasal insulin through the space of tight junction between olfactory epithelium cells and to reach the OB. Olfactory receptor neurons in the epithelium cells transport intranasal insulin, which extend to the olfactory bulb, and from olfactory bulb could project to various brain areas.

Our data indicated that intranasal insulin abundantly accumulated in the HDB and co-localised with cholinergic neurons through intranasal administration, implying that the HDB area could be the key region that is involved in intranasal insulin-dependent reduction of food intake. One reason we use mice to evaluate the physiology function of intranasal insulin is that we can take advantage of metabolic cages to collect data from mice after intranasal administration. Rats are not suitable for use in the metabolic cages available at Leeds. On the contrary, rats are more suitable to conduct knocking down insulin receptor in the HDB due to their larger brain compared to mice, and it is also much easier to manually weigh the food intake of rats because rats eat more than mice. Our *in vivo* data showed that knockdown of insulin receptor in the HDB increased food intake. Cholinergic neurons in the HDB provide the source of Ach to other brain areas. The release of Ach is increased after feeding, furthermore, the rise of Ach was delayed when the time course of a meal is prolonged such as in a case of binge eating (Mark et al., 1992; Avena et al., 2008), which suggested that the level of Ach is highly associated with feeding behaviour. Furthermore, it has been reported that local infusion of the Ach in the NAc could induce the cessation of a meal (Mark et al., 1992) and cause taste aversion (Taylor et al., 2011). Another elegant study found that impairment of cholinergic signalling in the HDB results in hyperphagia and obesity (Herman et al., 2016). In addition, neurotransmitter Ach can also influence the release of insulin from pancreas (Gilon and Henquin, 2001; Molina et al., 2014), which may be a direct way to reduce food intake. Intranasal insulin could act as a factor to likely increase the activity of cholinergic neurons which increases release of ACh in the brain regions, consequently reducing food intake (The potential mechanism of how intranasal insulin could reduce food intake is proposed in Figure 7.2). In the future, detecting efflux of acetylcholine by using microdialysis method (Calva et al., 2018) might provide some insights on whether intranasal insulin affects the level of Ach, and this effect regulates feeding behaviours. Specifically, by using microdialysis probes to collect extracellular fluid from the target brain regions (the HDB). Measure ACh levels in the dialysate using analytical techniques such as high-performance liquid chromatography (HPLC) after intranasal insulin administration to investigate the relationship between Ach and food intake.

increase food intake

②

Choline acetyltransferase
(ChAT)

Choline + Acetyl-CoA ⟶ Acetylcholine ① → decrease food intake
(Ach)

intranasal insulin ③

decrease food intake
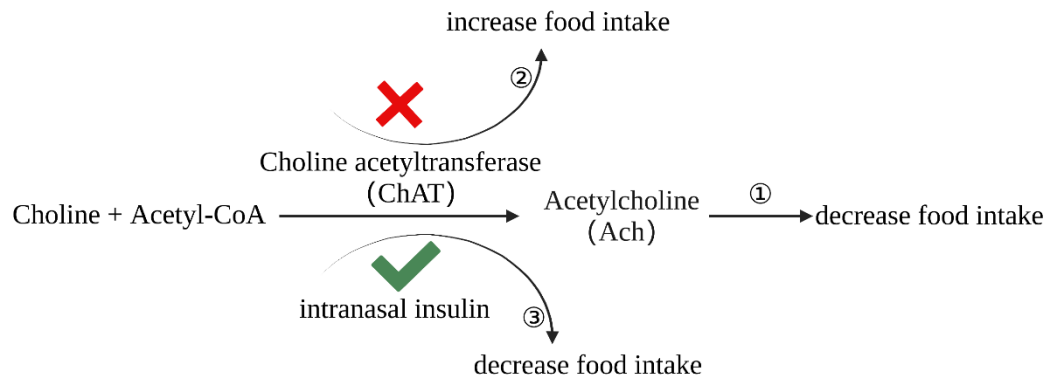
Figure 7. 2 The potential mechanism of how intranasal insulin reduce food intake.
① The level of Ach was increased following a meal and the high level of Ach could suppress the food intake. ② Impaired cholinergic neurons in the HDB leads to hyperphagia. ③ Intranasal insulin reaches the HDB as a factor to facilitate the process of the synthesis of Ach, which may be associated with the reduction in food intake.

It was reported that specifically ablating cholinergic neurons in the HDB using DT did not alter activity in mice (Herman et al., 2016), which is different to our findings that knockdown of the insulin receptor in the HDB caused a remarkable increase in activity in female rats. Neurotransmitter dopamine that is released from the substantia nigra, ventral tegmental area (VTA) and hypothalamus, which has been involved in locomotor activity (Juarez Olguin et al., 2016). Interestingly, we also observed that the VTA sent axons to the HDB, which is in line with previous reports (Beckstead et al., 1979; Geisler and Zahm, 2005; Do et al., 2016). One potential explanation of hyperactivity observed in our study is that knocking down insulin receptor in the HDB could enhance the release of dopamine from the VTA. In addition, the VTA consists of multiple neuronal populations, including dopaminergic neurons (65%), GABAergic neurons (33%) and glutamatergic neurons (2%) (Morales and Root, 2014; Nair-Roberts et al., 2008). The following question is which/how neuronal cell type and/or types in the VTA involved in regulation of the level of dopamine in the HDB and what the mechanisms are.

The projection from the VTA spread in various brain areas, such as cerebral cortex and basal forebrain (Beckstead et al., 1979; Fallon, 1981), which is involved in learning, feeding, and locomotor activity (Wise, 2004; Fields et al., 2007). A whole brain mapping study showed that the input to the basal forebrain from the VTA are parvalbumin, somatostatin, vesicular glutamate and choline acetyltransferase cells (Do

et al., 2016; Gaykema and Zaborszky, 1997). In addition, GABAergic neurons of the VTA could inhibit the cholinergic interneurons in the NAc, which suggested that GABA projection from the VTA could be a modulator of dopaminergic and cholinergic communication (Brown et al., 2012). Previous study further suggested intracerebral administration of GABA receptor agonist into the VTA increased dopamine concentrations in the HDB (Eaton et al., 1994), which may be related to active movement in rats. While our data further showed that the cell body in the VTA was colocalized with TH positive neurons (a marker for dopamine, norepinephrine, and catecholamine neurons), which implies that the dopaminergic neurons in the VTA may innervate the release of dopamine in the HDB.

Furthermore, Gaykema et al pointed that cholinergic neurons in the basal forebrain are the targets of dopaminergic VTA neurons, which implies that dopamine could direct modulate the release of Ach (Gaykema and Zaborszky, 1996). Ach level is associated with arousal, attention, learning and locomotor behaviour, this connection between the VTA and HDB provides as a therapeutic option for the cognitive symptoms and activity (Hangya et al., 2015; Malloy et al., 2019). Notably, the activity of dopamine transmission is also tightly modulated by cholinergic system. For example, nicotinic ACh receptor (nAChR) agonists could stimulate dopamine release (Quik and Mcintosh, 2006), which may be provide a new treatment for the Parkinson's disease (a movement disorder). Another study suggested that the HDB also projects to the VTA (Geisler and Zahm, 2005). While the activation of cholinergic terminals (an inhibitory neurotransmission) in the substantia nigra would inhibit dopamine neurons and lead to a decrease in movement (Estakhr et al., 2017). Here we proposed hypothesises that knockdown of the insulin receptor in the HDB may impede the cholinergic input to the dopamine neurons in the VTA, which disinhibits the activity of dopamine neurons and consequently causes hyperactivity (Figure 7.3). However, this neuronal circuits may be different in different sexes.
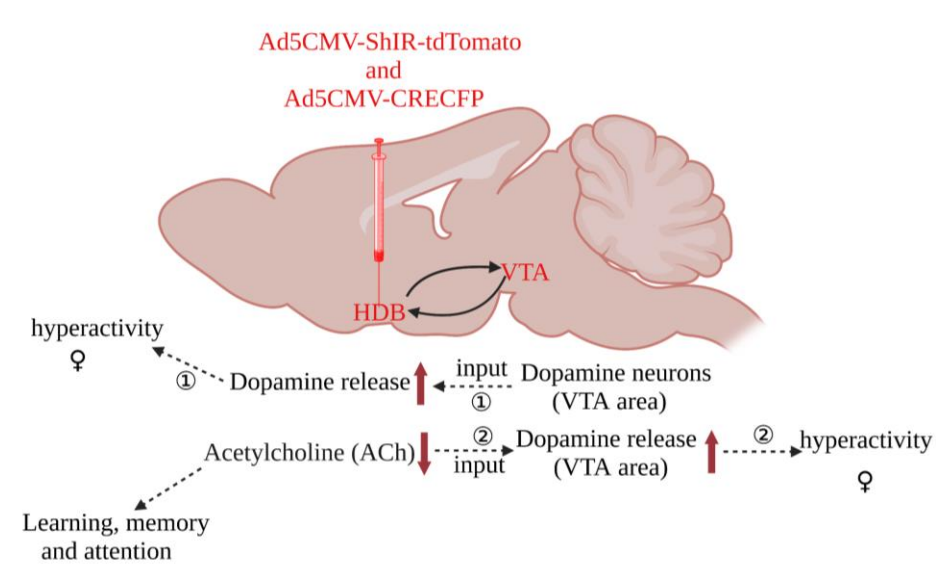
Figure 7. 3 The potential mechanism of knocking down insulin receptor in the HDB leading to hyperactivity in female rats but not male rats. ① Dopaminergic neurons in the VTA may affect the release of dopamine in the HDB to regulate activity. ② Impaired insulin receptor signalling in the HDB impedes the cholinergic input to the dopamine neurons in the VTA, which disinhibits the activity of dopamine neurons and consequently causes hyperactivity.

7.2 Future work

My current Ph.D project demonstrated that the insulin signaling in the HDB plays an important role in regulating feeding behavior and locomotor activity. However, due to the limited time resulting from the Covid pandemic, there are still more work to be done in order to gain a better understanding of this area in modulating metabolism.

Firstly, our data indicates that intranasal insulin reduced food intake within 2 to 5 hours in mice compared to the control, which illustrates the effect of intranasal insulin on feeding behavior *in vivo*. On the other hand, we also observed that with intranasal FITC-insulin administration, abundant insulin receptor positive signaling in the HDB area was detected. These findings led us to explore the relationship between insulin receptor signaling in the HDB and food intake. Interestingly, our *in vivo* work further suggested that insulin receptor knockdown in the HDB could significantly increase food intake in male rats, which implied that insulin signaling in the HDB might be the key to

151

the effect that intranasal insulin has on regulating feeding behaviour. In the future, we plan to knockdown the insulin receptor in the HDB area in rats and to evaluate that whether the effect of intranasal insulin induced decreased food intake will be prevented. But due to the restriction of animal license, currently we are unable to do this experiment.

Secondly, while we clearly show the importance of insulin sensing in the HDB in the regulation of feeding and activity, little is known regarding the cell populations that are insulin sensitive and which neuronal network is modulated by insulin sensing in the HDB. For example, work by Gritti et al estimated the proportion of different neuronal cell types in the basal forebrain, and the results suggested that only 5% of the total number of neurones represents cholinergic neurones, 25% of neurons are GABAergic, and 69% are glutamatergic (Gritti et al., 2006). Previous studies have mostly focused on one or two neural types in the HDB, however data about whether and/or how insulin interacts with these cell types to regulate feeding behaviour is still missing. In addition, our study and others also showed that some neurons co-express acetylcholine with glutamate and GABA, this also brings the challenge of selectively discerning different neural types (Ren et al., 2011; Herman et al., 2016). For example, a study from Herman et al suggested that the cholinergic neurones in the HDB are mostly GABAergic (Herman et al., 2016). However, how insulin signaling acts on the cholinergic neurones and/or GABAergic neurons has not yet been studied. For further work, we could impair insulin signaling exclusively in the GABAergic neurones and/or cholinergic neurones by using transgenic mice or using adenovirus system to investigate the role of insulin signaling in each type of neurons in regulating feeding behaviour and metabolic balance.

Third, our current study is just the first to demonstrate that the HDB might be a key area for the effect that intranasal insulin has on regulating feeding behaviour, however, the mechanisms of how insulin signaling in the HDB regulates food intake still unclear. Data from Herman et al indicated that dysfunction of cholinergic neurons in the HDB is related to decreased POMC activity in the hypothalamus, which might explain the increased food intake. Future work should therefore focus on if insulin receptor knockdown in the HDB influences the activity of other neurons involved in energy homeostasis, such as hypothalamic POMC or AgRP neurons. In order to investigate this possibility, we could use western blot or qPCR to check the gene expression of POMC

or AgRP. In addition, an electrophysiological technique could be an ideal tool to answer this question. We can record the POMC or AgRP neurons to see whether their neuronal activity is different when insulin receptor is knocked down in the HDB, and whether their neuronal activity will be changed when insulin is applied.

Fourth, we observed that female rats but not male rats were hyperactive after insulin receptor knockdown in the HDB, however more work needs to be done to explore the mechanism behind this phenomenon in the future. Previous reports showed that ablation of brain-derived neurotropic factor in mice causes obesity and increased activity (Rios et al., 2001). Specifically deleting FoxO1 in the POMC neurons increased α-Melanocyte-stimulating hormone (α-MSH) and melanocortin signaling in hypothalamus, these mice also exhibited increased locomotor activity (Plum et al., 2009). This increased locomotor activity was also observed in mice lacking FoxO1 in synapsin neurons, the mRNA level of Pcsk1 and Prcp (genes negatively regulated by α–MSH signaling) were remarkably reduced in the hypothalamus of FoxO1 depleted mice during the dark phase (Ren et al., 2013). In the future, we can also measure the mRNA level of Pcsk1 and Prcp in our animals with the insulin receptor knockdown in the HDB, which may provide some valuable insights into some genetic biomarkers which may be related to activity in these rodents. In addition, we have made the recombinant adenovirus expressing CRECFP from the insulin receptor promoter (Ad5IRP-CRECFP) that can be delivered with chemogenetic (FLEX-hM3Dq) virus to specifically target the insulin receptor positive cell in the HDB, and then by injecting CNO in the peripheral system we can selectively enhance the activity of insulin receptor in the HDB to monitor whether the activity of insulin receptor will reverse the food intake and locomotion. In addition, Chen et al reported that loss of insulin signalling in astrocytes led to the reduction of body weight in male and female mice (Chen et al., 2023). Their study also pointed out that knockout of IR in astrocytes could impair mitochondrial respiration and glycolysis, which suggested that insulin signalling in the astrocytes is also crucial to regulate metabolism. Our lab also developed GFAP promoter viruses to specifically target astrocyte. In the future, we can further investigate the effect of activating insulin signalling in the astrocytes in the HDB on the metabolism (Patel et al., 2021).

Fifth, eating behaviour is also related to emotional states, where studies suggest that there is a connection between eating habits and mood (Kaye et al., 2004). In addition to

eating behaviour, the HDB is also associated with cognition, awake and sleep (Anaclet et al., 2015; Heimer, 2000). Cassidy et al reported that GABAergic neurons in the HDB could receive monosynaptic inhibitory input from GABAergic neurons in the lateral hypothalamus (Cassidy et al., 2019). Activation of this circuit reduces anxiety and causes overeating (Cassidy et al., 2019). In our study, we observed that impaired insulin signaling in the HDB significantly increased food intake, however whether this is also related to emotional state has not been explored. On the other hand, our retrograde data suggested that dopaminergic neurons in the VTA might send projections to the HDB, which means the terminal of the VTA are in the HDB area. However, whether the projection from the VTA is crucial for the HDB to regulate mood and feeding is also important to study further. To answer this question, we can inject optogenetic viruses in the HDB and implant a fiber optic into the VTA to stimulate the cell body in the VTA, and investigate if enhancing the projection to the HDB will influence feeding behaviour.

7.3 Final conclusion

This project firstly confirmed that FITC-insulin has bioactivity using PC12 cells, activating the insulin downstream signaling p-Akt pathway but failing to activate p-Erk. In addition, FITC-insulin entered into PC12 cells showing a dynamic process, beginning from binding on the membranes, cytoplasm, then into the nucleus. Our experiments indicated that loss of insulin receptor alone markedly decrease FITC-insulin's internalization, which underscored that insulin receptors were necessary in insulin's internalization. In addition, our acute mouse brain slices also suggested that FITC-insulin as well as human insulin could activate p-Akt signaling in the hippocampus at 30 mins incubation compared with the same equal molar of FITC-Dye. Together, these investigations warrant that FITC-insulin is as a viable tool in scientific study as it performs like normal human insulin.

Intranasal insulin could suppress food intake within 2-5 hours in male mice, which is consistent with previous findings in human subjects. Also, intranasal delivery of FITC-insulin could reach various brain regions, including the olfactory bulb, HDB, hippocampus and brainstem. Among them, the HDB might be the key area to regulate feeding behaviour. Notably, knockdown of the insulin receptor in the HDB significantly increased food intake in male rats, these data demonstrated that insulin signaling

especially in the HDB might play an important role in modulating feeding behaviour. However, one of limitation in the current project is that we did not evaluate the knockdown efficiency in vivo. We cannot rule out the possibility that the virus may not have achieved 100% effectiveness, which might explain the absence of any significant effect on the cumulative food intake in female animals. To address this limitation, future studies should aim to incorporate in vivo analyses of insulin receptor knockdown in the specific brain region of interest (the HDB) to provide a more comprehensive understanding of its functional implications.

Another important finding is that the anorexigenic effect of intranasal insulin seems more sensitive in male rats compared to female rats, whereas insulin signaling on the HDB-related activity is more pronounced in female but not male rats. Our findings support the concept that the function of brain insulin signaling exhibited gender differences.

Finally, our findings also bring more opportunities for the clinical application of intranasal insulin. On the one hand, our study suggested that insulin reached the HDB through intranasal administration and insulin signaling in this area is closely associated with the feeding behaviour and activity. These observations further strengthen the value of developing non-invasive delivery insulin system.

References

Abu-Elheiga, L., Brinkley, W. R., Zhong, L., Chirala, S. S., Woldegiorgis, G. and Wakil, S. J. (2000). The subcellular localization of acetyl-coa carboxylase 2. Proc Natl Acad Sci U S A, *97*, 1444-9.

Adachi, M., Fukuda, M. and Nishida, E. (2000). Nuclear export of map kinase (erk) involves a map kinase kinase (mek)-dependent active transport mechanism. J Cell Biol, *148*, 849-56.

Adachi, M., Fukuda, M. and Nishida, E. (1999). Two co-existing mechanisms for nuclear import of map kinase: Passive diffusion of a monomer and active transport of a dimer. EMBO J, *18*, 5347-58.

Aime, P., Hegoburu, C., Jaillard, T., Degletagne, C., Garcia, S., Messaoudi, B., Thevenet, M., Lorsignol, A., Duchamp, C., Mouly, A. M. and Julliard, A. K. (2012). A physiological increase of insulin in the olfactory bulb decreases detection of a learned aversive odor and abolishes food odor-induced sniffing behavior in rats. PLoS One, *7*, e51227.

Air, E. L., Benoit, S. C., Blake Smith, K. A., Clegg, D. J. and Woods, S. C. (2002). Acute third ventricular administration of insulin decreases food intake in two paradigms. Pharmacol Biochem Behav, *72*, 423-9.

Akatsuka, A., Singh, T. J., Nakabayashi, H., Lin, M. C. and Huang, K. P. (1985). Glucagon-stimulated phosphorylation of rat liver glycogen synthase in isolated hepatocytes. J Biol Chem, *260*, 3239-42.

Akintola, A. A., Van Opstal, A. M., Westendorp, R. G., Postmus, I., Van Der Grond, J. and Van Heemst, D. (2017). Effect of intranasally administered insulin on cerebral blood flow and perfusion; a randomized experiment in young and older adults. Aging (Albany NY), *9*, 790-802.

Al Koborssy, D., Palouzier-Paulignan, B., Salem, R., Thevenet, M., Romestaing, C. and Julliard, A. K. (2014). Cellular and molecular cues of glucose sensing in the rat olfactory bulb. Front Neurosci, *8*, 333.

Alexander, G. M., Rogan, S. C., Abbas, A. I., Armbruster, B. N., Pei, Y., Allen, J. A., Nonneman, R. J., Hartmann, J., Moy, S. S., Nicolelis, M. A., Mcnamara, J. O. and Roth, B. L. (2009). Remote control of neuronal activity in transgenic mice expressing evolved g protein-coupled receptors. Neuron, *63*, 27-39.

Alves-Bezerra, M. and Cohen, D. E. (2017). Triglyceride metabolism in the liver. Compr Physiol, *8*, 1-8.

Anaclet, C., Pedersen, N. P., Ferrari, L. L., Venner, A., Bass, C. E., Arrigoni, E. and Fuller, P. M. (2015). Basal forebrain control of wakefulness and cortical rhythms. Nat Commun, *6*, 8744.

Andersson, K. E. (1992). Clinical pharmacology of potassium channel openers. Pharmacol Toxicol, *70*, 244-54.

Anthony, K., Reed, L. J., Dunn, J. T., Bingham, E., Hopkins, D., Marsden, P. K. and Amiel, S. A. (2006). Attenuation of insulin-evoked responses in brain networks controlling appetite and reward in insulin resistance: The cerebral basis for impaired control of food intake in metabolic syndrome? Diabetes, *55*, 2986-92.

Aponte, Y., Atasoy, D. and Sternson, S. M. (2011). Agrp neurons are sufficient to orchestrate feeding behavior rapidly and without training. Nat Neurosci, *14*, 351-5.

Arnold, S. E., Arvanitakis, Z., Macauley-Rambach, S. L., Koenig, A. M., Wang, H. Y., Ahima, R. S., Craft, S., Gandy, S., Buettner, C., Stoeckel, L. E., Holtzman, D. M. and Nathan, D. M. (2018). Brain insulin resistance in type 2 diabetes and alzheimer disease: Concepts and conundrums. Nat Rev Neurol, *14*, 168-181.

Ashcroft, F. M. (2005). Atp-sensitive potassium channelopathies: Focus on insulin secretion. J Clin Invest, *115*, 2047-58.

Avena, N. M., Rada, P. and Hoebel, B. G. (2008). Underweight rats have enhanced dopamine release and blunted acetylcholine response in the nucleus accumbens while bingeing on sucrose. Neuroscience, *156*, 865-71.

Balin, B. J., Broadwell, R. D., Salcman, M. and El-Kalliny, M. (1986). Avenues for entry of peripherally administered protein to the central nervous system in mouse, rat, and squirrel monkey. J Comp Neurol, *251*, 260-80.

Bally, L., Thabit, H., Hartnell, S., Andereggen, E., Ruan, Y., Wilinska, M. E., Evans, M. L., Wertli, M. M., Coll, A. P., Stettler, C. and Hovorka, R. (2018). Closed-loop insulin delivery for glycemic control in noncritical care. N Engl J Med, *379*, 547-556.

Band, G. C. and Jones, C. T. (1980). Functional activation by glucagon of glucose 6-phosphatase and gluconeogenesis in the perfused liver of the fetal guinea pig. FEBS Lett, *119*, 190-4.

Banks, W. A., Jaspan, J. B. and Kastin, A. J. (1997). Selective, physiological transport of insulin across the blood-brain barrier: Novel demonstration by species-specific radioimmunoassays. Peptides, *18*, 1257-62.

Banks, W. A. and Kastin, A. J. (1998). Differential permeability of the blood-brain barrier to two pancreatic peptides: Insulin and amylin. Peptides, *19*, 883-9.

Banting, F. G., Best, C. H., Collip, J. B., Campbell, W. R. and Fletcher, A. A. (1922). Pancreatic extracts in the treatment of diabetes mellitus. Can Med Assoc J, *12*, 141-6.

Banting, F. G., Best, C. H., Collip, J. B., Campbell, W. R. and Fletcher, A. A. (1991). Pancreatic extracts in the treatment of diabetes mellitus: Preliminary report. 1922. CMAJ, *145*, 1281-6.

Banting, F. G., Best, C. H., Collip, J. B., Campbell, W. R. and Fletcher, A. A. (1962). Pancreatic extracts in the treatment of diabetes mellitus: Preliminary report. Can

Med Assoc J, *87*, 1062-7.

Bartus, R. T., Dean, R. L., 3rd, Beer, B. and Lippa, A. S. (1982). The cholinergic hypothesis of geriatric memory dysfunction. Science, *217*, 408-14.

Baskin, D. G., Brewitt, B., Davidson, D. A., Corp, E., Paquette, T., Figlewicz, D. P., Lewellen, T. K., Graham, M. K., Woods, S. G. and Dorsa, D. M. (1986). Quantitative autoradiographic evidence for insulin receptors in the choroid plexus of the rat brain. Diabetes, *35*, 246-9.

Batista, T. M., Cederquist, C. T. and Kahn, C. R. (2019). The insulin receptor goes nuclear. Cell Res, *29*, 509-511.

Baura, G. D., Foster, D. M., Porte, D., Jr., Kahn, S. E., Bergman, R. N., Cobelli, C. and Schwartz, M. W. (1993). Saturable transport of insulin from plasma into the central nervous system of dogs in vivo. A mechanism for regulated insulin delivery to the brain. J Clin Invest, *92*, 1824-30.

Beale, E., Andreone, T., Koch, S., Granner, M. and Granner, D. (1984). Insulin and glucagon regulate cytosolic phosphoenolpyruvate carboxykinase (gtp) mrna in rat liver. Diabetes, *33*, 328-32.

Beckstead, R. M., Domesick, V. B. and Nauta, W. J. (1979). Efferent connections of the substantia nigra and ventral tegmental area in the rat. Brain Res, *175*, 191-217.

Begg, D. P., Mul, J. D., Liu, M., Reedy, B. M., D'alessio, D. A., Seeley, R. J. and Woods, S. C. (2013). Reversal of diet-induced obesity increases insulin transport into cerebrospinal fluid and restores sensitivity to the anorexic action of central insulin in male rats. Endocrinology, *154*, 1047-54.

Beirami, E., Oryan, S., Seyedhosseini Tamijani, S. M., Ahmadiani, A. and Dargahi, L. (2017). Intranasal insulin treatment alleviates methamphetamine induced anxiety-like behavior and neuroinflammation. Neurosci Lett, *660*, 122-129.

Benedict, C., Brede, S., Schioth, H. B., Lehnert, H., Schultes, B., Born, J. and Hallschmid, M. (2011a). Intranasal insulin enhances postprandial thermogenesis and lowers postprandial serum insulin levels in healthy men. Diabetes, *60*, 114-8.

Benedict, C., Frey, W. H., 2nd, Schioth, H. B., Schultes, B., Born, J. and Hallschmid, M. (2011b). Intranasal insulin as a therapeutic option in the treatment of cognitive impairments. Exp Gerontol, *46*, 112-5.

Benedict, C., Hallschmid, M., Hatke, A., Schultes, B., Fehm, H. L., Born, J. and Kern, W. (2004). Intranasal insulin improves memory in humans. Psychoneuroendocrinology, *29*, 1326-34.

Benedict, C., Hallschmid, M., Schmitz, K., Schultes, B., Ratter, F., Fehm, H. L., Born, J. and Kern, W. (2007). Intranasal insulin improves memory in humans: Superiority of insulin aspart. Neuropsychopharmacology, *32*, 239-43.

Benedict, C., Kern, W., Schultes, B., Born, J. and Hallschmid, M. (2008). Differential

sensitivity of men and women to anorexigenic and memory-improving effects of intranasal insulin. J Clin Endocrinol Metab, *93*, 1339-44.

Benoit, S. C., Air, E. L., Coolen, L. M., Strauss, R., Jackman, A., Clegg, D. J., Seeley, R. J. and Woods, S. C. (2002). The catabolic action of insulin in the brain is mediated by melanocortins. J Neurosci, *22*, 9048-52.

Berry, R., Jeffery, E. and Rodeheffer, M. S. (2014). Weighing in on adipocyte precursors. Cell Metab, *19*, 8-20.

Blindness, G. B. D., Vision Impairment, C. and Vision Loss Expert Group of the Global Burden of Disease, S. (2021). Causes of blindness and vision impairment in 2020 and trends over 30 years, and prevalence of avoidable blindness in relation to vision 2020: The right to sight: An analysis for the global burden of disease study. Lancet Glob Health, *9*, e144-e160.

Bloem, B., Schoppink, L., Rotaru, D. C., Faiz, A., Hendriks, P., Mansvelder, H. D., Van De Berg, W. D. and Wouterlood, F. G. (2014). Topographic mapping between basal forebrain cholinergic neurons and the medial prefrontal cortex in mice. J Neurosci, *34*, 16234-46.

Bode, B. W., Mcgill, J. B., Lorber, D. L., Gross, J. L., Chang, P. C., Bregman, D. B. and Affinity 1 Study, G. (2015). Inhaled technosphere insulin compared with injected prandial insulin in type 1 diabetes: A randomized 24-week trial. Diabetes Care, *38*, 2266-73.

Bohringer, A., Schwabe, L., Richter, S. and Schachinger, H. (2008). Intranasal insulin attenuates the hypothalamic-pituitary-adrenal axis response to psychosocial stress. Psychoneuroendocrinology, *33*, 1394-400.

Born, J., Lange, T., Kern, W., Mcgregor, G. P., Bickel, U. and Fehm, H. L. (2002). Sniffing neuropeptides: A transnasal approach to the human brain. Nat Neurosci, *5*, 514-6.

Bost, F., Aouadi, M., Caron, L., Even, P., Belmonte, N., Prot, M., Dani, C., Hofman, P., Pages, G., Pouyssegur, J., Le Marchand-Brustel, Y. and Binetruy, B. (2005). The extracellular signal-regulated kinase isoform erk1 is specifically required for in vitro and in vivo adipogenesis. Diabetes, *54*, 402-11.

Brabazon, F., Wilson, C. M., Jaiswal, S., Reed, J., Frey, W. H. N. and Byrnes, K. R. (2017). Intranasal insulin treatment of an experimental model of moderate traumatic brain injury. J Cereb Blood Flow Metab, *37*, 3203-3218.

Brange, J., Ribel, U., Hansen, J. F., Dodson, G., Hansen, M. T., Havelund, S., Melberg, S. G., Norris, F., Norris, K., Snel, L. and Et Al. (1988). Monomeric insulins obtained by protein engineering and their medical implications. Nature, *333*, 679-82.

Brito, M. N., Brito, N. A., Baro, D. J., Song, C. K. and Bartness, T. J. (2007). Differential activation of the sympathetic innervation of adipose tissues by melanocortin receptor stimulation. Endocrinology, *148*, 5339-47.

Brown, L. M., Clegg, D. J., Benoit, S. C. and Woods, S. C. (2006). Intraventricular insulin and leptin reduce food intake and body weight in c57bl/6j mice. Physiol Behav, *89*, 687-91.

Brown, M. T., Tan, K. R., O'connor, E. C., Nikonenko, I., Muller, D. and Luscher, C. (2012). Ventral tegmental area gaba projections pause accumbal cholinergic interneurons to enhance associative learning. Nature, *492*, 452-6.

Bruning, J. C., Gautam, D., Burks, D. J., Gillette, J., Schubert, M., Orban, P. C., Klein, R., Krone, W., Muller-Wieland, D. and Kahn, C. R. (2000). Role of brain insulin receptor in control of body weight and reproduction. Science, *289*, 2122-5.

Buettner, C., Patel, R., Muse, E. D., Bhanot, S., Monia, B. P., Mckay, R., Obici, S. and Rossetti, L. (2005). Severe impairment in liver insulin signaling fails to alter hepatic insulin action in conscious mice. J Clin Invest, *115*, 1306-13.

Cai, W., Xue, C., Sakaguchi, M., Konishi, M., Shirazian, A., Ferris, H. A., Li, M. E., Yu, R., Kleinridders, A., Pothos, E. N. and Kahn, C. R. (2018). Insulin regulates astrocyte gliotransmission and modulates behavior. J Clin Invest, *128*, 2914-2926.

Caillol, M., Aioun, J., Baly, C., Persuy, M. A. and Salesse, R. (2003). Localization of orexins and their receptors in the rat olfactory system: Possible modulation of olfactory perception by a neuropeptide synthetized centrally or locally. Brain Res, *960*, 48-61.

Calva, C. B. and Fadel, J. R. (2020). Intranasal administration of orexin peptides: Mechanisms and therapeutic potential for age-related cognitive dysfunction. Brain Res, *1731*, 145921.

Calva, C. B., Fayyaz, H. and Fadel, J. R. (2018). Increased acetylcholine and glutamate efflux in the prefrontal cortex following intranasal orexin-a (hypocretin-1). J Neurochem, *145*, 232-244.

Carlson, C. J., Koterski, S., Sciotti, R. J., Poccard, G. B. and Rondinone, C. M. (2003). Enhanced basal activation of mitogen-activated protein kinases in adipocytes from type 2 diabetes: Potential role of p38 in the downregulation of glut4 expression. Diabetes, *52*, 634-41.

Carvalheira, J. B., Ribeiro, E. B., Araujo, E. P., Guimaraes, R. B., Telles, M. M., Torsoni, M., Gontijo, J. A., Velloso, L. A. and Saad, M. J. (2003). Selective impairment of insulin signalling in the hypothalamus of obese zucker rats. Diabetologia, *46*, 1629-40.

Cassidy, R. M., Lu, Y., Jere, M., Tian, J. B., Xu, Y., Mangieri, L. R., Felix-Okoroji, B., Selever, J., Xu, Y., Arenkiel, B. R. and Tong, Q. (2019). A lateral hypothalamus to basal forebrain neurocircuit promotes feeding by suppressing responses to anxiogenic environmental cues. Sci Adv, *5*, eaav1640.

Cha, D. S., Best, M. W., Bowie, C. R., Gallaugher, L. A., Woldeyohannes, H. O., Soczynska, J. K., Lewis, G., Macqueen, G., Sahakian, B. J., Kennedy, S. H., Lui, J. P., Mansur, R. B. and Mcintyre, R. S. (2017). A randomized, double-blind,

placebo-controlled, crossover trial evaluating the effect of intranasal insulin on cognition and mood in individuals with treatment-resistant major depressive disorder. J Affect Disord, *210*, 57-65.

Cha, S. H. and Lane, M. D. (2009). Central lactate metabolism suppresses food intake via the hypothalamic amp kinase/malonyl-coa signaling pathway. Biochem Biophys Res Commun, *386*, 212-6.

Chapman, C. D., Schioth, H. B., Grillo, C. A. and Benedict, C. (2018). Intranasal insulin in alzheimer's disease: Food for thought. Neuropharmacology, *136*, 196-201.

Charron, M. J., Brosius, F. C., 3rd, Alper, S. L. and Lodish, H. F. (1989). A glucose transport protein expressed predominately in insulin-responsive tissues. Proc Natl Acad Sci U S A, *86*, 2535-9.

Chen, C., Turnbull, D. M. and Reeve, A. K. (2019). Mitochondrial dysfunction in parkinson's disease-cause or consequence? Biology (Basel), *8*.

Chen, M., Woods, S. C. and Porte, D., Jr. (1975). Effect of cerebral intraventricular insulin on pancreatic insulin secretion in the dog. Diabetes, *24*, 910-4.

Chen, W., Huang, Q., Lazdon, E. K., Gomes, A., Wong, M., Stephens, E., Royal, T. G., Frenkel, D., Cai, W. and Kahn, C. R. (2023). Loss of insulin signaling in astrocytes exacerbates alzheimer-like phenotypes in a 5xfad mouse model. Proc Natl Acad Sci U S A, *120*, e2220684120.

Chen, Y., Guo, Z., Mao, Y. F., Zheng, T. and Zhang, B. (2018). Intranasal insulin ameliorates cerebral hypometabolism, neuronal loss, and astrogliosis in streptozotocin-induced alzheimer's rat model. Neurotox Res, *33*, 716-724.

Chen, Y., Zhao, Y., Dai, C. L., Liang, Z., Run, X., Iqbal, K., Liu, F. and Gong, C. X. (2014). Intranasal insulin restores insulin signaling, increases synaptic proteins, and reduces abeta level and microglia activation in the brains of 3xtg-ad mice. Exp Neurol, *261*, 610-9.

Cherrington, A. D. (2005). The role of hepatic insulin receptors in the regulation of glucose production. J Clin Invest, *115*, 1136-9.

Chiu, S. L., Chen, C. M. and Cline, H. T. (2008). Insulin receptor signaling regulates synapse number, dendritic plasticity, and circuit function in vivo. Neuron, *58*, 708-19.

Choi, S. M., Tucker, D. F., Gross, D. N., Easton, R. M., Dipilato, L. M., Dean, A. S., Monks, B. R. and Birnbaum, M. J. (2010). Insulin regulates adipocyte lipolysis via an akt-independent signaling pathway. Mol Cell Biol, *30*, 5009-20.

Choi, Y. H., Park, S., Hockman, S., Zmuda-Trzebiatowska, E., Svennelid, F., Haluzik, M., Gavrilova, O., Ahmad, F., Pepin, L., Napolitano, M., Taira, M., Sundler, F., Stenson Holst, L., Degerman, E. and Manganiello, V. C. (2006). Alterations in regulation of energy homeostasis in cyclic nucleotide phosphodiesterase 3b-null mice. J Clin Invest, *116*, 3240-51.

Cholerton, B., Baker, L. D. and Craft, S. (2013). Insulin, cognition, and dementia. Eur J Pharmacol, *719*, 170-179.

Clark, J. T., Kalra, P. S., Crowley, W. R. and Kalra, S. P. (1984). Neuropeptide y and human pancreatic polypeptide stimulate feeding behavior in rats. Endocrinology, *115*, 427-9.

Claxton, A., Baker, L. D., Hanson, A., Trittschuh, E. H., Cholerton, B., Morgan, A., Callaghan, M., Arbuckle, M., Behl, C. and Craft, S. (2015a). Long acting intranasal insulin detemir improves cognition for adults with mild cognitive impairment or early-stage alzheimer's disease dementia. J Alzheimers Dis, *45*, 1269-70.

Claxton, A., Baker, L. D., Hanson, A., Trittschuh, E. H., Cholerton, B., Morgan, A., Callaghan, M., Arbuckle, M., Behl, C. and Craft, S. (2015b). Long-acting intranasal insulin detemir improves cognition for adults with mild cognitive impairment or early-stage alzheimer's disease dementia. J Alzheimers Dis, *44*, 897-906.

Clegg, D. J., Brown, L. M., Woods, S. C. and Benoit, S. C. (2006). Gonadal hormones determine sensitivity to central leptin and insulin. Diabetes, *55*, 978-87.

Clegg, D. J., Riedy, C. A., Smith, K. A., Benoit, S. C. and Woods, S. C. (2003). Differential sensitivity to central leptin and insulin in male and female rats. Diabetes, *52*, 682-7.

Collens, W. S. and Goldzieher, M. A. (1932). Absorption of insulin by nasal mucous membrane. 20. Proceedings of the Society for Experimental Biology and Medicine, *29*, 756 - 759.

Coomans, C. P., Biermasz, N. R., Geerling, J. J., Guigas, B., Rensen, P. C., Havekes, L. M. and Romijn, J. A. (2011). Stimulatory effect of insulin on glucose uptake by muscle involves the central nervous system in insulin-sensitive mice. Diabetes, *60*, 3132-40.

Cori, C. F. and Cori, G. T. (1925). Comparative study of the sugar concentration in arterial and venous blood during insulin action. American Journal of Physiology-Legacy Content, *71*, 688-707.

Corrigan, J. K., Ramachandran, D., He, Y., Palmer, C. J., Jurczak, M. J., Chen, R., Li, B., Friedline, R. H., Kim, J. K., Ramsey, J. J., Lantier, L., Mcguinness, O. P., Mouse Metabolic Phenotyping Center Energy Balance Working, G. and Banks, A. S. (2020). A big-data approach to understanding metabolic rate and response to obesity in laboratory mice. Elife, *9*.

Crea, R., Kraszewski, A., Hirose, T. and Itakura, K. (1978). Chemical synthesis of genes for human insulin. Proc Natl Acad Sci U S A, *75*, 5765-9.

Cushman, S. W. and Wardzala, L. J. (1980). Potential mechanism of insulin action on glucose transport in the isolated rat adipose cell. Apparent translocation of intracellular transport systems to the plasma membrane. J Biol Chem, *255*, 4758-62.

Czosnyka, M., Czosnyka, Z., Momjian, S. and Pickard, J. D. (2004). Cerebrospinal fluid dynamics. Physiol Meas, *25*, R51-76.

Dash, S., Xiao, C., Morgantini, C., Koulajian, K. and Lewis, G. F. (2015). Intranasal insulin suppresses endogenous glucose production in humans compared with placebo in the presence of similar venous insulin concentrations. Diabetes, *64*, 766-74.

De Leiva-Hidalgo, A. and De Leiva-Perez, A. (2020). Experiences of first insulin-treated patients (1922-1923). Am J Ther, *27*, e13-e23.

De Lorenzo, A. J. D. 1970. The olfactory neuron and the blood-brain barrier. *Ciba foundation symposium - internal secretions of the pancreas (colloquia on endocrinology).*

De Luca, C. and Olefsky, J. M. (2008). Inflammation and insulin resistance. FEBS Lett, *582*, 97-105.

Deltour, L., Leduque, P., Blume, N., Madsen, O., Dubois, P., Jami, J. and Bucchini, D. (1993). Differential expression of the two nonallelic proinsulin genes in the developing mouse embryo. Proc Natl Acad Sci U S A, *90*, 527-31.

Derkach, K. V., Ivantsov, A. O., Chistyakova, O. V., Sukhov, I. B., Buzanakov, D. M., Kulikova, A. A. and Shpakov, A. O. (2017). Intranasal insulin restores metabolic parameters and insulin sensitivity in rats with metabolic syndrome. Bull Exp Biol Med, *163*, 184-189.

Devaskar, S. U., Singh, B. S., Carnaghi, L. R., Rajakumar, P. A. and Giddings, S. J. (1993). Insulin ii gene expression in rat central nervous system. Regul Pept, *48*, 55-63.

Dhuria, S. V., Hanson, L. R. and Frey, W. H., 2nd (2010). Intranasal delivery to the central nervous system: Mechanisms and experimental considerations. J Pharm Sci, *99*, 1654-73.

Dimitriadis, G., Mitrou, P., Lambadiari, V., Maratou, E. and Raptis, S. A. (2011). Insulin effects in muscle and adipose tissue. Diabetes Res Clin Pract, *93 Suppl 1*, S52-9.

Do, J. P., Xu, M., Lee, S. H., Chang, W. C., Zhang, S., Chung, S., Yung, T. J., Fan, J. L., Miyamichi, K., Luo, L. and Dan, Y. (2016). Cell type-specific long-range connections of basal forebrain circuit. Elife, *5*.

Dodd, G. T., Michael, N. J., Lee-Young, R. S., Mangiafico, S. P., Pryor, J. T., Munder, A. C., Simonds, S. E., Bruning, J. C., Zhang, Z. Y., Cowley, M. A., Andrikopoulos, S., Horvath, T. L., Spanswick, D. and Tiganis, T. (2018). Insulin regulates pomc neuronal plasticity to control glucose metabolism. Elife, *7*.

Duan, X. and Mao, S. (2010). New strategies to improve the intranasal absorption of insulin. Drug Discov Today, *15*, 416-27.

Duncan, R. E., Ahmadian, M., Jaworski, K., Sarkadi-Nagy, E. and Sul, H. S. (2007). Regulation of lipolysis in adipocytes. Annu Rev Nutr, *27*, 79-101.

Duwaerts, C. C. and Maher, J. J. (2019). Macronutrients and the adipose-liver axis in obesity and fatty liver. Cell Mol Gastroenterol Hepatol, *7*, 749-761.

Eaton, M. J., Wagner, C. K., Moore, K. E. and Lookingland, K. J. (1994). Neurochemical identification of a13 dopaminergic neuronal projections from the medial zona incerta to the horizontal limb of the diagonal band of broca and the central nucleus of the amygdala. Brain Res, *659*, 201-7.

Edwin Thanarajah, S., Iglesias, S., Kuzmanovic, B., Rigoux, L., Stephan, K. E., Bruning, J. C. and Tittgemeyer, M. (2019). Modulation of midbrain neurocircuitry by intranasal insulin. Neuroimage, *194*, 120-127.

Elbrink, J. and Bihler, I. (1975). Membrane transport: Its relation to cellular metabolic rates. Science, *188*, 1177-84.

Emerging Risk Factors, C., Sarwar, N., Gao, P., Seshasai, S. R., Gobin, R., Kaptoge, S., Di Angelantonio, E., Ingelsson, E., Lawlor, D. A., Selvin, E., Stampfer, M., Stehouwer, C. D., Lewington, S., Pennells, L., Thompson, A., Sattar, N., White, I. R., Ray, K. K. and Danesh, J. (2010). Diabetes mellitus, fasting blood glucose concentration, and risk of vascular disease: A collaborative meta-analysis of 102 prospective studies. Lancet, *375*, 2215-22.

Erickson, J. C., Hollopeter, G. and Palmiter, R. D. (1996). Attenuation of the obesity syndrome of ob/ob mice by the loss of neuropeptide y. Science, *274*, 1704-7.

Estakhr, J., Abazari, D., Frisby, K., Mcintosh, J. M. and Nashmi, R. (2017). Differential control of dopaminergic excitability and locomotion by cholinergic inputs in mouse substantia nigra. Curr Biol, *27*, 1900-1914 e4.

Evans, M. C., Rizwan, M. Z. and Anderson, G. M. (2014). Insulin action on gaba neurons is a critical regulator of energy balance but not fertility in mice. Endocrinology, *155*, 4368-79.

Fabbrini, E., Mohammed, B. S., Magkos, F., Korenblat, K. M., Patterson, B. W. and Klein, S. (2008). Alterations in adipose tissue and hepatic lipid kinetics in obese men and women with nonalcoholic fatty liver disease. Gastroenterology, *134*, 424-31.

Fallon, J. H. (1981). Collateralization of monoamine neurons: Mesotelencephalic dopamine projections to caudate, septum, and frontal cortex. J Neurosci, *1*, 1361-8.

Fan, L. W., Carter, K., Bhatt, A. and Pang, Y. (2019). Rapid transport of insulin to the brain following intranasal administration in rats. Neural Regen Res, *14*, 1046-1051.

Fehm, H. L., Perras, B., Smolnik, R., Kern, W. and Born, J. (2000). Manipulating neuropeptidergic pathways in humans: A novel approach to neuropharmacology? Eur J Pharmacol, *405*, 43-54.

Fenzl, A. and Kiefer, F. W. (2014). Brown adipose tissue and thermogenesis. Horm Mol

Biol Clin Investig, *19*, 25-37.

Fernandez-Verdejo, R., Ravussin, E., Speakman, J. R. and Galgani, J. E. (2019). Progress and challenges in analyzing rodent energy expenditure. Nat Methods, *16*, 797-799.

Fields, H. L., Hjelmstad, G. O., Margolis, E. B. and Nicola, S. M. (2007). Ventral tegmental area neurons in learned appetitive behavior and positive reinforcement. Annu Rev Neurosci, *30*, 289-316.

Filippi, B. M., Abraham, M. A., Silva, P. N., Rasti, M., Lapierre, M. P., Bauer, P. V., Rocheleau, J. V. and Lam, T. K. T. (2017). Dynamin-related protein 1-dependent mitochondrial fission changes in the dorsal vagal complex regulate insulin action. Cell Rep, *18*, 2301-2309.

Filippi, B. M., Bassiri, A., Abraham, M. A., Duca, F. A., Yue, J. T. and Lam, T. K. (2014). Insulin signals through the dorsal vagal complex to regulate energy balance. Diabetes, *63*, 892-9.

Filippi, B. M., Yang, C. S., Tang, C. and Lam, T. K. (2012). Insulin activates erk1/2 signaling in the dorsal vagal complex to inhibit glucose production. Cell Metab, *16*, 500-10.

Fineberg, S. E., Galloway, J. A., Fineberg, N. S., Rathbun, M. J. and Hufferd, S. (1983). Immunogenicity of recombinant DNA human insulin. Diabetologia, *25*, 465-9.

Fisher, S. J. and Kahn, C. R. (2003). Insulin signaling is required for insulin's direct and indirect action on hepatic glucose production. J Clin Invest, *111*, 463-8.

Franke, T. F., Kaplan, D. R., Cantley, L. C. and Toker, A. (1997). Direct regulation of the akt proto-oncogene product by phosphatidylinositol-3,4-bisphosphate. Science, *275*, 665-8.

Franklin, I., Gromada, J., Gjinovci, A., Theander, S. and Wollheim, C. B. (2005). Beta-cell secretory products activate alpha-cell atp-dependent potassium channels to inhibit glucagon release. Diabetes, *54*, 1808-15.

Frauman, A. G., Jerums, G. and Louis, W. J. (1987). Effects of intranasal insulin in non-obese type ii diabetics. Diabetes Res Clin Pract, *3*, 197-202.

Frolich, L., Blum-Degen, D., Bernstein, H. G., Engelsberger, S., Humrich, J., Laufer, S., Muschner, D., Thalheimer, A., Turk, A., Hoyer, S., Zochling, R., Boissl, K. W., Jellinger, K. and Riederer, P. (1998). Brain insulin and insulin receptors in aging and sporadic alzheimer's disease. J Neural Transm (Vienna), *105*, 423-38.

Frotscher, M., Vida, I. and Bender, R. (2000). Evidence for the existence of non-gabaergic, cholinergic interneurons in the rodent hippocampus. Neuroscience, *96*, 27-31.

Fukumoto, H., Kayano, T., Buse, J. B., Edwards, Y., Pilch, P. F., Bell, G. I. and Seino, S. (1989). Cloning and characterization of the major insulin-responsive glucose transporter expressed in human skeletal muscle and other insulin-responsive

tissues. J Biol Chem, *264*, 7776-9.

Gabbouj, S., Natunen, T., Koivisto, H., Jokivarsi, K., Takalo, M., Marttinen, M., Wittrahm, R., Kemppainen, S., Naderi, R., Posado-Fernandez, A., Ryhanen, S., Makinen, P., Paldanius, K. M. A., Doria, G., Poutiainen, P., Flores, O., Haapasalo, A., Tanila, H. and Hiltunen, M. (2019). Intranasal insulin activates akt2 signaling pathway in the hippocampus of wild-type but not in app/ps1 alzheimer model mice. Neurobiol Aging, *75*, 98-108.

Gancheva, S., Koliaki, C., Bierwagen, A., Nowotny, P., Heni, M., Fritsche, A., Haring, H. U., Szendroedi, J. and Roden, M. (2015). Effects of intranasal insulin on hepatic fat accumulation and energy metabolism in humans. Diabetes, *64*, 1966-75.

Garcia-Caceres, C., Quarta, C., Varela, L., Gao, Y., Gruber, T., Legutko, B., Jastroch, M., Johansson, P., Ninkovic, J., Yi, C. X., Le Thuc, O., Szigeti-Buck, K., Cai, W., Meyer, C. W., Pfluger, P. T., Fernandez, A. M., Luquet, S., Woods, S. C., Torres-Aleman, I., Kahn, C. R., Gotz, M., Horvath, T. L. and Tschop, M. H. (2016). Astrocytic insulin signaling couples brain glucose uptake with nutrient availability. Cell, *166*, 867-880.

Garcia, N. H., Ramsey, C. R. and Knox, F. G. (1998). Understanding the role of paracellular transport in the proximal tubule. News Physiol Sci, *13*, 38-43.

Garner, A. R., Rowland, D. C., Hwang, S. Y., Baumgaertel, K., Roth, B. L., Kentros, C. and Mayford, M. (2012). Generation of a synthetic memory trace. Science, *335*, 1513-6.

Gavrilova, O., Haluzik, M., Matsusue, K., Cutson, J. J., Johnson, L., Dietz, K. R., Nicol, C. J., Vinson, C., Gonzalez, F. J. and Reitman, M. L. (2003). Liver peroxisome proliferator-activated receptor gamma contributes to hepatic steatosis, triglyceride clearance, and regulation of body fat mass. J Biol Chem, *278*, 34268-76.

Gaykema, R. P. and Zaborszky, L. (1996). Direct catecholaminergic-cholinergic interactions in the basal forebrain. Ii. Substantia nigra-ventral tegmental area projections to cholinergic neurons. J Comp Neurol, *374*, 555-77.

Gaykema, R. P. and Zaborszky, L. (1997). Parvalbumin-containing neurons in the basal forebrain receive direct input from the substantia nigra-ventral tegmental area. Brain Res, *747*, 173-9.

Gebrie, D., Manyazewal, T., D, A. E. and Makonnen, E. (2021). Metformin-insulin versus metformin-sulfonylurea combination therapies in type 2 diabetes: A comparative study of glycemic control and risk of cardiovascular diseases in addis ababa, ethiopia. Diabetes Metab Syndr Obes, *14*, 3345-3359.

Geisler, S. and Zahm, D. S. (2005). Afferents of the ventral tegmental area in the rat-anatomical substratum for integrative functions. J Comp Neurol, *490*, 270-94.

Gerozissis, K. (2004). Brain insulin and feeding: A bi-directional communication. Eur J

Pharmacol*, 490*, 59-70.

Ghasemi, R., Dargahi, L., Haeri, A., Moosavi, M., Mohamed, Z. and Ahmadiani, A. (2013). Brain insulin dysregulation: Implication for neurological and neuropsychiatric disorders. Mol Neurobiol*, 47*, 1045-65.

Gilon, P. and Henquin, J. C. (2001). Mechanisms and physiological significance of the cholinergic control of pancreatic beta-cell function. Endocr Rev*, 22*, 565-604.

Goldfine, I. D. and Smith, G. J. (1976). Binding of insulin to isolated nuclei. Proc Natl Acad Sci U S A*, 73*, 1427-31.

Gonzalez-Garcia, I., Gruber, T. and Garcia-Caceres, C. (2021). Insulin action on astrocytes: From energy homeostasis to behaviour. J Neuroendocrinol*, 33*, e12953.

Grassin-Delyle, S., Buenestado, A., Naline, E., Faisy, C., Blouquit-Laye, S., Couderc, L. J., Le Guen, M., Fischler, M. and Devillier, P. (2012). Intranasal drug delivery: An efficient and non-invasive route for systemic administration: Focus on opioids. Pharmacol Ther*, 134*, 366-79.

Greene, L. A. and Tischler, A. S. (1976). Establishment of a noradrenergic clonal line of rat adrenal pheochromocytoma cells which respond to nerve growth factor. Proc Natl Acad Sci U S A*, 73*, 2424-8.

Grillo, C. A., Piroli, G. G., Kaigler, K. F., Wilson, S. P., Wilson, M. A. and Reagan, L. P. (2011). Downregulation of hypothalamic insulin receptor expression elicits depressive-like behaviors in rats. Behav Brain Res*, 222*, 230-5.

Gritti, I., Henny, P., Galloni, F., Mainville, L., Mariotti, M. and Jones, B. E. (2006). Stereological estimates of the basal forebrain cell population in the rat, including neurons containing choline acetyltransferase, glutamic acid decarboxylase or phosphate-activated glutaminase and colocalizing vesicular glutamate transporters. Neuroscience*, 143*, 1051-64.

Gropp, E., Shanabrough, M., Borok, E., Xu, A. W., Janoschek, R., Buch, T., Plum, L., Balthasar, N., Hampel, B., Waisman, A., Barsh, G. S., Horvath, T. L. and Bruning, J. C. (2005). Agouti-related peptide-expressing neurons are mandatory for feeding. Nat Neurosci*, 8*, 1289-91.

Guthoff, M., Grichisch, Y., Canova, C., Tschritter, O., Veit, R., Hallschmid, M., Haring, H. U., Preissl, H., Hennige, A. M. and Fritsche, A. (2010). Insulin modulates food-related activity in the central nervous system. J Clin Endocrinol Metab*, 95*, 748-55.

Guthoff, M., Stingl, K. T., Tschritter, O., Rogic, M., Heni, M., Stingl, K., Hallschmid, M., Haring, H. U., Fritsche, A., Preissl, H. and Hennige, A. M. (2011). The insulin-mediated modulation of visually evoked magnetic fields is reduced in obese subjects. PLoS One*, 6*, e19482.

Haas, J. T., Miao, J., Chanda, D., Wang, Y., Zhao, E., Haas, M. E., Hirschey, M., Vaitheesvaran, B., Farese, R. V., Jr., Kurland, I. J., Graham, M., Crooke, R.,

Foufelle, F. and Biddinger, S. B. (2012). Hepatic insulin signaling is required for obesity-dependent expression of srebp-1c mrna but not for feeding-dependent expression. Cell Metab, *15*, 873-84.

Haemmerle, G., Zimmermann, R., Hayn, M., Theussl, C., Waeg, G., Wagner, E., Sattler, W., Magin, T. M., Wagner, E. F. and Zechner, R. (2002). Hormone-sensitive lipase deficiency in mice causes diglyceride accumulation in adipose tissue, muscle, and testis. J Biol Chem, *277*, 4806-15.

Hallschmid, M. (2021). Intranasal insulin for alzheimer's disease. CNS Drugs, *35*, 21-37.

Hallschmid, M., Benedict, C., Schultes, B., Born, J. and Kern, W. (2008). Obese men respond to cognitive but not to catabolic brain insulin signaling. Int J Obes (Lond), *32*, 275-82.

Hallschmid, M., Benedict, C., Schultes, B., Fehm, H. L., Born, J. and Kern, W. (2004). Intranasal insulin reduces body fat in men but not in women. Diabetes, *53*, 3024-9.

Hallschmid, M., Higgs, S., Thienel, M., Ott, V. and Lehnert, H. (2012). Postprandial administration of intranasal insulin intensifies satiety and reduces intake of palatable snacks in women. Diabetes, *61*, 782-9.

Halse, R., Bonavaud, S. M., Armstrong, J. L., Mccormack, J. G. and Yeaman, S. J. (2001). Control of glycogen synthesis by glucose, glycogen, and insulin in cultured human muscle cells. Diabetes, *50*, 720-6.

Hancock, M. L., Meyer, R. C., Mistry, M., Khetani, R. S., Wagschal, A., Shin, T., Ho Sui, S. J., Naar, A. M. and Flanagan, J. G. (2019). Insulin receptor associates with promoters genome-wide and regulates gene expression. Cell, *177*, 722-736 e22.

Hangya, B., Ranade, S. P., Lorenc, M. and Kepecs, A. (2015). Central cholinergic neurons are rapidly recruited by reinforcement feedback. Cell, *162*, 1155-68.

Hanson, L. R. and Frey, W. H., 2nd (2008). Intranasal delivery bypasses the blood-brain barrier to target therapeutic agents to the central nervous system and treat neurodegenerative disease. BMC Neurosci, *9 Suppl 3*, S5.

Hardaway, J. A., Crowley, N. A., Bulik, C. M. and Kash, T. L. (2015). Integrated circuits and molecular components for stress and feeding: Implications for eating disorders. Genes Brain Behav, *14*, 85-97.

Harishankar, N., Kumar, P. U., Sesikeran, B. and Giridharan, N. (2011). Obesity associated pathophysiological & histological changes in wnin obese mutant rats. Indian J Med Res, *134*, 330-40.

Harrison, T. C., Pinto, L., Brock, J. R. and Dan, Y. (2016). Calcium imaging of basal forebrain activity during innate and learned behaviors. Front Neural Circuits, *10*, 36.

Havrankova, J., Roth, J. and Brownstein, M. (1978). Insulin receptors are widely distributed in the central nervous system of the rat. Nature, *272*, 827-9.

Heimer, L. (2000). Basal forebrain in the context of schizophrenia. Brain Res Brain Res Rev, *31*, 205-35.

Heinemann, L., Schnell, O., Gehr, B., Schloot, N. C., Gorgens, S. W. and Gorgen, C. (2021). Digital diabetes management: A literature review of smart insulin pens. J Diabetes Sci Technol, 1932296820983863.

Heni, M., Kullmann, S., Ketterer, C., Guthoff, M., Bayer, M., Staiger, H., Machicao, F., Haring, H. U., Preissl, H., Veit, R. and Fritsche, A. (2014a). Differential effect of glucose ingestion on the neural processing of food stimuli in lean and overweight adults. Hum Brain Mapp, *35*, 918-28.

Heni, M., Kullmann, S., Ketterer, C., Guthoff, M., Linder, K., Wagner, R., Stingl, K. T., Veit, R., Staiger, H., Haring, H. U., Preissl, H. and Fritsche, A. (2012). Nasal insulin changes peripheral insulin sensitivity simultaneously with altered activity in homeostatic and reward-related human brain regions. Diabetologia, *55*, 1773-82.

Heni, M., Kullmann, S., Preissl, H., Fritsche, A. and Haring, H. U. (2015). Impaired insulin action in the human brain: Causes and metabolic consequences. Nat Rev Endocrinol, *11*, 701-11.

Heni, M., Schopfer, P., Peter, A., Sartorius, T., Fritsche, A., Synofzik, M., Haring, H. U., Maetzler, W. and Hennige, A. M. (2014b). Evidence for altered transport of insulin across the blood-brain barrier in insulin-resistant humans. Acta Diabetol, *51*, 679-81.

Heni, M., Wagner, R., Kullmann, S., Gancheva, S., Roden, M., Peter, A., Stefan, N., Preissl, H., Haring, H. U. and Fritsche, A. (2017). Hypothalamic and striatal insulin action suppresses endogenous glucose production and may stimulate glucose uptake during hyperinsulinemia in lean but not in overweight men. Diabetes, *66*, 1797-1806.

Heni, M., Wagner, R., Kullmann, S., Veit, R., Mat Husin, H., Linder, K., Benkendorff, C., Peter, A., Stefan, N., Haring, H. U., Preissl, H. and Fritsche, A. (2014c). Central insulin administration improves whole-body insulin sensitivity via hypothalamus and parasympathetic outputs in men. Diabetes, *63*, 4083-8.

Hennige, A. M., Sartorius, T., Lutz, S. Z., Tschritter, O., Preissl, H., Hopp, S., Fritsche, A., Rammensee, H. G., Ruth, P. and Haring, H. U. (2009). Insulin-mediated cortical activity in the slow frequency range is diminished in obese mice and promotes physical inactivity. Diabetologia, *52*, 2416-2424.

Herman, A. M., Ortiz-Guzman, J., Kochukov, M., Herman, I., Quast, K. B., Patel, J. M., Tepe, B., Carlson, J. C., Ung, K., Selever, J., Tong, Q. and Arenkiel, B. R. (2016). A cholinergic basal forebrain feeding circuit modulates appetite suppression. Nature, *538*, 253-256.

Hersom, M., Helms, H. C., Schmalz, C., Pedersen, T. A., Buckley, S. T. and Brodin, B.

(2018). The insulin receptor is expressed and functional in cultured blood-brain barrier endothelial cells but does not mediate insulin entry from blood to brain. Am J Physiol Endocrinol Metab, *315*, E531-E542.

Higgs, S. (2002). Memory for recent eating and its influence on subsequent food intake. Appetite, *39*, 159-66.

Hill, J. M., Lesniak, M. A., Pert, C. B. and Roth, J. (1986). Autoradiographic localization of insulin receptors in rat brain: Prominence in olfactory and limbic areas. Neuroscience, *17*, 1127-38.

Hilsted, J., Madsbad, S., Hvidberg, A., Rasmussen, M. H., Krarup, T., Ipsen, H., Hansen, B., Pedersen, M., Djurup, R. and Oxenboll, B. (1995). Intranasal insulin therapy: The clinical realities. Diabetologia, *38*, 680-4.

Hong, M. and Lee, V. M. (1997). Insulin and insulin-like growth factor-1 regulate tau phosphorylation in cultured human neurons. J Biol Chem, *272*, 19547-53.

Huang, S. and Czech, M. P. (2007). The glut4 glucose transporter. Cell Metab, *5*, 237-52.

Hubbard, S. R. (2013). The insulin receptor: Both a prototypical and atypical receptor tyrosine kinase. Cold Spring Harb Perspect Biol, *5*, a008946.

Ikeda, K., Maretich, P. and Kajimura, S. (2018). The common and distinct features of brown and beige adipocytes. Trends Endocrinol Metab, *29*, 191-200.

Imai, T. (2014). Construction of functional neuronal circuitry in the olfactory bulb. Semin Cell Dev Biol, *35*, 180-8.

Iravanpour, F., Dargahi, L., Rezaei, M., Haghani, M., Heidari, R., Valian, N. and Ahmadiani, A. (2021). Intranasal insulin improves mitochondrial function and attenuates motor deficits in a rat 6-ohda model of parkinson's disease. CNS Neurosci Ther, *27*, 308-319.

Iskandar, K., Cao, Y., Hayashi, Y., Nakata, M., Takano, E., Yada, T., Zhang, C., Ogawa, W., Oki, M., Chua, S., Jr., Itoh, H., Noda, T., Kasuga, M. and Nakae, J. (2010). Pdk-1/foxo1 pathway in pomc neurons regulates pomc expression and food intake. Am J Physiol Endocrinol Metab, *298*, E787-98.

Itaya, S. K. (1987). Anterograde transsynaptic transport of wga-hrp in rat olfactory pathways. Brain Res, *409*, 205-14.

Iwen, K. A., Scherer, T., Heni, M., Sayk, F., Wellnitz, T., Machleidt, F., Preissl, H., Haring, H. U., Fritsche, A., Lehnert, H., Buettner, C. and Hallschmid, M. (2014). Intranasal insulin suppresses systemic but not subcutaneous lipolysis in healthy humans. J Clin Endocrinol Metab, *99*, E246-51.

James, D. E., Brown, R., Navarro, J. and Pilch, P. F. (1988). Insulin-regulatable tissues express a unique insulin-sensitive glucose transport protein. Nature, *333*, 183-5.

Jauch-Chara, K., Friedrich, A., Rezmer, M., Melchert, U. H., H, G, S.-E., Hallschmid, M.

and Oltmanns, K. M. (2012). Intranasal insulin suppresses food intake via enhancement of brain energy levels in humans. Diabetes, *61*, 2261-8.

Jaworski, K., Sarkadi-Nagy, E., Duncan, R. E., Ahmadian, M. and Sul, H. S. (2007). Regulation of triglyceride metabolism. Iv. Hormonal regulation of lipolysis in adipose tissue. Am J Physiol Gastrointest Liver Physiol, *293*, G1-4.

Jensen, J., Rustad, P. I., Kolnes, A. J. and Lai, Y. C. (2011). The role of skeletal muscle glycogen breakdown for regulation of insulin sensitivity by exercise. Front Physiol, *2*, 112.

Jia, Y. L., Fu, Z. X., Zhang, B. H. and Jia, Y. J. (2017). Hippocampal overexpression of down syndrome cell adhesion molecule in amyloid precursor protein transgenic mice. Braz J Med Biol Res, *50*, e6049.

Jones, P. M., Pierson, A. M., Williams, G., Ghatei, M. A. and Bloom, S. R. (1992). Increased hypothalamic neuropeptide y messenger rna levels in two rat models of diabetes. Diabet Med, *9*, 76-80.

Juarez Olguin, H., Calderon Guzman, D., Hernandez Garcia, E. and Barragan Mejia, G. (2016). The role of dopamine and its dysfunction as a consequence of oxidative stress. Oxid Med Cell Longev, *2016*, 9730467.

Kalra, S. P., Dube, M. G., Sahu, A., Phelps, C. P. and Kalra, P. S. (1991). Neuropeptide y secretion increases in the paraventricular nucleus in association with increased appetite for food. Proc Natl Acad Sci U S A, *88*, 10931-5.

Kasuga, M. (2006). Insulin resistance and pancreatic beta cell failure. J Clin Invest, *116*, 1756-60.

Katsoyannis, P. G., Tometsko, A. M., Ginos, J. Z. and Tilak, M. A. (1966). Insulin peptides. Xi. The synthesis of the b chain of human insulin and its combination with the natural a chain of bovine insulin to generate insulin activity. J Am Chem Soc, *88*, 164-6.

Kaye, W. H., Bulik, C. M., Thornton, L., Barbarich, N. and Masters, K. (2004). Comorbidity of anxiety disorders with anorexia and bulimia nervosa. Am J Psychiatry, *161*, 2215-21.

Kellar, D., Lockhart, S. N., Aisen, P., Raman, R., Rissman, R. A., Brewer, J. and Craft, S. (2021). Intranasal insulin reduces white matter hyperintensity progression in association with improvements in cognition and csf biomarker profiles in mild cognitive impairment and alzheimer's disease. J Prev Alzheimers Dis, *8*, 240-248.

Kellett, G. L., Brot-Laroche, E., Mace, O. J. and Leturque, A. (2008). Sugar absorption in the intestine: The role of glut2. Annu Rev Nutr, *28*, 35-54.

Kern, W., Benedict, C., Schultes, B., Plohr, F., Moser, A., Born, J., Fehm, H. L. and Hallschmid, M. (2006). Low cerebrospinal fluid insulin levels in obese humans. Diabetologia, *49*, 2790-2.

Khokhlatchev, A. V., Canagarajah, B., Wilsbacher, J., Robinson, M., Atkinson, M., Goldsmith, E. and Cobb, M. H. (1998). Phosphorylation of the map kinase erk2 promotes its homodimerization and nuclear translocation. Cell, *93*, 605-15.

Kim, J. A., Wei, Y. and Sowers, J. R. (2008). Role of mitochondrial dysfunction in insulin resistance. Circ Res, *102*, 401-14.

Kimura, K., Tanida, M., Nagata, N., Inaba, Y., Watanabe, H., Nagashimada, M., Ota, T., Asahara, S., Kido, Y., Matsumoto, M., Toshinai, K., Nakazato, M., Shibamoto, T., Kaneko, S., Kasuga, M. and Inoue, H. (2016). Central insulin action activates kupffer cells by suppressing hepatic vagal activation via the nicotinic alpha 7 acetylcholine receptor. Cell Rep, *14*, 2362-74.

King, G. L. and Johnson, S. M. (1985). Receptor-mediated transport of insulin across endothelial cells. Science, *227*, 1583-6.

Kinney, J. W., Bemiller, S. M., Murtishaw, A. S., Leisgang, A. M., Salazar, A. M. and Lamb, B. T. (2018). Inflammation as a central mechanism in alzheimer's disease. Alzheimers Dement (N Y), *4*, 575-590.

Kitamura, K., Judkewitz, B., Kano, M., Denk, W. and Hausser, M. (2008). Targeted patch-clamp recordings and single-cell electroporation of unlabeled neurons in vivo. Nat Methods, *5*, 61-7.

Kitamura, T., Feng, Y., Kitamura, Y. I., Chua, S. C., Jr., Xu, A. W., Barsh, G. S., Rossetti, L. and Accili, D. (2006). Forkhead protein foxo1 mediates agrp-dependent effects of leptin on food intake. Nat Med, *12*, 534-40.

Knox, D. and Keller, S. M. (2016). Cholinergic neuronal lesions in the medial septum and vertical limb of the diagonal bands of broca induce contextual fear memory generalization and impair acquisition of fear extinction. Hippocampus, *26*, 718-26.

Koch, L., Wunderlich, F. T., Seibler, J., Konner, A. C., Hampel, B., Irlenbusch, S., Brabant, G., Kahn, C. R., Schwenk, F. and Bruning, J. C. (2008). Central insulin action regulates peripheral glucose and fat metabolism in mice. J Clin Invest, *118*, 2132-47.

Kong, D., Tong, Q., Ye, C., Koda, S., Fuller, P. M., Krashes, M. J., Vong, L., Ray, R. S., Olson, D. P. and Lowell, B. B. (2012). Gabaergic rip-cre neurons in the arcuate nucleus selectively regulate energy expenditure. Cell, *151*, 645-57.

Konishi, M., Sakaguchi, M., Lockhart, S. M., Cai, W., Li, M. E., Homan, E. P., Rask-Madsen, C. and Kahn, C. R. (2017). Endothelial insulin receptors differentially control insulin signaling kinetics in peripheral tissues and brain of mice. Proc Natl Acad Sci U S A, *114*, E8478-E8487.

Konner, A. C., Janoschek, R., Plum, L., Jordan, S. D., Rother, E., Ma, X., Xu, C., Enriori, P., Hampel, B., Barsh, G. S., Kahn, C. R., Cowley, M. A., Ashcroft, F. M. and Bruning, J. C. (2007). Insulin action in agrp-expressing neurons is required for suppression of hepatic glucose production. Cell Metab, *5*, 438-49.

Kousteni, S. (2012). Foxo1, the transcriptional chief of staff of energy metabolism. Bone, *50*, 437-43.

Kozorovitskiy, Y., Saunders, A., Johnson, C. A., Lowell, B. B. and Sabatini, B. L. (2012). Recurrent network activity drives striatal synaptogenesis. Nature, *485*, 646-50.

Krashes, M. J., Koda, S., Ye, C., Rogan, S. C., Adams, A. C., Cusher, D. S., Maratos-Flier, E., Roth, B. L. and Lowell, B. B. (2011). Rapid, reversible activation of agrp neurons drives feeding behavior in mice. J Clin Invest, *121*, 1424-8.

Krashes, M. J., Shah, B. P., Madara, J. C., Olson, D. P., Strochlic, D. E., Garfield, A. S., Vong, L., Pei, H., Watabe-Uchida, M., Uchida, N., Liberles, S. D. and Lowell, B. B. (2014). An excitatory paraventricular nucleus to agrp neuron circuit that drives hunger. Nature, *507*, 238-42.

Krebs, E. G. (1981). Phosphorylation and dephosphorylation of glycogen phosphorylase: A prototype for reversible covalent enzyme modification. Curr Top Cell Regul, *18*, 401-19.

Kristensson, K. and Olsson, Y. (1971). Uptake of exogenous proteins in mouse olfactory cells. Acta Neuropathol, *19*, 145-54.

Kroemer, N. B., Krebs, L., Kobiella, A., Grimm, O., Vollstadt-Klein, S., Wolfensteller, U., Kling, R., Bidlingmaier, M., Zimmermann, U. S. and Smolka, M. N. (2013). (still) longing for food: Insulin reactivity modulates response to food pictures. Hum Brain Mapp, *34*, 2367-80.

Kuang, Q., Purhonen, P. and Hebert, H. (2015). Structure of potassium channels. Cell Mol Life Sci, *72*, 3677-93.

Kullmann, S., Frank, S., Heni, M., Ketterer, C., Veit, R., Haring, H. U., Fritsche, A. and Preissl, H. (2013). Intranasal insulin modulates intrinsic reward and prefrontal circuitry of the human brain in lean women. Neuroendocrinology, *97*, 176-82.

Kullmann, S., Heni, M., Fritsche, A. and Preissl, H. (2015a). Insulin action in the human brain: Evidence from neuroimaging studies. J Neuroendocrinol, *27*, 419-23.

Kullmann, S., Heni, M., Veit, R., Scheffler, K., Machann, J., Haring, H. U., Fritsche, A. and Preissl, H. (2015b). Selective insulin resistance in homeostatic and cognitive control brain areas in overweight and obese adults. Diabetes Care, *38*, 1044-50.

Kullmann, S., Kleinridders, A., Small, D. M., Fritsche, A., Haring, H. U., Preissl, H. and Heni, M. (2020a). Central nervous pathways of insulin action in the control of metabolism and food intake. Lancet Diabetes Endocrinol, *8*, 524-534.

Kullmann, S., Valenta, V., Wagner, R., Tschritter, O., Machann, J., Haring, H. U., Preissl, H., Fritsche, A. and Heni, M. (2020b). Brain insulin sensitivity is linked to adiposity and body fat distribution. Nat Commun, *11*, 1841.

Kullmann, S., Veit, R., Peter, A., Pohmann, R., Scheffler, K., Haring, H. U., Fritsche, A.,

Preissl, H. and Heni, M. (2018). Dose-dependent effects of intranasal insulin on resting-state brain activity. J Clin Endocrinol Metab, *103*, 253-262.

Kuo, L. E., Kitlinska, J. B., Tilan, J. U., Li, L., Baker, S. B., Johnson, M. D., Lee, E. W., Burnett, M. S., Fricke, S. T., Kvetnansky, R., Herzog, H. and Zukowska, Z. (2007). Neuropeptide y acts directly in the periphery on fat tissue and mediates stress-induced obesity and metabolic syndrome. Nat Med, *13*, 803-11.

Kwon, E., Joung, H. Y., Liu, S. M., Chua, S. C., Jr., Schwartz, G. J. and Jo, Y. H. (2020). Optogenetic stimulation of the liver-projecting melanocortinergic pathway promotes hepatic glucose production. Nat Commun, *11*, 6295.

Lafontaine, D. L. and Tollervey, D. (2001). The function and synthesis of ribosomes. Nat Rev Mol Cell Biol, *2*, 514-20.

Lalej-Bennis, D., Boillot, J., Bardin, C., Zirinis, P., Coste, A., Escudier, E., Chast, F., Peynegre, R., Selam, J. L. and Slama, G. (2001). Efficacy and tolerance of intranasal insulin administered during 4 months in severely hyperglycaemic type 2 diabetic patients with oral drug failure: A cross-over study. Diabet Med, *18*, 614-8.

Lam, C. K., Chari, M., Wang, P. Y. and Lam, T. K. (2008). Central lactate metabolism regulates food intake. Am J Physiol Endocrinol Metab, *295*, E491-6.

Lam, T. K. (2010). Neuronal regulation of homeostasis by nutrient sensing. Nat Med, *16*, 392-5.

Le, L., Jiang, B., Wan, W., Zhai, W., Xu, L., Hu, K. and Xiao, P. (2016). Metabolomics reveals the protective of dihydromyricetin on glucose homeostasis by enhancing insulin sensitivity. Sci Rep, *6*, 36184.

Leary, A. C., Stote, R. M., Breedt, H. J., O'brien, J. and Buckley, B. (2005). Pharmacokinetics and pharmacodynamics of intranasal insulin administered to healthy subjects in escalating doses. Diabetes Technol Ther, *7*, 124-30.

Leary, A. C., Stote, R. M., Cussen, K., O'brien, J., Leary, W. P. and Buckley, B. (2006). Pharmacokinetics and pharmacodynamics of intranasal insulin administered to patients with type 1 diabetes: A preliminary study. Diabetes Technol Ther, *8*, 81-8.

Lee, J. and Kim, M. S. (2007). The role of gsk3 in glucose homeostasis and the development of insulin resistance. Diabetes Res Clin Pract, *77 Suppl 1*, S49-57.

Leto, D. and Saltiel, A. R. (2012). Regulation of glucose transport by insulin: Traffic control of glut4. Nat Rev Mol Cell Biol, *13*, 383-96.

Li, J., Defea, K. and Roth, R. A. (1999). Modulation of insulin receptor substrate-1 tyrosine phosphorylation by an akt/phosphatidylinositol 3-kinase pathway. J Biol Chem, *274*, 9351-6.

Li, X., Yu, B., Sun, Q., Zhang, Y., Ren, M., Zhang, X., Li, A., Yuan, J., Madisen, L., Luo, Q., Zeng, H., Gong, H. and Qiu, Z. (2018). Generation of a whole-brain atlas for

the cholinergic system and mesoscopic projectome analysis of basal forebrain cholinergic neurons. Proc Natl Acad Sci U S A, *115*, 415-420.

Liao, W., Nguyen, M. T., Yoshizaki, T., Favelyukis, S., Patsouris, D., Imamura, T., Verma, I. M. and Olefsky, J. M. (2007). Suppression of ppar-gamma attenuates insulin-stimulated glucose uptake by affecting both glut1 and glut4 in 3t3-l1 adipocytes. Am J Physiol Endocrinol Metab, *293*, E219-27.

Lin, H. V. and Accili, D. (2011). Hormonal regulation of hepatic glucose production in health and disease. Cell Metab, *14*, 9-19.

Lin, H. V., Plum, L., Ono, H., Gutierrez-Juarez, R., Shanabrough, M., Borok, E., Horvath, T. L., Rossetti, L. and Accili, D. (2010). Divergent regulation of energy expenditure and hepatic glucose production by insulin receptor in agouti-related protein and pomc neurons. Diabetes, *59*, 337-46.

Lindahl, E., Nyman, U., Zaman, F., Palmberg, C., Cascante, A., Shafqat, J., Takigawa, M., Savendahl, L., Jornvall, H. and Joseph, B. (2010). Proinsulin c-peptide regulates ribosomal rna expression. J Biol Chem, *285*, 3462-9.

Liu, Q., Bengmark, S. and Qu, S. (2010). The role of hepatic fat accumulation in pathogenesis of non-alcoholic fatty liver disease (nafld). Lipids Health Dis, *9*, 42.

Lochhead, J. J., Kellohen, K. L., Ronaldson, P. T. and Davis, T. P. (2019). Distribution of insulin in trigeminal nerve and brain after intranasal administration. Sci Rep, *9*, 2621.

Loh, K., Zhang, L., Brandon, A., Wang, Q., Begg, D., Qi, Y., Fu, M., Kulkarni, R., Teo, J., Baldock, P., Bruning, J. C., Cooney, G., Neely, G. G. and Herzog, H. (2017). Insulin controls food intake and energy balance via npy neurons. Mol Metab, *6*, 574-584.

Lu, M., Wan, M., Leavens, K. F., Chu, Q., Monks, B. R., Fernandez, S., Ahima, R. S., Ueki, K., Kahn, C. R. and Birnbaum, M. J. (2012). Insulin regulates liver metabolism in vivo in the absence of hepatic akt and foxo1. Nat Med, *18*, 388-95.

Luquet, S., Perez, F. A., Hnasko, T. S. and Palmiter, R. D. (2005). Npy/agrp neurons are essential for feeding in adult mice but can be ablated in neonates. Science, *310*, 683-5.

Lv, H., Tang, L., Guo, C., Jiang, Y., Gao, C., Wang, Y. and Jian, C. (2020). Intranasal insulin administration may be highly effective in improving cognitive function in mice with cognitive dysfunction by reversing brain insulin resistance. Cogn Neurodyn, *14*, 323-338.

Ma, M. and Luo, M. (2012). Optogenetic activation of basal forebrain cholinergic neurons modulates neuronal excitability and sensory responses in the main olfactory bulb. J Neurosci, *32*, 10105-16.

Maik-Rachline, G., Hacohen-Lev-Ran, A. and Seger, R. (2019). Nuclear erk:

Mechanism of translocation, substrates, and role in cancer. Int J Mol Sci, *20*.

Maimaiti, S., Anderson, K. L., Demoll, C., Brewer, L. D., Rauh, B. A., Gant, J. C., Blalock, E. M., Porter, N. M. and Thibault, O. (2016). Intranasal insulin improves age-related cognitive deficits and reverses electrophysiological correlates of brain aging. J Gerontol A Biol Sci Med Sci, *71*, 30-9.

Malloy, C. A., Somasundaram, E., Omar, A., Bhutto, U., Medley, M., Dzubuk, N. and Cooper, R. L. (2019). Pharmacological identification of cholinergic receptor subtypes: Modulation of locomotion and neural circuit excitability in drosophila larvae. Neuroscience, *411*, 47-64.

Manschot, S. M., Biessels, G. J., De Valk, H., Algra, A., Rutten, G. E., Van Der Grond, J., Kappelle, L. J. and Utrecht Diabetic Encephalopathy Study, G. (2007). Metabolic and vascular determinants of impaired cognitive performance and abnormalities on brain magnetic resonance imaging in patients with type 2 diabetes. Diabetologia, *50*, 2388-97.

Mansur, R. B., Fries, G. R., Subramaniapillai, M., Frangou, S., De Felice, F. G., Rasgon, N., Mcewen, B., Brietzke, E. and Mcintyre, R. S. (2018). Expression of dopamine signaling genes in the post-mortem brain of individuals with mental illnesses is moderated by body mass index and mediated by insulin signaling genes. J Psychiatr Res, *107*, 128-135.

Marciniak, S. J., Yun, C. Y., Oyadomari, S., Novoa, I., Zhang, Y., Jungreis, R., Nagata, K., Harding, H. P. and Ron, D. (2004). Chop induces death by promoting protein synthesis and oxidation in the stressed endoplasmic reticulum. Genes Dev, *18*, 3066-77.

Mark, G. P., Rada, P., Pothos, E. and Hoebel, B. G. (1992). Effects of feeding and drinking on acetylcholine release in the nucleus accumbens, striatum, and hippocampus of freely behaving rats. J Neurochem, *58*, 2269-74.

Marks, D. R., Tucker, K., Cavallin, M. A., Mast, T. G. and Fadool, D. A. (2009). Awake intranasal insulin delivery modifies protein complexes and alters memory, anxiety, and olfactory behaviors. J Neurosci, *29*, 6734-51.

Marks, J. L., Porte, D., Jr., Stahl, W. L. and Baskin, D. G. (1990). Localization of insulin receptor mrna in rat brain by in situ hybridization. Endocrinology, *127*, 3234-6.

Matikainen-Ankney, B. A., Garmendia-Cedillos, M., Ali, M., Krynitsky, J., Salem, G., Miyazaki, N. L., Pohida, T. and Kravitz, A. V. (2019). Rodent activity detector (rad), an open source device for measuring activity in rodent home cages. eNeuro, *6*.

Matsubayashi, Y., Fukuda, M. and Nishida, E. (2001). Evidence for existence of a nuclear pore complex-mediated, cytosol-independent pathway of nuclear translocation of erk map kinase in permeabilized cells. J Biol Chem, *276*, 41755-60.

Matsuda, M., Liu, Y., Mahankali, S., Pu, Y., Mahankali, A., Wang, J., Defronzo, R. A., Fox, P. T. and Gao, J. H. (1999). Altered hypothalamic function in response to

glucose ingestion in obese humans. Diabetes, *48*, 1801-6.

Matsuhisa, M., Yamasaki, Y., Shiba, Y., Nakahara, I., Kuroda, A., Tomita, T., Iida, M., Ikeda, M., Kajimoto, Y., Kubota, M. and Hori, M. (2000). Important role of the hepatic vagus nerve in glucose uptake and production by the liver. Metabolism, *49*, 11-6.

Matsumoto, M., Pocai, A., Rossetti, L., Depinho, R. A. and Accili, D. (2007). Impaired regulation of hepatic glucose production in mice lacking the forkhead transcription factor foxo1 in liver. Cell Metab, *6*, 208-16.

Maurer, S. V. and Williams, C. L. (2017). The cholinergic system modulates memory and hippocampal plasticity via its interactions with non-neuronal cells. Front Immunol, *8*, 1489.

Mccall, A. L. (2012). Insulin therapy and hypoglycemia. Endocrinol Metab Clin North Am, *41*, 57-87.

Mccrimmon, R. J., Ryan, C. M. and Frier, B. M. (2012). Diabetes and cognitive dysfunction. Lancet, *379*, 2291-9.

Mcgaughy, J., Dalley, J. W., Morrison, C. H., Everitt, B. J. and Robbins, T. W. (2002). Selective behavioral and neurochemical effects of cholinergic lesions produced by intrabasalis infusions of 192 igg-saporin on attentional performance in a five-choice serial reaction time task. J Neurosci, *22*, 1905-13.

Mergenthaler, P., Lindauer, U., Dienel, G. A. and Meisel, A. (2013). Sugar for the brain: The role of glucose in physiological and pathological brain function. Trends Neurosci, *36*, 587-97.

Miki, T., Liss, B., Minami, K., Shiuchi, T., Saraya, A., Kashima, Y., Horiuchi, M., Ashcroft, F., Minokoshi, Y., Roeper, J. and Seino, S. (2001). Atp-sensitive k+ channels in the hypothalamus are essential for the maintenance of glucose homeostasis. Nat Neurosci, *4*, 507-12.

Mina, A. I., Leclair, R. A., Leclair, K. B., Cohen, D. E., Lantier, L. and Banks, A. S. (2018). Calr: A web-based analysis tool for indirect calorimetry experiments. Cell Metab, *28*, 656-666 e1.

Mineur, Y. S., Obayemi, A., Wigestrand, M. B., Fote, G. M., Calarco, C. A., Li, A. M. and Picciotto, M. R. (2013). Cholinergic signaling in the hippocampus regulates social stress resilience and anxiety- and depression-like behavior. Proc Natl Acad Sci U S A, *110*, 3573-8.

Minkowski, O. (1989). Historical development of the theory of pancreatic diabetes by oscar minkowski, 1929: Introduction and translation by rachmiel levine. Diabetes, *38*, 1-6.

Mogi, M. and Horiuchi, M. (2011). Neurovascular coupling in cognitive impairment associated with diabetes mellitus. Circ J, *75*, 1042-8.

Molina, J., Rodriguez-Diaz, R., Fachado, A., Jacques-Silva, M. C., Berggren, P. O. and

Caicedo, A. (2014). Control of insulin secretion by cholinergic signaling in the human pancreatic islet. Diabetes, *63*, 2714-26.

Molnar, G., Farago, N., Kocsis, A. K., Rozsa, M., Lovas, S., Boldog, E., Baldi, R., Csajbok, E., Gardi, J., Puskas, L. G. and Tamas, G. (2014). Gabaergic neurogliaform cells represent local sources of insulin in the cerebral cortex. J Neurosci, *34*, 1133-7.

Morales, M. and Root, D. H. (2014). Glutamate neurons within the midbrain dopamine regions. Neuroscience, *282*, 60-8.

Moran, C., Phan, T. G., Chen, J., Blizzard, L., Beare, R., Venn, A., Munch, G., Wood, A. G., Forbes, J., Greenaway, T. M., Pearson, S. and Srikanth, V. (2013). Brain atrophy in type 2 diabetes: Regional distribution and influence on cognition. Diabetes Care, *36*, 4036-42.

Morgan, H. E., Regen, D. M. and Park, C. R. (1964). Identification of a mobile carrier-mediated sugar transport system in muscle. J Biol Chem, *239*, 369-74.

Morton, G. J., Cummings, D. E., Baskin, D. G., Barsh, G. S. and Schwartz, M. W. (2006). Central nervous system control of food intake and body weight. Nature, *443*, 289-95.

Mosconi, L., Mistur, R., Switalski, R., Tsui, W. H., Glodzik, L., Li, Y., Pirraglia, E., De Santi, S., Reisberg, B., Wisniewski, T. and De Leon, M. J. (2009). Fdg-pet changes in brain glucose metabolism from normal cognition to pathologically verified alzheimer's disease. Eur J Nucl Med Mol Imaging, *36*, 811-22.

Mullen, R. J., Buck, C. R. and Smith, A. M. (1992). Neun, a neuronal specific nuclear protein in vertebrates. Development, *116*, 201-11.

Muller, T. D., Klingenspor, M. and Tschop, M. H. (2021). Revisiting energy expenditure: How to correct mouse metabolic rate for body mass. Nat Metab, *3*, 1134-1136.

Mullins, R. J., Diehl, T. C., Chia, C. W. and Kapogiannis, D. (2017). Insulin resistance as a link between amyloid-beta and tau pathologies in alzheimer's disease. Front Aging Neurosci, *9*, 118.

Murata, K., Kinoshita, T., Fukazawa, Y., Kobayashi, K., Kobayashi, K., Miyamichi, K., Okuno, H., Bito, H., Sakurai, Y., Yamaguchi, M., Mori, K. and Manabe, H. (2019). Gabaergic neurons in the olfactory cortex projecting to the lateral hypothalamus in mice. Sci Rep, *9*, 7132.

Nair-Roberts, R. G., Chatelain-Badie, S. D., Benson, E., White-Cooper, H., Bolam, J. P. and Ungless, M. A. (2008). Stereological estimates of dopaminergic, gabaergic and glutamatergic neurons in the ventral tegmental area, substantia nigra and retrorubral field in the rat. Neuroscience, *152*, 1024-31.

Nakae, J., Barr, V. and Accili, D. (2000). Differential regulation of gene expression by insulin and igf-1 receptors correlates with phosphorylation of a single amino acid residue in the forkhead transcription factor fkhr. EMBO J, *19*, 989-96.

Nakae, J., Kitamura, T., Silver, D. L. and Accili, D. (2001). The forkhead transcription factor foxo1 (fkhr) confers insulin sensitivity onto glucose-6-phosphatase expression. J Clin Invest, *108*, 1359-67.

Nakae, J., Park, B. C. and Accili, D. (1999). Insulin stimulates phosphorylation of the forkhead transcription factor fkhr on serine 253 through a wortmannin-sensitive pathway. J Biol Chem, *274*, 15982-5.

Navarro, M., Olney, J. J., Burnham, N. W., Mazzone, C. M., Lowery-Gionta, E. G., Pleil, K. E., Kash, T. L. and Thiele, T. E. (2016). Lateral hypothalamus gabaergic neurons modulate consummatory behaviors regardless of the caloric content or biological relevance of the consumed stimuli. Neuropsychopharmacology, *41*, 1505-12.

Nedelcovych, M. T., Gadiano, A. J., Wu, Y., Manning, A. A., Thomas, A. G., Khuder, S. S., Yoo, S. W., Xu, J., Mcarthur, J. C., Haughey, N. J., Volsky, D. J., Rais, R. and Slusher, B. S. (2018). Pharmacokinetics of intranasal versus subcutaneous insulin in the mouse. ACS Chem Neurosci, *9*, 809-816.

Nedergaard, J., Bengtsson, T. and Cannon, B. (2007). Unexpected evidence for active brown adipose tissue in adult humans. Am J Physiol Endocrinol Metab, *293*, E444-52.

Niu, S. N., Huang, Z. B., Wang, H., Rao, X. R., Kong, H., Xu, J., Li, X. J., Yang, C. and Sheng, G. Q. (2011). Brainstem hap1-ahi1 is involved in insulin-mediated feeding control. FEBS Lett, *585*, 85-91.

Novak, V., Mantzoros, C. S., Novak, P., Mcglinchey, R., Dai, W., Lioutas, V., Buss, S., Fortier, C. B., Khan, F., Aponte Becerra, L. and Ngo, L. H. (2022). Memaid: Memory advancement with intranasal insulin vs. Placebo in type 2 diabetes and control participants: A randomized clinical trial. J Neurol.

Novak, V., Milberg, W., Hao, Y., Munshi, M., Novak, P., Galica, A., Manor, B., Roberson, P., Craft, S. and Abduljalil, A. (2014). Enhancement of vasoreactivity and cognition by intranasal insulin in type 2 diabetes. Diabetes Care, *37*, 751-9.

Obici, S., Feng, Z., Karkanias, G., Baskin, D. G. and Rossetti, L. (2002a). Decreasing hypothalamic insulin receptors causes hyperphagia and insulin resistance in rats. Nat Neurosci, *5*, 566-72.

Obici, S., Zhang, B. B., Karkanias, G. and Rossetti, L. (2002b). Hypothalamic insulin signaling is required for inhibition of glucose production. Nat Med, *8*, 1376-82.

Ogg, M. C., Ross, J. M., Bendahmane, M. and Fletcher, M. L. (2018). Olfactory bulb acetylcholine release dishabituates odor responses and reinstates odor investigation. Nat Commun, *9*, 1868.

Okamoto, H., Obici, S., Accili, D. and Rossetti, L. (2005). Restoration of liver insulin signaling in insr knockout mice fails to normalize hepatic insulin action. J Clin Invest, *115*, 1314-22.

Oleck, J., Kassam, S. and Goldman, J. D. (2016). Commentary: Why was inhaled

insulin a failure in the market? Diabetes Spectr, *29*, 180-4.

Ott, V., Lehnert, H., Staub, J., Wonne, K., Born, J. and Hallschmid, M. (2015). Central nervous insulin administration does not potentiate the acute glucoregulatory impact of concurrent mild hyperinsulinemia. Diabetes, *64*, 760-5.

Owens, D. R. and Griffiths, S. (2002). Insulin glargine (lantus). Int J Clin Pract, *56*, 460-6.

Ozougwu, J., Obimba, K., Belonwu, C. and Unakalamba, C. (2013). The pathogenesis and pathophysiology of type 1 and type 2 diabetes mellitus. J Physiol Pathophysiol, *4*, 46-57.

Pang, Y., Lin, S., Wright, C., Shen, J., Carter, K., Bhatt, A. and Fan, L. W. (2016). Intranasal insulin protects against substantia nigra dopaminergic neuronal loss and alleviates motor deficits induced by 6-ohda in rats. Neuroscience, *318*, 157-65.

Park, C. R., Bornstein, J. and Post, R. L. (1955). Effect of insulin on free glucose content of rat diaphragm in vitro. Am J Physiol, *182*, 12-6.

Patel, B., New, L. E., Griffiths, J. C., Deuchars, J. and Filippi, B. M. (2021). Inhibition of mitochondrial fission and inos in the dorsal vagal complex protects from overeating and weight gain. Mol Metab, *43*, 101123.

Patel, J. M., Swanson, J., Ung, K., Herman, A., Hanson, E., Ortiz-Guzman, J., Selever, J., Tong, Q. and Arenkiel, B. R. (2019). Sensory perception drives food avoidance through excitatory basal forebrain circuits. Elife, *8*.

Peeyush, K. T., Savitha, B., Sherin, A., Anju, T. R., Jes, P. and Paulose, C. S. (2010). Cholinergic, dopaminergic and insulin receptors gene expression in the cerebellum of streptozotocin-induced diabetic rats: Functional regulation with vitamin d3 supplementation. Pharmacol Biochem Behav, *95*, 216-22.

Perry, R. J., Camporez, J. G., Kursawe, R., Titchenell, P. M., Zhang, D., Perry, C. J., Jurczak, M. J., Abudukadier, A., Han, M. S., Zhang, X. M., Ruan, H. B., Yang, X., Caprio, S., Kaech, S. M., Sul, H. S., Birnbaum, M. J., Davis, R. J., Cline, G. W., Petersen, K. F. and Shulman, G. I. (2015). Hepatic acetyl coa links adipose tissue inflammation to hepatic insulin resistance and type 2 diabetes. Cell, *160*, 745-758.

Picard, F. and Auwerx, J. (2002). Ppar(gamma) and glucose homeostasis. Annu Rev Nutr, *22*, 167-97.

Pinto, L., Goard, M. J., Estandian, D., Xu, M., Kwan, A. C., Lee, S. H., Harrison, T. C., Feng, G. and Dan, Y. (2013). Fast modulation of visual perception by basal forebrain cholinergic neurons. Nat Neurosci, *16*, 1857-1863.

Plum, L., Lin, H. V., Dutia, R., Tanaka, J., Aizawa, K. S., Matsumoto, M., Kim, A. J., Cawley, N. X., Paik, J. H., Loh, Y. P., Depinho, R. A., Wardlaw, S. L. and Accili, D. (2009). The obesity susceptibility gene cpe links foxo1 signaling in hypothalamic pro-opiomelanocortin neurons with regulation of food intake. Nat

Med, *15*, 1195-201.

Plum, L., Ma, X., Hampel, B., Balthasar, N., Coppari, R., Munzberg, H., Shanabrough, M., Burdakov, D., Rother, E., Janoschek, R., Alber, J., Belgardt, B. F., Koch, L., Seibler, J., Schwenk, F., Fekete, C., Suzuki, A., Mak, T. W., Krone, W., Horvath, T. L., Ashcroft, F. M. and Bruning, J. C. (2006). Enhanced pip3 signaling in pomc neurons causes katp channel activation and leads to diet-sensitive obesity. J Clin Invest, *116*, 1886-901.

Pocai, A., Lam, T. K., Gutierrez-Juarez, R., Obici, S., Schwartz, G. J., Bryan, J., Aguilar-Bryan, L. and Rossetti, L. (2005a). Hypothalamic k(atp) channels control hepatic glucose production. Nature, *434*, 1026-31.

Pocai, A., Obici, S., Schwartz, G. J. and Rossetti, L. (2005b). A brain-liver circuit regulates glucose homeostasis. Cell Metab, *1*, 53-61.

Pontvianne, F., Carpentier, M. C., Durut, N., Pavlistova, V., Jaske, K., Schorova, S., Parrinello, H., Rohmer, M., Pikaard, C. S., Fojtova, M., Fajkus, J. and Saez-Vasquez, J. (2016). Identification of nucleolus-associated chromatin domains reveals a role for the nucleolus in 3d organization of the a. Thaliana genome. Cell Rep, *16*, 1574-1587.

Porniece Kumar, M., Cremer, A. L., Klemm, P., Steuernagel, L., Sundaram, S., Jais, A., Hausen, A. C., Tao, J., Secher, A., Pedersen, T. A., Schwaninger, M., Wunderlich, F. T., Lowell, B. B., Backes, H. and Bruning, J. C. (2021). Insulin signalling in tanycytes gates hypothalamic insulin uptake and regulation of agrp neuron activity. Nat Metab, *3*, 1662-1679.

Puigserver, P., Rhee, J., Donovan, J., Walkey, C. J., Yoon, J. C., Oriente, F., Kitamura, Y., Altomonte, J., Dong, H., Accili, D. and Spiegelman, B. M. (2003). Insulin-regulated hepatic gluconeogenesis through foxo1-pgc-1alpha interaction. Nature, *423*, 550-5.

Qiu, J., Zhang, C., Borgquist, A., Nestor, C. C., Smith, A. W., Bosch, M. A., Ku, S., Wagner, E. J., Ronnekleiv, O. K. and Kelly, M. J. (2014). Insulin excites anorexigenic proopiomelanocortin neurons via activation of canonical transient receptor potential channels. Cell Metab, *19*, 682-93.

Qiu, R., Miao, T., Lin, L. and Wei, Z. (2022). Biological functions of nuclear-localized insulin receptor (ir) on a549 lung cancer cells. Endokrynol Pol, *73*, 121-130.

Quik, M. and Mcintosh, J. M. (2006). Striatal alpha6* nicotinic acetylcholine receptors: Potential targets for parkinson's disease therapy. J Pharmacol Exp Ther, *316*, 481-9.

Rajas, F., Gautier-Stein, A. and Mithieux, G. (2019). Glucose-6 phosphate, a central hub for liver carbohydrate metabolism. Metabolites, *9*.

Ralph-Williams, R. J., Paulus, M. P., Zhuang, X., Hen, R. and Geyer, M. A. (2003). Valproate attenuates hyperactive and perseverative behaviors in mutant mice with a dysregulated dopamine system. Biol Psychiatry, *53*, 352-9.

Ramalingam, M., Kwon, Y. D. and Kim, S. J. (2016). Insulin as a potent stimulator of akt, erk and inhibin-betae signaling in osteoblast-like umr-106 cells. Biomol Ther (Seoul), *24*, 589-594.

Rao, Z. R., Yamano, M., Wanaka, A., Tatehata, T., Shiosaka, S. and Tohyama, M. (1987). Distribution of cholinergic neurons and fibers in the hypothalamus of the rat using choline acetyltransferase as a marker. Neuroscience, *20*, 923-34.

Reger, M. A., Watson, G. S., Frey, W. H., 2nd, Baker, L. D., Cholerton, B., Keeling, M. L., Belongia, D. A., Fishel, M. A., Plymate, S. R., Schellenberg, G. D., Cherrier, M. M. and Craft, S. (2006). Effects of intranasal insulin on cognition in memory-impaired older adults: Modulation by apoe genotype. Neurobiol Aging, *27*, 451-8.

Reger, M. A., Watson, G. S., Green, P. S., Baker, L. D., Cholerton, B., Fishel, M. A., Plymate, S. R., Cherrier, M. M., Schellenberg, G. D., Frey, W. H., 2nd and Craft, S. (2008). Intranasal insulin administration dose-dependently modulates verbal memory and plasma amyloid-beta in memory-impaired older adults. J Alzheimers Dis, *13*, 323-31.

Ren, H., Plum-Morschel, L., Gutierrez-Juarez, R., Lu, T. Y., Kim-Muller, J. Y., Heinrich, G., Wardlaw, S. L., Silver, R. and Accili, D. (2013). Blunted refeeding response and increased locomotor activity in mice lacking foxo1 in synapsin-cre-expressing neurons. Diabetes, *62*, 3373-83.

Ren, J., Qin, C., Hu, F., Tan, J., Qiu, L., Zhao, S., Feng, G. and Luo, M. (2011). Habenula "cholinergic" neurons co-release glutamate and acetylcholine and activate postsynaptic neurons via distinct transmission modes. Neuron, *69*, 445-52.

Renner, D. B., Svitak, A. L., Gallus, N. J., Ericson, M. E., Frey, W. H., 2nd and Hanson, L. R. (2012). Intranasal delivery of insulin via the olfactory nerve pathway. J Pharm Pharmacol, *64*, 1709-14.

Rensink, A. A., Otte-Holler, I., De Boer, R., Bosch, R. R., Ten Donkelaar, H. J., De Waal, R. M., Verbeek, M. M. and Kremer, B. (2004). Insulin inhibits amyloid beta-induced cell death in cultured human brain pericytes. Neurobiol Aging, *25*, 93-103.

Rhea, E. M., Humann, S. R., Nirkhe, S., Farr, S. A., Morley, J. E. and Banks, W. A. (2017). Intranasal insulin transport is preserved in aged samp8 mice and is altered by albumin and insulin receptor inhibition. J Alzheimers Dis, *57*, 241-252.

Rhea, E. M., Rask-Madsen, C. and Banks, W. A. (2018). Insulin transport across the blood-brain barrier can occur independently of the insulin receptor. J Physiol, *596*, 4753-4765.

Riccardi, G., Giacco, R. and Rivellese, A. A. (2004). Dietary fat, insulin sensitivity and the metabolic syndrome. Clin Nutr, *23*, 447-56.

Richardson, T. and Kerr, D. (2003). Skin-related complications of insulin therapy:

Epidemiology and emerging management strategies. Am J Clin Dermatol, *4*, 661-7.

Riera, C. E., Tsaousidou, E., Halloran, J., Follett, P., Hahn, O., Pereira, M. M. A., Ruud, L. E., Alber, J., Tharp, K., Anderson, C. M., Bronneke, H., Hampel, B., Filho, C. D. M., Stahl, A., Bruning, J. C. and Dillin, A. (2017). The sense of smell impacts metabolic health and obesity. Cell Metab, *26*, 198-211 e5.

Rios, M., Fan, G., Fekete, C., Kelly, J., Bates, B., Kuehn, R., Lechan, R. M. and Jaenisch, R. (2001). Conditional deletion of brain-derived neurotrophic factor in the postnatal brain leads to obesity and hyperactivity. Mol Endocrinol, *15*, 1748-57.

Rodriguez-Raecke, R., Sommer, M., Brunner, Y. F., Muschenich, F. S. and Sijben, R. (2020). Virtual grocery shopping and cookie consumption following intranasal insulin or placebo application. Exp Clin Psychopharmacol, *28*, 495-500.

Rodriguez, J. and Crespo, P. (2011). Working without kinase activity: Phosphotransfer-independent functions of extracellular signal-regulated kinases. Sci Signal, *4*, re3.

Roth, B. L. (2016). Dreadds for neuroscientists. Neuron, *89*, 683-94.

Ruhm, C. J. (2012). Understanding overeating and obesity. J Health Econ, *31*, 781-96.

Rye, D. B., Wainer, B. H., Mesulam, M. M., Mufson, E. J. and Saper, C. B. (1984). Cortical projections arising from the basal forebrain: A study of cholinergic and noncholinergic components employing combined retrograde tracing and immunohistochemical localization of choline acetyltransferase. Neuroscience, *13*, 627-43.

Sahu, A., Sninsky, C. A., Phelps, C. P., Dube, M. G., Kalra, P. S. and Kalra, S. P. (1992). Neuropeptide y release from the paraventricular nucleus increases in association with hyperphagia in streptozotocin-induced diabetic rats. Endocrinology, *131*, 2979-85.

Sakaguchi, M., Cai, W., Wang, C. H., Cederquist, C. T., Damasio, M., Homan, E. P., Batista, T., Ramirez, A. K., Gupta, M. K., Steger, M., Wewer Albrechtsen, N. J., Singh, S. K., Araki, E., Mann, M., Enerback, S. and Kahn, C. R. (2019). Foxk1 and foxk2 in insulin regulation of cellular and mitochondrial metabolism. Nat Commun, *10*, 1582.

Salameh, T. S., Bullock, K. M., Hujoel, I. A., Niehoff, M. L., Wolden-Hanson, T., Kim, J., Morley, J. E., Farr, S. A. and Banks, W. A. (2015). Central nervous system delivery of intranasal insulin: Mechanisms of uptake and effects on cognition. J Alzheimers Dis, *47*, 715-28.

Saleeba, C., Dempsey, B., Le, S., Goodchild, A. and Mcmullan, S. (2019). A student's guide to neural circuit tracing. Front Neurosci, *13*, 897.

Salzman, R., Manson, J. E., Griffing, G. T., Kimmerle, R., Ruderman, N., Mccall, A., Stoltz, E. I., Mullin, C., Small, D., Armstrong, J. and Et Al. (1985). Intranasal

aerosolized insulin. Mixed-meal studies and long-term use in type i diabetes. N Engl J Med, *312*, 1078-84.

Samuel, V. T., Choi, C. S., Phillips, T. G., Romanelli, A. J., Geisler, J. G., Bhanot, S., Mckay, R., Monia, B., Shutter, J. R., Lindberg, R. A., Shulman, G. I. and Veniant, M. M. (2006). Targeting foxo1 in mice using antisense oligonucleotide improves hepatic and peripheral insulin action. Diabetes, *55*, 2042-50.

Sanchez-Perez, A. M., Arnal-Vicente, I., Santos, F. N., Pereira, C. W., Elmlili, N., Sanjuan, J., Ma, S., Gundlach, A. L. and Olucha-Bordonau, F. E. (2015). Septal projections to nucleus incertus in the rat: Bidirectional pathways for modulation of hippocampal function. J Comp Neurol, *523*, 565-88.

Sandoval, D. A., Obici, S. and Seeley, R. J. (2009). Targeting the cns to treat type 2 diabetes. Nat Rev Drug Discov, *8*, 386-98.

Sara, V. R., Hall, K., Von Holtz, H., Humbel, R., Sjogren, B. and Wetterberg, L. (1982). Evidence for the presence of specific receptors for insulin-like growth factors 1 (ige-1) and 2 (igf-2) and insulin throughout the adult human brain. Neurosci Lett, *34*, 39-44.

Sartorius, T., Peter, A., Heni, M., Maetzler, W., Fritsche, A., Haring, H. U. and Hennige, A. M. (2015). The brain response to peripheral insulin declines with age: A contribution of the blood-brain barrier? PLoS One, *10*, e0126804.

Scherer, T., Lindtner, C., O'hare, J., Hackl, M., Zielinski, E., Freudenthaler, A., Baumgartner-Parzer, S., Todter, K., Heeren, J., Krssak, M., Scheja, L., Furnsinn, C. and Buettner, C. (2016). Insulin regulates hepatic triglyceride secretion and lipid content via signaling in the brain. Diabetes, *65*, 1511-20.

Scherer, T., O'hare, J., Diggs-Andrews, K., Schweiger, M., Cheng, B., Lindtner, C., Zielinski, E., Vempati, P., Su, K., Dighe, S., Milsom, T., Puchowicz, M., Scheja, L., Zechner, R., Fisher, S. J., Previs, S. F. and Buettner, C. (2011). Brain insulin controls adipose tissue lipolysis and lipogenesis. Cell Metab, *13*, 183-94.

Schilling, T. M., Ferreira De Sa, D. S., Westerhausen, R., Strelzyk, F., Larra, M. F., Hallschmid, M., Savaskan, E., Oitzl, M. S., Busch, H. P., Naumann, E. and Schachinger, H. (2014). Intranasal insulin increases regional cerebral blood flow in the insular cortex in men independently of cortisol manipulation. Hum Brain Mapp, *35*, 1944-56.

Schmid, V., Kullmann, S., Gfrorer, W., Hund, V., Hallschmid, M., Lipp, H. P., Haring, H. U., Preissl, H., Fritsche, A. and Heni, M. (2018). Safety of intranasal human insulin: A review. Diabetes Obes Metab, *20*, 1563-1577.

Schneider, E., Spetter, M. S., Martin, E., Sapey, E., Yip, K. P., Manolopoulos, K. N., Tahrani, A. A., Thomas, J. M., Lee, M., Hallschmid, M., Rotshtein, P., Dourish, C. T. and Higgs, S. (2022). The effect of intranasal insulin on appetite and mood in women with and without obesity: An experimental medicine study. Int J Obes (Lond), *46*, 1319-1327.

Schulingkamp, R. J., Pagano, T. C., Hung, D. and Raffa, R. B. (2000). Insulin receptors

and insulin action in the brain: Review and clinical implications. Neurosci Biobehav Rev, *24*, 855-72.

Schwartz, M. W., Figlewicz, D. P., Baskin, D. G., Woods, S. C. and Porte, D., Jr. (1992a). Insulin in the brain: A hormonal regulator of energy balance. Endocr Rev, *13*, 387-414.

Schwartz, M. W., Marks, J. L., Sipols, A. J., Baskin, D. G., Woods, S. C., Kahn, S. E. and Porte, D., Jr. (1991). Central insulin administration reduces neuropeptide y mrna expression in the arcuate nucleus of food-deprived lean (fa/fa) but not obese (fa/fa) zucker rats. Endocrinology, *128*, 2645-7.

Schwartz, M. W., Sipols, A. J., Marks, J. L., Sanacora, G., White, J. D., Scheurink, A., Kahn, S. E., Baskin, D. G., Woods, S. C., Figlewicz, D. P. and Et Al. (1992b). Inhibition of hypothalamic neuropeptide y gene expression by insulin. Endocrinology, *130*, 3608-16.

Seghers, V., Nakazaki, M., Demayo, F., Aguilar-Bryan, L. and Bryan, J. (2000). Sur1 knockout mice. A model for k(atp) channel-independent regulation of insulin secretion. J Biol Chem, *275*, 9270-7.

Shaul, Y. D. and Seger, R. (2007). The mek/erk cascade: From signaling specificity to diverse functions. Biochim Biophys Acta, *1773*, 1213-26.

Shi, H., Asher, C., Chigaev, A., Yung, Y., Reuveny, E., Seger, R. and Garty, H. (2002). Interactions of beta and gamma enac with nedd4 can be facilitated by an erk-mediated phosphorylation. J Biol Chem, *277*, 13539-47.

Shimura, T., Imaoka, H. and Yamamoto, T. (2006). Neurochemical modulation of ingestive behavior in the ventral pallidum. Eur J Neurosci, *23*, 1596-604.

Shin, A. C., Filatova, N., Lindtner, C., Chi, T., Degann, S., Oberlin, D. and Buettner, C. (2017). Insulin receptor signaling in pomc, but not agrp, neurons controls adipose tissue insulin action. Diabetes, *66*, 1560-1571.

Shiota, C., Larsson, O., Shelton, K. D., Shiota, M., Efanov, A. M., Hoy, M., Lindner, J., Kooptiwut, S., Juntti-Berggren, L., Gromada, J., Berggren, P. O. and Magnuson, M. A. (2002). Sulfonylurea receptor type 1 knock-out mice have intact feeding-stimulated insulin secretion despite marked impairment in their response to glucose. J Biol Chem, *277*, 37176-83.

Shipley, M. T. (1985). Transport of molecules from nose to brain: Transneuronal anterograde and retrograde labeling in the rat olfactory system by wheat germ agglutinin-horseradish peroxidase applied to the nasal epithelium. Brain Res Bull, *15*, 129-42.

Simpson, I. A., Appel, N. M., Hokari, M., Oki, J., Holman, G. D., Maher, F., Koehler-Stec, E. M., Vannucci, S. J. and Smith, Q. R. (1999). Blood-brain barrier glucose transporter: Effects of hypo- and hyperglycemia revisited. J Neurochem, *72*, 238-47.

Sindelar, D. K., Balcom, J. H., Chu, C. A., Neal, D. W. and Cherrington, A. D. (1996). A

comparison of the effects of selective increases in peripheral or portal insulin on hepatic glucose production in the conscious dog. Diabetes, *45*, 1594-604.

Sindelar, D. K., Chu, C. A., Rohlie, M., Neal, D. W., Swift, L. L. and Cherrington, A. D. (1997). The role of fatty acids in mediating the effects of peripheral insulin on hepatic glucose production in the conscious dog. Diabetes, *46*, 187-96.

Sindelar, D. K., Chu, C. A., Venson, P., Donahue, E. P., Neal, D. W. and Cherrington, A. D. (1998). Basal hepatic glucose production is regulated by the portal vein insulin concentration. Diabetes, *47*, 523-9.

Sipols, A. J., Baskin, D. G. and Schwartz, M. W. (1995). Effect of intracerebroventricular insulin infusion on diabetic hyperphagia and hypothalamic neuropeptide gene expression. Diabetes, *44*, 147-51.

Sivitz, W. I. and Yorek, M. A. (2010). Mitochondrial dysfunction in diabetes: From molecular mechanisms to functional significance and therapeutic opportunities. Antioxid Redox Signal, *12*, 537-77.

Skipor, J. and Thiery, J. C. (2008). The choroid plexus--cerebrospinal fluid system: Undervaluated pathway of neuroendocrine signaling into the brain. Acta Neurobiol Exp (Wars), *68*, 414-28.

Skolnik, E. Y., Lee, C. H., Batzer, A., Vicentini, L. M., Zhou, M., Daly, R., Myers, M. J., Jr., Backer, J. M., Ullrich, A., White, M. F. and Et Al. (1993). The sh2/sh3 domain-containing protein grb2 interacts with tyrosine-phosphorylated irs1 and shc: Implications for insulin control of ras signalling. EMBO J, *12*, 1929-36.

Smith, S. M. and Vale, W. W. (2006). The role of the hypothalamic-pituitary-adrenal axis in neuroendocrine responses to stress. Dialogues Clin Neurosci, *8*, 383-95.

Song, M. Y. and Yuan, J. X. (2010). Introduction to trp channels: Structure, function, and regulation. Adv Exp Med Biol, *661*, 99-108.

Soria-Gomez, E., Bellocchio, L., Reguero, L., Lepousez, G., Martin, C., Bendahmane, M., Ruehle, S., Remmers, F., Desprez, T., Matias, I., Wiesner, T., Cannich, A., Nissant, A., Wadleigh, A., Pape, H. C., Chiarlone, A. P., Quarta, C., Verrier, D., Vincent, P., Massa, F., Lutz, B., Guzman, M., Gurden, H., Ferreira, G., Lledo, P. M., Grandes, P. and Marsicano, G. (2014). The endocannabinoid system controls food intake via olfactory processes. Nat Neurosci, *17*, 407-15.

Speakman, J. R. (2013). Measuring energy metabolism in the mouse - theoretical, practical, and analytical considerations. Front Physiol, *4*, 34.

Spielman, L. J., Bahniwal, M., Little, J. P., Walker, D. G. and Klegeris, A. (2015). Insulin modulates in vitro secretion of cytokines and cytotoxins by human glial cells. Curr Alzheimer Res, *12*, 684-93.

Staib, J. M., Della Valle, R. and Knox, D. K. (2018). Disruption of medial septum and diagonal bands of broca cholinergic projections to the ventral hippocampus disrupt auditory fear memory. Neurobiol Learn Mem, *152*, 71-79.

Stockhorst, U., De Fries, D., Steingrueber, H. J. and Scherbaum, W. A. (2004). Insulin and the cns: Effects on food intake, memory, and endocrine parameters and the role of intranasal insulin administration in humans. Physiol Behav, *83*, 47-54.

Stolk, R. P., Meijer, R., Mali, W. P., Grobbee, D. E., Van Der Graaf, Y. and Secondary Manifestations of Arterial Disease Study, G. (2003). Ultrasound measurements of intraabdominal fat estimate the metabolic syndrome better than do measurements of waist circumference. Am J Clin Nutr, *77*, 857-60.

Stouffer, M. A., Woods, C. A., Patel, J. C., Lee, C. R., Witkovsky, P., Bao, L., Machold, R. P., Jones, K. T., De Vaca, S. C., Reith, M. E., Carr, K. D. and Rice, M. E. (2015). Insulin enhances striatal dopamine release by activating cholinergic interneurons and thereby signals reward. Nat Commun, *6*, 8543.

Studenski, S., Perera, S., Patel, K., Rosano, C., Faulkner, K., Inzitari, M., Brach, J., Chandler, J., Cawthon, P., Connor, E. B., Nevitt, M., Visser, M., Kritchevsky, S., Badinelli, S., Harris, T., Newman, A. B., Cauley, J., Ferrucci, L. and Guralnik, J. (2011). Gait speed and survival in older adults. JAMA, *305*, 50-8.

Sun, X. J., Rothenberg, P., Kahn, C. R., Backer, J. M., Araki, E., Wilden, P. A., Cahill, D. A., Goldstein, B. J. and White, M. F. (1991). Structure of the insulin receptor substrate irs-1 defines a unique signal transduction protein. Nature, *352*, 73-7.

Suzuki, K. and Kono, T. (1980). Evidence that insulin causes translocation of glucose transport activity to the plasma membrane from an intracellular storage site. Proc Natl Acad Sci U S A, *77*, 2542-5.

Sweeney, P., Li, C. and Yang, Y. (2017). Appetite suppressive role of medial septal glutamatergic neurons. Proc Natl Acad Sci U S A, *114*, 13816-13821.

Sweeney, P. and Yang, Y. (2016). An inhibitory septum to lateral hypothalamus circuit that suppresses feeding. J Neurosci, *36*, 11185-11195.

Sylow, L., Kleinert, M., Pehmoller, C., Prats, C., Chiu, T. T., Klip, A., Richter, E. A. and Jensen, T. E. (2014). Akt and rac1 signaling are jointly required for insulin-stimulated glucose uptake in skeletal muscle and downregulated in insulin resistance. Cell Signal, *26*, 323-31.

Sylow, L., Tokarz, V. L., Richter, E. A. and Klip, A. (2021). The many actions of insulin in skeletal muscle, the paramount tissue determining glycemia. Cell Metab, *33*, 758-780.

Tago, H., Mcgeer, P. L., Bruce, G. and Hersh, L. B. (1987). Distribution of choline acetyltransferase-containing neurons of the hypothalamus. Brain Res, *415*, 49-62.

Taha, S. A., Katsuura, Y., Noorvash, D., Seroussi, A. and Fields, H. L. (2009). Convergent, not serial, striatal and pallidal circuits regulate opioid-induced food intake. Neuroscience, *161*, 718-33.

Tang, Y., Ge, J., Liu, F., Wu, P., Guo, S., Liu, Z., Wang, Y., Wang, Y., Ding, Z., Wu, J., Zuo, C. and Wang, J. (2016). Cerebral metabolic differences associated with

cognitive impairment in parkinson's disease. PLoS One, *11*, e0152716.

Taylor, K. M., Mark, G. P. and Hoebel, B. G. (2011). Conditioned taste aversion from neostigmine or methyl-naloxonium in the nucleus accumbens. Physiol Behav, *104*, 82-6.

Thorne, R. G., Emory, C. R., Ala, T. A. and Frey, W. H., 2nd (1995). Quantitative analysis of the olfactory pathway for drug delivery to the brain. Brain Res, *692*, 278-82.

Thorne, R. G., Pronk, G. J., Padmanabhan, V. and Frey, W. H., 2nd (2004). Delivery of insulin-like growth factor-i to the rat brain and spinal cord along olfactory and trigeminal pathways following intranasal administration. Neuroscience, *127*, 481-96.

Tilg, H. and Diehl, A. M. (2000). Cytokines in alcoholic and nonalcoholic steatohepatitis. N Engl J Med, *343*, 1467-76.

Tong, J., Mannea, E., Aime, P., Pfluger, P. T., Yi, C. X., Castaneda, T. R., Davis, H. W., Ren, X., Pixley, S., Benoit, S., Julliard, K., Woods, S. C., Horvath, T. L., Sleeman, M. M., D'alessio, D., Obici, S., Frank, R. and Tschop, M. H. (2011). Ghrelin enhances olfactory sensitivity and exploratory sniffing in rodents and humans. J Neurosci, *31*, 5841-6.

Tsalamandris, S., Antonopoulos, A. S., Oikonomou, E., Papamikroulis, G. A., Vogiatzi, G., Papaioannou, S., Deftereos, S. and Tousoulis, D. (2019). The role of inflammation in diabetes: Current concepts and future perspectives. Eur Cardiol, *14*, 50-59.

Tsao, T. S., Burcelin, R., Katz, E. B., Huang, L. and Charron, M. J. (1996). Enhanced insulin action due to targeted glut4 overexpression exclusively in muscle. Diabetes, *45*, 28-36.

Tschop, M. H., Speakman, J. R., Arch, J. R., Auwerx, J., Bruning, J. C., Chan, L., Eckel, R. H., Farese, R. V., Jr., Galgani, J. E., Hambly, C., Herman, M. A., Horvath, T. L., Kahn, B. B., Kozma, S. C., Maratos-Flier, E., Muller, T. D., Munzberg, H., Pfluger, P. T., Plum, L., Reitman, M. L., Rahmouni, K., Shulman, G. I., Thomas, G., Kahn, C. R. and Ravussin, E. (2011). A guide to analysis of mouse energy metabolism. Nat Methods, *9*, 57-63.

Tschritter, O., Hennige, A. M., Preissl, H., Grichisch, Y., Kirchhoff, K., Kantartzis, K., Machicao, F., Fritsche, A. and Haring, H. U. (2009). Insulin effects on beta and theta activity in the human brain are differentially affected by ageing. Diabetologia, *52*, 169-71.

Tschritter, O., Preissl, H., Hennige, A. M., Stumvoll, M., Porubska, K., Frost, R., Marx, H., Klosel, B., Lutzenberger, W., Birbaumer, N., Haring, H. U. and Fritsche, A. (2006). The cerebrocortical response to hyperinsulinemia is reduced in overweight humans: A magnetoencephalographic study. Proc Natl Acad Sci U S A, *103*, 12103-8.

Tsujimoto, K., Tsuji, N., Ozaki, K., Minami, M., Satoh, M. and Itoh, N. (1995).

Expression of insulin receptor-related receptor mrna in the rat brain is highly restricted to forebrain cholinergic neurons. Neurosci Lett, *188*, 105-8.

Turchi, J. and Sarter, M. (1997). Cortical acetylcholine and processing capacity: Effects of cortical cholinergic deafferentation on crossmodal divided attention in rats. Brain Res Cogn Brain Res, *6*, 147-58.

Unger, J., Mcneill, T. H., Moxley, R. T., 3rd, White, M., Moss, A. and Livingston, J. N. (1989). Distribution of insulin receptor-like immunoreactivity in the rat forebrain. Neuroscience, *31*, 143-57.

Updegraff, B. L. and O'donnell, K. A. (2013). Stressing the importance of chop in liver cancer. PLoS Genet, *9*, e1004045.

Van Den Berg, M. P., Romeijn, S. G., Verhoef, J. C. and Merkus, F. W. (2002). Serial cerebrospinal fluid sampling in a rat model to study drug uptake from the nasal cavity. J Neurosci Methods, *116*, 99-107.

Van Nassauw, L., Wu, M., De Jonge, F., Adriaensen, D. and Timmermans, J. P. (2005). Cytoplasmic, but not nuclear, expression of the neuronal nuclei (neun) antibody is an exclusive feature of dogiel type ii neurons in the guinea-pig gastrointestinal tract. Histochem Cell Biol, *124*, 369-77.

Varela, L. and Horvath, T. L. (2012). Leptin and insulin pathways in pomc and agrp neurons that modulate energy balance and glucose homeostasis. EMBO Rep, *13*, 1079-86.

Vasselli, J. R., Pi-Sunyer, F. X., Wall, D. G., John, C. S., Chapman, C. D. and Currie, P. J. (2017). Central effects of insulin detemir on feeding, body weight, and metabolism in rats. Am J Physiol Endocrinol Metab, *313*, E613-E621.

Verkhratsky, A. and Nedergaard, M. (2018). Physiology of astroglia. Physiol Rev, *98*, 239-389.

Vidarsdottir, S., Smeets, P. A., Eichelsheim, D. L., Van Osch, M. J., Viergever, M. A., Romijn, J. A., Van Der Grond, J. and Pijl, H. (2007). Glucose ingestion fails to inhibit hypothalamic neuronal activity in patients with type 2 diabetes. Diabetes, *56*, 2547-50.

Villar, P. S., Hu, R. and Araneda, R. C. (2021). Long-range gabaergic inhibition modulates spatiotemporal dynamics of the output neurons in the olfactory bulb. J Neurosci, *41*, 3610-3621.

Wallum, B. J., Taborsky, G. J., Jr., Porte, D., Jr., Figlewicz, D. P., Jacobson, L., Beard, J. C., Ward, W. K. and Dorsa, D. (1987). Cerebrospinal fluid insulin levels increase during intravenous insulin infusions in man. J Clin Endocrinol Metab, *64*, 190-4.

Wang, D., He, X., Zhao, Z., Feng, Q., Lin, R., Sun, Y., Ding, T., Xu, F., Luo, M. and Zhan, C. (2015). Whole-brain mapping of the direct inputs and axonal projections of pomc and agrp neurons. Front Neuroanat, *9*, 40.

Wang, L., Li, J. and Di, L. J. (2022). Glycogen synthesis and beyond, a comprehensive

review of gsk3 as a key regulator of metabolic pathways and a therapeutic target for treating metabolic diseases. Med Res Rev, *42*, 946-982.

Warner-Schmidt, J. L., Schmidt, E. F., Marshall, J. J., Rubin, A. J., Arango-Lievano, M., Kaplitt, M. G., Ibanez-Tallon, I., Heintz, N. and Greengard, P. (2012). Cholinergic interneurons in the nucleus accumbens regulate depression-like behavior. Proc Natl Acad Sci U S A, *109*, 11360-5.

Weisberg, S. P., Mccann, D., Desai, M., Rosenbaum, M., Leibel, R. L. and Ferrante, A. W., Jr. (2003). Obesity is associated with macrophage accumulation in adipose tissue. J Clin Invest, *112*, 1796-808.

Weyer, C., Funahashi, T., Tanaka, S., Hotta, K., Matsuzawa, Y., Pratley, R. E. and Tataranni, P. A. (2001). Hypoadiponectinemia in obesity and type 2 diabetes: Close association with insulin resistance and hyperinsulinemia. J Clin Endocrinol Metab, *86*, 1930-5.

Willette, A. A., Bendlin, B. B., Starks, E. J., Birdsill, A. C., Johnson, S. C., Christian, B. T., Okonkwo, O. C., La Rue, A., Hermann, B. P., Koscik, R. L., Jonaitis, E. M., Sager, M. A. and Asthana, S. (2015). Association of insulin resistance with cerebral glucose uptake in late middle-aged adults at risk for alzheimer disease. JAMA Neurol, *72*, 1013-20.

Wilson, R. C., Vacek, T., Lanier, D. L. and Dewsbury, D. A. (1976). Open-field behavior in muroid rodents. Behav Biol, *17*, 495-506.

Wise, R. A. (2004). Dopamine, learning and motivation. Nat Rev Neurosci, *5*, 483-94.

Wishart, T. B., Bland, B. H., Vanderwolf, C. H. and Altman, J. L. (1973). Electroencephalographic correlates of behaviors elicited by electrical stimulation of the septum: Seizure induced feeding. Behav Biol, *9*, 763-9.

Wong, A. D., Ye, M., Levy, A. F., Rothstein, J. D., Bergles, D. E. and Searson, P. C. (2013). The blood-brain barrier: An engineering perspective. Front Neuroeng, *6*, 7.

Woods, S. C., Seeley, R. J., Baskin, D. G. and Schwartz, M. W. (2003). Insulin and the blood-brain barrier. Curr Pharm Des, *9*, 795-800.

Wu, Z., Kim, E. R., Sun, H., Xu, Y., Mangieri, L. R., Li, D. P., Pan, H. L., Xu, Y., Arenkiel, B. R. and Tong, Q. (2015). Gabaergic projections from lateral hypothalamus to paraventricular hypothalamic nucleus promote feeding. J Neurosci, *35*, 3312-8.

Xu, A. W., Kaelin, C. B., Takeda, K., Akira, S., Schwartz, M. W. and Barsh, G. S. (2005). Pi3k integrates the action of insulin and leptin on hypothalamic neurons. J Clin Invest, *115*, 951-8.

Xu, M., Chung, S., Zhang, S., Zhong, P., Ma, C., Chang, W. C., Weissbourd, B., Sakai, N., Luo, L., Nishino, S. and Dan, Y. (2015a). Basal forebrain circuit for sleep-wake control. Nat Neurosci, *18*, 1641-7.

Xu, P. T., Song, Z., Zhang, W. C., Jiao, B. and Yu, Z. B. (2015b). Impaired translocation of glut4 results in insulin resistance of atrophic soleus muscle. Biomed Res Int, *2015*, 291987.

Xu, W. L., Qiu, C. X., Wahlin, A., Winblad, B. and Fratiglioni, L. (2004). Diabetes mellitus and risk of dementia in the kungsholmen project: A 6-year follow-up study. Neurology, *63*, 1181-6.

Yang, J. P., Liu, H. J., Cheng, S. M., Wang, Z. L., Cheng, X., Yu, H. X. and Liu, X. F. (2009). Direct transport of vegf from the nasal cavity to brain. Neurosci Lett, *449*, 108-11.

Yip, C. C. and Ottensmeyer, P. (2003). Three-dimensional structural interactions of insulin and its receptor. J Biol Chem, *278*, 27329-32.

Yoo, S., Cha, D., Kim, S., Jiang, L., Adebesin, M., Wolfe, A., Riddle, R., Aja, S. and Blackshaw, S. (2019). Ablation of tanycytes of the arcuate nucleus and median eminence increases visceral adiposity and decreases insulin sensitivity in male mice. bioRxiv, 637587.

Zaborszky, L., Carlsen, J., Brashear, H. R. and Heimer, L. (1986). Cholinergic and gabaergic afferents to the olfactory bulb in the rat with special emphasis on the projection neurons in the nucleus of the horizontal limb of the diagonal band. J Comp Neurol, *243*, 488-509.

Zaborszky, L., Csordas, A., Mosca, K., Kim, J., Gielow, M. R., Vadasz, C. and Nadasdy, Z. (2015). Neurons in the basal forebrain project to the cortex in a complex topographic organization that reflects corticocortical connectivity patterns: An experimental study based on retrograde tracing and 3d reconstruction. Cereb Cortex, *25*, 118-37.

Zhan, X., Yin, P. and Heinbockel, T. (2013). The basal forebrain modulates spontaneous activity of principal cells in the main olfactory bulb of anesthetized mice. Front Neural Circuits, *7*, 148.

Zhang, Y., Zhou, J., Corll, C., Porter, J. R., Martin, R. J. and Roane, D. S. (2004). Evidence for hypothalamic k+(atp) channels in the modulation of glucose homeostasis. Eur J Pharmacol, *492*, 71-9.

Zhao, J., Wu, Y., Rong, X., Zheng, C. and Guo, J. (2020). Anti-lipolysis induced by insulin in diverse pathophysiologic conditions of adipose tissue. Diabetes Metab Syndr Obes, *13*, 1575-1585.

Zheng, Y., Feng, S., Zhu, X., Jiang, W., Wen, P., Ye, F., Rao, X., Jin, S., He, X. and Xu, F. (2018). Different subgroups of cholinergic neurons in the basal forebrain are distinctly innervated by the olfactory regions and activated differentially in olfactory memory retrieval. Front Neural Circuits, *12*, 99.

Zheng, Y., Tao, S., Liu, Y., Liu, J., Sun, L., Zheng, Y., Tian, Y., Su, P., Zhu, X. and Xu, F. (2022). Basal forebrain-dorsal hippocampus cholinergic circuit regulates olfactory associative learning. Int J Mol Sci, *23*.

Zhu, C., Yao, Y., Xiong, Y., Cheng, M., Chen, J., Zhao, R., Liao, F., Shi, R. and Song, S. (2017). Somatostatin neurons in the basal forebrain promote high-calorie food intake. Cell Rep, *20*, 112-123.

Zisman, A., Peroni, O. D., Abel, E. D., Michael, M. D., Mauvais-Jarvis, F., Lowell, B. B., Wojtaszewski, J. F., Hirshman, M. F., Virkamaki, A., Goodyear, L. J., Kahn, C. R. and Kahn, B. B. (2000). Targeted disruption of the glucose transporter 4 selectively in muscle causes insulin resistance and glucose intolerance. Nat Med, *6*, 924-8.

Zlokovic, B. V. (2008). The blood-brain barrier in health and chronic neurodegenerative disorders. Neuron, *57*, 178-201.

Zou, X. H., Sun, L. H., Yang, W., Li, B. J. and Cui, R. J. (2020). Potential role of insulin on the pathogenesis of depression. Cell Prolif, *53*, e12806.

Appendix

2.3.7 Analysis of CLAMS data

#install packages and libraries

```
install.packages("tidyverse")

install.packages("ggplot2")

library(rstatix)

library(ggplot2)

library(tidyverse)

install.packages("emmeans")

library(readr)

library(emmeans)
```

 # input database

```
library(readr)

df <- read_csv ("D:\\summary\\metabolic_cage\\ANCOVA\\Foldername.CSV")
```

 # summarize data of food comsumption and body mass

```
library(rstatix)

library(emmeans)

df    %>%    group_by(Group)    %>%    get_summary_stats(FoodComsumped,
type="common")

df %>% group_by(Group) %>%   get_summary_stats(BodyMass, type="common")
```

 # output data of body mass

```
write.csv(df    %>%    group_by(Hours)    %>%    get_summary_stats(BodyMass,
type="common"), file=" D:\\summary\\metabolic_cage\\ANCOVA\\groupby.CSV ")
```

#anova test to get mass effect and group effect

```
anova_test(data = df, formula = FoodComsumped ~ BodyMass + Group, type = 3,
detailed = TRUE)
```
 # type 3 SS should be used in ANCOVA

 # plot regression liner model between food consumption and body mass

```
install.packages("ggpubr")

library(ggpubr)

library(ggscatter)

ggscatter(df, x = "BodyMass", y = "FoodComsumped", color = "Group", add =
"reg.line")+ stat_regline_equation(aes(label =    paste(..eq.label.., ..rr.label.., sep =
"~~~~"), color = Group))
```

 # Get adjusted means according to the model:

```
adj_means <- emmeans_test(data = df, formula = FoodComsumped ~ Group, covariate
= BodyMass)
get_emmeans(adj_means)
```